CRANFIELD UNIVERSITY

L E ORR

RAMAN SPECTROSCOPY OF LARYNGEAL AND LYMPHOID TISSUE – AN APPLICATION IN OPTICAL DIAGNOSIS OF MALIGNANCY

CRANFIELD HEALTH

DM Thesis

Academic Year: 2009-2010

Supervisors: Dr N. Stone, Dr. I.E. Tothill & Mr M. Thomas

March 2010

CRANFIELD UNIVERSITY

CRANFIELD HEALTH

DM Thesis

Academic Year: 2009-2010

L E ORR

Raman Spectroscopy of Biological Tissue for Application in Optical Diagnosis of Malignancy

Supervisors: Dr N. Stone, Dr. I.E. Tothill & Mr M. Thomas

March 2010

This thesis is submitted in partial fulfilment of the requirements for the degree of Doctor of Medicine.

Abstract

The use of Raman spectroscopy in the detection and classification of malignancy within the human larynx and lymph nodes of the head and neck has been evaluated. Currently histopathology is considered the diagnostic gold standard. The potential for Raman spectroscopy to be used as an *in vivo* diagnostic tool in the detection of dysplasia and malignancy has been demonstrated. A consensus opinion from three expert histopathologists has been obtained and spectral diagnostic models developed by correlation with these results.

The ability of Raman spectroscopy to differentiate between disease entities and normal tissue within the larynx has been shown. Raman spectroscopy was able to identify non-neoplastic vocal cord mucosa (sensitivity 85 %, specificity 95%) from laryngeal mucosa showing neoplastic change (sensitivity 95 %, specificity 85%) with an increase in sensitivity to 89% for the non-neoplastic tissue and a reduction to73% in tissues showing neoplastic changes after cross-validation. For the first time benign changes in the structure of vocal cords such as those exhibiting hyperkeratosis and hyperplasia, where also identified with sensitivity of 97.9% for tissue exhibiting hyperplasia/hyperkeratosis and 100% for normal squamous cell epithelium. Research into the ability of Raman spectroscopy to interrogate lymphoid tissue in order to differentiate reactive nodes (sensitivity 90 %, specificity 88%) from those containing cancer (sensitivity 88 %, specificity 90%) was successful and fully independently validated. This work was further developed and the efficacy of Raman spectroscopy in differentiating between squamous cell carcinoma (sensitivity 76%, specificity 95%), adenocarcinoma (sensitivity 93 %, specificity 99%), Hodgkin's lymphoma (sensitivity 80%, specificity 90%) and reactive lymph nodes (sensitivity 81%, specificity 88%) was shown. This model was also independently cross-validated by node producing further improvements to give a spectral performance of sensitivity/specificity for SCC of 75/97%, adenocarcinoma 100/99%, Hodgkin's lymphoma 83/92% and reactive lymph nodes 85/86%.

Acknowledgements

I would like to thank my supervisors Dr Nick Stone, Dr Sam Tothill and Mr. Mike Thomas for their support, help and enthusiasm throughout this work. Thanks to Professor Barr for his vision in involving clinicians from differing surgical specialties in research of this type also to Mr. Mike Thomas, consultant ear, nose and throat (ENT) surgeon, for his help during the collection of the tissue samples and his continuing operative teaching and encouragement. On a day-by-day basis help on the scientific aspects of this work received from Dr Nick Stone and Dr Catherine Kendall has been much appreciated.

I would also like to thank the pathologists for reviewing the tissue specimens and for the time they spent explaining their work. Thanks also to the pathology technicians for meticulously cutting the specimens, the operating theatre teams and anaesthetists particularly Dr Jean Walters whose patience and help was much appreciated as was her quiet confidence and support.

To my colleagues in the Biophotonics Group thanks are due for all their help and for creating an atmosphere within the team that has made participating in this work such a pleasure.

Thanks to the south west ENT Training Committee, the Subspecialty Advisory Committee of the Royal College of Surgeons (SAC) and Defence Medical Services. Also thanks to the south west postgraduate deanery and my defence consultant advisors, Surgeon Commander Chris Pearson and Group Captain John Skipper, for allowing me the time to undertake this work. To my ENT Specialist Registrar colleagues for putting up with the changes in the 'Master Plan', for making me so welcome on the rotation and for continuing to be interested when I talk about Raman spectroscopy!

Thank you to my husband Evan, Alice, Sampson, my family and friends for their enduring interest and patience throughout, particularly their encouragement to complete this work over the difficult times. Who said it couldn't be done? I promise no more!

List of Figures

List of Tables

Chapter 1: Introduction

The work presented in this thesis is a programme of rigorous *in vitro* studies investigating the possible application of Raman spectroscopy in the study of biological tissues obtained from the head and neck. The potential of Raman spectroscopy to act as an objective, non-invasive technique capable of identifying focal biochemical changes is explored, particularly the progression of benign disease towards malignancy within the human laryngopharynx and in lymph nodes.

This chapter discusses the demographics of cancer with the emphasis on those which occur in the throat and lympho-reticular system. The context of the research described in the thesis is placed within the wider picture of resource allocation for cancer services. Raman spectroscopy is introduced as one of several optical diagnostic techniques that have potential for use in this area. The objectives of this research are summarised and the chapter concludes with an outline summary of the structure of this thesis as a whole.

1.1 Context of Research

1.1.1 Overview

Medicine has been described as primarily an art rather than a science. This is never more apparent than in surgery. Despite extraordinary advances in technology there is no machine that can discriminate between the subtle shades and textures that allow us to find the correct plane in which to operate in order to avoid a frustrating procedure performed in an ever-increasing field of blood. To watch a really gifted surgeon is to be in no doubt that surgery truly is an art however increasingly there is an appropriate call for the justification of practices based on science and research. This is particularly true in the emotive areas of cancer diagnosis and treatment.

Histopathology has historically been the gold standard in the assessment of disease within biological tissue however it is still haunted by difficulties of time and subjectivity. The basic workload of histopathologists is enormous and increasing. Technological advances allow for more tests, on more specimens and this is coupled with an increase in public and professional expectations on the speed of service delivery and accuracy of results.

It is envisaged that this research will contribute to progress in the development of Raman spectroscopy as an effective, efficient technique used in support of histological diagnosis; the ultimate goal of which is the development of a diagnostic and surgical tool to be used as a new gold standard.

1.1.2 Demographics of Cancer

Statistics published by the World Health Organization (WHO) estimate that in 2005 of a total of 58 million deaths worldwide 7.6 million were due to cancer. Of these more than 70% were in countries where incomes are classified to be in the low or middle brackets and where the provision off cancer services is considered poor. The WHO has predicted that by 2015 there will be 9 million deaths from cancer per year and by 2030, 11.4 million (WHO, 2007).

In England between 1971 and 2004 the age standardized incidence of cancer increased by approximately 41% in women and 21% in men. The vast majority of cancers occur in the elderly with less than 0.5% of registered cancers diagnosed in children under the age of 15 (National Statistics Online, 2006a). The mortality rate from cancer has broadly remained the same with one in four people in the United Kingdom (UK) dying from cancer during the period 1950 to 2004 (National Statistics Online, 2006b).

The highest incidence of laryngeal cancer within the UK occurs in Scotland (Table 1.1). To place this in the context of the overall incidence of cancer diagnoses made in Scotland studies have shown that 26, 400 new cancer diagnoses were made per annum over the period 1996-2000 and the prediction has been made that this will rise to 33, 700 per annum in the period 2016 - 2020. This represents an increase of 28% in cancer diagnoses as a whole over the next 20 years, 1.4% per year. In actual patient numbers approximately an extra 650 newly diagnosed cases in the under 75 age group and a further 1200 cases in the over 75s per annum. This increase is not due primarily to an increase in the individual risk of developing a particular cancer type, although the incidence of some cancers are predicted to increase, but is mainly due to an aging population (Cancer Incidence Projections for Scotland, 2001-2020).

Table 1.1: Number of new cases and rates of laryngeal cancer, UK, 2004. (Cancer Research UK, 2007)

	England		**Wales**		**Scotland**		**N. Ireland**	
Cases								
Males	1,424		91		234		40	
Females	269		24		71		13	
Persons	1,693		115		305		53	
Crude rate per 100,000 population								
Male	5.8		6.3		9.6		4.8	
Female	1.1		1.6		2.7		1.5	
Persons	3.4		3.9		6.0		3.1	
Age-standardised rate (European) per 100,000 population								
Males	5.0		5.1		8.3		4.9	
CI95%	4.8	5.3	4.0	6.1	7.3	9.4	3.4	6.4
Females	0.8		1.1		2.0		1.4	
CI95%	0.7	0.9	0.7	1.5	1.6	2.5	0.7	2.2
Persons	2.8		2.9		4.9		3.0	
CI95%	2.7	2.9	2.4	3.5	4.4	5.5	2.2	3.9

Cancer of the larynx has historically been associated with smoking and alcohol consumption, particularly spirits. In all regions of the UK men have a significantly

greater risk of developing the disease compared to women. The peak age range at which a diagnosis of laryngeal cancer is made in men is 60 - 64 years and for women slightly older 65 - 69 years. In 2004 there were a total of 2,166 new cases diagnosed in the UK of these 1789 (82.6%) were in men and 377 in women (17.4%). Age-standardised mortality rates for laryngeal cancer in the UK between 1971 and 2005 show that from the early 1990's there has been a decline in mortality for men and from 2000 there has also been a decline for women but this has been less pronounced (Cancer Research UK, 2007).

Cancers which affect lymph nodes can be either primary or due to secondary, metastatic spread from other sites. Of the lymph nodes cancers classified as primary lymphoma is the most common. Hodgkin's lymphoma makes up approximately 0.5% of all cancers presenting each year. In 2004 there were 1519 new cases diagnosed, of these 844 (55.6%) were in men and 675 (44.4%) in women (Table 1.2). There are two age periods were presentation occurs most frequently 15-29 years and 75-84 years. Within these age groups different disease subtypes predominate. Hodgkin's Lymphoma ranks as the 6th most common cancer occurring in children under 15 years of age.

Table 1.2: Number of new cases and rates of Hodgkin's lymphoma within the UK, 2004. (Cancer Research UK, 2007)

	England		**Wales**		**Scotland**		**N. Ireland**	
Cases								
Males	697		45		79		23	
Females	560		27		71		17	
Persons	1,257		72		150		40	
Crude rate per 100,000 population								
Male	2.8		3.1		3.2		2.7	
Female	2.2		1.8		2.7		1.9	
Persons	2.5		2.4		3.0		2.3	
Age-standardised rate (European) per 100,000 population								
Males	2.7		2.9		3.2		2.7	
CI95%	2.5	2.9	2.1	3.8	2.5	3.9	1.6	3.9
Females	2.1		1.8		2.6		2.0	
CI95%	2.0	2.3	1.1	2.4	2.0	3.2	1.0	2.9
Persons	2.4		2.3		2.9		2.3	
CI95%	2.3	2.6	1.8	2.8	2.4	3.3	1.6	3.0

Over the period 1970-1980 the age-standardised incidence rates for Hodgkin's lymphoma in the UK appeared to decrease. This is felt to be a reflection of reclassification of some disease as Non-Hodgkin's Lymphoma. From the mid 1980s to

2003 the age-standardised incidence rates have remained basically unchanged at approximately 3 per 100, 000 male and 2 per 100, 000 for females.

Non-Hodgkin's lymphoma accounts for approximately 4% of all cancer that present per annum, in 2004, 8316 new diagnoses were made in England (Table 1.3). A significantly higher incidence of non- Hodgkin's lymphoma is found in persons over the age of 50 and 69% of diagnoses being made in the over 60s.

Table 1.3: Number of new cases and rates of Non-Hodgkin lymphoma within the UK, 2004. (Cancer Research UK, 2007)

	England		**Wales**		**Scotland**		**N. Ireland**	
Cases								
Males	4,417		283		453		135	
Females	3,899		242		427		147	
Persons	8,316		525		880		282	
Crude rate per 100,000 population								
Male	18.0		19.7		18.6		16.1	
Female	15.3		15.9		16.3		16.8	
Persons	16.6		17.8		17.4		16.5	
Age-standardised rate (European) per 100,000 population								
Males	15.6		16.3		16.1		16.0	
CI95%	15.2	16.1	14.7	18.5	14.8	17.8	13.7	19.2
Females	11.4		10.8		11.8		13.4	
CI95%	11.0	11.7	9.4	12.1	10.7	12.9	11.2	15.6
Persons	13.3		13.4		13.8		14.6	
CI95%	13.0	13.6	12.2	14.5	12.9	14.7	12.9	16.3

1.1.3 Utilisation of Cancer Resources

The 58th World Health Assembly (WHA) resolution on cancer prevention and control in May, 2005 called upon all member states to 'intensify action against cancer by developing and reinforcing cancer control programmes.' The WHA suggested this be done using a framework of:

- Prevention
- Early Detection
- Diagnosis and Treatment
- Palliative Care

As the population of the UK ages the number of people diagnosed with cancer also increases and with this the amount of funding required to diagnose, treat and support

patients. The planning of provision for the management of patients with cancer is challenging. Trends in population growth, cancer incidence along with variations in survival as a consequence of new treatment regimes must all be taken into consideration. The NHS Cancer Plan published in July 2000 outlined the governments' strategy for investment and reform within the cancer services network. The stated aims were to improve the 'speed, quality and equality of cancer services.' The cancer plan outlines the strategies for improving cancer services in all areas not just those related to waiting times. It prioritises the provision of a unified, comprehensive cancer service focusing on service reorganisation, provision of equipment for diagnosis and treatment, improved levels of appropriately trained staff, facilities and research. To support these targets the government has undertaken a significant programme of additional investment in the NHS (The NHS Cancer Plan, 2000a & 2000b);

£280 million in 2001-2002
£407 million in 2002/2003
£570 million in 2003/2004
By 2003, £20 million each year towards the infrastructure of cancer research the aim being to match the investment made by the voluntary sector.
£50 million towards palliative care

Waiting list targets specified that by 2005 there would be a maximum wait of two months from receipt of an urgent referral to treatment of cancer and a one month maximum wait from diagnosis to treatment. The ultimate aim being that there was a maximum wait of one month from urgent GP referral to the commencement of treatment of all cancer patients by 2008 (The NHS Cancer Plan, 2000c). In order to make a diagnosis of laryngeal cancer or lymphoma patients usually require surgical removal of tissue for histological review. A technique that is significantly less expensive and could be used in the outpatients' clinic would be enormously advantageous in improving the speed of primary diagnosis and efficacy of screening for recurrence after treatment. This would ultimately help move clinical practice to a position where by it can offer a management plan for cancer sufferers that meets the criteria laid out in the NHS Cancer Plan. This work investigates the potential for Raman spectroscopy to be used as such a diagnostic technique.

1.2 Research Objectives

The primary aim of this work is to evaluate the potential of Raman spectroscopy as a tool capable of being used alongside histopathology techniques in the diagnosis of disease, specifically cancer occurring in tissues of the laryngopharynx and in lymph nodes.

In order to achieve this hypotheses listed below will be tested;

- Raman spectra obtained from biological tissue can be used to develop models capable of assigning pathological disease entities correctly for tissue obtained from the laryngopharynx and lymph nodes.
- When used to formulate diagnostic algorithms for diseases in these anatomical areas Raman spectroscopy processes both the sensitivity and the specificity to compare with that of the gold standard, histopathology.

- Raman spectroscopy can be used to distinguish diseased and normal vocal cord tissue.

Surgical skills and core medical knowledge have been maintained throughout the period of research as all tissue samples used were acquired during operations done by the author of this thesis.

1.2.1 Laryngopharyngeal Study

The aim of this study is to assess the ability of Raman Spectroscopy to differentiate between normal and diseased tissue in the laryngopharynx. If Raman Spectroscopy is found to be a viable tool in this respect it could be developed for use in the outpatient clinic. Using a thin flexible probe passed down the side port of a nasendoscope it may be possible to obtain an 'optical biopsy' to assess if cancer is present, if recurrence diagnostic accuracy and give a reduction in the number of biopsies required. This is particularly important as the cohort of patients who present with cancer of the larynx often have significant co-morbidity resulting in higher risks associated with receiving a general anaesthetic.

1.2.2 Lymph Node Study

The aim of this work is to assess the ability of Raman spectroscopy to differentiate between normal and diseased lymphoid tissue in the neck. If Raman spectroscopy is a viable tool in this respect then it may be possible to use this technique to introduce a Raman probe by means of a needle obtaining an 'optical biopsy' of enlarged lymph nodes in the neck without surgery. Work has begun on the development of an *in vivo* probe; however, there is a need to both clarify the validity of the technique when applied to this type of tissue and to formulate a baseline set of spectra for different lymphoid diseases.

1.3 Thesis Structure

Chapter 2 contains a review of the relevant literature. It begins with a section summarising the history and theory of Raman spectroscopy followed by a discussion of the characteristics required in an ideal diagnostic technique for the detection of malignancy and the positive attributes that Raman spectroscopy shows in this respect. A summary follows outlining the component parts of a classical Raman system and how Raman spectroscopy instrumentation has developed over time to give the system used in this work. A description of other relevant spectroscopic techniques is included and a discussion of various applications of Raman spectroscopy with particular emphasis on biomedical uses. The general theory of cancer development is then summarised along with clinical information relevant to this research. This includes a basic outline of anatomy and its influence on disease progression also the classification, aetiology, staging and treatment options for malignant diseases in the two anatomical areas studied. A discussion of the clinical relevance of Raman spectroscopy as a diagnostic tool in the investigation of disease in these areas concludes each of these sections. *Chapter 3* details the materials and methods used including details of system calibration. The results of this work, along with a discussion of the findings are contained in *Chapter 4*. *Chapter 5* summarises the conclusions drawn and discusses areas of future study.

Chapter 2: Literature Review

2.1 Raman Spectroscopy

After a brief outline of the historical context of the discovery of Raman spectroscopy the theoretical basis by which it is explained is discussed. The main emphasis is placed on the classical theory and only a brief description of the quantum theory is given.

2.1.1 History of Raman Spectroscopy

The possibility of inelastic scattering of light was first postulated in 1923 (Smekal, 1923). Sir Chandreskhara Venkata Raman C.B.E (1880-1970) and K.S. Krishnan observed the Raman effect in 1928. Their work was carried out at the University of Calcutta and the Indian Association for the Cultivation of Science (IACS) and published in Nature the same year (Raman & Krishnan, 1928). This discovery was also independently reported by Russian physicists (Landsberg & Mandelstam, 1928). Raman's experiment used sunlight as the source of incident radiation. This light was focused using a telescopic lens onto samples of either gases or dust free vapours. A further lens and series of optical filters were placed beyond the sample at an angle to the direction of the incident beam of sunlight. Initially the naked eye then photographic plates were used to record the presence of the scattered radiation. This processed an altered frequency compared to that of the incident beam – the basic fundamental finding underpinning the theory of Raman spectroscopy and called by Raman and Krishnan 'a new radiation.' Raman was knighted in 1928 and awarded the Nöbel prize in 1930. His other major scientific interests were in the physics of sound and theory of harmonics. Since the first observations of Raman peaks within the spectra obtained from the exposure of a chemical compound to incident monochromatic light there have been enormous developments in this technique. These advances will be discussed in more detail later, however, it is noted that they have resulted in an increasing number of biomedical and industrial applications for the technique of Raman spectroscopy.

2.1.2 Theoretical Basis of Raman Spectroscopy

When monochromatic light shines on a molecule it can pass through unchanged or interact with it in several ways undergoing either undergoing an absorption such as that which occurs in infrared (IR) spectroscopy or the light can be scattered as seen in Raman spectroscopy. Both IR and Raman spectroscopy are classified as vibrational spectroscopic techniques. In the case where no absorption reaction takes place the polarisability and the vibrational state of the molecule can change producing two distinct effects, Raman and Rayleigh scattering. The majority of photons undergo elastic scattering where the wavelength of the scattered light remains unchanged, this is called Rayleigh scattering. The energy of the incident photon and emitted photon are connected by a quantum of energy hence the interaction can be regarded as a single photon event rather than the type of two photon event, absorption followed by emission seen in IR spectroscopy (Nafie, 2001). A much smaller proportion of photons undergo inelastic scattering where energy is exchanged and the wavelength of the light is altered, this is called Raman scattering. Raman scattered light undergoes a frequency shift corresponding to the vibrational energy gained or lost by the change in the vibration motion of the molecule. Raman spectroscopy can be defined as an inelastic scattering, vibrational spectroscopic technique. It exploits a change in frequency in monochromatic

light occurring as a result of the interaction of incident photons with a test substance which results in the molecules within the test substance undergoing an alteration in their vibrational or rotational states. The signal obtained from Raman scattering is much weaker than that of Rayleigh scattering. If a million molecules are present approximately 100 000 will undergo an absorption reaction, 900 of these will undergo vibrational changes and of these only one will show the Raman effect. In Raman spectroscopy the speed of interaction between molecule and light is of the order of picoseconds. In absorption spectroscopy, such as infrared spectroscopy, the timescale over which absorption or fluorescence occurs is much slower nanoseconds. This allows the interaction seen in Raman spectroscopy to be thought of as a perturbation rather than an absorption reaction (Stone, 2001a). A Raman spectrum, such as that seen for 2-propanone (acetone) in Figure 2.1, is a plot of scattered light intensity as a function of the energy difference between the incident and scattered photons.

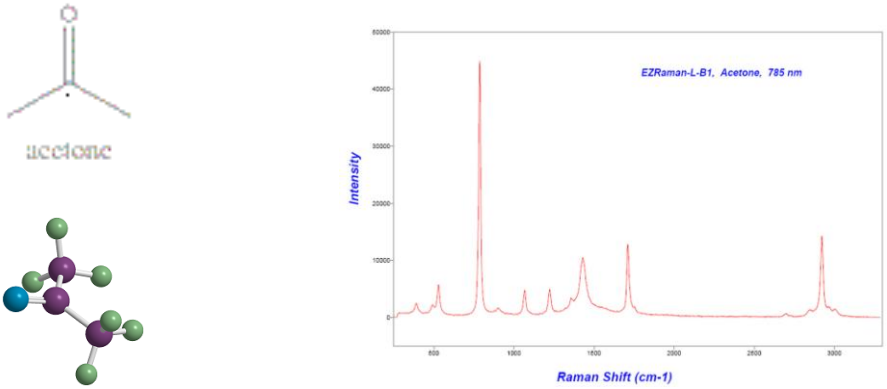

Figure 2.1: Raman spectrum of acetone

The efficiency of scattering increases as the fourth power of the frequency of the incident light used. The energy gained or lost by the photon equals the change in energy of the molecule and is called the Raman shift and is measured in wavenumbers (cm^{-1}). The position of peaks within a Raman spectrum is independent of the wavelength of the excitation photons; the more intense the peak the greater the number of Raman scattering events has occurred for that particular vibrational mode. The more energy required to produce a perturbation reaction within a molecule the larger the Raman shift. This energy is not used to initiate an electronic transition but to alter the conformational shape of the molecular bonds by setting up a vibration, stretch or bending motion that reflects the orientation of the atomic nuclei and arrangement of the chemical bonds within the molecule. This provides a highly specific method by which molecular vibrations can be probed and allows the attainment of a vibrational spectral finger print for each molecule species.

Figure 2.2 shows the Raman spectrum of cyclohexane, the Raman peaks are narrow and correlate well with the vibrations of specific bonds within the molecules.

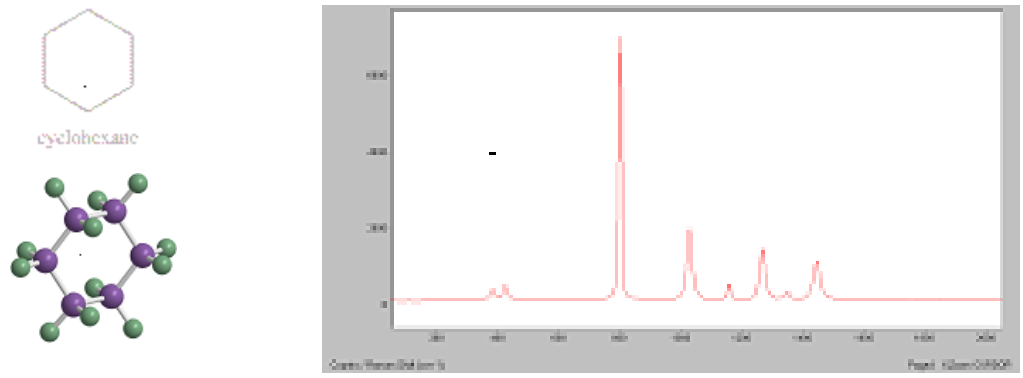

Figure 2.2: Raman spectrum of cyclohexane.

Biological tissues are very complex and often highly heterogeneous; this can result in significant energy absorption and emission in the form of fluorescence. This has always been a problem limiting the scope of Raman spectroscopy in the analysis of biological tissue. Raman spectroscopy for *in vivo* analysis of biological tissue also requires the use of low power density lasers as the excitation light source in order to avoid tissue damage. Most biological molecules are Raman active and can provide their own spectral fingerprint, there is considerable cellular and molecular information contained within these spectra. Recent advances in instrumentation and improvements in data analysis have brought Raman spectroscopy to the forefront of the search to find a tool that can provide a viable, real time optical biopsy of tissue *in vivo* that differentiates between normal tissue and that which shows neoplastic change.

2.1.3 Models Explaining Raman Spectroscopy

The classical theory of Raman scattering is based on the wave theory of light. This approach has also been complemented by quantum theory, which reflects the nature of vibrations as being made up of discreet packets of energy - photons.

Classical model

Monochromatic light such as that of a laser beam is an electromagnetic wave whose field strength fluctuates with time. This fluctuating electric field can interact with that of a molecule and in so doing induces an oscillating dipole moment, made up of multiple harmonic components, within the target molecule. This elevates the molecule to a short lived, unstable 'virtual state' whose energy is determined by the frequency of the incident light. The resultant oscillating dipole emits light in all possible directions at the frequency of each component of this oscillation. The electron cloud of a molecule is relatively light compared to the mass of the nucleus and as a consequence the energy change, hence the frequency change, of the light scattered by these molecular components is small. Whilst interacting with the electric field of the incident light should the molecule being studied undergo some internal motion i.e. of the nucleus such as bending, rotation or vibration then the primary oscillating dipole will have a further oscillation superimposed relating to each of these internal modes. The energy of the scattered light will differ from the incident beam by one vibrational unit (Smith & Dent 2005a). This is Raman scattering and is considered inelastic. There are two forms depending on which vibrational state the molecule is in at the time of interaction. If the molecule is in the lowest vibrational state and as a result of an interaction with the

incident light electric field gains energy and is elevated into a higher vibrational state Stokes scattering occurs. A proportion of molecules will already be in an elevated vibrational state and the interaction of the electric field with these will result in a transfer of energy to the scattered photon and a fall in the molecules vibrational state, this is called anti-Stokes scattering. Whilst the convention in Raman spectroscopy is to record Stokes scattering there are occasions when measuring anti-Stokes scattering can be useful. Where fluorescence occurs it often does so at a frequency lower frequency than that of vibrational excitation. In these circumstances recording anti-Stokes scattering to avoid fluorescence interference may be helpful.

At room temperature there are relatively few molecules in the higher vibrational states and Stokes scattering predominates. Anti-Stokes scattering will be weak and become weaker as the frequency of the vibration increases. One way to increase the amount of anti-Stokes scattering is to increase the temperature. The relationship between the number of molecules in the higher vibrational state and temperature is expressed in the Boltzmann equation.

$$N_v / N_o = \exp (- E_v / kT) \qquad \text{Eq. 2.1}$$

Where;

N_v = the numbers of molecules in the excited vibrational state.
N_o= the numbers of molecules in the ground state.
Ev = the energy in the vibrational state.
K = Boltzmann constant.
T = absolute temperature.

Light of any frequency can induce a Raman effect however the cross section for the inelastic scattering process is proportional to λ_{in}^{-4} where λ_{in} is the wavelength of the incident photon. For example incident light of wavelength 200nm will have a cross section of inelastic scattering 16 times that of light of wavelength 400nm. This important feature allows the energy level of the incident photons to be lower than that required for a molecular transition into a higher electronic state where resonance effects and fluorescence may come into play. The ease with which the dipole moment associated with a molecule can be distorted by an external electric field is called polarisability (α). The intensity of a Raman band is dependent on the degree to which the polarisability of the electron cloud around the molecule is changed by the vibration. Symmetrical vibrations will give the greatest change and so produce the most intense Raman bands. Unlike Raman spectroscopy in infrared absorption spectroscopy it is the change in dipole moment, maximal in asymmetric vibrations, that give the most intense peaks. Not all vibrations of a molecule will be both infrared and Raman active. Figure 2.3 shows the Raman and infrared spectra of phenylaniline. The intensities of the spectral signals vary considerably and these two spectroscopic techniques are considered complementary.

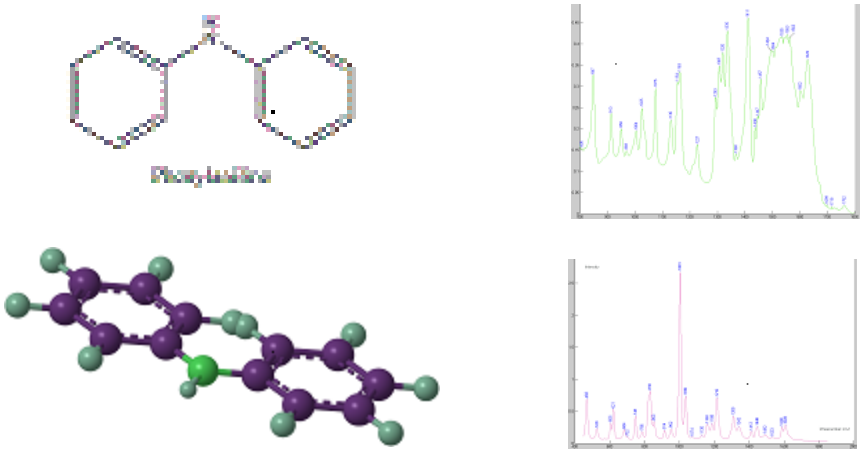

Figure 2.3: IR and Raman spectra obtained from phenylaniline.

Centrosymmetric molecules are those where a reflection of any point through the centre of the molecule produces an identical configuration e.g. C_2 H_6 (Figure 2.4). These molecules abide by a rule of mutual exclusion which states that in centrosymmetric molecules no band can be both Raman and infrared active.

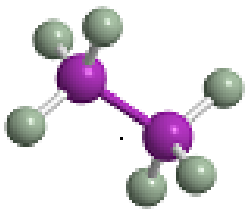

Figure 2.4: A centrosymmetric molecule in 3 dimensions - Ethane (C_2 H_6).

Molecular vibrational model.

As previously discussed the frequency at which a molecular vibration occurs is dependent on the mass of the atoms and their bond strength and this determines the position of the bands within the spectra. The bond between nuclei can be approximated to a spring which obeys Hooke's Law (Eq 2.2). Hooke's Law describes the relationship between a force applied to an unstretched spring and the amount the spring will stretch when that force is exerted. It states that the resultant extension or compression of a spring is directly proportional to the loading force. The negative sign shows that the force exerted by the spring is in a direction opposite to that of the displacement.

$$F=-kX \qquad \text{Eq. 2.2}$$

Where;
F = force (N).
K = spring constant (Nm^{-1})
X = the distance moved by the object from its position of equilibrium

Whilst a molecule remains in one electronic energy level the energy it processes can be expressed in terms of 'degrees of freedom.' Translation in space accounts for three degrees of freedom and a further 3 describe rotational movement for all except linear molecules. Thus the dynamics of a molecule can be expressed in terms of its' nuclei. A molecule with N nuclei will have a total of 3N degrees of freedom. For non -linear molecules subtraction of rotational and translation degrees of freedom will result in 3N - 6 degrees of internal freedom, 3N - 5 degrees for a linear molecule.

The degree, to which polarisation and dipole changes occur and hence changes in the strength of the signals in the Raman or IR spectra, is dependent on the type of vibrational mode. A symmetrical stretching vibration will cause the largest change in polarisability hence the strongest Raman band. In this vibrational mode the dipole moment change will be very small and so the infrared band if seen at all will be very weak. The deformation mode of the molecule will produce the reverse as the change in dipole moment is comparatively large compared with the change in polarisability.

Diatomic Molecules
Symmetrical diatomic molecules e.g. Oxygen (O_2), were N = 2, have 1 degree of internal freedom; linear stretch. This vibration will produce a change in polarisability but not in dipole so the resultant band will be present in the Raman spectrum but not in the infrared spectrum.

Asymmetrical diatomic molecules e.g. nitric oxide (NO) also have one degree of freedom but in this case a simple stretch will result in both a change in polarisability and dipole hence the vibration will result in a single band but this will appear in both the Raman and infrared spectra.

Triatomic Molecules
Linear tri-atomic molecules e.g. carbon dioxide (CO_2) were N = 3 have four modes of vibration (Figure 2.5), non- linear tri-atomic molecules such as water have three (Figure 2.6).

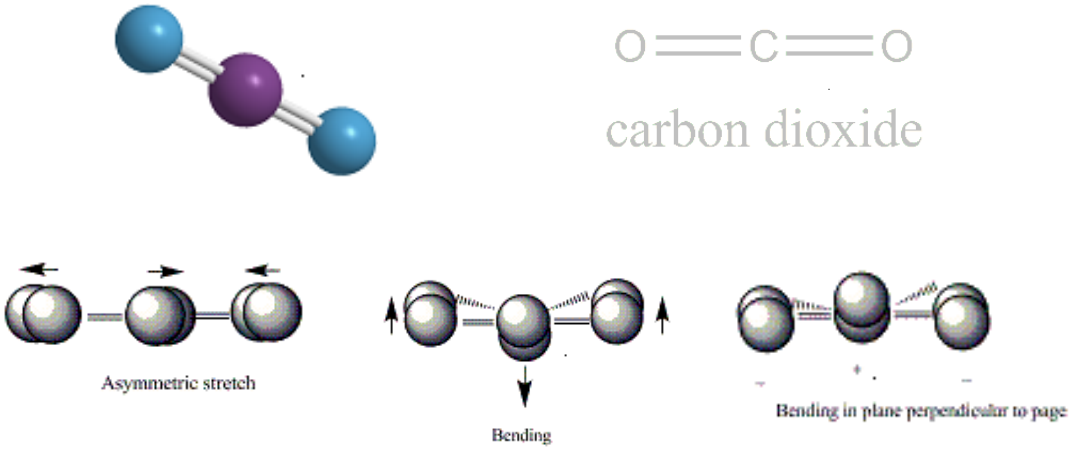

Figure 2.5: Vibrational modes of carbon dioxide (CO_2).

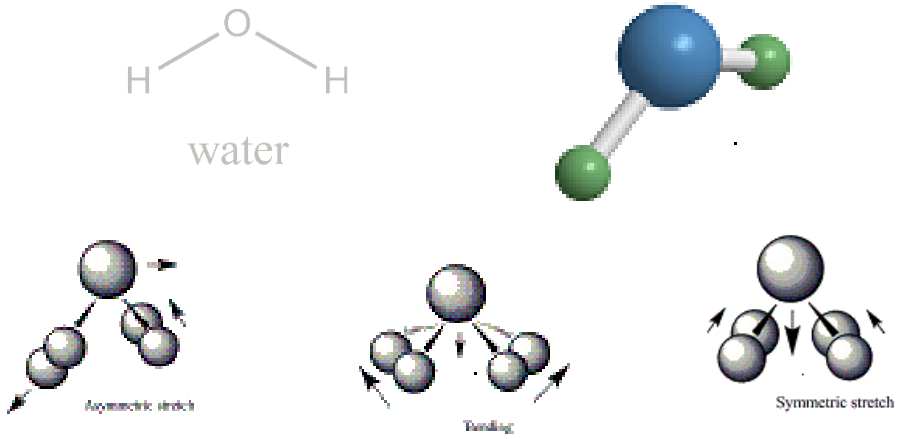

Figure 2.6: Vibrational modes of water (H_2O).

Quantum theory model

To look in more detail at the relationship between molecular properties and Raman scattering for a particular molecular entity quantum mechanics can be used. Whilst detailed analysis of Raman spectroscopy based on these principles is beyond the scope of this work the basic grounding of this theory with respect to Raman spectroscopy is outlined below.

If a photon of energy E = hν collides with a molecule the collision may be either perfectly elastic, and the photon of energy will be detected unchanged (Rayleigh scattering), or the collision may be inelastic (Raman scattering). In quantum mechanics if an inelastic collision occurs energy (ΔE) is exchanged between photon and molecule. The molecule may only loose or gain energy equal to the difference between two allowed energy states (Eq 2.3-2.5). Only transitions involving Δν = +/- 1 are allowed for a harmonic oscillator in quantum mechanics. If the molecule struck gains energy the

photon will be scattered with energy $h\nu - \Delta E$, (Stokes scattering). If the molecule looses energy to the photon of radiation it is scattered with a higher frequency (anti-Stokes scattering). This can only occur if the molecule is in an excited vibrational or rotational state to begin with.

$$E_{out} = E_{in} (+/- E_{vib}) \quad \text{Eq. 2.3}$$

$$h\nu_{out} = h\nu_{in} +/- h\nu_{vib} \quad \text{Eq. 2.4}$$

$$\nu_{out} = \nu_{in} +/- \nu_{vib} \quad \text{Eq. 2.5}$$

When E_{vib} equals zero elastic (Rayleigh) scattering has occurred.

Where;

E_{out} and E_{in} = the values for the energy of the emitted and incident radiation.
E_{vib} = the energy absorbed or emitted in order to alter the vibrational state.
h = Planck's constant.
ν_{out} and ν_{in} = the frequency of the emitted and incident radiation.
ν_{vib} = the frequency of the energy absorbed or emitted in order to alter the vibrational state.

A rigorous application of Quantum mechanics would necessitate that both the incident radiation and target molecule were treated as quantum particles. A good approximation can be made if the incident radiation is considered to be a perturbation of the wave function of the scattered molecule. This is considered valid, as the applied external electromagnetic field is small in comparison to the electromagnetic fields within the molecule. Deeper analysis using Quantum mechanics is beyond the scope of this thesis.

2.2 Raman Spectroscopy as an Optical Diagnostic Technique

The characteristics of the ideal spectroscopic technique used to diagnose disease are discussed, as are the advantages and disadvantages of Raman spectroscopy with particular reference to the detection of malignancy in biological tissues. The component parts of a classical Raman system are described, as are landmark developments in Raman instrumentation.

2.2.1 Characteristics of the Ideal Optical Diagnostic Technique.

The scope of applications for optical diagnostic techniques is vast both as a 'stand alone' procedure and as part of a series of investigations aimed at confirming a diagnosis with maximum speed, sensitivity and specificity. The assessment of disease without the need for an invasive or surgical procedure is the ultimate goal. Where outpatient assessment of the disease is purely subjective, for example in dysplasia of the larynx, improved diagnostic specificity would be of great benefit. At present multiple biopsies are often required to monitor disease progression and repeated excision of vocal cord tissue can significantly damage voice quality. Intra-operative, real time accurate assessment of surgical resection margins would be an invaluable tool for all surgeons. This would reduce the need for secondary procedures which occur when histological review suggests resection margins are too close to tumour. It would improve morbidity and in some cases the mortality associated with these procedures

whilst reducing surgical lists and hence costs. The ideal optical diagnostic technique would allow real time mapping of disease as an outpatient procedure with accurate, highly specific, reproducible results. It should be non- or minimally invasive and not require the use of a general or local anaesthetic. The acquisition of the spectra should be over the shortest time frame possible to reduce the risk of thermal damage to tissue and make the technique attractive to clinicians. Tissue penetration is wavelength dependant and should be optimised in order that extension of disease beyond the mucosal layer may be identified. The ideal system should produce a small signal from water. The proportion of water in biological tissue is high and the signal it gives should not be allowed to obviate the signal from other molecular species. The spectra obtained should be molecular specific with sharp peaks providing excellent quantitative information and no fluorescence unless fluorescence spectroscopy is being utilised and vice versa. The spectra obtained should be consistent enough to allow standardisation over different systems in order to compile a comprehensive and generic spectral library for normal and diseased tissue. Of paramount importance is that the system is safe. It should use the lowest power laser possible, be stable over a wide range of ambient temperatures and high detector sensitivity should not be at the expense of specificity. An inexpensive, portable system that is compatible with current endoscopic and monitor technology would be a great advantage to the speed, scope and cost of introduction into clinical practice.

2.2.2 Why Raman Spectroscopy?

Raman spectroscopy as a diagnostic technique for the detection of malignancy fulfils many of these criteria. Progress in instrumentation has allowed more rapid spectral acquisition times and the future commercial production of the Raman probe is likely to be suitable for use in the outpatient setting. For many epithelial cancers a reasonably comprehensive spectral library now exists and its content is constantly expanding.

2.2.3 Component Parts of a Classical Raman System.

At present most groups use one of two basic systems. The first has a UV, visible or near infrared laser as the excitation source, a dispersive spectrometer containing a monochromator or series of filters and a charge coupled device for detecting scattered light. The alternative uses a near infrared laser combined with a system based on an interferometer with Fourier-transform analysis of the scattered light signal recorded by an indium-gallium-arsenide (InGaAs) detector sensitive to NIR radiation (FTRS).

2.2.4 Developments in Raman Spectroscopy Instrumentation.

The original experiment undertaken by C.V Raman and K.S Krishan (Raman, 1928) used the sun as an illuminating light source, simple blue-violet filters, a prism as a spectrometer, highly purified liquid samples, the naked eye and photographic plates as detectors. Much of the early Raman work was limited by fluorescence and poor instrumentation particularly in the detection of the inherently weak Raman signal. Advances in optical diagnostic instrumentation combined with better understanding of disease processes and how they relate to changes at a molecular level have allowed Raman spectroscopy to move forward towards clinical relevance. Portable instruments small enough to gain access to key anatomical areas are now under development (Boppart, 2005). The Raman probe used in part of this work can fit within the biopsy port of a flexible nasendoscope; these instruments can be passed into the larynx, without any form of anaesthetic. The Raman probe is also small enough to pass through the

lumen of a 21 gauge needle. This size of needle is routinely used in the outpatients department for obtaining fine needle aspiration cytology specimens from enlarged lymph nodes percutaneously. The major steps taken in key areas of instrument development to bring us to this point are summarised below.

2.2.4.1 Excitation Light Source

Visible light Raman spectroscopy using sunlight as an illuminating light source was almost immediately superseded by the use of a mercury lamp combined with filters to produce monochromatic light. The Toronto mercury arc lamp became the mainstay excitation light source until the development of lasers in the 1960s (Maiman, 1960). From that point on, the work to produce an ideal light source has centred on laser technology.

In the 1970s visible light Raman spectroscopy studies on biological tissue were done using continuous-wave noble gas ion lasers (Goheen, 1978). Argon lasers (351.1-514.5nm) were used to produce intense monochromatic light, the scattered light was separated into different frequencies using a monochromator and a series of filters to isolate photons of a particular frequency. A photomultiplier was used to improve the signal to noise ratio and measure the light intensity over the chosen frequency range (Yu, 1975). In laser systems a noble gas is contained within an externally cooled plasma tube to improve the signal to noise ratio. A high current is passed through the tube and the gas ionises moving atoms to an excited state capable of lasing. For emission in the visible range the ends of the plasma tube are closed off by windows made of silica which are orientated at specific angles. Mirrors reflect the emission back and forth within the system providing indirect amplification and a prism can be used to select a specific wavelength. The prism can be removed if several laser transmissions are required for example in dye lasers.

Pulsed lasers such as the neodymium-yttrium-aluminium-garnet laser, Nd:YAG , (1064nm) were developed in the late 1960s and early 1970s. Nd:YAG lasers emit over the blue-green range and gives excellent tissue penetration with minimal absorption by water and little fluorescence (Hirschfield, 1996). The YAG portion of the system carries the Nd ions. Early versions were initiated with flash lamps this was subsequently superseded by arrays of diode lasers (800-900nm). In the 1970 to 80s development of tuneable dye lasers such as the Ti-sapphire laser allowed laser line emission over a wide range of frequencies. Driven by commercial applications diode lasers have now come to the fore. Characteristics such as modest cost, small size and high efficiency to power and cooling ratio has enabled them to be used extensively in information technology systems. Diode lasers produce emissions at the junctions of semiconductors. Their main limitation is one of beam instability with a tendency for the wavelength of light they produce to drift over time. In diode lasers the cavity is the actual silicon chip itself and the edges of the chip act in a similar way to the mirrors seen in early systems. As the silicon chip heats it undergoes a changes in size which is then reflected in a drift in the wavelength of the laser light emitted.

Many characteristics of lasers make them ideally suited for use in spectroscopy. They can produce excellent power profiles; continuous wave lasers have a range of 1 to 2 watts, pulsed lasers 10 to 100 megawatts and a wide range of wavelengths are available

particularly if dye lasers are used. The light produced has superb monochromisity and any small amounts of light of different frequencies can be removed easily. The illuminating light beam produced by lasers can be focused to a small spot size and this characteristic in combination with microscopy allows volumes as small as $2\mu m^3$ to be studied (Ferrano, 2003b).

Choice of frequency for excitation source.

Raman scattering is weak and the intensity of the scattered light produced is related to three factors; laser power, the fourth power of the frequency of the excitation light and the polarisability of the molecular species studied (Smith & Dent, 2005b). The choice of which region of the electromagnetic spectrum to use to probe a molecular vibration, near infrared (NIR), visible (Vis) or ultraviolet (UV) light, is not straight forward each has advantages and disadvantages; the ultimate choice is invariably a compromise.

At first glance to optimise the intensity of the Raman signal produced lasers emitting in the UV range would seem the best choice as light from this region of the electromagnetic spectrum has a higher frequency than that from the NIR region. However NIR excitation sources produce less fluorescence than UV excitation when used to investigate biological tissues. Another significant disadvantage of using UV-radiation is that many biological molecules absorb UV light more strongly than visible light altering the appearance of their Raman spectra. Energy absorption can also cause photo and thermal degradation of the sample being studied, because of this and the potentially mutagenic effect on biological tissue, lasers emitting in this region are less applicable to *in vivo* applications (Wang, 2001; Runger, 2008). Ultraviolet radiation has very short penetration depth (Coohill, 1987) and systems require high specification optics and tend to be relatively expensive. Development of UV laser technology, driven by commercial applications, continues to make this form of Raman spectroscopy attractive however *in vivo* applications at present look very limited.

Visible light lasers are widely available, they are small and inexpensive. Their main disadvantages over lasers using NIR and UV excitation is the degree of fluorescence they stimulate. Fluorescence can also occur below the molecular excitation energy of the main molecule being studied if other species are present which process energy transitions near the value of electronic absorption, producing near Raman resonance and masking Stokes Raman scattering. The energy of the photons emitted from visible light lasers can cause thermal and photo degradation effectively reducing the power profile available to the spectroscopist. Even at lower power values the fluorescence stimulated from the sample and contaminants can completely mask the Raman spectrum

Near-infrared (785-860nm) lasers are now used extensively in Raman spectroscopy; they optimise signal to noise ratio and have fast integration times as a result of reduced tissue fluorescence and high sensitivity. FTRS uses NIR lasers for example the Nd^{3+}:YAG laser. This laser excites at a frequency of 1064nm which is a great advantage as there are very few molecules which process excited states low enough in energy to fluoresce at this wavelength. As the fourth power of the frequency of the excitation radiation determines the intensity of Raman scattered light, NIR radiation produces relatively weak Raman scattering compared to that seen with visible and UV light. Higher laser powers are achievable compared to those obtained from visible light lasers because

excitation energy is lower in photons from the NIR region and these photons are minimally absorbed by most biological molecules. One disadvantage for NIR lasers (785-860nm) is that they operate right at the limit of CCD efficiency; other detectors such as InGaAs detectors are sensitive to photons from this region however they are more expensive.

2.2.4.2 Collection and Amplification of Raman Scattered Light

To optimise the signal detected from Raman scattered light it is imperative to remove the more prominent Rayleigh scattered light and all other forms of extraneous light such as that from specular reflection.

Prisms and grating monochromators

Prisms were first used for this purpose but were superseded by single and then multiple monochromators. When a single grating monochromator is used the frequency shifted Raman scattered light is seen to separate out however some stray light still persists, mainly undiffracted light scattered from the surface of the grating. A second and even a third monochromator will act to further isolate the Raman scattered light. These systems produce excellent separation of peaks close to the laser-line, an advantage over some filter systems. Systems using monochromators rather than notch filters can be tuned to a range of excitation frequencies. Disadvantages include the need to keep monochromators at a constant temperature to avoid variation in band width position. Grating characteristics such as size and density of surface grooves affect spectral resolution as do slit width and the speed of scanning. Triple monochromators are generally no longer used, they do produce very high spectral resolution, but only permit small amounts of light to be transmitted and hence require much higher acquisition times than the single monochromator systems. For Raman systems which use monochromators and single detectors, the scattered radiation is focused onto a photomultipler tube for amplification of the Raman signal.

2.2.4.3 Wavelength Selection

Optical filters are used to remove specific frequencies of light for example the laser-line; light of frequency equal to that of the excitation source. They are imperative in order to eliminate any stray light which might otherwise saturate the detecting system.

Holographic notch filters

Holographic notch filters are interference filters made by a holographic process. They are a very effective tool used to filter out elastic scattered radiation. Characteristically they have a narrow spectral bandwidth and high optical density however they contain gelatin and the optical properties of this can decay over time. This allows variation in the frequency of light passing through the filter and hence variation in the spectra obtained. Holographic notch filters have the advantage over edge filters in allowing Stokes and anti-Stokes spectra to be measured. If a change in the excitation frequency is required a disadvantage of holographic notch filter systems is that the filter must be removed and replaced with one that will remove the new laser- line. Holographic notch filters do not allow the measurement of Raman scattering as close to the laser-line as multiple monochromator systems but they are small, efficient and very effective when used to collect and focus scattered light onto a monochromator

Edge filters

Edge filters are metal oxide filters and are generally more robust than holographic notch filters. The pattern of signal noise seen in these systems can be altered by changing the angle of the filter however they are limited by the fact that they can only measure anti-Stokes spectra.

Band-pass filters

Band-pass filters allow only the signal recorded over a specific band of frequencies.

2.2.4.4 Detectors

Photographic plates were used in the early Raman work however these were cumbersome and required long exposure times to record the weak Raman signal. For efficient detection both amplification systems and specialised detectors were developed.

Photomultiplier tubes

Spectrometers which utilise monochromators use photomultiplier tubes (PM) to amplify the Raman signal. PM tubes convert photons into an electrical signal. Each individual photon hitting the photocathode of a PM tube releases one or more electrons which in turn are attracted to a second dynode where each stimulates the release of more electrons. Successive dynodes are progressively less negatively charged and the resulting cascade effectively amplifies the signal. PM tubes require thermoelectric cooling to reduce 'dark current'. Dark current is that produced by emission from components of the system themselves. A further drawback is the need for the tubes to be dismantled and serviced regularly in order to dry out condensation in the lens system. There are two methods by which the amplified Raman signal can be quantified. In early systems the electron stream was averaged over time and the direct current amplified and measured. The second method, photon counting, is considered more sensitive and produces a better signal to noise ratio however the speed at which individual photons producing electron pulses can be counted is the rate determining step. Photomultipler tubes are single channelled and very sensitive however detecting Raman signals for each individual frequency in the range being studied was time consuming so multichannel photon detectors, called photoarrays, were developed to address this problem.

Photoarrays

Multichannel photon detectors are made up of a collection of small devices which are photosensitive. They can change an optical signal into a charge pattern which can then be read as a Raman spectrum. They have the advantage over single channel systems as they can detect the Raman signal over the entire frequency range simultaneously and as a consequence have much shorter acquisition times. This is of particular benefit in the study of unstable compounds

Charge coupled devices (CCDs)

Driven by advances in information technology and camera imaging CCDs have been a huge step in the development of more widely accessible and efficient detector systems. A CCD is a semiconductor based on silicon containing an array of pixels. When struck by photons each one of the photosensitive elements produces an electric charge proportional to the number of photons striking it and a charge transfer process allows

the pixels to be read. Time-resolved spectra are obtained by shifting a horizontal section of the CCD vertically as a function of time. There are no gratings and the component parts do not have to move allowing CCDs to be small and robust. They generate very little noise and have a superb signal to noise ratio. CCDs are very sensitive to light in the range of frequency used in Raman spectroscopy. They detect efficiently in the wavelength range 120-1000nm hence a CCD coupled with dye or diode lasers can be used to measure Raman signals from highly fluorescent compounds. Over 1000nm their sensitivity drops however other detectors which cover this region are available such as Indium-Gallium-Arsenic (InGaAs) detectors.

Indium-Gallium-Arsenic (InGaAs) detectors

InGaAs detectors are thermally stable and can be used at room temperature, they have a lower signal to noise ratio than CCDs however some improvement is seen when the system is cooled. These detectors are used in FTRS where the excitation light used is in the IR region but are limited in detecting spectra above 3000 cm^{-1}. They produce minimal dark current and fluorescence and can record from a wide variety of samples in different states.

2.2.5 Refinements

Fourier-transform Raman spectroscopy (FTRS)

Conventional Raman spectroscopy also known as dispersive Raman spectroscopy measures scattered light intensity against frequency or wavenumber whereas FTRS, also known as time-domain spectroscopy, measures light intensity against wavenumber over all frequencies simultaneously. Computer processing by Fourier transform converts the data obtained into a conventional spectrum. The development of Michelson interferometers (Michelson, 1920) allowed visible light Raman spectroscopy to be superseded by FTRS as a technique to probe biological tissue (Chantry & Gebbie, 1964). Both visible light and NIR-FT systems are used however commonly FTRS systems use a continuous-wave Nd^{3}:YAG solid state laser (1064nm). The power range is 1 to 10 watts with most systems operating at the lower end. Using NIR light significantly lowers the intensity of the Raman signal compared to that which would be obtained using lasers emitting visible light so the use of filtering optics to remove stray light is imperative. Holographic notch filters have been used extensively. Systems often incorporate a reference Helium-Neon (He-Ne) laser however the detectors used are sensitive to radiation of this frequency and so it must also be filtered out. FTRS has good acquisition times and signal to noise ratios. Large surface areas can be studied without loss of spectral resolution; however a disadvantage is that the spectral noise signal is split between all spectral components

Micro-Raman spectroscopy

Delhaye developed the first micro-Raman spectrometers 1974 (Delhaye, 1974). A year later Rosasco developed the first Raman microprobe (Rosasco, 1975). The spatial resolution of Raman scattered light was greatly improved by the development of micro-spectroscopy systems. General advances in the technical specifications of the component parts, particularly detectors and distal end optics continue to improve this technique. Micro-Raman spectroscopy is based on the characteristic that light from lasers emitting in the visible region can pass through samples and then can be focused by a lens. Optical channels for excitation and reflected light are separated and

extraneous light such as specular reflectance is minimised with careful alignment of the excitation beam and sample. Maximum signal is detected by using the largest collection angle possible and a large collector aperture. Light can be focused to a very small spot size increasing the power density over the area studied and this allows a relatively low powered laser to be used. Spatial resolution is also dependant on the spot size. This technique gives excellent imaging of tissue epithelial surfaces, but is limited in the submucosa, deeper tissue and in the assessment of heterogeneous samples. This latter point is a great disadvantage to the development of this technique as a useful clinical tool.

Confocal microspectroscopy

In confocal microspectroscopy scattered light is collected from the area of the sample in focus only, off-axis light is removed. In confocal microscopes the X-Y mapping plane is extended to the z direction allowing focusing at different depths. A confocal microscope contains what is effectively a pin hole in the focal plane of the microscope. In some cases two separated slits at right angles are used, one in the microscope the other in the spectrometer. These block all light except that which is in the focal plane. The development of this refinement to Raman systems has allowed depth profiling and Raman signals to be obtained from well defined, small volumes. (Rosasco, 1980; Delhaye, 1990; Baldwin, 2001).

Mapping and imaging Systems

Much of the Raman spectroscopy work to date has utilised data from single point analysis; this remains a very valuable tool however motorised stage systems are now widely used to map larger areas. Two dimensional mapping involves mounting a sample on a mobile X-Y stage. The sample is moved in the X-Y plane by incremental amounts and after each movement a point measurement is taken. Mapping can also use an XYZ stage to obtain three dimensional images. Comprehensive mapping is a time consuming process and it is this problem which has been one of the major drawbacks encountered with this technique however it is excellent at identifying substances accurately and for showing the distribution of other components within the specimen. Recent developments may greatly reduce the time required for mapping. Systems such as the Renishaw Streamline system look very promising. In this system spectral measurements are taken whilst the stage is moving. It is a much quicker technique however it is limited by the small amount of scattered light captured compared to that seen with conventional mapping (Hutchings, 2008)). Each frequency of scattered light is focused at a specific point along a line on a CCD; alternatively a series of filters allows only one frequency of light through that corresponds to a particular vibrational excitation in the molecules being studied. In both these cases the detector can act like a camera and a Raman image of the specimen is obtained.

Probe and portable Systems

In 1988 technological advances were made in the development of fibreoptic probes to be used for *in situ* Raman spectral measurements (Hendra, 1988). The development of fibreoptic technology has allowed samples to be analysed remotely from spectrometers (Lieber, 2004). CCDs, developed in the video and digital camera commercial world, have helped to make systems more portable, as have miniature gratings based on fibreoptic interfaces and solid-state semiconductor lasers. The design of Raman *in vivo* probe systems is an active area of research (Utzinger & Richards-Kortum, 2003). Many

prototype probes are based on a ring of collecting optical fibers surrounding an illuminating fibre. Problems associated with these systems include the low intensity of Raman signal and the high signal to noise ratio from both the Raman system and the endoscope optics (Mahadevan-Jensen, 1998a). Systems such as the Visonex probe have beveled fibres to maximise the capture of scattered light and other recent advances include band-pass filters which allow only laser light through and remove the Raman silicon signal which emanates from the illuminating fibre optics.

2.2.6 Limitations and Hazards Associated with Raman Spectroscopy

Very slight biochemical changes must be detected in order that successful early diagnosis of disease can be made through analysis of Raman spectra. This, in conjunction with an inherently weak Raman signal, is the crux of the technical challenge faced in the development of medical diagnostic Raman spectroscopy. To optimise a Raman spectroscopy system a balance must be struck between the need for high laser power, a sensitive detector and the practicalities of whether these components are readily and inexpensively available. Much of the research in Raman spectroscopy has addressed these technical aspects. Raman spectroscopy has a great many useful properties. It can be used to probe molecular vibrational motion at much lower frequencies than IR spectroscopy i.e. less than 400cm^{-1} and has a spatial resolution of 1μm x 1μm compared to that of IR which is in the order of 20μm x 20μm, although FTIR in mapping mode can produce higher resolution than this. Raman spectral bands are usually narrower than those obtained from IR excitation allowing better peak resolution and more accurate assignment to specific molecular vibrational entities. The water content within biological tissue is high resulting in stronger IR absorption compared to that seen when Raman spectroscopy is used. This gives Raman spectroscopy an advantage over IR in the assessment of some biological tissues. There are however some major drawbacks in the *in vivo* use of Raman spectroscopy for the study of these types of tissue. Biological tissue is often heterogeneous and absorbs light from the whole UV-Visible range producing a strong fluorescence emission which can swamp the much weaker Raman signal; this is largely overcome by the use of NIR excitation. The choice of excitation source has been discussed in detail and whist UV light has many advantages and it has been used *in vitro* studies extensively it can be mutagenic (Pfeifer, 2005). It is considered unsafe for *in vivo* applications and consideration of energy transfer to tissue producing both thermal and photo degradation must be considered.

There are national and international guidelines for the acceptable levels of exposure of biological tissue to laser light. This data give the maximum permissible exposure (MPE) for skin but to date there are no values for the larynx or lymph nodes. The British guidelines (BS EN 60825, 2007) give the MPE for different wavelengths of light. For light of 790nm the limit of exposure is 95μW for a spot diameter of 200μm, for 830 nm the MPE is equivalent to 114 μW. If these MPEs were adhered to it would not be possible to obtain adequate Raman spectra however work on tissue *in vitro* suggests much higher levels of exposure can be used without thermal damage being caused (Puppels, 2001). Shim has not only published work on the effects on Raman spectra from different handling of *ex vivo* mammalian tissue (Shim, 1996) but has also more recently investigated the thermal effects of laser light (Shim, 2000). Using an 830nm laser, giving 250mW of power focused into a spot size of 500μm for 60 seconds no

thermal damage was detected. In the use of Raman spectroscopy there continue to be problems with optimisation of signal to noise ratio and reduction of dark current, although detector cooling has resulted in an improvement in this area. Progress has been made in compilation of molecular spectral databases which do not contain spectra contaminated with instrument signals or signatures but a truly standardised database is some way off. Despite great advances much work is still required for the development of a truly portable and clinically relevant system that can be used *in vivo* and which is affordable.

2.3 Current Applications for Raman Spectroscopy

An outline of the development of Raman spectroscopy as a biomedical diagnostic tool is given in this section. A more detailed overview for applications relating to specific anatomical areas is also listed and the section concludes with a synopsis of selected non-clinical uses. Multiple reviews of the biomedical applications of Raman spectroscopy have been undertaken in the past (Mahadevan-Jansen, 1996; Fulljames, 1999; Hanlon, 2000, Wilson, 2007) so the aim of this chapter is to highlight the development and scope of this technique.

2.3.1 General.

In 1970 the first Raman spectra of proteins were obtained from cellular lysozymes using a He: Ne laser (Lord, 1970). A study done in 1974 (Larsson & Hellgren, 1974) was the first to highlight the possible value of Raman spectroscopy in the detection of disease. Raman and fluorescence spectroscopy were performed on the plasma component of blood from patients with a variety of diseases. The plasma from healthy patients showed Raman peaks attributed to the presence of carotenoids and aromatic amino acid side chains; these were not visible in the spectra obtained from the plasma of patients with disease. These spectra also showed a greatly increased fluorescence signal. Spectroscopy was shown to be able to distinguish between health and diseased plasma better than the standard measurement of erythrocyte sedimentation rate (ESR) but was not able to separate out the different disease entities. Instrumentation development in the 1970s (Delhaye, 1975) combined a dispersion Raman spectrometer with a microscope. This system allows Raman spectroscopy to be used for studies at a cellular level. From the mid 1970s to late 1980s much work was done on the analysis of individual proteins e.g. within the eye lens (Yu, 1974) and to study the RNA and DNA content of viruses (Hartman, 1973). Early work also included the study of foreign inclusion bodies, material that can become embedded within biological tissues and which the body has no way of removing e.g. asbestos and silicon particles. The first study analysed silicon inclusion bodies *in vitro* within lymph nodes (Abraham, 1979). Inclusion bodies generally give strong, distinctive spectral signals and work continued on refining Raman spectroscopy in order that it might be used to detect the small changes found in the biochemical profile of tissue that accompanies the pathological disease process. The advantage of visible light Raman spectroscopy used in studies undertaken at a cellular level is that it produces less fluorescence than that seen in studies of complete tissues. Even so technical advances such as the development of Confocal Raman microscopy have allowed more detailed work on cellular proteins to be undertaken (Puppels, 1990). Throughout the 1990s studies done using cultured cell lines yielded information on cellular structure (Sureau, 1990) and on protein conformation and concentration (Yazdi, 1999). As Raman spectroscopy evolved and was used to

study more complex tissue so fluorescence was increasingly a limiting factor. In the early 1990s skin studies using NIR and visible Raman spectroscopy showed good correlation between peak assignments obtained from *in vitro* and *in vivo* experiments (Williams, 1993 & 1994). In 1993 Alfano et al applied for a patent to cover the use of Raman spectroscopy in cancer diagnostics. Through the analysis of cellular constituents and metabolites a great deal has been learnt and extensive spectral library data bases now exist. Early work on individual cells was of fundamental importance in establishing the use of Raman spectroscopy as a tool for the detection of malignancy by showing that changes such as cytoplasm to nuclear ratio could be demonstrated in the presence of malignancy. Beyond oncology Raman spectroscopy has also been used as a tool for microbiological analysis and has been used successfully to classify strains of bacteria (Maquelin, 2000) and quantify the presence of viruses in cells (Wu, 2000).

2.3.2 Clinical

Larynx/pharynx

Much progress has been made in the use of Raman spectroscopy in the study of epithelial cell changes in different anatomical sites (Stone, 2002). Yang et al used a series of spectroscopic investigations, including FT-IR and Raman spectroscopy, to study molecular changes that occur in the presence of squamous cell carcinoma within head and neck tissues (Yang, 1998). In 2000 preliminary studies showed that Raman spectroscopy could be used to discriminate between normal, dysplastic and malignant changes in squamous epithelial cells of the larynx (Stone, 2000; Kendall, 2000). An excitation wavelength of 830nm was used and 5 -12 spectra obtained from each sample, multivariate statistical methods – principal component and linear discriminant analysis were performed on the data to maximise spectral differences. These were most pronounced in the 850- 950 cm^{-1} and 1200-1350 cm^{-1} range. Peaks were identified that corresponded to conformational changes in proteins and stretches in the C-H bonds found in nucleic acid bases. As disease progressed towards malignancy the relative intensity of the peaks relating to nucleic acids increased. Cross validation of the discriminant model gave excellent specificities, 94%, 91% and 90% and good sensitivities 83%, 76% and 92% for normal, dysplastic and squamous cell carcinoma. This study was limited by a small sample number and part of the work contained in this thesis expands on these results. Stone et al extended their work to other anatomical sites; tonsil, oesophagus, stomach, bladder and prostate and using Raman spectroscopy classified normal and diseased epithelial tissue with similar sensitivities and specificities as that obtained from laryngeal tissue (Stone, 2002). A study published in 2005 used slightly larger sample numbers than seen in the preceding studies and looked at the ability of Raman spectroscopy to discriminate between normal, malignant and laryngeal tissue infected with the human papilloma virus (Lau, 2005). Sensitivities of 89%, 69% and 88% and specificities of 86%, 94%, and 94% were obtained for normal, laryngeal carcinoma and papilloma infected tissue respectively.

Lymph nodes

Raman studies of lymph nodes have been limited and most have been in association with the investigation of breast disease. Studies to date have shown the ability of Raman spectroscopy to interrogate lymph nodes for the presence of silicone in patients who have undergone breast augmentation with silicon implants (Feng, 2004; Katzin, 2005). More recently *in vivo* mice experiments have been undertaken to assess if Raman

spectroscopy can discriminate between normal and breast cancer metastatic disease in regional lymph nodes (Kast, 2008).

Breast

FT-Raman was first used to study breast cancer in 1991 (Lui, 1991) and has now been successfully used *in vitro* to detect the presence of lymph node metastases from breast cancer (Smith, 2003 & 2005). More recently *in vivo* experiments have been undertaken on mice using Raman spectroscopy to differentiate between normal breast tissue and that infiltrated with tumour (Thakur, 2007; Kast, 2008). Kast et al extended their study to also investigate metastatic disease in regional lymph nodes groups. Spectral classification of normal, tumour and inflammatory tissue correlated well with that obtained from histology.

Lung

Several review articles (Kraft, 2006; Zeng, 2004) have summarised the evidence in support of the application of spectroscopic techniques, such as Raman spectroscopy, in the diagnosis of lung malignancies. Raman spectroscopy has also been used for the study of the mechanism by which lung surfactants work (Vincent, 1991; Levin, 1993) and in the diagnosis of non-malignant pulmonary diseases such as alveolar proteinosis lung disease (De Silva 1999). Raman spectroscopy has been used to identify inhalation toxins such as ricin and sulphur mustard gas and it has been successfully used to assess pulmonary cell viability post exposure to these gases (Notingher, 2004). In the assessment of cells and subcellular components Raman spectroscopy has been used to identify the morphological changes associated with apoptosis in lung fibroblasts (Krafft, 2006). Novel uses of Raman spectroscopy include the identification of foreign material in lung parenchyma biopsies (Bayder, 2005). In this study bisphenol-A-polycarbonate was identified in a granulomatous pulmonary lesion. This material is thought to have originated from an indwelling medical catheter which had degraded. More recently Raman spectroscopy has been used to assess the toxicity of inhaled nanoparticles (Baker, 2008) and the efficacy of drug delivery systems and pulmonary inhalation aerosols (Mansour, 2007).

Thyroid

Raman spectroscopy systems were initially used in the development of thyroid stimulating hormone immunoassays (Rohr, 1989), more recently they have been used in the assessment of thyroid stimulating hormone in rats (Medina-Gutierrez, 2005). In the study of thyroid disease Schultz et al used a combination of infrared and Raman spectroscopy, including *in vitro* fibre optic probe studies, to examine the cellular components of the thyroid gland and thyroid specific molecules such as thyroglobulins (Schultz, 2000). The first study to show the ability of Raman spectroscopy to differentiate between benign and malignant pathology in the thyroid was published in 2000 (Manfait, 2000) and a more recent summary of the changes associated with malignancy in several tissues including the thyroid has also been published (Lui, 2005). Significant differences between normal thyroid tissue and thyroid follicular carcinoma samples were identified in particular Raman spectral bands at 1585 and 1634 cm^{-1} were found to be absent in samples containing carcinoma.

Vascular

An enormous amount of work has been undertaken using Raman spectroscopy to study vascular lesions and several comprehensive reviews have been published (Yu, 1996; Naghavi, 2001; Landini, 2003). Salenius et al have used Raman spectroscopy to analyse the structure of the human arterial wall for lipid and calcium salt content (Salenius, 1998). Whilst Buschman et al have demonstrated the use of Raman spectroscopy *in vivo* on the arterial wall in sheep (Buschman 2000). The use of Raman spectroscopy in the characterisation of vascular plaques, in particular determining those features which flag a lesion as unstable has been extensive (de Romer, 1998; Korte, 2000; Ozer, 2005)

Gynaecological (cervical)

Most of the work using Raman spectroscopy in gynaecology has concentrated on the spectral characteristics of cervical neoplasias and the changes that occur in the progression from carcinoma in situ to invasive disease (Mahadevan-Jansen, 1998; Utzinger, 2001; Krishna, 2006), some *in vivo* studies have also been completed (Chang, 2002; Robichaux, 2002). Correlation with the biochemical changes which occur during cervical disease progression have now been made (Lyng, 2007). More recently Raman spectroscopy has been used to show the presence of cells expressing the human papilloma virus (HPV) 16 E7 gene. The cellular effects of infection with this virus identified at a biochemical level, even in fixed tissue samples, suggests it may be a useful and compatible adjunct to current screening programmes (Jess, 2007). Transvaginal sonography is a common way of screening for ovarian cancer however although this technique is good for detecting an abnormal mass it discriminates poorly between benign and malignant disease. A definitive diagnosis requires open biopsy however studies assessing the efficacy of Raman spectroscopy for the diagnosis of ovarian cancer have been promising (Leiber, 2000).

Brain

Raman spectroscopy is taking an increasingly valuable rôle in the investigation of the mechanisms by which neurological diseases occur and it has also been used in the assessment of many neuro-oncological conditions. Mizuno et al suggested that near-infrared FT-Raman spectroscopy might be able to differentiate between rat brain grey and white matter (Mizuno, 1992) and later spectral analysis of human brain tissue showed that solvents applied to brain tissue removed nucleic acid and lipid components inducing conformational changes in proteins which could be followed using Raman spectroscopy (Sajid, 1997). Raman spectroscopy has been used to differentiate glioblastoma from necrotic tissue and mooted as a possible means of defining resection margins during stereotactic surgery (Koljenovic, 2002). It has also been used for the characterisation of brain tissue lipids in the hope that detection of their presence and variations in concentration profile might also be used as a diagnostic tool in neurological diseases (Krafft, 2005a, 2005b & 2006). Tumour maps have also been complied for glioma, meningeoma and schwannoma tissue (Krafft, 2006). A review of neuro-oncological applications of optical spectroscopy was published by Toms et al in 2006 (Toms, 2006).

The mechanism by which Alzheimer's disease occurs is still poorly understood however Raman spectroscopy is beginning to play an important rôle in Alzheimer research. It has been used in the confirmation of the importance of adequate Cu (II) levels which

competitively inhibit Zn (II) and reduce the aggregation of amyloid β-peptide, a key step in the development of the disease (Suzuki, 2001). More recent studies have looked at the ability of Raman spectroscopy to differentiate between Alzheimer's disease, normal brain tissue and other neurological diseases such as Huntington's chorea (Sudworth, 2005), this work has been further refined by utilising more sophisticated Raman systems (Archer, 2007).

Advances in Raman technology have allowed a fibre-optic Raman probe to be used to characterise and differentiate between different anatomical areas within pig brain tissue (Koljenovic, 2007). In a fascinating study a Raman spectroscopy-based biosensor was combined with an image-guided surgery system. The Raman probe was connected to a passively articulated mechanical arm which was able to correctly classify a number of objects within a 'phantom skull' (Reisner, 2007). This represents a further step towards a system which combines intraoperative diagnosis and the delineation of surgical resection margins by Raman spectroscopy combined with stereotactic surgery using image guidance systems.

Raman spectroscopy has also been used to study the effects of radiation on rat neural tissue. Such exposure can produce changes some distance from the actual site of injury and the authors have used this evidence to support the hypothesis that radiation exposure produces systemically released protective factors (Lakshmi, 2002). This may be of importance to the use of Raman spectroscopy in the study of recurrent neoplastic disease in the head and neck where one of the primary treatment modalities is radiotherapy.

The assessment of the severity of brain trauma and monitoring the progress of brain injured patients can be very difficult. A rat model has been developed were brain tissue ischaemia is used as a damage model and surface-enhanced Raman spectroscopy used to analyse the rat neural tissue *ex vivo*. This work has shown a correlation between Raman spectra features and areas of ischaemia (O'Neal, 2000) and may be useful in the detection of highly vascularised tumours some of which occur in the head and neck. Cerebral oedema can be a life threatening complication of head trauma and is also of concern in patients with intracranial neoplasms. Raman spectroscopy has been mooted as a possible technique for measuring water concentration in brain tissues directly (Wolthius, 2001). After head injury damaged neurons release excitatory amino acids and these are thought to be associated with a risk of acquiring a secondary injury. Surface-enhanced Raman spectroscopy has been used in rats to investigate the possibility of rapid quantification of these compounds as a measure of the risk of further deterioration and assessment of the need for pharmacological intervention (O'Neal, 2003). Over the last ten years there has been an increase in the recorded incidence of prion disease and the neurodegenerative disorders it produces which in turn has stimulated an enormous amount of research. Surgical instrument cleaning has been greatly influenced by this and there is now a general move towards disposable instruments particularly in operations such as neurosurgery and tonsillectomy were it is necessary to resect tissue which processes an increased risk of containing prions. Raman spectroscopy has been used to investigate the affinity and binding properties of the precursor forms of the infectious isoform of prion particles for Cu (II) ions and how this binding alters with pH. It has been suggested that the presence of specific Cu(II)

bridged forms of the protein may be important in the aggregation of prion protein in its' pathogenic form and that the formation of these Cu(II) bridges can be influenced by the pH of the micro-environment of the neural tissue (Miura, 1999 & 2005).

Skin

The use of Raman spectroscopy for the *in vivo* study of skin (Williams, 1992 & 1993; Caspers, 2001) and skin lesions occurred early in the modern development of Raman spectroscopic techniques (Sterenborg, 1993). Raman spectroscopy has been used to show that the essential building blocks of skin from the 5200 year old 'Similaun man' have remained essentially unchanged through time (Williams, 1995). The non-destructive nature of this technique and the ease of access to skin has facilitated great progress in the assessment of protein structure, lipids and water content (Gniadecka, 1998) and this has led to a clearer understanding of skin diseases, such as psoriasis (Bernard, 2007), vitiligo (Schallreuter, 2008) and basal cell carcinoma (Nijssen, 2007). In 1998 the mode of action of salicylic acid with verrucae was studied using Raman spectroscopy (Lawson, 1998) and in the following year the first work towards clarifying the mechanism by which simple compounds are absorbed transcutaneously was published (Williams, 1999). A comprehensive review of methods available for the assessment of transcutaneous drug availability including Raman spectroscopy was published in 2008 (Herkenne, 2008). There has been a great commercial drive to find topical products that reduce the signs of aging and this has facilitated advances in the use of Raman spectroscopy in this field. Of particular interest has been changes seen in lycopenes and carotene derived compounds by external factors such as diet (Darvin, 2007), ultra violet light (Hata, 2000; Darvin, 2006) and the effectiveness of absorption of topical moisturisers (Seig, 2006) and sun screens (Lademann, 1999).

Bladder

Work published by Stone et al summarised Raman studies outlining diagnostic algorithms for the classification of epithelial cancers and precancers in different anatomical areas including the bladder (Stone, 2002). The five group bladder model developed gave sensitivities of 78-98% and specificities of 96-99%. In the same year it was shown that Raman spectroscopy could be used to identify *in vitro* the different layers of the bladder wall in guinea pigs and that the spectra obtained from urothelium showed a particularly strong lipid signal (De Jong, 2002). *In vitro* studies of the Raman spectral characteristics of human bladder urothelium have shown that normal, inflammatory and malignant tissues can be differentiated. Within the malignant subset containing transitional cell carcinomas it has also been shown that it is possible for the grade and degree of invasion of to be correctly assigned paving the way for *in vivo* cystoscopic studies (Crow, 2004). Studies have now been published which outline the possible applications of Raman spectroscopy in the diagnosis of interstitial cystitis (Hsieh, 2007) and in the determination of the biochemical basis for disease in the prostate (Stone, 2007).

Mineralised Tissue (Bone & Teeth)

Raman spectroscopy has been used extensively to analyses bone and its' biocompatibility with prosthetic devices, particularly those used in dentistry and orthopaedics (Carden, 2000; Dippel, 1998; Bertoluzza, 1992). There have been some novel uses for this technique in the study of mineralised tissue including the study of the human remains of a seventh century cist burial in Anglesey (Edwards, 2007). In what

the paper describes as ‘a complex and dynamic environment’ the forensic evaluation of the archaeological human remains by Raman spectroscopy showed that the environment surrounding the remains in which the tissue degraded played a part in the final composition of the tissue . Raman spectroscopy has also been put forward as a possible alternative to the use of dual x-ray absorptometry in the evaluation of osteoporosis. A recent study has suggested analysis of sulphation and the integrity of disulphide bonds in keratin, a protein contained in nails may correlate with changes in bone chemistry (Towler, 2007). Raman spectroscopy has also been used to investigate the link between the characteristics of mineral crystals and the mechanical properties of bone (Yerramshetty, 2008). An ongoing area of research is the effect of weightlessness on human physiology. Prolonged periods of weightlessness result in loss of bone mass and renal stones. Drugs to minimise these problems are given prophylactically to astronauts however their metabolism is also affected by weightlessness and as a consequence the reliability of earth based studies are limited. Standard analytical techniques employed on earth are not feasible in space and Raman spectroscopy has been investigated as an alternative (Inscore, 2006). From the 1990s Raman spectroscopy has been used in the study of human tooth enamel and the biocompatibility and penetration of resins used in dentistry (Suzuki, 1991). The differences in the Raman spectra obtained in the presence of caries has been studied (Hill, 2000; Ko, 2006) and Raman spectroscopy used to differentiate between normal teeth and resin restorations (Hill, 1997).Raman spectroscopy has also been used to study dental calculus; spectra obtained showed marked differences from those obtained from dentin. These spectral changes did not appear to alter with the age of the calculus (1 to 6 months). At the interface between calculus and saliva or dentine the Raman spectra were almost unchanged and it is thought that the distribution within dental calculus of the major constituent minerals does not alter significantly along the axis of growth (Tsuda, 1993). A detailed analysis of the internal vibrational modes obtained from Raman spectroscopy of human tooth enamel crystallites was published in 2002 (Leroy, 2002). UV resonance Raman spectroscopy has been used to study the impact of age on dentine and bone. An increase in the amide I peak was noted when teeth from donors aged 23 to 73 years were studied (Ager, 2006).

Ophthalmic

The eye is made up, in part, by media through which light is transmissible. This property makes the eye particularly amenable to study using Raman spectroscopy. Some of the earliest work utilising Raman spectroscopy in biomedical research was done using animal eye models (Rinai, 1970; Yu, 1982). Early applications mainly concentrated on the diagnosis of cataracts. In 1987 multichannel Raman spectroscopy was used to study the human lens *in vitro* (Ozaki, 1987). Since that time much work has been carried out to characterise lens pigmentation and opacities (Nei, 1990; Kellar, 1994; Yu, 1996; Duidam, 1998; Furic, 2005). The association between UV light exposure and the development of cataracts instigated the use of Raman spectroscopy in a novel application to assess the degree of penetration of UV light through contact lenses (Bergbauer, 1993). Macular degeneration is a common eye disease related to increasing age. It is the leading cause of irreversible blindness in the elderly and is associated with a decrease in macular carotenoid pigments. Raman spectra of human lenses, *in vivo*, show a linear relationship between spectral peak size and carotenoids concentration. In addition Raman signal strength can be demonstrated to decline with

increasing age (Gellermann, 2002; Bernstein, 2004; Ermakov, 2005; Obana, 2008). Raman spectroscopy of the eye has also been used to determine concentrations of glucose (Lambert, 2005) and drugs such as *Amphotericin B* and other antibiotics (La Via, 2006; Sideroudi, 2006 & 2007).

Upper gastrointestinal tract - Oesophagus

Much progress has been made building on important early work using Raman spectroscopy to investigate the characteristics of the epithelium from several different tissues, including tissue from the upper gastro-intestinal tract. A NIR (850nm) dispersion spectrometer was used and a difference between the glycogen content of normal and diseased oesophageal tissue (Barrett's oesophagus) shown (Bakker-Schut, 1997; Wolthius, 1999). Raman spectroscopy was also used successfully to assign classifications to the three main groups of tissue; normal, Barrett's and adenocarcinoma. Work published by Shim et al investigated the effects of *ex vivo* handling of biological tissue such as drying and snap freezing (Shim, 1996). It has also been shown that a 250mW laser focused to a spot size of 500μm does not produce a rise (< 1^{o}C) in the temperature in the tissue sample being examined (Shim, 2000). Detailed work has been published discussing the ability of Raman spectroscopy to classify epithelial cancers and pre-cancers, including those found in the oesophagus (Stone, 2002). This work also drew attention to the fact that it was difficult to spectroscopically differentiate tissue exhibiting early changes related to the development of cancer e.g. dysplasia from those that could be unambiguously be classified as neoplasia. Subsequent work has shown a great improvement in the ability of these models to classify disease when they are developed using consensus pathology reporting (Kendall, 2003). Stone et al have taken their work forward using the lessons learned and have shown it is possible to correctly assign pathological groups to epithelial tissue samples from different anatomical areas using a commercially available Raman microspectrometer (Stone, 2004). In another step forward Raman mapping studies have been used to clarify the possible biochemical changes, particularly in levels of glycogen and DNA, present during the development of adenocarcinoma of the oesophagus (Shetty, 2006). The hollow, tube like structure of the gastro-intestinal tract enables the passage of endoscopic instruments and this facilitates the use of fibre-optic Raman probes. Boere et al published work in 2003 that outlined the results of experiments using a Raman probe to study the characteristics of *ex vivo* Barrett's oesophagus from rats (Boere, 2003) and work continues towards *in vivo* human studies.

Lower gastrointestinal tract – Colon/Rectum

The incidence of colorectal carcinoma is increasing however treatment protocols are improving and one of the key factors in their success is early diagnosis. Raman spectroscopy has been investigated as a technique to fulfil this rôle. Initially UV resonance (Manoharan, 1995; Boustany, 1999) and NIR Raman spectroscopy (Feld, 1995) were both used and review papers have discussed the advantages and disadvantages of these different modalities (Manoharan, 1996; Zonios, 1998). More recently studies with larger sample numbers, ex and *in vivo*, have explored the use of Raman probes in the diagnosis of different types of colonic polyps (Molckovsky, 2003). Several reviews outlining the use of Raman spectroscopy in the diagnosis of colonic lesions have been written (Da Costa, 2005; Dekker, 2005). In 2007 a study was published in which laser-induced fluorescence spectroscopy (LIF) and Raman

spectroscopy were used to investigate the presence of markers within serum that are associated with an increased risk of colorectal cancer (Li, 2007).

2.3.3 Non Clinical

Gemstones

The 11th century reliquary Heinrich's Cross has been examined in situ with the aid of a Raman probe. Not all the gems contained in the cross were unambiguously identified but of those that were it was shown that they were mainly glass quartz and paste. Some precious stones such as rubies were found but it is unclear if the non-precious stones were original or replacements (Reiche, 2004). Raman spectroscopy can be used for both the identification of gemstones and gemstone treatments. Emerald fissure can be treated with oil to improve the clarity of the stone and brown diamonds can be treated with a high temperature and pressure process that can render them almost colourless. Gemstones which have undergone either of these processes can be detected by Raman spectroscopy (Kiefert, 2000).

The food industry

Raman spectroscopy has been used in the assessment of the content of amylose in rice (Ootake, 1998), a compound which is closely related to stickiness. It has also been used in the study of soils. Over a prolonged period (22years) areas of soil were treated with different substances one of which was cattle manure. This work showed that the composition of the soil organic matter varied considerably between areas (Francioso, 2000). It was suggested that in soil that had been 'amended' with cattle manure the organic matter was made up of material that might prove more resistant to decomposition. Significant amounts of perchlorate from fertilisers have been found to have leached into drinking water sources in the USA and this has caused concern. Raman spectroscopy studies of perchlorate levels in water and vegetables have highlighted its' potential as a possible monitoring technique (Williams, 2001). Studies have also identified Raman spectroscopy as a possible way of analysing pesticides on and in fruit. The current world food crisis is likely to focus research on techniques which allow rapid and inexpensive methods for the assessment of plant components in order that the strongest specimens can be selected for cultivation. Raman spectroscopy has been shown to be a viable tool in these assessments and potentially also in the quality control of raw food materials and their end products (Schulz, 2007).

Sport

Raman spectroscopy has been put forward as a possible means of non-invasive evaluation of muscle fitness by the detection of lactic acid levels (Williams, 2001). It has also been used to detect substances banned in sport (Perez, 1998) and as previously discussed can now be used to detect and monitor a wide range of drugs which can be identified from human plasma and urine samples.

2.4 The Pathogenesis of Cancer

Cancer evolves as a result of a complex, multi-factorial sequence of events. There are many contributing factors related to both the individual patient and the external environment. Aetiological factors relating to both the host and environment are outlined briefly in this chapter. The mechanism by which carcinogensis occurs has been elucidated greatly by research in these areas and a summary is given. More detailed

studies of aetiological factors specifically relevant to diseases of the larynx and lymph nodes are to be found in *Sections 2.5* and *2.6*.

2.4.1 Theory of Cancer Development

Host Factors

Genetic predisposition for the development of certain tumours has been clearly demonstrated in many neoplasms for example the breast and in the colon (Weatherall, 1987). *Familial polyposis coli* is an autosomal dominant condition where multiple premalignant polyps are found in the colon and invariably transform to become malignant. In this disease in addition to the genetic predisposition there is also a loss of a tumour suppressor (antioncogene) gene. Although there are cancers that predominately occur in children such as retinoblastoma and certain leukaemias most neoplasia occurs in adults. Whilst increased age is certainly a risk factor the exact changes that cause this are still unclear, exposure to carcinogens may be accumulative and changes in hormones with age may also play a part. Immunosuppression is also known to increase the risk of neoplasia either acquired as a result of poor nutrition or resulting from an infective process such as *Acquired Immunodeficiency Syndrome* (*AIDS*) (Scheifele, 2005, Robbins, 1989a). Approximately a third of patients with *AIDS* develop the neoplasia *Karposi's sarcoma*. Other systemic diseases can result in an increase in cancer risk such as atropic gastritis seen in pernicious anaemia patients which is associated with carcinoma of the stomach.

Environmental factors

Environmental factors such as geography and racial influences have been extensively studied. Geographic influences are considered mainly attributable to exposure to environment factors. The incidence of certain stomach cancer in Japan is much greater than that seen in the United States of America however the children of Japanese immigrants living in the USA have a similar risk to those not of Japanese origin. Cultural influences can also play a part in the development of cancer for example chewing beetle nut, common in South America, increases the risk of carcinoma of the oral cavity. Cancer risk can be increased by exposure to carcinogens either chemical, infective or as a result of radiation. Chemical carcinogens can be divided into those that act to initiate and promote carcinogensis (complete) and those that can only fulfil one of these functions (incomplete). Some carcinogens occur naturally in the environment such as aflatoxin B1. This compound is produced by *Aspergillus flavus* found on poorly stored grain and it is a strong hepatocarcinogen. It is also an example of a procarcinogen as it requires metabolic activation by liver enzymes to give the 'ultimate' carcinogen; dihydrodiol epoxide. Synthetic compounds can act directly or indirectly as carcinogens. Chemotherapeutic agents such as cyclophosphamide and chlorambucil are weak alkylating agents but never the less do act to damage cellular DNA, cyclophosphamide is also a very powerful immunosuppressant and it is these characteristics that cause its' carcinogenic properties. Indirect carcinogens require metabolic activation; there are an enormous number of these compounds. Aflatoxin B1 has been discussed but food additives have also been shown to act as indirect carcinogens. Azo dyes, used in the past to colour food e.g. margarine are metabolised in humans by urinary glucuronidase. The carcinogen produced predisposes to the development of bladder cancer (Robbins, 1989b). Many infective agents, particularly viruses, both DNA and RNA have been shown to be oncogenic and their study has led to many breakthroughs in the

understanding of carcinogenesis. Infection with the Epstein-Barr virus, particularly in the presence of malaria increases the risk of Burkitt's lymphoma, hepatitis C virus is associated with hepatocellular carcinoma and certain strains of human papilloma virus (HPV 16 and 18), cervical carcinoma. The RNA virus human T cell leukaemia virus 1 (HTLV-1) is implicated in the development of adult T cell leukaemia and lymphoma (ATLL). The correlation between radiation exposure and cancer has been clearly demonstrated. Ultraviolet light exposure and skin cancer have a strong correlation and there is an increase in the incidence of many different cancers in populations exposed to radiation after nuclear explosions. The ability of ionising radiation to produce mutagenic changes in DNA depends on the type and strength of the radiation, the duration of exposure and the nature of the tissue for example the thyroid is particularly radiation sensitive as are children compared to adults.

The Mechanism of Cancer Pathogenesis

Carcinogensis represents a series of steps beginning with initiation then promotion to produce a focal proliferative lesion. The cells of this lesion become autonomous, independent of normal homeostatic control. A cancer does not occur as the result of a single cellular event but as a consequence of a number of mutagenic events thus explaining the spectrum of disease seen from benign through precancerous lesions to true malignancy. Figure 2.7 is a diagrammatic representation of the steps involved. There can be a genetic predisposition to cancer however many carcinogens can also cause abnormal gene expression. Malignant neoplasias must develop certain characteristics; autonomy of growth, invasiveness and the ability to metastasize. It is in these areas that oncogenes and tumour suppressor genes have a rôle. The presence of mutations does not necessitate their expression and the body has developed both local and systemic controls utilising the immune system. Many tumours are weakly antigenic and vaccinations which protect against the development of certain cancers now exist. A vaccination against the human papilloma virus to reduce the risk of developing cervical carcinoma has proved very effective in clinical trials. Certain tumours have been shown to regress spontaneously. The degree to which the immune system can influence the development of neoplasia has, and still is, hotly debated. There is evidence to support the idea of T cell surveillance. Neoplasia induced by exposure to chemicals would appear to stimulate the formation of antigens that are unique. Tumours induced by exposure to viruses produce antigens that share characteristics with the virus itself. Certain antigens present in the embryo but not in adults are found to be re-expressed when neoplasia is present for example carcino-embryonic antigen (CEA) in the presence of carcinoma of the colon. These antigens are used to assess the presence of disease and response to treatment. Both natural and adaptive immunity play a part in the response to cancer. Natural immunity involving activated natural killer cells and macrophages can inhibit tumour cell growth and on occasions kill tumour cells by the release of compounds such as tumour necrosis factor. Adaptive immunity with the production of antibody is more likely to be effective against free cells such as those found in leukaemia than in solid mass tumours. Cell-mediated immunity against tumour cells by cytotoxic T cells has been shown to eliminate tumours in animal experiments and suppressor T cells can inhibit cytotoxic T cell function and stimulate tumour growth. This is seen in patients with Burkitt's lymphoma were high levels of an antibody similar to that found in infectious mononucleosis are found. It is felt that a

concomitant disease, in this case malaria, suppresses the normal cytotoxic T cell response allowing proliferation of the virus infected B cells (Robbins, 1989c).

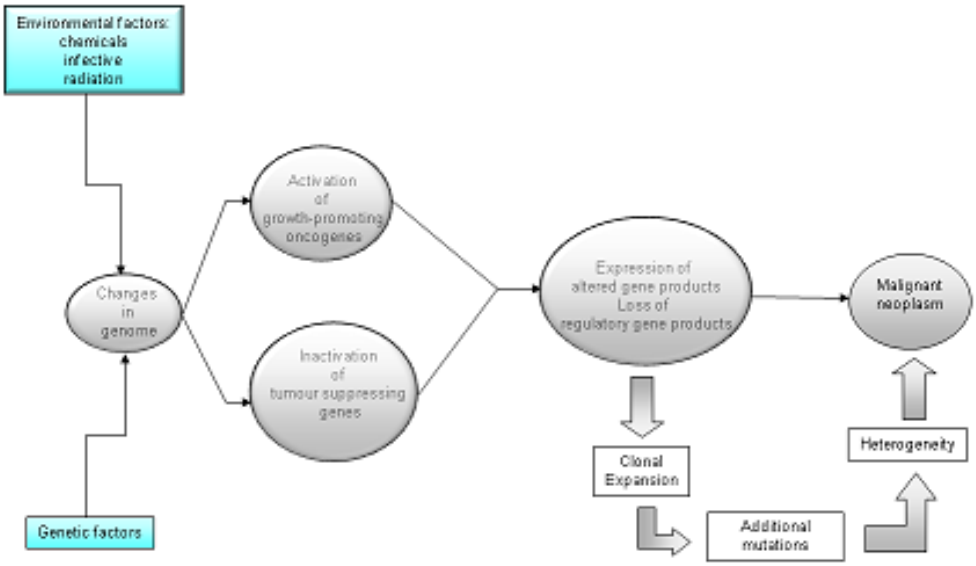

Figure 2.7: Pathogenesis of cancer (Adapted from Robbins, 1989d)

2.5 Diseases of the Laryngopharynx

A basic understanding of the anatomy of the larynx, and lymphoid system is extremely important to the understanding of the context of this work. The scope of the diseases that occur, their spread and treatment protocols all influence the type of diagnostic techniques that will be of use. It is the nature and anatomical configuration of the larynx and lymphoid system which dictate the type of diseases that occur and the ease and efficacy by which these diseases can be investigated, diagnosed and treated.

2.5.1 Relevant Anatomy

The structure of the pharynx and larynx plays has an intimate relationship with the way disease manifests in these areas and spreads beyond them. The three dimensional anatomy is complex so a simplified explanation of the main points is given in this section in order to place aspects of this research work in context and to clarify the references made to anatomical structures in the classification and staging protocols for laryngeal disease.

The pharynx is a tube like structure approximately 12cm in length. It begins at the base of the skull and extends caudally to the level of the sixth cervical vertebra were it is contiguous with the oesophagus. It contains a series of defects anteriorly that allow for communication with the nose and mouth, distally it also communicates with the larynx via the laryngeal inlet. The walls of the pharynx are fibromuscular and are made up of four layers. When examined from inside to out; a mucosal, submucosal, muscular and fascial layer. The pharynx is divided anatomically into three parts, nasopharynx, oropharynx and laryngopharynx as seen in Figure 2.8. The nasopharynx extends from

the base of the skull to the level of the soft palate, the oropharynx from this point to the upper edge of the epiglottis, where the laryngopharynx begins. This lower portion ends at the point where the oesophagus starts. The cricopharyngeus muscle acts as a sphincter at the entrance to the oesophagus. The pharynx from the laryngeal inlet to cricopharyngeus may be referred to as the hypopharynx. In this part, on either side of the opening to the larynx, lie the piriform recesses. These recesses are obliterated as the wedge shaped hypopharynx narrows towards the cricopharyngeus muscle. Lying anteriorly at the level of the laryngopharynx the pharynx communicates with the trachea via the larynx and becomes contiguous with it at the same level as the laryngopharynx does with the oesophagus behind i.e. the sixth cervical vertebra which is also the level of the cricoid cartilage.

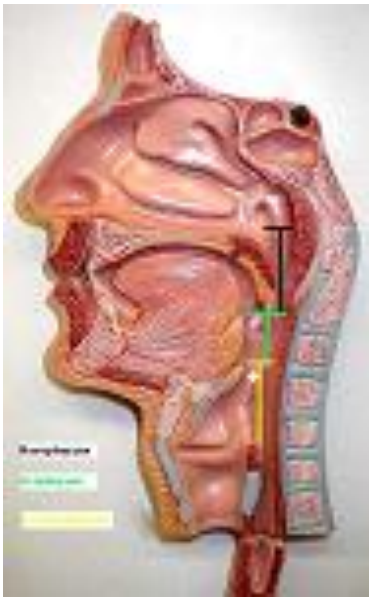

Figure 2.8: Schematic diagram of the pharynx and larynx.

The larynx is classified as a respiratory organ, in humans it has developed into the organ that is used for phonation but its primary rôle is to act as a sphincter to protect the airway. The larynx has a cartilaginous framework, the thyroid, cricoid and pair of arytenoids cartilages are composed of hyaline cartilage whilst the epiglottic and pairs of corniculate and cuneiform cartilages are made up of fibroelastic tissue. All cartilage elements of the larynx play an important rôle as attachments for the laryngeal ligaments and muscles but they also act as a structure over which the inner most mucosal lining of the larynx is draped allowing support for the vocal cords and the formation of a series of spaces. The thyroid cartilage lies a little higher than the cricoid cartilage and has two laminae which lie anteriorly meeting at the midline to form the laryngeal prominence; the Adam's apple. The cricoid cartilage is the main cartilaginous building block of the larynx and is the only complete cartilaginous ring. Its shape, articulation with the arytenoid cartilages and relationships to the thyroid cartilage are shown in Figure 2.9.

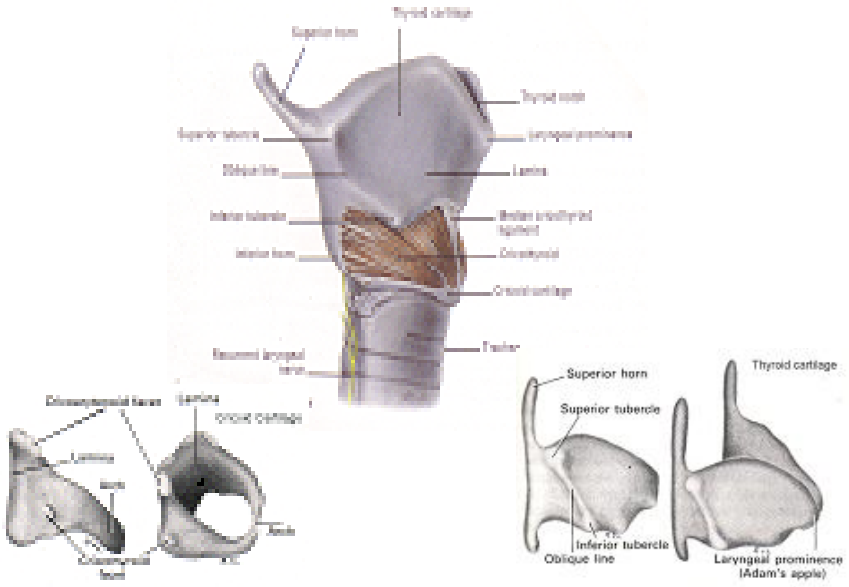

Figure 2.9: Anatomy of Thyroid and cricoid cartilages.

The cricovocal membrane is the name given to the upper part of the cricothyroid ligament. The vocal folds, or cords, are formed from the free edges of the cricovocal membranes, one from each side. These membranes slant upwards from the inner surface of the arch of the cricoid cartilage and have an anterior attachment to the inner surface of the thyroid cartilage at the level of the laryngeal prominence. The arytenoid cartilages articulate with the cricoid cartilage posteriosuperiorly and are the posterior attachment of the vocal folds. The gap between the folds is called the rima glottis and is a V shaped space in the horizontal plane with the apex of the V lying anteriorly (Last, 1995). The drawings in Figure 2.10 show lateral views of the larynx. In these figures the lateral wall of the larynx, above the level of the cricoid cartilage has been cut away to show the inner part of the larynx at the level of the vocal folds and rima glottis.

The space that exists between the laryngeal inlet below and the vestibular folds above is called the vestibule. There is a second space between the vestibular and vocal fold on each side which is slit like and projects laterally; these are called the laryngeal ventricles. Whilst diseases of the vocal cords themselves usually present early with symptoms of a hoarse voice disease present in these spaces can remain occult until directly visualised.

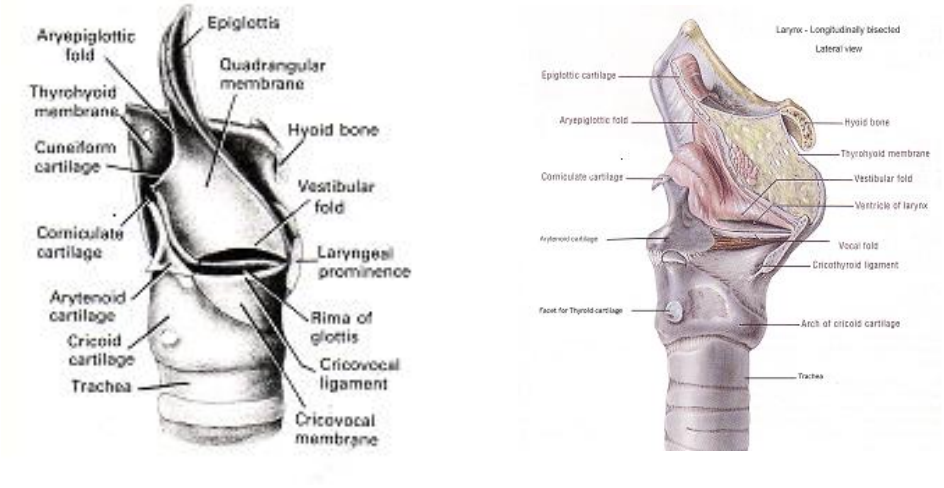

Figure 2.10: Human larynx - Line diagram and operative drawing of lateral view with outer wall cut away.

2.5.2 Aetiology

The development of epithelial cell tumours is thought to be multifactorial involving a series of steps underpinned by genomic instability and exposure to environmental risk factors (Hittelman, 2001). Koufman et al have presented a multifactorial model for carcinogenesis of laryngeal mucosa (Koufman, 1997).

Genetic and molecular biology

Both genetic and mutagenic factors are thought to have a rôle in the aetiology of head and neck squamous cell carcinomas (HNSCC), much work has been done to investigate the expression of molecular markers for premalignant laryngeal lesions with clinical prognosis and to establish genetic factors that determine susceptibility. There have been several review articles that summarise this work (Cattaruzza, 1996; Maier, 1997; Sadri, 2006). Genetic predisposition can be investigated using the bleomycin sensitivity assay (BSA) which assesses chromosomal instability and hence the risk of developing a laryngeal cancer associated with exposure to environmental risks. Broadly speaking the risk of induced mutagenic changes from environmental exposure to carcinogens appears to decrease from the oral cavity caudally through the aero-digestive tract towards the larynx (Szekely, 2005). Studies of polymorphism in carcinogen-metabolising enzymes such as glutathione-S-transferase and cytochrome P-450 have shown an association with genetic predisposition to development of laryngeal carcinoma, but not pharyngeal carcinoma (Jahnke, 1996; Matthias, 1998). Other gene polymorphisms have been investigated as possible markers for genetic susceptibly (Varzim, 2003). In this study the presence of the CYP1A1 NcoI HT genotype was associated with a 2.3 fold increase in the risk of developing laryngeal cancer especially in smokers who had inherited certain genotypes. Known molecular alterations associated with tobacco smoking and resulting in an increased risk of developing laryngeal cancer now include mutations of the p53 tumour-suppressor gene, loss of heterozygosity (LOH) in chromosomal loci encoding for the p53, p16 genes (Szyfter, 1999; Lewensohn-Fuchs, 1994) and other tumour suppressor loci (Sasiadek, 2001). Over expression of the cyclin D1 gene (CCND1) is found in approximately 20% of laryngeal carcinomas. The three main

subgroups of head and neck squamous cell carcinoma are, oral, pharyngeal and laryngeal. Studies have demonstrated that specific differences exist in the pattern of genetic alterations between these anatomical sites and hypotheses have been formulated as to the most important initiating chromosomal events and the oncogenetic tree models complied for tumour progression (Huang, 2002).

Smoking and Alcohol

Since the early 1970s studies have correlated the increased risk of developing laryngeal cancer with cigarette smoking. It was established early that subjects smoking unfiltered cigarettes, particularly cigarettes containing high tar content had a relatively increased associated risk of developing laryngeal cancer (Wyder, 1979). A large, case-controlled study has shown an overall increase in the risk of developing cancer in the upper aero-digestive tract in patients with significant alcohol consumption and to a lesser degree in smokers. In this study alcohol consumption was associated much more strongly with oral cavity, pharyngeal and extrinsic laryngeal tumours whereas smoking without excessive alcohol consumption increased the risk of developing intrinsic laryngeal carcinoma (Elwood, 1984). Different types of alcohol appear to confer differing risks with red wine and strong spirits causing the greatest increase in risk (De Stefani, 1987). Smokers have an increased risk of developing a carcinoma throughout the whole aero-digestive tract however the risk appears to decline in those subjects who stop smoking (Choi, 1991). In male smokers the risk at all sites increased with increasing duration of smoking and increased consumption per day. Alcohol consumption also linearly increased risk, 15-fold for oral cavity cancers and 11-fold for the pharynx and larynx. Overall alcohol was felt to be a weaker risk factor in the larynx than smoking but that a synergistic effect existed. DNA damage and mutations in the p53 gene have been shown to be related to inhalation of tobacco smoke (Pfeifer, 2002).

Diet

In 1981 variation in the dietary intake of vitamins was associated with changes in the risk of developing laryngeal carcinoma with reduced intake of vitamins A and C increasing the risk 2-fold (Graham, 1981). Investigations into the possible effects of dietary iron and zinc have been inconclusive. Subjects who reported a diet high in these elements appeared initially to have a reduced risk however after further study with analysis of nail clippings no actual increase in the concentration of iron or zinc in tissue was detected. A case-controlled study of salted meat consumption has shown that high intake has a significant association with an increased risk of developing laryngeal cancer and that this is compounded by smoking in a synergistic way. Fresh meat also showed this trend however after the consumption of fresh meat was accounted for the results for salted meat persisted (De Stefani, 1995). A multi-centre European study published in 1996 noted cancers of the larynx were less prevalent in subjects who had a diet rich in vitamin C and A, fruit, vegetables, vegetable oils and fish along with low intake of butter and processed meat (Esteve, 1996). Using a case-control study it has also been shown that consumption of raw tomatoes and other lycopene containing foods is strongly associated with a reduced risk of development of upper aero-digestive tract neoplasia. (De Stefani, 2000). More recent epidemiological studies have evaluated and confirmed the generally perceived protective influence of a Mediterranean diet against these types of cancers (Bosetti, 2002 & 2003) in addition increased risk was observed with higher consumption of eggs, red and processed meats, sugars and mixed seed oils.

Gastro-oesophageal Reflux Disease (GORD)

In the 1980s attention was drawn to the possibility that GORD might be a risk factor for the development of laryngeal disease (Morrison, 1988). This study was limited by a small sample number as was a more recent retrospective review of patients with GORD (Freije, 1996). Both these studies looked at patients who lacked the generally accepted common risk factors however there are larger studies, using pH monitoring within the oesophagus, which cast doubt on this association (Chen, 1998; Pellicano, 2000)

Occupational and Radiation Exposure

A large case-controlled study published in 1984 investigated some of the possible occupational risks that might be associated with the development of laryngeal cancer, particularly nickel and chromium (Olsen, 1984). A positive correlation was demonstrated for unskilled and semiskilled workers, particularly those exposed to dust and those working in the cement and port industries. The study found no support to implicated chromium however exposure to nickel was felt to significantly increase the risk of developing laryngeal cancer. More recent case-controlled studies have confirmed the risk conferred by cement dust exposure (Dietz, 2004). Hypopharyngeal cancer has also been shown to be associated with exposure to coal dust and formaldehyde (Laforest, 2000). A study in Sweden seeking to correlate increased risk in meat workers did not concluded that the apparent increased risk associated with employment as a butcher could be explained when other lifestyle choices were taken into consideration such as smoking and alcohol consumption. It did however postulate that the increased risk demonstrated in other meat industry workers might be due to exposure to nitrosamines and polycyclic hydrocarbons (Boffetta, 2000). Exposure to aluminium and lead has been implicated in the development of precancerous lesions such as laryngeal papillomatosis and laryngeal cancer (Olszewski, 2006).

Asbestos

Stell et al first noted the association of asbestos exposure and laryngeal carcinoma in work published in 1973 (Stell, 1973). Since then there have been several studies but the situation remains unclear and more recent review articles have cast doubt on this association (Griffiths, 2003).

HPV

This association was first noted in 1983 and shortly after a case study was published of a 6 year old child with recurrent laryngeal papillomatosis. At post mortem area of laryngeal mucosa were shown to have undergone malignant transformation (Solomon, 1985). This association has been extensively investigated but the rôle of infection with the human papilloma virus (HPV) in the aetiology of laryngeal cancer remains controversial. A study has shown that the p53 genetic mutation is associated with the integration of HPV-11 in malignant lesions (Rady, 1998). HPV DNA has been detected in cancers of the head and neck and in patients with respiratory papillomatosis however viral subset profiles differ and increased levels of oncogenic HPV are not universally present in patients with laryngeal carcinoma and leucoplakia (Major, 2005). After correction for smoking and alcohol consumption patients with HPV infection do show an increased risk of developing laryngeal cancer (Smith, 2000).More recent work has investigated the link between the presence of HPV and transfusion transmitted virus (TTV) in the aetiology of laryngeal disease concluding that co-infection with genogroup

1 TTV and HPV was associated with more rapid laryngeal tumour progression (Szladek, 2005).

Immune Deficiency

Oral, pharyngeal and laryngeal carcinomas have been shown to arise more commonly in immunosuppressed patients such as those that have undergone liver transplantation and appear also develop at a much earlier age in patients infected with the human immunodeficiency virus (HIV) (Scheifele, 2005).

Novel Ideas

Mitomycin C has been used topically within the larynx to reduce scarring however a case report has been published suggesting that its use may be implicated in the development of a laryngeal carcinoma (Agrawal, 2006)

2.5.3 Classification and Staging of Disease

2.5.3.1 General classification

The classification of disease within a specific anatomical area can be done in many ways. The most widely used and practical concept used by surgeons is called the 'surgical sieve'. A clinician will approach the diagnosis of a lesion in a step-wise fashion with all the possibilities assigned under a heading that link them such as vascular, infective, inflammatory or neoplastic. These possibilities are then narrowed down in light of the clinical picture and results of investigations. For example a lesion that appears to fall into the neoplastic group may be either benign or malignant and may also be subclassified in relation to the type of cell from which it originated. The most common neoplastic lesion found within the larynx is squamous cell carcinoma; it is malignant and originates from squamous epithelial cells. Figure 2.11 summarises part of this surgical sieve and more full describes the differential diagnoses of neoplasms found within the larynx. It must be emphasised that the largest contribution by far in the section classifying possible malignancies are SCCs.

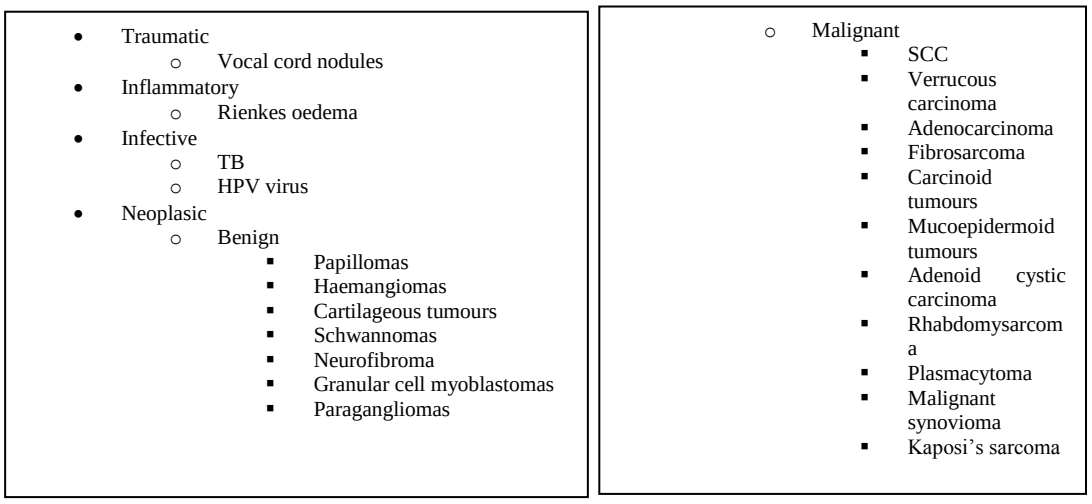

Figure 2.11: Part of the 'surgical sieve' used to classifiy diseases of the larynx.

2.5.3.2 Staging

Aims of Staging

Staging is a process by which cancers are divided into groups which behave in a similar ways. The grade of a specific tumour is defined as the degree of differentiation present in the cells and it is convention to grade a tumour with respect to the area with the most advanced disease. There are correlations between tumour grade and prognosis but they are considered weak, tumour stage has a much more significant prognostic value. The first defining staging parameter is the anatomical site of the primary tumour, additionally histological type, size and extent of the tumour, particularly in respect to haematological and lymphatic spread, are important. With progress in areas such as molecular biology other parameters are now beginning to play an important rôle in defining the stage of some diseases. This is particularly important for some neoplasms, notably in lymphomas were the natural history of the diseases are such that they do not lend themselves to this classical view of staging; this will be further discussed in *Section 2.6.2.*

Staging is primarily used as a guide to treatment and as part of the assessment of suitability for adjuvant therapy. A patient presenting with a small vocal cord carcinoma requires a completely different treatment plan to that of a patient presenting with a large invasive tumour and regional lymph node metastases. Staging is also used as a guide to prognosis; this is of immense importance to the patient and also to the clinician and researcher. For laryngeal disease clinical stage and anatomical subsite still offer the strongest practical predictors of outcome although the presence of molecular and cellular markers such as apoptosis index, p53 aberration and angiogenesis may play a rôle in the staging of laryngeal neoplasia in the future (Teppo, 2003). Staging also allows the results of different treatment protocols to be compared between groups of patients with the same stage of disease. This is imperative in the assessment of new techniques and to allow accurate audit and comparison of results between treatment centres.

Criteria for staging laryngeal malignancy

There are two principle staging classifications for head and neck cancer One published by the American Joint Committee on Cancer (AJCC) and the second by the Union Internationale Contre le Cancer (UICC). The most recent handbooks published by these organizations are The Manual for Staging Cancer, Ed 6 (AJCC) and the TNM Classification of Malignant Tumours, Ed 6, (UICC). To establish uniformity between these two classifications a supplementary publication is available; The TNM Supplement: A Commentary on uniform use, 3rd Ed. For the purposes of this thesis the TNM staging classification has been used for all neoplasias of the head and neck, excluding lymphomas.

TNM Classification of Malignant Tumours- Larynx

This classification was developed between 1943 and 1952 by Prof Pierre Denoix at the Institute Gustave-Roussy in France. It is anatomically based and records the site of the primary tumour (T), any regional lymph node involvement (N) and the presence or absence of metastases (M). To simplify the number of permutations the different categories are grouped. These groups are designated as stages and given Roman numerals, stage I, II, III and IV. The system can be used to assign a pre and post-

surgical clinical stage as well as a pathological stage (pTNM). The former are anatomically based relying on clinical examination, imaging, laboratory tests and biopsy results and is determined before any treatment is given. The latter utilises additional information obtained from pathological examination of the tumour after resection. Both systems are of practical use, the clinical TNM stage is used to formulate an initial management strategy and the pathological TNM stage is used to help determine what adjuvant therapy and follow-up will be required. The full TNM classification of laryngeal carcinoma can be found in *Appendix B*, Figure 2.12 is a summary for the glottis.

Summary—Glottis

T1	Limited to vocal cord(s), normal mobility a. one cord b. two cords
T2	Supraglottis, subglottis, impaired cord mobility
T3	Cord fixation, paraglottic space, thyroid cartilage erosion
T4a	Through thyroid cartilage; trachea, soft tissues of neck: deep/extrinsic muscle of tongue, strap muscles, thyroid, oesophagus
T4b	Prevertebral space, mediastinal structures, carotid artery

Figure 2.12: Summary of the TNM classification of malignant disease of the glottis.

2.5.4 Non-spectroscopic Diagnostic Techniques for Laryngeal Disease

2.5.4.1 General

Accurate outpatient assessment of the larynx in patients presenting with laryngeal disease is imperative. A great many patients are referred for otolaryngological assessment with altered voice but in many cases these symptoms are not due to cancer. In those cases were suspicious areas of mucosal change are found a simple, accurate and acceptable procedure aids early diagnosis, subsequent follow-up and ultimately improves prognosis.

2.5.4.2 Optical

Indirect Laryngoscopy

In the past outpatient examination of the larynx was by indirect laryngoscopy. This technique involved placing a mirror behind the uvula at an angle resulting in an image that could be viewed per orally. The great advantage of this technique is its simplicity; the only equipment needed was a mirror, light source and swab to hold the tongue. The disadvantages are that the view is often limited particularly if the patient has an over hanging epiglottis or a sensitive throat and cannot tolerate the procedure.

Nasendoscopy

In the developed world indirect laryngoscopy has been superceded by the use of the flexible nasendoscope, Figure 12.13. This technique involves passing a fine, flexible endoscope through one side of the nose, the post nasal space and over the superior aspect of the soft palate to view the laryngeal inlet below. By asking the patient to say certain vowel sounds an assessment of the vocal cords may be made. This procedure is often done without anaesthetic but if required this can be applied using a nasal spray. Whilst this procedure is usually tolerated very well there are a very few patients in whom it is not or in whom the anatomical configuration does not allow an adequate view. In these patients, were there is any suspicion of malignancy, a formal endoscopy is performed under general anaesthetic.

Figure 2.13: Flexible nasendoscopy; equipment, technique and view of normal vocal cords.

Stroboscopy

Laryngostroboscopy has been used for many years and remains an extremely useful tool in the assessment of the vocal cords for the presence of invasive malignancy (Bigenzahn, 1998). Even superficial lesions of the cords that invade the muscle below produce interruptions in the stroboscopic signal.

Contact Endoscopy

Contact endoscopy of the larynx has been used in the past to help delineate areas of mucosal change in the larynx but is no longer widely practiced; it is a form of chromendoscopy. A compound, for example toluidine or methylene blue, was applied to the area of the vocal cord under investigation with malignant tissue showing an improved uptake of the dye (Thomsen, 1975). Whist the results suggested that this technique might be useful the practical problems encountered during its use such as leaching of dye has limited uptake of the technique.

2.5.4.3 Histopathology

General

The larynx is considered part of the respiratory tract and for the most part it is lined with pseudostratified columnar ciliated epithelium, however the stratified squamous epithelium which covers the anterior epiglottis can project onto its posterior surface and by varying amounts can creep caudally onto the aryepiglottic folds and into the vestibule of the larynx. Areas of squamous metaplasia can also be found within the ciliated epithelium of the vestibule however the normal mucosa over the vocal folds is always stratified squamous and is firmly attached to the vocal ligaments. Scattered mucous glands can be found throughout the larynx but these are generally concentrated in the saccule. The step wise progression of disease change within the larynx, particularly on the vocal cords is one of the reasons Raman spectroscopy might offer a viable diagnostic tool. The criteria for histological classification of laryngeal disease, including grades of dysplasia are summarised in *Appendix C*.

Cytology has been used in the past to assess cells removes from the vocal cord by brushing during microlaryngoscopy (Lundgren, 1982) but this is no longer regularly practiced. Certain cell markers namely mini-chromosomal maintenance protein-2 and Ki67 found in laryngeal squamous epithelial lesions may improve the diagnosis by increasing objectivity and reliability of disease grade when used in conjunction with confocal microscopy to assess expression patterns. Flow cytometric analysis has recently been used to diagnose carcinoma occurring in the head and neck (Abou-Elhamd, 2007). In this study DNA image cytometry was used to assess if DNA ploidy could predict clinical outcome. Imprint cytology has also been mooted as future diagnostic technique (Loncar, 2007). The results of this study appeared very promising however the inherent drawbacks of cytology, inter-observer error and error induced by poor handling and preparation of the tissue, remain problematic.

There has been a great deal of interest in the use of molecular biology in the study of head and neck cancers. Investigation of tumour biology has concentrated on analysis of treatment results and the search for prognostic indicators. This is a huge area of ongoing work and as yet no single test has been found to be predominant however there is a great deal of work on the expression of the p53 gene. It is known that over expression of p53 at the edges of resected laryngeal cancers which macroscopically appeared free from disease reflects a similar poor prognosis to those specimens resected with positive margins (Brennan, 1995). Similarly the assessment of dysplastic lesions using immunohistochemical markers for differentiation such as cytokeratins and involucrin (Mills, 2008)

2.5.4.4 Imaging

Computed Tomography Scanning (CT) and Magnetic Resonance Imaging (MRI)

In the past patients with laryngeal cancer underwent chest x-ray to detect the presence of concomitant bronchial tumours or the presence of lung metastases. This investigation has now been superceded by the use of computed tomography scanning (CT). CT scanning also gives good visualization of thyroid cartilage infiltration form laryngeal tumours. Comparative studies of CT scanning with other investigative modalities were

done in the 1980s (Charlin, 1989).This study compared the abilities of CT and endoscopy to stage laryngeal malignancy and found them to be complementary. CT is both low in cost and widely available and with the advent of spiral-CT scanning which allows three dimensional reconstruction it may in the future be utilised further (Xu, 2007). One way to achieve this may be the development of a computer tomography virtual endoscopy (CTVE), (Sanuki, 1997; Gallivant, 1999). MRI and CT have historically been seen as competitors. MRI facilitated multiplanar imaging earlier than CT scanning and produces better delineation of soft tissue (Casselman, 1992). Its ability to delineate the extent of disease allows for accurate staging and improved operative planning. In 2006 a preliminary study assessed the ability of diffusion-weighted MRI to evaluate the larynx after patients had been treated with radiotherapy (Vandecaveye, 2006). This type of scanning is non-invasive and probes tissue by determining the movement of water. This study had a very small sample size however it is likely this will be an area for future investigation and may offer an alternative to Positron Emission Tomography (PET).

Positron Emission Tomography (PET) scanning

PET scanning is based on the detection of a radioactive tracer which is introduced to the body intravenously and can be varied depending on which tissue is under investigation.PET scanning can be used to assess physiological function such as blood flow and metabolism. Using a fluorine 18 radioactive glucose analogue, 18-fluorooxyglucose, the rate of cellular glucose consumption can be measured and used to distinguish between malignant and benign tissue in the head and neck (Foehrenbach, 2002; Israel, 2007). This type of scan is not widely available and the cost of the equipment is large however it is now used in specific areas such as the detection of occult head and neck malignancy particularly in patients who have radionecrosis and/or surgical scarring and in whom clinical assessment can be very difficult. The lack of PET scanners in the UK means many suitable patients still undergo CT scanning as an alternative.

The efficacy of different imaging modalities for the detection of metastatic lymph node disease arising from a primary tumour in the larynx has been studied (Kau, 2000). In this study CT and MRI scanning were felt to be superior to neck palpation. Ultra sound examination also appeared slightly better, PET scanning and ultrasound guided fine needle aspiration cytology gave the best results.

Scintigraphy and Super-imposed Dual Isotope Scanning (SPECT)

99mTc-tetrofosim scintigraphy has been investigated as a possible way of staging laryngeal cancer (Fattori, 2005). This study compared the results of scintigraphy with those obtained from CT scanning. Both modalities were found to be equally sensitive (96%) for identification of the primary tumour. CT was significantly more sensitive in detecting lymph nodes containing metastatic disease (100% vs. 50%) however the specificity of 99mTc-tetrofosim scintigraphy was much higher than CT scanning (100% vs. 56%). The invasion of thyroid cartilage is normally assessed with CT initially then with histology from a resected specimen. In 2004 a study investigated the use of isotope scanning with dual-isotope SPECT images obtained from tumour being superimposed onto SPECT bone scans which were taken simultaneously. Although the numbers in this study were small the results were encouraging.

Colour Duplex Echography

Colour duplex echography is not widely used in the UK but is in the United States as a way of assessing blood flow (Leuwer, 1997). This study assessed the ability of colour duplex echography to help distinguish the margins of malignant tissue within the head and neck by analysis of blood flow. It was noted that the central portion of tumours where relatively poorly vascularised compared with those seen at the periphery of the lesion and it was felt that this technique would only be a useful adjunct to other staging procedures.

Endolaryngeal high-frequency ultrasound

This technique has also be used in the assessment of diseases of the head and neck (Arens, 1998) but has not as yet borne out its' early potential because of the availability of less invasive and more cost effective procedures.

2.5.5 Treatment

The treatment of laryngeal cancer is currently undergoing great change. Treatment of primary tumours and metastatic spread to regional lymph nodes has been based around three modalities; surgery, radiotherapy and chemotherapy. Generally the TNM stage of a tumour has determined which of these, or which combination of these, should be used however technology is advancing and so too are surgical techniques and this in turn is greatly influencing options for treatment. The ideal aim of treatment is cure however where this is felt to be impossible then local control is of paramount importance. The guidelines for the treatment of cancer of the head and neck are published by the British Association of Otorhinolaryngologists and Head and Neck Surgeons (BAO-H&N). Carcinoma of the larynx at the in situ, T1 or T2 stages have a 80-90% chance of cure independent of the treatment modality; surgery or radiotherapy (Marioi, 2006), and until recently early cancers of the larynx have been treated with radiotherapy ensuring voice preservation. The disadvantage of this approach has always been the fact that there is a limit to the radiation tissue can be exposed too. This has meant that should a recurrence or another primary tumour of the head and neck occur salvage surgery has been the only treatment available for local control. This type of surgery is technically very difficult as it is done on a background of tissue radiation damage which destroys anatomical landmarks, can make haemostasis difficult and healing poor. Surgery for small primary laryngeal cancers has changed enormously over the last few years with the advent of laser surgery. Cancers up to T3 can be removed using a CO_2 laser and this opens up the possibility of retaining radiotherapy as a second line management strategy.

2.5.6 Clinical Relevance of Raman Spectroscopy

There are a large range of techniques available, both spectroscopic and non-spectroscopic for the diagnosis and staging of laryngeal malignancy. The key in treatment is early detection but the progression of cellular changes through the disease spectrum is continuous. Determination of the cut off points for histological grading are difficult to make and interpret consistently. Definitive diagnosis is reliant on histology from tissue resected from the larynx. This procedure is not without risk as it involves manipulation of the airway and the patient requires a general anaesthetic. Nasendoscopic evaluation of the larynx is highly subjective but is the mainstay of outpatient clinic assessment, both at presentation and during follow-up. A way of objectively assessing the degree of dysplasia present on a vocal cord in clinic or at the edge of a laser resection of a vocal cord lesion during surgery would be a tremendous

step forward. It is hoped that Raman spectroscopy will, in time be able to fulfil these rôles.

2.6 Diseases of the Lymphoreticular System

The lymphatic system comprises of all lymphoid tissue in the body and the lymphatic vessels connecting them. *Section 2.6.1* gives an explanation of the structure and function of the different components of this system.

2.6.1 Relevant Anatomy

2.6.1.1 Lymphatic vessels

These vessels are analogous to those found in the vascular system but are smaller and contain lymph not blood. In subcutaneous tissue they generally run alongside veins and in deeper tissue arteries. The two systems, lymphatic and vascular are intimately related but not directly connected except via the thoracic duct. Hydrostatic pressure and electrolyte differences allow the transfer of fluid from vascular capillaries through the tissue interstitum into lymphatic vessels which then form a plexus present in all tissues. Groups of lymph nodes are scattered throughout the body and are usually related to larger blood vessels. Lymph nodes contain both afferent and efferent lymphatic vessels and the route lymph takes after passing through a node can vary enormously depending on which efferent vessels it chooses. The only lymphoid organs that do not have afferent lymphatic vessels are the thymus and spleen. Lymph fluid eventually returns to the circulation via the thoracic duct which joins the vascular system at the confluence of the left subclavian artery and internal jugular vein in the root of the neck. The lymphatic system is generally considered ‘one-way’ as larger lymph vessels contain valves however despite this the clinical spread of disease by the lymphatic system, infective and neoplastic, does not always follow a strict anatomical progression. Lymph nodes can be by-passed, alternative efferent vessels used and distal increases in pressure, for example as a consequence of obstruction, can compromise lymph valves and cause back flow. One of the consequences of the vast number of interconnections within the lymphatic system is that surgeons can tie off the thoracic duct with impunity and lymph will always find a path which allows it to recirculate back into the vascular system. This is one of the mechanisms by which ‘surveillance’ information can be shared with other areas of the body where immune mediators are produced.

2.6.1.2 Lymph

Lymph is the name given to the fluid which circulates in lymphatic vessels and is an ultra-filtrate of blood. It contains proteins and cells such as B and T lymphocytes, macrophages and antigen-presenting cells (APCs) which mediate in the response to disease. The body has several defence systems the most basic being the physical barrier provided by skin however it can also mount a defence against attack by using non-specific mechanisms to recognise, engulf and destroy foreign material - phagocytosis. The immune response is a more specific defence mechanism reacting to foreign particles and micro-organisms.

There are two types of immune response, humoral and cell-mediated, both require lymphocytes. All lymphocytes arise from a common stem cell and before birth they are produced by the embryological liver and the yolk sac, after birth by the bone marrow. Lymphocytes that settle and proliferate in the thymus are called T lymphocytes as they

are dependent on the thymus for development. After maturation they are released into the blood stream and colonise lymphoid organs. T lymphocytes are responsible in part for the cell-mediated immune response where by cells which circulate in the blood destroy and facilitate the destruction by phagocytosis of organisms and antigens perceived as foreign. Several subsets of T cells exist such as T helper cells, T killer cells and T suppressor cells. The second type of lymphocyte is the B cell, these are formed and mature in the bone marrow and are responsible for the humoral immune response. Normal B cells migrate from bone marrow into secondary lymphoid tissues such as lymph nodes and when exposed to an antigen they form germinal centres, proliferate and mature. B cells can develop into B memory cells or plasma cells and plasma cells in turn can produce protein molecules called immunoglobulins which attach to antigens allowing the combination of the two to be recognised and destroyed. B cells are not named after bone marrow but from the Bursa of Fabricus an organ in chickens in which the humoral antibody response was first noted.

2.6.1.3 Lymphatic organs

Lymphoid follicle

Lymphoid follicles, also called lymphoid nodules are made up of a spherical collection of lymphocytes. The central area of the follicles is paler as the lymphocytes here are less densely packed together. Isolated lymphoid follicles can be found throughout the respiratory and gastrointestinal system mucosa and submucosa; those found in the ileum are known as Peyer's patches.

Bone Marrow

This is where B lymphocytes are produced and mature and its function with respect to the lymphoid system is described in *Section 2.6.1.2.*

Thymus

The thymus, as previously described, is where T cell lymphocytes are produced and mature. Its' structure is dissimilar to the other lymphoid organs as it is formed from several lobules and rather than having spherical follicular concentrations of lymphocytes they are arranged as a band around the outer cortex of the lobules.

Lymph nodes

The primary functions of lymph nodes are to act as filters and to facilitate lymphopoiesis and its related functions. Lymph nodes have simple connective tissue capsules, afferent and efferent lymphatics and contain the classical spherical arrangement of lymphoid follicles arranged around their periphery within the cortex of the node. The afferent lymphatics enter the node at its outer edge and continue through the paracortical areas via a series of anastomosing sinusoids which join together forming the medullary sinuses. They leave the node as the efferent lymphatic vessels at the hilum of the node. Sinusoids are lined with macrophages which filter material perceived as foreign and help in the initiation of specific immune responses. All cells within a lymph node work together but in certain types of response different cells which mediate in the response to disease will dominate. T cells are found in the deeper paracortical areas and will proliferate in response to organisms such as viruses otherwise most of the lymphocytes within lymph nodes are B lymphocytes, contained within primary follicles. Secondary follicles are those in which a germinal centre has

been formed and in which B cells are proliferating and this occurs in response to bacterial infections. Where there is enlargement of lymphoid follicles and increased production of B cells the term follicular hyperplasia is used. The structure of a normal lymph node is illustrated in Figure 2.14 and Figure 2.15 shows how they are classified to levels within the neck.

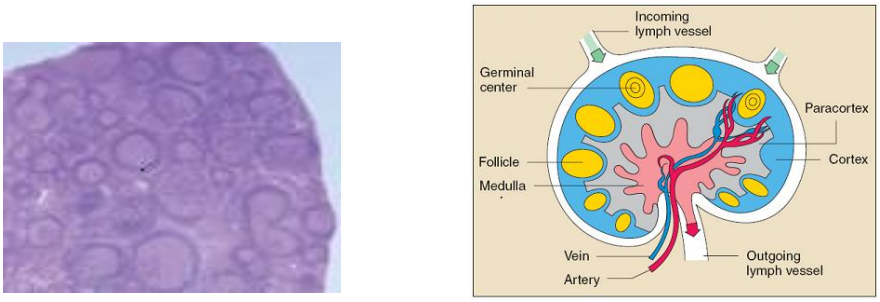

Figure 2.14: Sectioned lymph node and explanatory diagram of structure.

Figure 2.15:Lymph node levels in the neck.

Spleen

The spleen is analogous to lymph nodes in many ways however it has a thicker connective tissue capsule and has blood rather than lymph passing through it. It plays a more prominent rôle when an antigen passes into the blood stream and acts by trapping organisms and stimulating immune cell proliferation.

Tonsils

The tonsils, both the palatine and pharyngeal are very similar to lymph nodes but differ from them in one major way. Both types of structures are encapsulated however the tonsil capsule is lined by stratified squamous epithelium which dips inwards forming crypts. This is an important point as it differentiates between lymph nodes and tonsillar tissue and means that a primary squamous cell carcinoma of the tonsil can occur where as it can only be found as metastatic disease within lymph nodes.

2.6.2 Classification and Staging of Disease

The general classification of diseases which affect lymph nodes can be done in a similar way to those of the larynx using the 'surgical sieve.' The most common neoplastic lesions found in lymph nodes are metastatic cancer arising from a different primary site and lymphoma. In neck lymph nodes metastatic disease is usually squamous cell carcinoma originating from the upper aero-digestive tract however a smaller number of other cancers do on occasions spread to nodes in this region for example adenocarcinoma. Lymphomas are a primary malignancy occurring in lymph nodes and are considered to be haematological malignancies manifest as solid tumours and include any tumour which arises from a lymphoid cell line.

In 1971 a meeting was held in Ann Arbor in order to formulate a clinical classification for Hodgkin's disease (Carbone, 1971). This classification replaced the Rye histological classification and has been adopted by both the AJCC and UICC. It was later slightly modified to take into account disease bulk and number of sites affected; the Cotswold modification (Lister, 1989). The Ann Arbor classification has now been extended to include non-Hodgkin's lymphoma (NHL). Although the classification of lymphoma is complex there are very clear clinical and histological distinctions between the two groups. Hodgkin's lymphoma is comparatively amenable to treatment compared to the more resistant NHL and histologically NHL can be very hard to interpret. NHL appears to be a series of distinct diseases and clear delineation between them often requires sophisticated immunohistological diagnostic techniques and prediction of outcome has historically been based on an overview of several prognostic indicators.

The clinical staging classification of lymphoma is primarily determined by the location of the tumour. This is then modified depending on the presence of additional symptoms which are subdivided into an A and B classification. Pathological staging follows the same criteria but in addition uses information gleaned from a laparotomy. If a full pathological stage is to be assigned the spleen must be removed for evaluation and liver, lymph node biopsies and a bone marrow trephine results included. The full Revised European American Lymphoma classification (REAL) and WHO classifications can be found in *Appendix D.*

The classification of NHL has been a cause of great debate and the REAL classification is now widely used for the diseases that collectively make up NHL. It is based on a combination of clinical features, morphology and immunophenotyping (Harris, 1994). The REAL classification has also been the basis on which a World Health Organisation classification has been developed in the hope of unifying and developing an overall consensus document (Harris, 1999). Changes in the emphasis of the newer classifications have allowed these diseases to be subdivided on the basis of their clinical picture rather than just histological features. The division of NHL into low-grade and high-grade NHLs is commonly used and is based on the natural history of the diseases. Low-grade NHLs are generally considered less aggressive, responding well to treatment initially but with ultimately a fairly poor cure rate. High-grade NHLs are more aggressive initially but have good long term survival if the patient responds well to primary treatment.

2.6.3 Aetiology

Hodgkin's lymphoma can present at any age but most commonly in young adults. The cervical lymph nodes are involved in 60-70% of patients (Hoffbrand, 2006a) and are usually enlarged, firm and rubbery to palpate. NHL is a group of diseases that have very diverse presentations however all lymphomas are malignancies that originate from a genetic aberration of a single bone marrow or lymphoid tissue cell. The remainder of this section and *Section 2.6.4* summarises the principal aetiological and prognostic factors. Familial factors seem to play only a small part in the risk of developing lymphomas as does exposure to radiation, organic solvents and certain drugs. There is clear evidence of an increased risk in patients who also suffer from specific infections, for example malaria and Epstein-Barr virus (EBV). EBV is associated with the development of Burkitt's lymphoma, a high-grade, B-cell NHL. Other infections that have been implicated include the human immunodeficiency virus (HIV), human T-lymphotropic virus type 1 and the herpes viruses. Bacteria such as *Helicobacter pylori* have an association with lymphoma of the gastro-intestinal tract. Patients with primary Sjögren's disease, a chronic autoimmune disorder of salivary glands, are at increased risk of developing non-Hodgkin's lymphoma (Hoffbrand, 2006b).

2.6.4 Prognostic Factors in Lymphoproliferative Disease

Hodgkin's lymphoma

Hodgkin's disease is highly amenable to treatment; prognostic indicators are used to determine what levels of intervention are required and to predict their chance of success. In stages I and II the extent of disease is felt to be a major prognostic indicator as is the volume of disease within an individual region. The presence of B symptoms is also felt to be a poor prognostic indicator as they are an indirect reflection of disease bulk. In a similar way haematological parameters such as anaemia, decreased serum albumin and elevated erythrocyte sedimentation rate (ESR) are also felt to predict a poor outcome. Older patients have generally been thought to have a poorer prognosis but it is now felt that early diagnosis in the older patient with early disease negates this and is a strong point in favour of the development of early, accurate diagnostic techniques. Patients with immunodeficiency appear to have a poorer prognosis as do males. Certain histological features are also regarded as prognostic indicators and it was on this that the Rye classification was based. Race has not been found to be a clear prognostic indicator for early disease but access to sophisticated diagnostic and treatment regimes have been. In stages III and IV the bulk of disease is much harder to evaluate. The number of sites involved, the amount of disease below the diaphragm, within the spleen and in the mediastinum are all considered important. In addition elevated, alkaline phosphatase and a reduction in white cell count, particularly in lymphocytes, are poor prognostic indicators.

NHL

In NHL the immunophenotype of the tumour is particularly important in determining prognosis. The majority of NHLs are B-cell in origin and these patients general fair better than those with tumours which have a T-cell phenotype. Tumour bulk is again a major prognostic indicator as are the presence of B symptoms, elevated serum LDH, on occasions elevated serum calcium and malnutrition. There are now many haematological, biochemical and molecular markers which can act as prognostic indicators and some of these are highly specialised for example the amount of protein

found in the cerebro-spinal fluid (CSF) of patients with primary brain lymphoma. Older age is an adverse prognostic indicator in all NHLs and seems to be related to the degree of tolerance that patients over 60 exhibit to treatment. Gender seems to be only related to poor outcome for males with early NHL. Immunocompromised patients do particularly badly with NHL the second commonest malignancy in patients with HIV.

2.6.5 Non-spectroscopic Diagnostic Techniques for Lymphoproliferative Diseases

Staging lymphoma is imperative in order to help choose the correct treatment modality for a patient, over and above a detailed clinical examination certain tests outlined below are usually carried out for accurate staging.

Haematological and Biochemical Tests

Haematological and biochemical tests used for staging include full blood count (FBC), erythrocyte sedimentation rate (ESR), liver function tests, lactate dehydrogenase (LDH) and C-reactive protein measurements. Surgery at present is mandatory before treatment to obtain a definitive diagnosis through histological and immunohistological analysis of affected lymphoid tissue although in some cases a tru-cut biopsy of a prominent lymph node may be done. Fine needle aspiration cytology will not confirm the diagnosis of lymphoma but can be used to confirm the presence of metastatic squamous cell carcinoma in a lymph node. In the past for full pathological staging a bone marrow trephine was taken from the iliac crest and diagnostic laparotomy done with splenectomy. Clinical assessment is thought to underestimate the amount of abdominal involvement in a large percentage of patients with clinical stage (CS) I and II of Hodgkin's disease but there is no recorded improvement in survival in patients who have undergone staging with laparatomy so this has now been abandoned (Carde, 1993).

Imaging

Imaging plays a vital rôle in staging at all points during diagnosis, treatment and follow-up. CT scanning of the chest and thorax has largely superceded the use of chest x-ray and is done for both staging and to monitor response to treatment. MRI scanning is commonly utilised and in certain centres full body PET scanning is used in the staging of both non-Hodgkin's and Hodgkin's lymphoma. It is particularly useful in combination with CT for the detection of small residual tumour masses post treatment. Bone scans can also be useful in detecting extralymphatic deposits.

Histopathology and Immunohistochemistry

Lymphoma cannot be reliably diagnosed from tissue frozen sections and requires paraffin sections. The definitive diagnosis of lymphoma is made on assessment of an excised lymph node and the histological feature which divides Hodgkin's lymphoma and NHL is the presence of Reed-Sternberg cells which are found in Hodgkin's lymphoma.

There are five sub-groups of Hodgkin's lymphoma defined histologically;

- Nodular-sclerosing (NS)
- Mixed cellularity (MC)
- Lymphocyte depleted (LD)
- Lymphocyte rich (LR)
- Nodular lymphocyte-predominant. (LP)

The majority of early Hodgkin's lymphoma is of the nodular-sclerosing (NS) and mixed-cellularity (MC) types. There is now scope within this classification for the presence of a lymphocyte predominant (LP) subgroup which in the early stages has an excellent response to treatment. Histological definition of NHL subgroups is difficult and immunohistochemistry is very useful in determining phenotype. If certain markers are present for example κ or λ light chains the presence of NHL is confirmed differentiating the node from a purely reactive one. This is off great importance particularly in children who often present with non-specific lymphadenopathy. Analysis of tumour cell antigens, immunoglobulin and T-cell receptors may also be useful. Cryogenetics, the study of specific chromosomal translocations is a relatively new and exciting field, certain translocations may be important in the diagnosis and prognosis of NHL (Hoffbrand, 2006c).

2.6.6 Treatment

Treatment of Hodgkin's disease

Patients with early stage Hodgkin's lymphoma are treated with either radiotherapy or combined radio and chemotherapy. Patients with early disease, particularly the LP sub-group, are often treated with external beam radiotherapy alone. Fractionation and new ways of planning and delivering radiotherapy are making this an even more valuable form of treatment helped in some cases by the addition of chemotherapy which has led to a decrease in the amount of radiation required. Radiotherapy can be used to reduce the size of bulky tumours which are causing pressure effects and in the treatment of painful isolated bone deposits. Chemotherapy is used as the primary treatment modality in stages III and IV and also in patients with early disease but who have B symptoms, bulky disease or have relapsed after radiotherapy. In patients who relapse different combinations of chemotherapy can be used and autologous stem cell grafting. Stem cell transplantation involves the obliteration of the patient's immune and haemopoietic systems by chemotherapy, radiotherapy or both then the reintroduction of stem cells either from another person (allogenic) or a previously harvested set of cells from the patient which have been treated to allow re-colonisation to be successful (autologous).

Treatment of Non-Hodgkin's Disease

It is impossible to generalise the treatment options for NHL as they constitute such a diverse group, however the low-grade NHLs diseases such as lymphocytic lymphoma are often very slowly progressing and require little treatment. Others such as follicular lymphoma can also have a benign course presenting in middle to old age with only a few cases transforming to the more aggressive form. The early localised stages of these diseases are often treated by radiotherapy alone; however the treatment of disseminated disease can vary from conservative management to chemotherapy and stem cell transplantation. The high-grade NHLs are generally more aggressive but with rapid,

targeted treatment patients have a good chance of long term survival. Treatment regimes for these diseases include radiotherapy, chemotherapy and stem cell transplantation with the main modality usually being chemotherapy. For example, diffuse large B-cell lymphoma is treated with an extended period of chemotherapy of 6 to 8 courses.

2.6.7 Clinical Relevance of Raman Spectroscopy

The development of lymphadenopathy is by no means pathognonic of lymphoma and in many cases is due to a response to infection. The need to clearly and simply differentiate between the two is imperative. This is true in all age groups but is particularly relevant in children as some of the investigative procedures such as fine needle aspiration cytology are very poorly tolerated. The pressure to undertake lymph node excision can be great however in children and in some adults this will often necessitate a general anaesthetic with its inherent risks as well as the risks to other vital structures in the neck and the inevitable resultant scarring. The greatest factor at play to support the development of Raman spectroscopy in this field is that the major prognostic factor for the response to disease in lymphoma is the extent of the disease at presentation. This presents a compelling argument for investment in the development of accurate, sensitive and minimally invasive diagnostic techniques, such as Raman spectroscopy

Chapter 3: Materials and Methods

3.1 Materials

3.1.1 Laser and Static Spectrometer System

The aim of using the system whose configuration is described below was to obtain good quality spectra with high signal-to-noise ratio and the lowest laser power possible to avoid damage to the biological tissue specimens. It was also hoped that by using a configuration consistently between different research work comparisons between results could be made. This was particularly true of the work carried out on lymph nodes from the head and neck where squamous cell carcinoma and lymphomas predominate compared to those obtained from the axillae and areas adjacent to the upper gastrointestinal tract where adenocarcinomas are most common.

A customized Raman spectrometer system based on the commercially available Renishaw System 1000 microspectrometer coupled with an excitation source and confocal, polarized light, microscope (Leica DML) was used in this work. A labelled schematic diagram of this system can be seen in Figure 3.1 and a summary of the major components are given in Table 3.1. The path of the laser light before illumination of the specimen is nominally drawn in red and after illumination in green. A photograph of the Renishaw spectrometer and experimental configuration used for obtaining point spectra is shown in Figure 3.2. Further pertinent details on individual parts of the system configuration are contained in the remainder of this section.

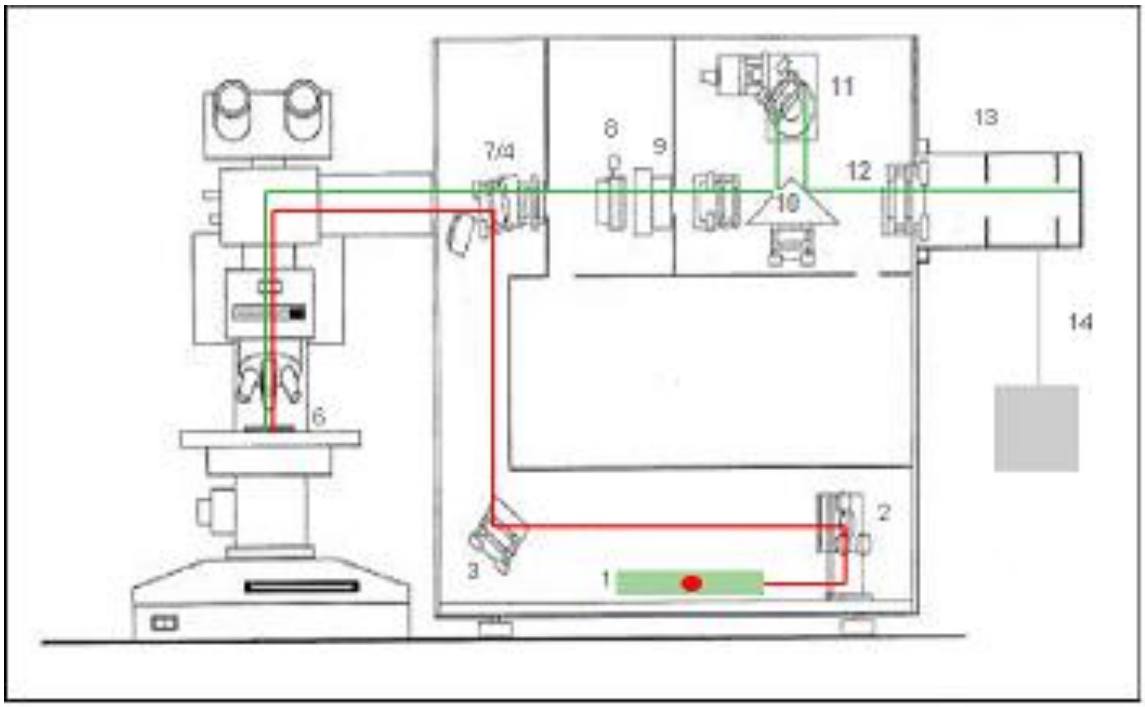

Figure 3.1: Schematic diagram of Renishaw System 1000 microspectrometer (reproduced by kind permission of Renishaw spectrometer division).

Table 3.1: Major components of experimental configuration.

Key	Component	Technical Detail
1	Excitation radiation source	Diode Laser
2	Mirror	Directs laser light into the horizontal plane
3	Steering mirror	Direct laser light onto the laser-line rejection apparatus (4/7).
4a & 4b	Laser-line rejection filter apparatus	This is made up of two parts (4a) a fixed mirror which is aligned to reflect only light of the laser-line towards the microscope (5) and (4b) an edge filter which removes any light with wavelength equal to that of the laser-line from the scattered radiation; allowing only light with an energy shift greater than $150cm^{-1}$ from the laser-line to pass through.
5	Lieca confocal microscope	Light passes through the microscope and illuminates the specimen after which it is collected and redirected back horizontally towards the laser-line rejection filter apparatus. The laser-line light is reflected off the horizontal axis and the remainder of the scattered light is allowed to pass forwards in this plane towards the focusing lens (7)
6	Specimen presentation stage	A motorized, computer controlled x-y-z translational stage used to allow accurate movement of the sample by computer control. This in turn allowed large numbers of spectra to be obtained with detailed signal positioning, of particular importance in mapping studies.
7	Focusing lens	Focuses the collected light onto an entry slit in the monochromator (8)
8	Monochromator entry slit	Removes any scattered light which is out of focus from the sample volume. This improves spatial resolution and removes any fluorescence contribution from the tissue. A slit width of 50μm was used throughout these experiments.
9	Beam expanding lens	
10	Prism mirror	A prism mirror with two reflective surfaces which allows light to be both directed towards a grating (11) and then collected from the grating after it has been dispersed into its' constituent wavelength components.
11	Dispersion grating	A single dispersion grating containing 300lines/mm used to separates the light into its' constituent wavelengths and allows it to be directed towards the CCD focusing lens (12).
12	CCD focusing lens	This lens focuses the dispersed light onto the CCD array detector (13)

13	CCD array detector	Sensitive to NIR radiation.
14	Control and analysis systems	

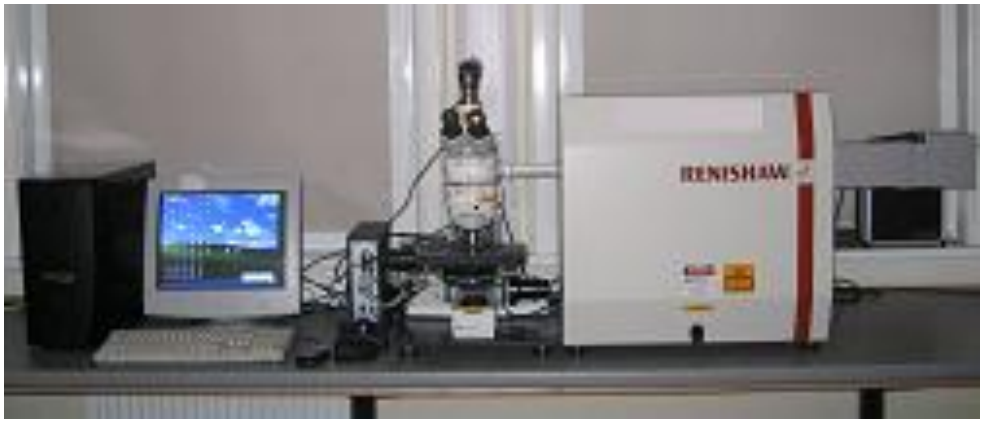

Figure 3.2: Renishaw spectrometer and experimental configuration for point spectra experiments.

General points

The laser system was bolted to a laboratory bench and the environment closely monitored and kept at 23^{o}C. This was to reduce inaccuracies that might be caused in calibration and spectra signal by vibration and changes in ambient temperature.

Excitation Source (1)

The excitation source used was a high power, tuneable (750 to 950nm) Argon ion (Stabilite 2017, Spectra Physics) pumped Ti: Sapphire laser (3900S Spectra Physics). When NIR radiation is used as an excitation source it is unlikely to produce electronic absorptions and hence fluorescence within biological tissue. Using a radiation source with longer wavelength has the disadvantage of being within a range less efficiently detected by a CCD. This is because Raman scattering cross-section is inversely proportional to the fourth power of the wavelength of the excitation source used and as a consequence very high sensitivity detectors are needed. Work has shown that using this system 830nm is the optimum excitation source wavelength for measuring the Raman spectra from biological tissue such as that obtained from the larynx (Stone, 2001a; Kendall, 2002b) and from lymph node tissue (Smith, 2005). This wavelength allows for optimisation of the Raman signal with minimisation of interference from fluorescence and was used in this work. A 300 lines/mm grating and a pair of edge filters (Semrock) were used to separate the Raman from the elastically scattered light and to disperse the spectrum across the deep depletion CCD detector. This was Peltier cooled to -70oC to reduce thermal noise. The beam of laser light was launched into the

spectrometer through a series of delivery optics which included the initial alignment mirror (2).

Microscope (5)

A confocal, polarizing light microscope was used with a x80 ultra-long-working-distance objective. Both reflectance and transmission white light images could be recorded and the Raman signal was collected in backscattering geometry. Each component of the laser system absorbs energy and reduces the power available at the surface of the specimen (Stone, 2001b). When a x80 (Olympus) ultra-long-working-distance (ULWD) objective is used in conjunction with a 500mW power output from the Ti: Sapphire laser 60mW power is detected at the sample (Kendall, 2002c). The choice of objective used was a balance. The numerical aperture (NA) is a way of describing the collection angle of a lens and is related to the refractive index of the material surrounding the lens and the maximum angle of collection from the optical axis of the lens. For the x80 ULWD objective NA=0.75, the maximum collection angle is 48.6^{o} and collection efficiency 16.9%. The collection efficiency of this objective is greater than that of a x20 objective (4.2%) and whilst this reflects a greater ability to collect photons of light by the x80 objective the corresponding larger numerical aperture reduces the working distances and depth of field. This is an important consideration as the depth at which a Raman signal can be collected by different objectives will be very important in the design of equipment used clinically. In the larynx, malignant changes occur within the surface layer epithelium which is approximately 500 microns thick. This epithelium consists of layers of cells 10-20 microns in diameter and work analyzing the depth intensity profile for a Raman signal using different objectives has shown that has shown that the x80 objective has a poorer depth of field than a x50 objective and this in turn is poorer than a x20. As a consequence using a x80 objective the Raman signal from only a depth of 2 to 3 cell will be obtained but for a x20 objective this is increased by at least ten-fold however the background Raman signal seen with a x80 ULWD objective is lower than that from a x20 ULWD lens (Kendall, 2002d). The objective chosen for use in the point studies in this work was the x80 ULWD lens.

Specimen presentation stage (6)

The x-y-z stage used allowed specimens to be moved along all axes in pre-designated step sizes.

Dispersion grating (11)

Although the use of a single dispersion grating is advantageous in that it allows high signal through-put, its disadvantage is that it is inefficient at removal of stray light. The use of a single grating is made possible by the laser-line rejection apparatus, which contains edge filters (4b) and is placed in a position earlier in the system. The dispersion grating is mounted on a stage that allows for precision rotation and as a consequence permits selection of the spectral range studied. The grating was made up of 300 lines/mm and this allowed signals up to $1980cm^{-1}$ to be recorded when the grating was static.

CCD Array Detector (13)

A peltier cooled depletion charge coupled device (CCD) was used which was sensitive to light in the NIR range of the electromagnetic spectrum. The CCD was made up of a

384 x 576 pixel array and the silicon wafer kept cooled to -70^{o}C to reduce thermal noise.

Control and Analysis Systems (14)

The laser system was controlled using a Hewlett Packard Pentium II Vectra PC which allowed system configuration, calibration and data acquisition via a CCD interface card installed in the computer. The software used was Galactic GRAMS/32 (Graphic Relational Array Management System) and WiRE (Windows based Raman Environment), version 1.3.15. Galactic Grams software is a stand- alone 32 bit data processor software package designed to facilitate the analysis, display and storage of large datasets from spectroscopy. It also allows for automatic file conversion whereby foreign type data files are treated as having a SPC format. The WiRE software was designed by Renishaw for use with their spectrometers specifically and it provides all the basic instrument controls, calibration, data acquisition and analysis functions.

3.1.2 Probe System

This section is included for completeness and refers to work in which a portion of each lymph node sample underwent investigation using a Raman probe. The experimental work has been completed and data analysis is ongoing. A 2mm diameter (GASER level 10), reusable Visonex fibreoptic probe was used in this series of experiments. The GASER scale is used to define depth of field with lower values indicating a longer working distance and larger depth of field. This probe consists of a central delivery fibre (400µm diameter) surrounded by seven collection fibres (300µm diameter) the actual experimental configuration is shown in Figure 3.3.

Each probe fibre has a numerical aperture of 0.22 and is capable of sampling a volume of 1mm^3 to a depth of 500µm (Crow, 2004).The delivery fibre commences at the laser excitation source and the collection fibres finish at the spectrometer. These two sets of fragile fibres are combined and held surrounded by a metal jacket for protection; this in turn was held by a retort clamp placed above the sample to be measured. The proximity of the sample could be finely adjusted in the vertical plane by using a movable stage on which the mounted sample was positioned.

Figure 3.3: Experimental configuration using Visonex Raman fibreoptic probe.

3.1.3 Tissue

Laryngopharynx study

Micro-biopsies, approximately 2mm in diameter, were taken from the vocal cords including those that appeared macroscopically normal. Specimens were also acquired from other sites within the laryngopharynx when areas of suspicion where identified. Where ever possible a biopsy was taken from the contralateral side in order to act as an 'internal' control.

Lymph node study

For the lymph node study biopsies were obtained from lesions presenting as masses in the neck and obtained by open neck dissection. The dimensions of the neck masses excised varied enormously from approximately 0.5cm to 14cm. In some cases the mass proved to be multiple lesions in close proximity which had on external manual palpation appeared to be one. The size of biopsies taken from the main operative specimens for research purposes were 0.25cm to 1.5 cm in diameter.

3.2 Methods

3.2.1 System Calibration

Renishaw static system.

Raman spectrometers measures light intensity as a function of wavelength and both these parameters need to be calibrated accurately. Where calibration error remains constant throughout the development of a model analysis of the spectra will not be affected, however if a different system is used or an instrument drift occurs the model may produce spurious results. Instrument calibration allows spectra acquired at different times and using different systems to be compared as knowledge of the calibration error in wavelength and light intensity measurements allows their influence to be calculated and removed from the Raman spectra measured. Calibration of wavenumber and light intensity can be thought of as full and daily.

The full wavenumber calibration for the modified Renishaw system is necessary should changes in the excitation wavelength or system alignment occur. Full wavenumber calibration of the Renishaw spectrometer used in point spectra studies was done using a Neon-Argon atomic emission lamp standard, Figure 3.4 (Renishaw Plc).

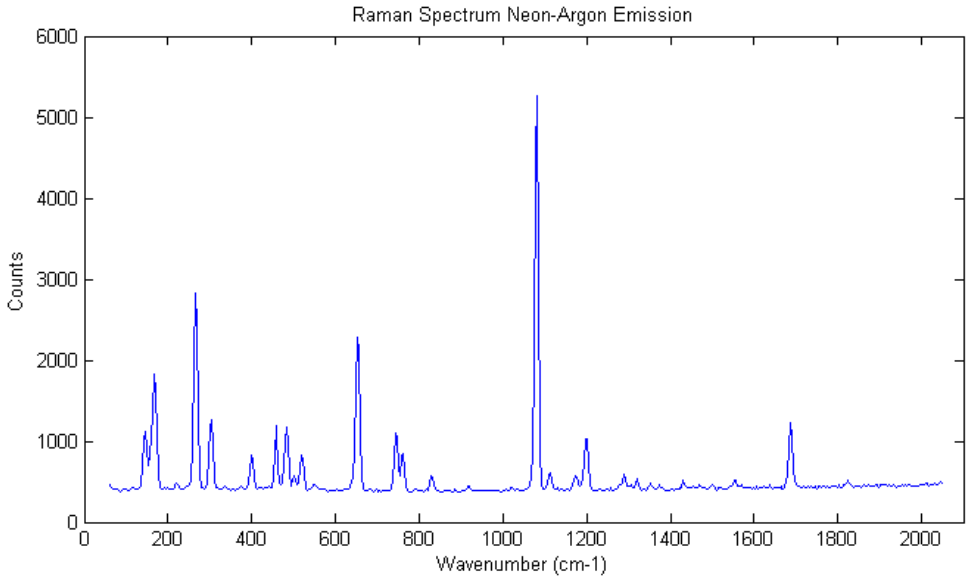

Figure 3.4: Raman spectrum obtained from Neon-Argon emission lamp standard.

To perform a full calibration, several atomic emission lines within the spectral range to be studied are selected and their absolute position defined by a line file. Using a x20 objective, an entrance slit of 10-20µm and acquisition time of 20 seconds the emission from the Neon-Argon lamp is measured over the range 10 000 -12 100 wavenumbers (cm^{-1}). The grating is moved in 25cm^{-1} steps over this wavenumber range and the emission spectrum recorded at each point. The WiRE software supplied by Renishaw is then used to fit the peaks measured to those in the line file which contains the absolute peak positions. For the daily calibration of wavenumber, Silicon was used as the test substance to test peak position. Cyclohexane (Sigma Chemicals) held in a UV-grade quartz cuvette (Jensons) shows standard peaks that when recorded over time allows calibration drift to be measured. Equal alteration of all peak positions suggests a variation in laser wavelength has occurred. Other standard substances used in the daily calibration of this system were a plastic pipette tip and the diffuse output from the Neon-Argon lamp.

The efficiency by which a Raman signal is detected is wavenumber dependent as a result of the fact that both the efficiency of the scattered light detector and the system optics are both wavenumber dependent. Therefore the shape of any spectrum measured depends not only on the molecular composition of the test specimen but also on the intrinsic response profile of the spectrometer. In these experiments the energy calibration relies on the measurement of a substance with a spectrum of standard, known shape. By comparing the ratio of the emitted light from the measured and standard spectra an instrument response profile can be developed and used to correct spectra obtained from tissue specimens. The energy calibration of this system was done using a tungsten-filament lamp whose spectral output was calibrated by the National Physics laboratory (Teddington, UK). Laser light was shone at a barium fluoride disc which was orientated at 45^{o} to the axis of the illuminating source. This causes the light

to be scattered almost completely diffusely which has the advantage of reducing any effects from beam geometry.

3.2.2 Specimen Collection

All tissue used in this work was obtained by myself, assisted by Mr. M Thomas, consultant ENT surgeon, Gloucestershire NHS Trust (GNHST) during surgical procedures. These procedures were performed on patients under general anaesthetic in accordance with an approved ethical proposal (*Appendix H*). Prior to surgery the aims of this research were explained to each patient by me and a written explanatory leaflet given. The patient was then allowed time to read the leaflet and decide if they wished to participate after which they were asked to sign a consent form in triplicate; one copy was retained in the patient's notes, another given to the patient and the final copy kept by myself in their research file. At all times the General Medical Council (GMC) guidelines on good clinical practice were followed. No patients declined to participate.

Laryngopharynx study specimens

After administration of a general anaesthetic the first step of the surgical procedure was an assessment of the neck and base of tongue done by manual palpation. Figure 3.7.

After this the patient's head was repositioned with the neck extended to help obtain an adequate view of the larynx. A gum shield was then inserted to protect the teeth and a thorough initial visual assessment of the laryngopharynx made using a hand held laryngoscope. After this a suspension apparatus was used to hold the laryngoscope in place allowing the surgeon to have both hands free to use other instruments (Figure 3.7). Pictures of the standard laryngoscope and the microlaryngoscopy instruments used during these procedures are shown in Figure 3.5.

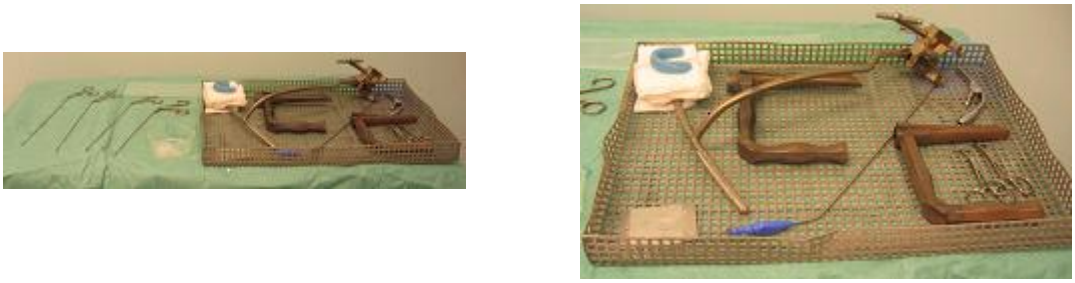

Figure 3.5: Standard laryngoscope and microlaryngoscopy instruments.

An operating microscope was wheeled into position and orientated to allow the rest of the surgery to be carried out under magnification, Figure 3.6. A typical view of the vocal cords seen through the microscope is seen in Figure 3.7.

Figure 3.6: Operative configuration for microlaryngoscopy.

Figure 3.7: View of vocal cords with SCC on right as seen through operating microscope.

Each patient had a micro-biopsy taken from the suspicious area of vocal cord epithelium and a further biopsy taken from the macroscopically normal cord. This biopsy was taken in an area that was not adjacent to the first biopsy to avoid complications such as laryngeal web formation. No adrenalin was applied to either vocal cord for haemostasis before these biopsies were taken in order to avoid specimen contamination. Each specimen was then carefully placed on acetate paper and oriented so that the epithelial surface could be clearly identified by placing this surface adjacent to a mark on the paper. This was imperative for further processing of the specimens and to allow comparison between H&E slides prepared for regular histopathological assessment and the results obtained from the Raman studies. The mounted specimens were then placed in a cryo-vial labelled with the date, coded patient identification and sample number for example 1LP1 corresponds to the first sample taken from patient number 1, 1LP2 the second sample. The vial was then placed in liquid nitrogen, snap frozen and stored at minus 85^{o}C. At the time of surgery a card was written detailing the exact position of the biopsies and this was added to the research file kept for each patient. A written comment was also made on the histopathology request form used for the main operative samples that further biopsies had been taken and from which positions.

Lymph node study specimens

During open neck dissection, biopsies were taken of all neck masses presenting in patients recruited to this study, in many cases multiple masses could be delineated and a research biopsy was taken from each. All operations were done under general anaesthetic and local anaesthetic infiltration was confined to the area of the skin incision and if near to the mass was superficial to it. Only specimens located away from areas

where bipolar diathermy had been used for haemostasis were included. The patient was positioned prone with the head resting in a gel ring or pillow and turned towards the unaffected side if the lesion was unilateral or held centrally for bilateral lesions (Figure 3.8).

Figure 3.8: Operative position for neck dissection.

A skin incision was marked and local anaesthetic infiltrated. Research biopsies were obtained from as many separate nodes as possible and each assigned a side and anatomical level. Figure 3.9 shows a photo of a lymph node resection from a neck.

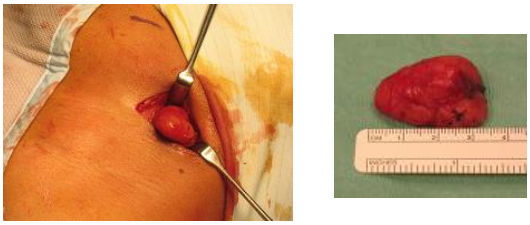

Figure 3.9: Photographs of a neck lymph node excision.

The research biopsies were placed on acetate paper and wherever present the capsule of the node was placed uppermost next to a mark on the paper in order that orientation could be maintained throughout processing. Each specimen was placed in a cryo-vial labelled in the same way as for the laryngopharyngeal study except that the letters assigning the sample to a particular study were changed from LP to NN, for example 1NN1 was the label given to the first sample from patient number one recruited to the lymph node study. The specimens were snap frozen and stored in the same way as that done for the laryngopharyngeal study. A card was written at the time of surgery identifying the exact location on the main specimen from which each biopsy had been taken and placed in the patient's research file. A comment was also written on the histopathology request form sent with the main specimen(s) to keep the reporting pathologist informed. After processing to give H & E slides, each research specimen from the lymph node study was bisected. This was to allow two studies on the same node, one using point spectra and one using the fibreoptic Raman probe.

Probe Study Specimens

The remaining portion of the bisected lymph node specimens were used in these studies in order that the results could be compared with the results from point spectra obtained using the Renishaw static configuration. Larger bisected specimens were divided in half again in order that they could be studied using the Visonex probe. In time the remaining specimens will be used in a comparison study of the Visonex probe and a needle probe that our research group hopes to develop.

3.2.3 Specimen Processing

Details of all samples collected were entered into databases developed for each study and specimens assigned a unique identifying code as described above. Other information contained within these databases included, hospital number, patient age, number and collection date of spectra; number, type and location of samples and research specimen pathology assignments from each histopathologist and those deduced from the histopathology report issued on the main operative specimen(s).

For every specimen histological tissue cross sections were obtained and H&E slides of the frozen section made. Distortion of spectra from the contamination that occurs during normal histological processing (Sajid, 1997) was avoided by obtaining H&E slides from the frozen sections using a freezing microtome. The acetate paper on which the specimen was mounted in the operating theatre acted not only to orient the sample but also allowed the specimens to adhere to the microtome chuck without the need for cutting agents. Ice crystal artefact was avoided throughout by snap freezing the specimens using liquid nitrogen. Figure 3.10 shows the order in which the histological sections were obtained.

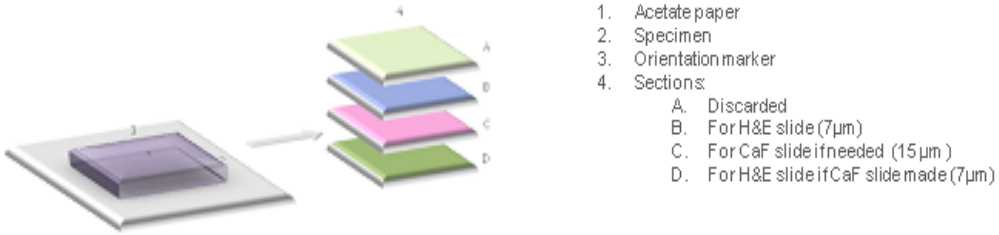

Figure 3.10: Tissue sectioning.

The freezing microtome was used to first obtain a flat specimen surface then a 7 micron section was cut and mounted on a plain glass slide for H&E staining. If the specimen had been selected as a possible candidate for mapping studies at a later date a thicker section (15 microns) was then cut and mounted onto a calcium fluoride (CaF_2) slide and a further 7 micron section taken for a second H&E slide. This slide was used to compare with the one obtained from above the mapping section in order to confirm consistency of tissue structure above and below the mapping section. All H&E slides were assessed by three histopathologists independently. The blocks of tissue remaining and mapping

specimen mounted on CaF_2 slides were stored at -85^{o}C and before being used in any of the Raman experiments were allowed to passively thaw at 23^{o}C.

3.2.4 Specimen Presentation and Acquisition of Spectra

The following sections describe how the specimens were presented for each study and experimental parameters used in spectra acquisition.

Point Spectra Studies

Specimens were individually mounted in their anatomical position on CaF_2 slides and held oriented in the correct position by two other pieces of CaF_2 (Figure 3.11).

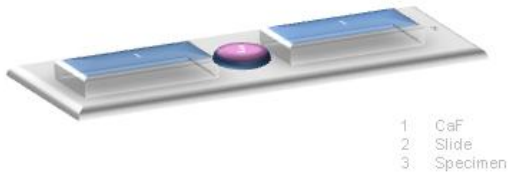

Figure 3.11: CaF_2 mounted block specimens.

CaF_2 was used for this purpose as it has a well defined spectrum with only one Raman peak at 323cm^{-1}, a peak which falls outside the main wavenumber range being studied (400-1800 cm^{-1}). The CaF_2 unit was placed on the microscope presentation stage and by moving the stage up or down a basic focus was achieved which was fine tuned by using the microscope manual controls. Multiple point spectra were obtained in a step wise progression across the specimen by moving the presentation stage. The microscope fitted with the x20 objective was used to focus the laser prior to the acquisition of each spectrum. The excitation source used provided light with a wavelength of 830nm, the spectra acquisition time was set at 10 seconds. The range over which scattered light was detected was 400-1800 wavenumbers (cm^{-1}).

3.3 Histopathology

The main operative specimens from which the research biopsies were taken underwent standard histopathological assessment and in some cases immunohistochemistry where lymphoma was suspected. Each research biopsy had histological frozen sections taken and H&E slides produced as described in *Section 3.2.3*. A consensus approach was taken to the assessment of these slides with three senior consultant pathologists making independent assessments of each one. Each pathologist was blinded to patient details, type of tissue presented and other relevant histological reports. The histopathologists used for these studies were Dr Christie-Brown (GNHST), Dr Keith McCarthy (GNHST) and Dr Simon Rose (Royal United Hospital, Bath).

In the assessment of the H&E slides from each research biopsy histopathologists were invited to comment on the homogeneity of the samples, type of tissue present and to give a diagnosis based on their findings. Where laryngeal epithelium exhibited any degree of dysplasia the pathologists were asked to assign a grade in accordance with

specific criteria (*Appendix B2*). One area of difficulty in the assessment of the H&E research biopsy slides is in the diagnosis of lymphoma. Lymphoma cannot be reliably diagnosed from H&E slides of frozen sections and requires assessment of formalin fixed specimens however certain histological features seen in the H&E slides of frozen sections can arouse suspicion. These features were used to assign a diagnosis from H & E slides of frozen sections and these results were analysed latter to formulate a majority consensus result which was also compared to the definitive report given for the main operative specimen. The results of these two studies are contained in *Section 4.1*. In both studies all slides on which the diagnosis differed between different pathologists and the cases in which specimens were poorly predicted by the relevant diagnostic models were looked at in more detail.

Only the standard histological and supplementary immunochemistry reports of the main operative specimen(s) are available to clinicians when patients attend postoperatively for discussion of their diagnosis and treatment plan. It was felt important to investigate the efficacy of a model based on these reports as well as the reports of the specific H&E slides obtained from research biopsies. The standard reports were obtained at the end of the study and the research biopsies assigned a diagnosis solely from these reports by correlation with positional data recorded at the time of surgery.

3.4 Data Processing

The data processing used in this work is discussed below and summarised in Figure 3.12.

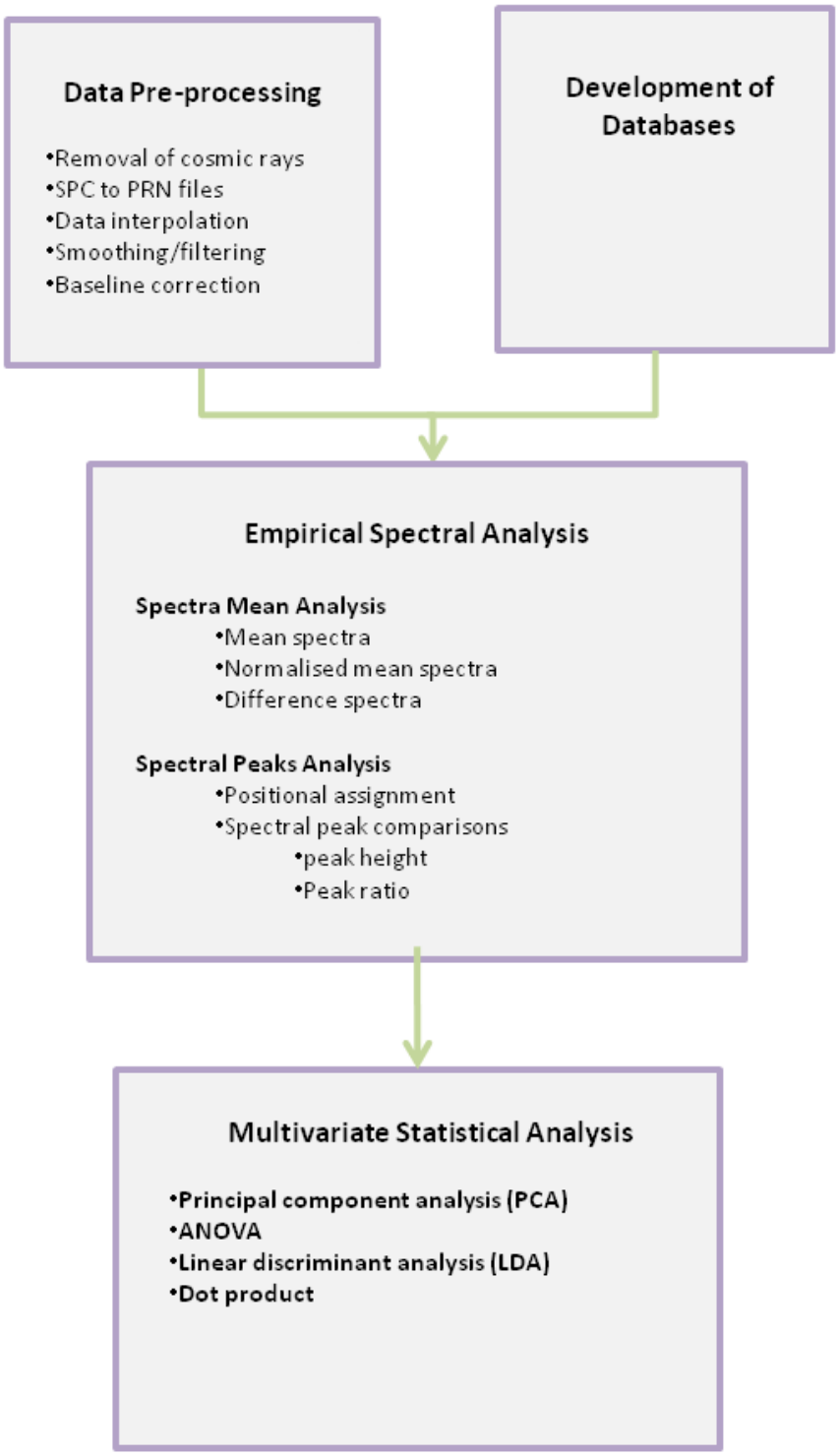

Figure 3.12: Data processing.

3.4.1 Database development

From the outset of this work an excel database has been built for each of the two main areas of work; laryngopharynx and lymph nodes.. Each database contains information under identical headings and this facilitated the use of similar Matlab processing scripts for most of the studies. A text file was made from each complete excel database and used within the Matlab data loading script. For each spectrum a corresponding H&E slide of the tissue sample from which it was obtained was reviewed by three expert consultant histopathologists. A diagnostic numerical code called the 'pathology code' was then assigned to each consultant opinion and recorded in the database against each sample and spectra. The databases were used to generate and record a consensus pathology decision for each sample from the three individual consultant opinions.

A surgeon relies greatly on the written histopathology report, compiled after examination of the origin resected surgical specimen, to make a management plan for the treatment of the patient. Whilst there are inherent difficulties in comparing the diagnoses made by consultant consensus of individual slides and the original pathology report it was considered interesting to examine the similarities and differences and so a further consensus was formulated between consultant opinions and the diagnosis given in the original pathology report.

Within each of the three main study areas 'mini-models' were developed by comparing different groupings of diseases, each disease having been assigned its' own numerical 'pathology code'. For ease of computer programming each of these groupings were also given a further numerical 'study group code'. For example in the larynx study mini-model, L2a, was developed by comparing squamous cell carcinoma made up of pathology groups 12, 13 and 14 (poorly, moderately and well differentiated SCC) against a group made up of normal laryngeal mucosa taken from the vocal cords and given pathology codes 7 and 15 respectively. Pathology codes 12, 13 and 14 were given a study group code of 1 whilst 7 and 15 were assigned the study group code 5. A summary of the pathology and study group numerical codes is recorded at the beginning of the relevant results sections and also in *Appendix D.2*.

3.4.2 Pre-processing

Conversion of spc to prn files

The original data for each spectrum was saved as a spc file however in order to use Matlab for data analysis these files required conversion to a prn format.

Removal of cosmic rays and fluorescence spectra

The ability of the models developed to separate different disease entities relies on the accuracy of the information used to build the model. In order to achieve a clean and accurate dataset spectra containing cosmic rays and those in which fluorescence obscured signal from tissue components were discarded from the larynx and lymph node point spectra dataset before any analysis was undertaken.

Baseline correction

To adjust for variations in Raman system throughput two corrections were made to the experimental data. A correction was made to account for the effects of variation in the

baseline of spectra (y axis). For this an absolute green glass reference and daily green glass calibration spectra were used and each spectrum individually corrected with reference to the corresponding green glass spectrum.

It was noted that after undergoing green glass correction when all sample normalised mean spectra were plotted together they had an x axis offset manifest as the appearance of double peaks seen particularly prominently for the major phenylaniline peak at or near 1001.5 cm^{-1}. To correct for this an adjustment was made during data loading which gave all phenylaniline peaks an x coordinate of 1001.5cm^{-1} exactly.

Interpolation

Interpolation was done between 350 and 1850cm^{-1} wavenumbers during data loading but after baseline correction.

Smoothing/filtering

Before undergoing green glass correction the experimental data produced spectra which where relatively smooth however it was noted that after green glass correction the spectra appeared much noisier. The green glass calibration spectra themselves did show more noise than the actual dataset and this noise appeared to be passed to the experimental data during correction and so was removed from the green glass spectra only, by smoothing using a savgol function.

3.4.3 Empirical Spectral Analysis

3.4.3.1 Spectra Mean Analysis

Mean and normalised spectra

Within each study group the mean spectra was determined and each of these spectra where normalised so certain comparisons could be made between the mean spectra of different groups such as peak height and area ratios.

Difference spectra

Difference spectra were generated in each mini model by subtracting the mean spectra from each other. For example in mini- model study L1 the mean spectra representing non-malignant tissue was subtracted from that for squamous cell carcinoma. The resulting difference spectrum is constructed about a y axis value of 0 and shows both positive and negative peaks. Positive peaks represent tissue constituents that are present in greater amounts in the squamous cell carcinoma group and negative peaks those that are more prevalent in the non-malignant tissue group. This technique allowed a visual representation to be used to pick out those peaks, and hence tissue constituents, that might be significantly different between the two groups and subsequently allowed more focused investigation to be undertaken.

3.4.3.2 Spectra Peak Analysis

Spectral peak comparisons-peak height, intensity and peak area ratios

Using customised Matlab scripts prominent peaks particularly those present in the difference spectra were identified and marked on the normalised, mean spectra of each study group. Ratios of peak heights, intensities and areas were calculated and entered into a database. This formed a representation of the similarities and differences between the groups not unlike that shown by difference spectra but in a numerical form.

Peak assignment to tissue constituents

This proved to be the most difficult part of the data analysis as the complex structures found in biological tissue produce peak assignments that in many cases overlap. Standard tables of some biological tissue peak assignments now exist and the table used in this work was compiled by Catherine Kendall (Kendall, 2002e) and a copy can be found in *Appendix E*.

Mean centering of spectra

This technique is used before PCA is undertaken and helps ensure that the first PC is not simply a reflection of the variance about the mean.

3.4.4 Multivariate Statistical Analysis

Multivariate analysis was used in this work to identify and quantify differences in spectra. It has a major advantage over the univariate analytical techniques described above as it uses all the data measured and also allows inspection of very small differences in spectra more easily.

Principal component analysis (PCA)

PCA allows extraction of spectral components which best describe the variance over the entire dataset. This allows reduction and optimisation of the number of dimensions of the original variables to a minimum value which is capable of adequately describing the variance of the original dataset and can then be used in linear discriminant analysis of promising models. Two things are generated during PCA; loads, also called components, and scores. The first principal component (PC) represents the spectral features which best represents the variance over the whole dataset and as the number of the PC increases the degree to which it does this reduces. Each group's mean centred spectrum is broken down into a series of PCs and a score allocated depending on the degree to which it is represented in that individual spectrum. The sum of each principal component multiplied by its score should reproduce the spectrum.

Analysis of variance (ANOVA)

ANOVA is used to compare the means where more than two groups exist and allows the effects of multiple interrelated factors to be assessed simultaneously. For example it can be used to determine whether more than two independent samples originate from the same group. In this work it is used to identify diagnostically significant PCs. An F statistic is formulated which is the ratio of the mean square of the variance between the groups to the mean square of the variance within the groups; the greater the difference between the groups the greater the F value. A critical F value (Fcrit) is the value over which a particular PC score represents true variance within the dataset and is dependent on the level of significance the investigator has chosen.

Linear discriminant analysis (LDA)

This is a technique in which information on the origin of the samples is applied to the analysis and is an example of a 'supervised' technique as information relating to the samples in the training set is used for the analysis and the number of groups in the study is specified rather than found as a result of the analysis. Using spectral data LDA allows identification of the dimension of maximal variance between a designated number of groups within the dataset. The scores for selected PCs are used as the input data and the groups correspond to the study group codes each one representing a group of samples

containing one or more pathology codes. The results of LDA are presented as the proportion of spectra correctly predicted by the model as belonging to a specific group.

Cross-validation

Once a classification model has been developed by using data to train the model it is usually tested by using a different validation dataset. When the results of analysis of the two datasets are the same or very similar the model can be thought of as robust. When no independent validation data is available a 'leave one out' cross validation technique can be used. This is where one piece of data is withheld, a multivariate model made from the remaining data and the process repeated. In this work the type of data withheld could have been either a single spectrum, the data relating to a single sample or that relating to a single patient. A leave one out (LOO) cross validation was chosen and the data relating to a single specimen in each cycle was removed. This allowed optimisation of validation whilst ensuring each analysis ran in a reasonable time.

3.4.5 Summary

The use of empirical methods such as comparison of normalised mean spectra allows a simple overview that helps focus further analysis and by producing difference spectra from the SGs normalised mean spectra the main wavenumber areas where a difference is present can be clearly seen. Difference spectra are produced by subtraction of the normalised mean spectra and utilise all data from these plots. The intensity of the difference spectra at a particular wavenumber reflects the absolute difference in the amount of the compound(s) present that are responsible for that particular signal. If spectra B is subtracted from spectra A and no peaks are seen compound A and B must be the same. If a positive peak is seen the molecular entity/entities responsible for it are present in a greater amount in compound A, and this amount is directly proportional to peak height. The difficulty in interpretation of Raman spectra in general is that more than one entity can be attributed to the Raman signal at a certain wavenumber. This is a limiting factor in the conclusions that can be drawn from empirical analysis.

The other main interrogative tool used in the empirical analysis is peak intensity ratios (PIRs). This technique compares the data between study groups in a different way. Firstly the values for the main peaks within a normalised mean spectrum are ratioed to a single peak that occurs in that spectrum and in the spectra of the other study groups. For each study group a set of ratio values is produced, one for each peak, that describe the relative amounts present of the entity/entities responsible for the peak signals in that study group alone. The pattern of ratios can be compared within a study group to give clues as to the molecular construction of the sample and between study groups to assess how this composition may differ between them. The difference in the PIRs between study groups can be calculated giving values that reflect the difference in the proportion of the constituents; they do not reflect absolute values. In both cases a single ratio taken in isolation is less useful than a pattern of the ratios or ratio differences between study groups as peaks may have more than one molecular assignment. One drawback with this technique is that only a relatively small amount of the data is used. The power of interrogation can be increased by also considering the peaks that do not occur in the spectra of all the study groups in the mini model. These peaks may in fact be of enormous importance because by definition they are absent in at least one of the study groups and if they can be given a peak assignment there is potential to learn a great deal

about that group, again this information is given more power if it can be linked with a pattern of ratio changes.

Multivariate analysis treats the data as a whole and is a very powerful tool. However it is not as useful as empirical analysis in helping determine molecular composition in a study group or molecular differences between them. Multivariate analysis does enables the variance across the data set to be analysed in detail and gives a clear objective assessment of the ability of a model to discriminate between groups of samples.

Each tool within the empirical and multivariate analyses has a part to play and this is demonstrated in the diagnostic mini model results. *Section 4.2.3.7* contains the results for mini model L4 and this mini model is a good example of how all these techniques can be combined to maximally interrogate the data.

Chapter 4: Results and Discussion

This chapter is divided into three main sections, consensus studies relating to the histopathological classification of tissue samples and two sections relating to diagnostic models; larynx and lymph node studies.

The results and discussion for the two diagnostic model studies are organised in a similar way with the first section in each summarising general information relating to the data and how this data is organised to form the diagnostic 'mini models'. This is followed by a section outlining findings related to the spectra from tissue samples of individual pathology codes and for the combinations of these that are used to form study groups. The section that follows contains a detailed look at the data for each diagnostic mini model and is divided into three parts; results obtained from the empirical and multivariate analysis and finally a discussion section.

To avoid repetition the results and discussion section for mini model L1 is written in the most detail as it aims to show the systematic approach by which the models and studies developed.

4.1 Consensus Studies

Three consultant histopathologists independently assessed H&E slides of frozen sections for all tissue samples used in these experiments. Each pathologist was blinded to the history of the patient, the site of surgery and the opinion of the other pathologists. They were also unaware of the histopathology report given for the main operative specimen. Table 4.1 is an example of how data relating to the histological classification of tissue samples was recorded. Columns 2 to 5 contain the numerical pathology codes representing the opinion of each consultant as to the type of tissue and any disease process present. Column 2 refers to the diagnoses gleaned from the histology report of the main operative specimen and columns 3 to 5 are coded A, B and C to identify clearly the relevant histopathology consultants. The codes for the histopathology diagnoses for the larynx study are summarised in Table 4.2 and in Table 4.3 for the lymph node study.

Table 4.1: Example of data compiled in order to obtain a consultant majority consensus on histological classification of H & E slides of frozen sections obtained from each tissue sample.

Sample	Report	A	B	C	Consultant Consensus	Consultants Agree/Disagree	Count of Agree	Count of Disagree
10L1	7	7	7	7	7	All Agree	1	0
11L1	9	7	7	7	7	All Agree	1	0
11L2	7	7	7	7	7	All Agree	1	0
12L1	15	15	15	15	15	All Agree	1	0
12L2	15	15	15	15	15	All Agree	1	0
13L1	17	17	17	17	17	All Agree	1	0
13L2	17	17	17	17	17	All Agree	1	0
17L1	7	7	7	7	7	All Agree	1	0
17L2	7	7	7	7	7	All Agree	1	0
17L3	1	1	1	1	1	All Agree	1	0
18L1	1	1	1	1	1	All Agree	1	0
18L2	13	13	11	11	11	Someone Disagrees	0	1

A majority consensus histological classification (consensus) was then used to build a series of mini models within the two main studies; larynx and lymph node. The consensus classification was kept as detailed as possible so that combinations of related codes and hence related histological findings could be used. For example codes 16 to 20 in the lymph node study all refer to types of Hodgkin's lymphoma. In the future as more specimens are added to the study this data may be used to test the ability of Raman spectroscopy to interrogate specimens of Hodgkin's lymphoma further to ascertain if subgroups can be identified.

Table 4.2: Pathology codes assigned to different histological diagnoses in larynx study.

Pathology Code	Description
1	Laryngeal polyp
2	CT/Stroma
3	Muscle
4	Tonsil/Lymphoid Tissue
5	Papilloma
6	TB
7	Controls - Hyperplasia/Hyperkeratosis
8	V/C Dysplasia - mild
9	V/C Dysplasia - moderate
10	V/C Dysplasia - severe
11	Carcinoma in situ
12	SCC Poorly differentiated
13	SCC Moderate differentiated
14	SCC Well differentiated
15	Controls - Normal squamous epithelium
16	Not used
17	Reactive lymph node
01	Cleaned SCC Well differentiated

Table 4.3: Pathology codes assigned to different histological diagnoses in lymph node study.

Pathology Code	Description
1	Reactive Lymph node
2	Branchial cyst
3	Fibrous connective tissue
4	Normal squamous epithelium
5	Fat
6	Parotid salivary tissue
7	Normal thyroid tiassue
8	SCC - Poorly differenciated
9	SCC - Moderately differentiated
10	SCC - well differentiated
11	Adenocarcinoma
12	Pleomorphic adenoma
13	Poorly differentiated carcinoma
14	Thyroid - papillary carcinoma
15	Thyroid - follicular carcinoma
16	Hodgkin's lymphoma (HL) - mixed cellularity
17	HL - nodular sclerosing
18	HL - follicular cell
19	HL - classical lymphocyte predominant
20	HL - Non-classical
21	Non-Hodgkin's lymphoma (NHL) - diffuse large B cell
22	NHL - Low grade malignant
23	NHL - MALT type

4.1.1 Results and Discussion - Consultant consensus study.

As expected there was a range of diagnoses given to different tissue samples and to the diseases which affected them. Tables 4.4 and 4.7 summarise the consensus for tissue samples from the larynx and lymph node studies respectively. There are very important limitations on the interpretation of these results as much larger numbers of samples would be needed for a rigorous analysis of the variation in histopathology classification between consultants however there are some interesting features in the results of this work that might prove helpful in directing future studies.

Table 4.4: Histopathology consultant majority consensus for larynx study tissue samples.

PathologyCode	Name	Instances All Consultants Agree with Consensus	Instances Some Consultants Disagree with the Consensus
1	Laryngeal polyp	2	0
2	CT/Stroma	3	0
3	Muscle	0	0
4	Tonsil/Lymphoid Tissue	6	0
5	Papilloma	1	0
6	TB	0	0
7	Control V/C - Hyperplasia/Hyperkeratosis	13	0
8	V/C Dysplasia - mild	1	0
9	V/C Dysplasia - moderate	0	1
10	V/C Dysplasia - severe	1	0
11	Carcinoma in situ	1	1
12	SCC Poorly differentiated	7	2
13	SCC Moderate differentiated	15	0
14	SCC Well differentiated	0	5
15	Control - Normal Squamous epithelium	10	0
16	Not used	0	0
17	Reactive lymph node	14	0
		74	9
			83

Variation in the histological classification of laryngeal disease has always been a concern particularly in the classification of dysplasia and carcinoma in situ and also in the assignment of the degree of differentiation of a squamous cell carcinoma. In this work the classification of the experimental tissue samples was even more challenging as it was done on H&E slides prepared from frozen sections. Table 4.5 shows an example of the classifications given by different consultants for a tissue sample were a disagreement exists. Overall the degree to which consultants agreed on the histological classification of specimens in the larynx study was excellent, 74 specimens out of 83 (89.1%) had complete agreement.

Table 4.5: Larynx study tissue samples were a disagreement in consultant histological classification exists.

Sample	Report	A	B	C	Consultant Consensus	Consultants Agree/Disagree	Count of Agree	Count of Disagree
10L1	7	7	7	7	7	All Agree	1	0
11L1	9	7	7	7	7	All Agree	1	0
11L2	7	7	7	7	7	All Agree	1	0
12L1	15	15	15	15	15	All Agree	1	0
12L2	15	15	15	15	15	All Agree	1	0
13L1	17	17	17	17	17	All Agree	1	0
13L2	17	17	17	17	17	All Agree	1	0
17L1	7	7	7	7	7	All Agree	1	0
17L2	7	7	7	7	7	All Agree	1	0
17L3	1	1	1	1	1	All Agree	1	0
18L1	1	1	1	1	1	All Agree	1	0
18L2	13	13	11	11	11	Someone Disagrees	0	1

The diagnosis of moderate dysplasia and carcinoma in situ evoked some disagreement as might have been expected. One specimen was classified by A as mild dysplasia whilst the other two consultants felt this to be moderate dysplasia. The operative specimen was classified as exhibiting moderate dysplasia. Of the two specimens the consensus classified as showing the presence of carcinoma in situ one was agreed on by all consultants and one specimen had a single consultant (A) disagreement were a classification of a moderately well differentiated squamous cell carcinoma (SCC) was

given. This classification was supported by the histology report of the main operative specimen.

Of the 9 samples classified by consensus as exhibiting features of poorly differentiated SCC seven were agreed by all consultants and 2 were classified by A as moderately differentiated SCC, the same classification as given in the main specimen histology report. Interestingly the histology reports for the main operative specimens correlating to the seven fully agreed experimental tissue samples were very interesting. Whilst two agreed with the consensus five did not and of these, the reports classified the main operative specimens as showing features of reactive lymph nodes in 4 cases, the presence of papilloma in one case.

The diagnosis of well differentiated squamous cell carcinoma was not agreed by all consultants for any of the samples. Table 4.6 shows the breakdown of consultant opinion. For all five samples two out of three consultants assigned a classification of well differentiated squamous cell carcinoma (SCC). The third consultant assigned a classification of moderately well differentiated SCC in 4 out of the five cases and poorly differentiated SCC for the remaining sample. Interestingly the reports from the operative specimen classified them all as showing moderately well differentiated SCC.

Table 4.6: Break down of the individual diagnoses for samples which ultimately had a consensus diagnosis of well differentiated squamous cell carcinoma in the larynx study.

Sample	Report	A	B	C	Consultant Consensus
24n5	13	13	14	14	14
23n1	13	12	14	14	14
23n10	13	13	14	14	14
23n12	13	13	14	14	14
23n13	13	13	14	14	14

In all cases of disagreement between consultants, apart from that of carcinoma in situ, the discrepancies between classifications was slight and related to the degree of expression of a disease and was not a disagreement in the fundamental nature of that change. In the single case of carcinoma in situ this also held true but rather than one degree of change between the consensus and the disagreeing consultant in this case the disagreement suggested the changes noted by the consultant were two degrees more advanced than the consensus classification. The view of the disagreeing consultant was upheld by the full histology report and as the patient treatment plan is always based on the histology report of the main specimen no under treatment resulted. The difference in the slide preparation between the experimental and main operative specimens may account from some differences in classification as might variation between the weights consultants put on certain histological features when assigning the degree of differentiation. Whilst consultants all reviewed the same slide for each experimental specimen the slides prepared from the main operative specimen will not have been prepared from exactly the same tissue. As the disease process may not be uniformly expressed over the whole of the diseased area variations in histology classification between the main operative specimen and the experimental specimens may arise. This is

particularly true where tissue samples were taken from large main operative specimen such as those obtained from total laryngectomy patients or where the tissue samples themselves were large, increasing the possibility of disease variance over the sample itself.

Table 4.7: Histopathology consultant majority consensus for lymph node study tissue samples.

Pathology Code	Name	Instances Consultants Agree with Consensus	Instances Consultants Disagree with their Consensus
1	Reactive Lymph node	55	0
2	Branchial cyst	0	1
3	Fibrous connective tissue	5	1
4	Normal squamous epithelium	8	0
5	Fat	0	0
6	Parotid salivary tissue	8	0
7	Normal thyroid tiassue	5	0
8	SCC - Poorly differenciated	6	0
9	SCC - Moderately differentiated	8	10
10	SCC - well differentiated	0	0
11	Adenocarcinoma	8	0
12	Pleomorphic adenoma	1	2
13	Poorly differentiated carcinoma	8	0
14	Thyroid - papillary carcinoma	0	5
15	Thyroid - follicular carcinoma	7	0
16	Hodgkin's lymphoma (HL) - mixed cellularity	2	0
17	HL - nodular sclerosing	4	0
18	HL - follicular cell	0	1
19	HL - classical lymphocyte predominant	4	0
20	HL - Non-classical	1	1
21	Non-Hodgkin's lymphoma (NHL) - diffuse large B ce	8	0
22	NHL - Low grade malignant	0	0
23	NHL - MALT type	0	0
	CheckSum	*138*	*21*
			159

The consensus between the consultants who reviewed the H&E slides of the frozen section specimens entered into the lymph node study was also excellent; 138 samples out of 159 (86.8%) had complete agreement. Most tissue samples included in this study were larger than those in the larynx study. The homogenicity of the samples and hence H&E slides of the lymph node study specimens were also better. The diseases present in the tissue samples used in the lymph node study do not tend to show the same step wise progression from normal to invasive cancer that SCC of the larynx shows and all these points would suggest that the consensus for the lymph node study should be better than that for the larynx study.

There are some general difficulties in the classification of the type of specimens used in the lymph node study which might explain the slightly poorer consensus result. Lymphoma frozen sections are notoriously difficult to interpret and are in fact never used as a definitive diagnostic technique for these diseases. The classification of moderately differentiated SCC showed some disagreement between consultants and this is summarised in Table 4.8. In all these samples the diagnosis of SCC was made but it was in the classification of the degree of tumour call differentiation that differences arose. This is a common occurrence and reflects the subjective nature of the histological classification process. In the one case were there was no agreement between any consultant; the full report on the operative specimen confirmed the presence of moderately differentiated SCC. In the other cases the diagnosis was still one of SCC but

classification of the degree of differentiation assigned was different. In six samples one consultant made a classification of poor differentiation in four cases a single consultant thought the samples well differentiated. In the latter case the full histology reported moderately differentiated SCC whilst for the former the report classified the disease as poorly differentiated. Whilst the prognosis of the patient may be affected by the degree of differentiation of tumour cells the initial treatment plan for these patients would not have been altered.

Table 4.8: Majority consensus for lymph node study tissue samples classified as moderately differentiated SCC but where a disagreement in classification exists.

Sample	Report	A	B	C	Consultant Consensus
22n10	8	9	9	8	9
22n11	8	9	9	8	9
22n12	8	9	9	8	9
22n2	8	9	9	8	9
22n9	8	9	9	8	9
23n12	8	9	9	8	9
3n2	9	9	10	9	9
3n3	9	9	10	9	9
3n4	9	9	10	9	9

The consensus relating to classification of thyroid tissue was very interesting. In the 5 cases classified by consensus as papillary carcinoma one case was reported by pathologist A as poorly differentiated carcinoma and this classification agreed with that given for the main operative specimen. In the four other cases where a consultant disagreed with the consensus the classification was by consultant B who felt the samples possibly represented a pleomorphic adenoma. These tumours are aggressive locally invasive neoplasias usually affecting the parotid gland in the head neck. The main histology for these 4 specimens classified 3 of them as papillary carcinoma and one as a normal lymph node. The latter classification suggests that the section of the operative specimen examined was of a normal lymph node however the diagnosis was not missed as the large specimen had multiple areas examined and the diagnosis of papillary carcinoma was made from these. Some tissue in or near the parotid was entered into the study from a formal parotidectomy. The full histology report classified this tissue as showing a pleomorphic adenoma in two cases and in one as showing fat. Two consultants felt that two samples showed a pleomorphic tumour in all three cases. One consultant thought this true of one of the samples and that the other two showed features of a poorly differentiated carcinoma. Table 4.9 shows the consensus classification result for the samples designated as pleomorphic adenoma.

Table 4.9: Samples classified as pleomorphic adenoma by majority consensus in lymph node

Sample	Report	A	B	C	Consultant Consensus
19L1a	12	13	12	12	12
19L1b	12	13	12	12	12
2L2	5	12	12	12	12

The degree to which the consultants were able to reach full agreement was recorded using pivot tables and the results have been illustrated in Figures 4.1, 4.2, 4.3 and 4.4 in the form of histograms. Percentage plots have been shown but it is noted that in some cases actual pathology numbers are small.

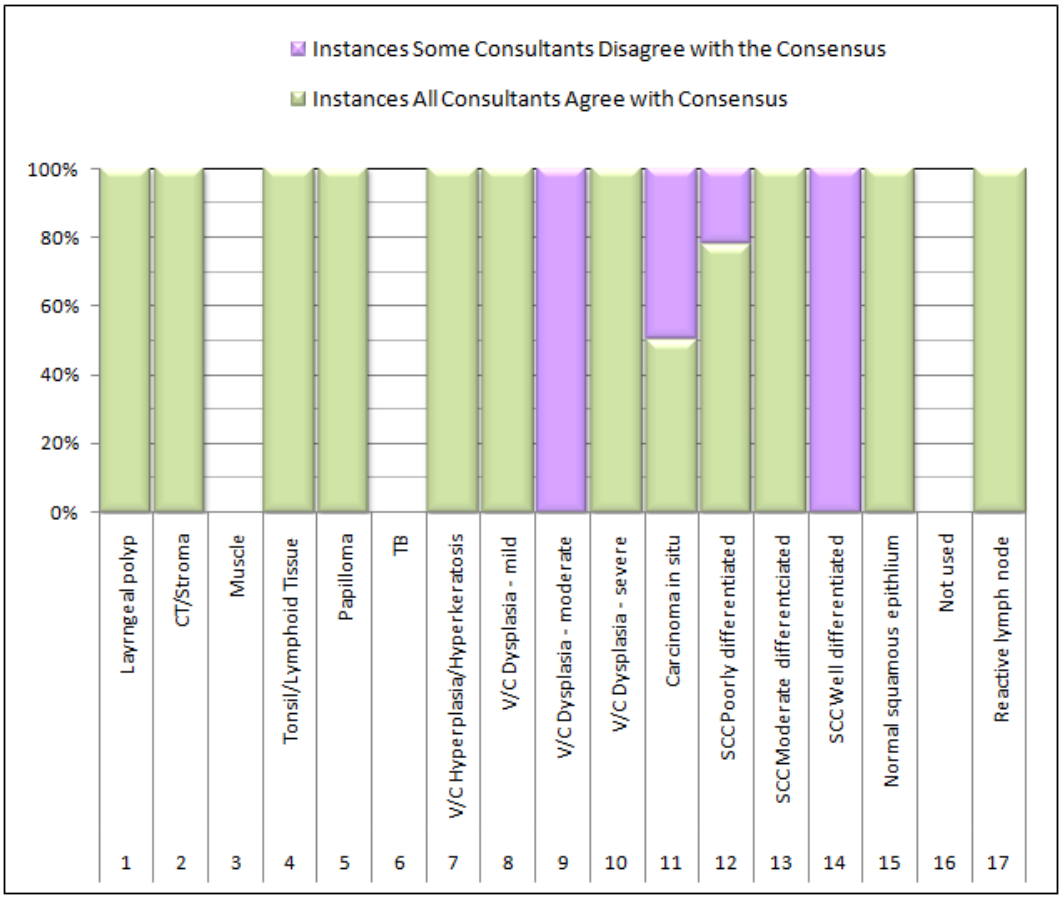

Figure 4.1: Consultant consensus for histopathological classification of tissue specimens in the larynx study - expressed as a percentage.

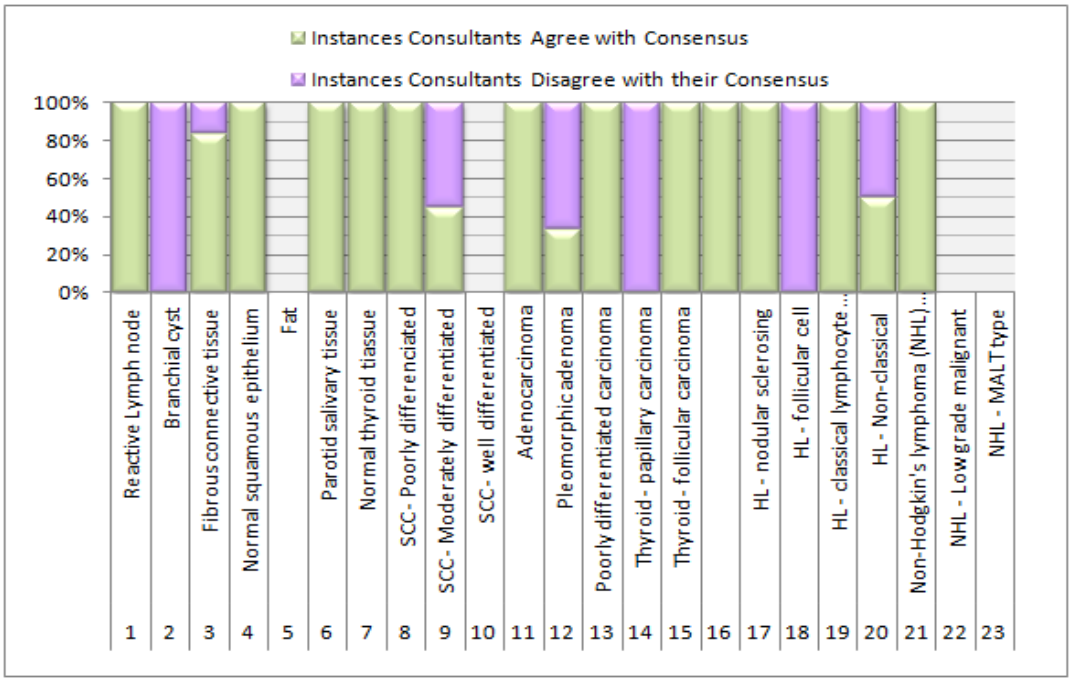

Figure 4.2: Consultant consensus for histopathological classification of tissue specimens in the lymph node study - expressed as a percentage.

4.1.2 Results and Discussion –Comparison of consultant consensus and histopathology report issued for main operative specimen.

The histopathological classification assigned to the main operative specimen was obtained and a comparison made to the histopathology consultant majority consensus for the experimental tissue samples for both the larynx and lymph node studies.

The larynx study dataset contained tissue samples unrelated to the main operative specimen (pathology codes 7 and 15/study group 5) and so no meaningful comparison could be made between the consultant consensus and the histology report for the main operative specimen for these larynx samples. In order to make a valid comparison of the consensus histology and the operative specimen histology reports these tissue samples were removed from the analysis for this section only. For the larynx the consultant consensus agreed with the main histology report in 40 out of 53 specimens (75.5%) and in the lymph node study in 115 out of 159 samples (72.3%).

Tables 4.10 and 4.11 compare the agreement/disagreement between consultant consensus and main specimen histology report. Figure 4.3 compares the agreement/disagreement between consultant consensus and main specimen histology report expressed as a percentage for the larynx study patients. Figure 4.4 does this for the lymph node study. In some cases where there was also a disagreement within the consultant consensus comments and discussion relating to these samples may have already been included in *Section 4.1.1.* Agreement between the consensus and the histology report for the main operative specimen is, as expected much lower that for that of the consensus alone. The most obvious problem is that the full histology report is based on the review of slides that may not have any direct spatial relation to the samples

taken for consensus review. This is more of a problem where the operative specimen is large but does highlight a difficulty for both traditional histology and Raman spectroscopy. How do we ensure that enough of the specimen is reviewed to ensure no areas of disease are missed? In histology large number of slides are prepared and reviewed which is enormously time consuming, expensive and potentially open to error. In Raman spectroscopy probing at depth is still a problem, as is limitation of speed that makes the scanning of areas in real time clinically challenging. For small areas of disease such as those found on vocal cord this may be less of a problem but if Raman spectroscopy was applied to large pieces of tissue which might only contain foci of disease then these concerns increase.

Table 4.10: Comparison between consultant consensus and histopathology report issued on main operative specimens in larynx study.

Pathology Code	Name	Instance Consultant Consensus Agrees with Report	Instance Consultant Consensus Disagrees with Report
1	Laryngeal polyp	2	0
2	CT/Stroma	0	3
3	Muscle	0	0
4	Tonsil/Lymphoid Tissue	5	1
5	Papilloma	1	0
6	TB	0	0
8	V/C Dysplasia - mild	0	1
9	V/C Dysplasia - moderate	1	0
10	V/C Dysplasia - severe	0	1
11	Carcinoma in situ	1	1
12	SCC Poorly differentiated	4	5
13	SCC Moderate differentiated	9	6
14	SCC Well differentiated	0	5
16	Not used	0	0
17	Reactive lymph node	6	8
		29	31
			60

With smaller areas of tissue it would have been expected that the consensus and main reports might be more in agreement for the larynx rather than for the lymph node study however this is not the case and it appears that two reasons are the difficulties in classifying dysplasia and differentiation of SCCs. For the three cases the consensus classified as connective tissue/stroma the full histology picked up a poorly differentiated squamous cell carcinoma. This case was carefully reviewed and the two sets of slides had quite different appearances and SCC was not thought to appear in the study slides so no adverse clinical incident occurred. The one case of discrepancy relating to tonsil/lymphoid tissue showed that the main specimen whist containing lymphoid tissue also had sections showing normal squamous epithelium. The cases of severe dysplasia and carcinoma in situ reported by consensus that did not agree with the full histology report did so because full histology classified them as moderately well differentiated SCC. Severe dysplasia and carcinoma in situ are difficult to assess and often there is great debate as to the best way forward clinically, treat/intervention or a watchful waiting approach. If the latter were adopted these patients would often undergo repeat endoscopy and likely biopsy usually within a few weeks of the original procedure. The treatment of moderately differentiated SCC is very different and requires significant

surgery so this difference in opinion for these cases has real clinical significance and is an example of the diagnostic difficulties were grades of disease can coexist. All samples classified by consensus as showing moderately differentiated SCC and this disagreeing with report was because the report graded the tumour as a poorly differentiated SCC.

The lymph node specimens included in the larynx study were obtained from en bloc laryngectomy dissections and where a discrepancy exists this is due to the slides used in the study being from different areas of the large specimen compared to the ones used for the main report and in some cases the level at which the lymph node was obtained was reported as containing reactive lymph nodes where the main specimen showed SCC.

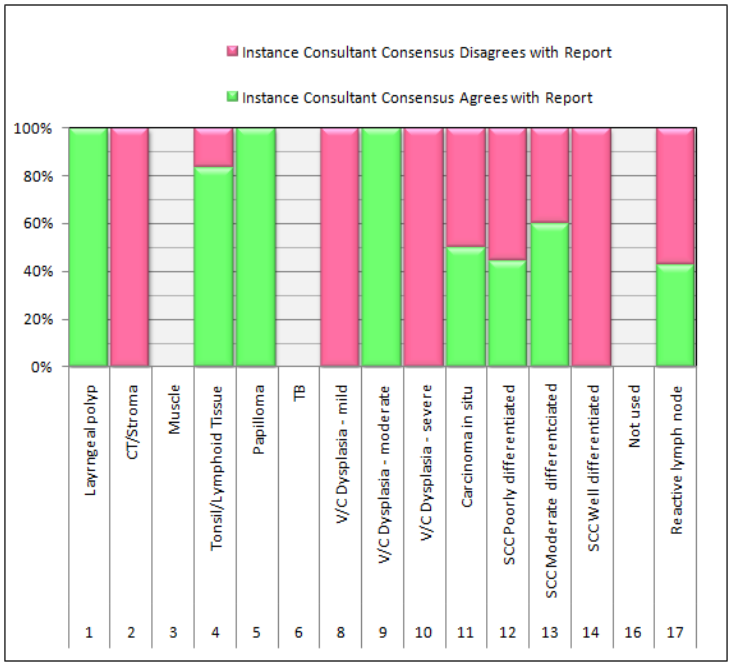

Figure 4.3: Comparison between consultant consensus and histopathology report issued for main specimens in larynx study - expressed as a percentage.

One of the very interesting points to note in relation to the consensus and its agreement with the reported main histology in the lymph node study is the surprising degree of accuracy the consensus shows for the diagnosis of lymphomas. As discussed the pathologists involved in reporting the consensus slides would never rely on them for a firm diagnosis but it is a reflection of their clinical judgement and experience that they had such good agreement when pressed hard to give their 'best guess.' In the case of fat as a consensus all samples were reported by full histological examination as either showing lymph node or a SCC and this is a reflection of different tissue sampling. The disagreements between consensus and main histology report relating to the thyroid tissue have been discussed in *Section 4.1.1* as have the disagreements relating to classification of SCCs. It is important clinically to note that there was a large disagreement for samples classified by consensus as reactive lymph nodes. The main histology specimens showed these patients as having lymph nodes at the same level as

the study samples positive for poorly differentiated SCC (4), moderately differentiated SCC (1), NHL (1) and Hodgkin's' lymphoma in one case. No complete lymph nodes were taken from the main specimens and these finding confirm that in these cases, other than the lymphomas, that lymph nodes either contained foci of disease or that some nodes at these levels did not contain disease.

Table 4.11: Comparison between consultant consensus and histopathology report issued for main operative specimens in lymph node study.

Pathology Code	Name	Instance Consultant Consensus Agrees with Report	Instance Consultant Consensus Disagrees with Report
1	Reactive Lymph node	44	9
2	Branchial cyst	1	1
3	Fibrous connective tissue	2	3
4	Normal squamous epithelium	2	0
5	Fat	0	2
6	Parotid salivary tissue	7	0
7	Normal thyroid tiassue	5	0
8	SCC - Poorly differenciated	2	17
9	SCC - Moderately differentiated	12	1
10	SCC - well differentiated	0	0
11	Adenocarcinoma	8	0
12	Pleomorphic adenoma	2	0
13	Poorly differentiated carcinoma	8	1
14	Thyroid - papillary carcinoma	3	7
15	Thyroid - follicular carcinoma	0	0
16	Hodgkin's lymphoma (HL) - mixed cellularity	2	1
17	HL - nodular sclerosing	4	0
18	HL - follicular cell	1	0
19	HL - classical lymphocyte predominant	4	0
20	HL - Non-classical	0	0
21	Non-Hodgkin's lymphoma (NHL) - diffuse large B ce	8	0
22	NHL - Low grade malignant	0	0
23	NHL - MALT type	0	2
	CheckSum	*115*	*44*
			159

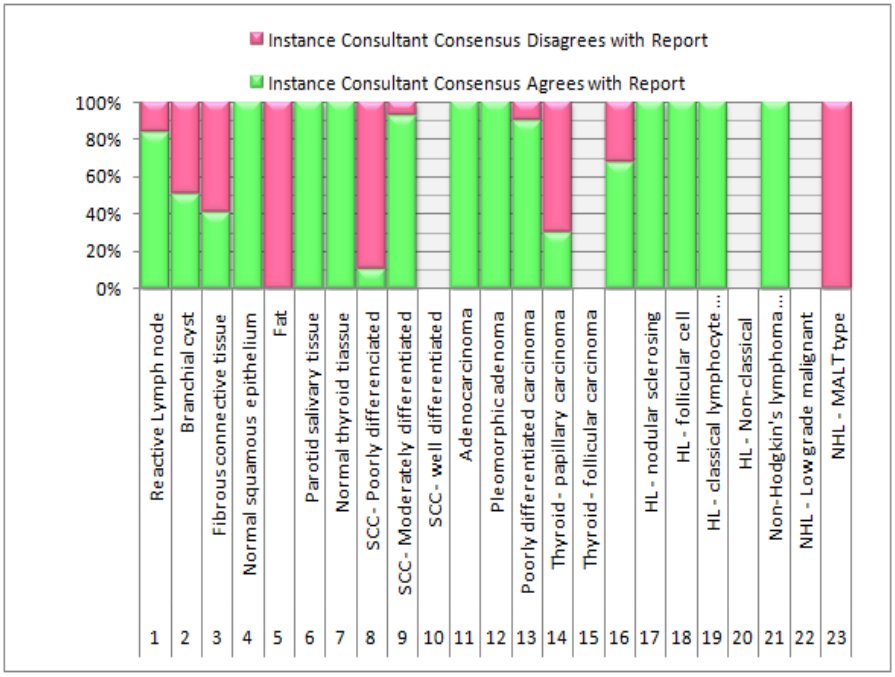

Figure 4.4: Comparison between consultant consensus and histopathology report issued for main specimens in lymph node study - expressed as a percentage.

4.2 Larynx Study

4.2.1 Data summary

The tissue sample dataset for the larynx study is summarised in Table 4.12. The number of patients recruited the number of samples with specific histopathology classifications and the numbers of spectra obtained are recorded.

39 patients were recruited to the larynx study and from these patients 83 tissue samples were collected. In total 2422 individual point spectra were obtained. The mean number of spectra obtained from a sample being 29 (range 11 to 44).

Tissue samples were each assigned to a pathology group. Pathology group 6 contained only specimens thought to be infected with TB. These specimens were not used as facilities for the processing of this type of sample were not available. A sample of muscle yielded no useful spectra as it was inadvertently defrosted and degraded as a result. No samples were assigned to group 16 which was held as a ‘spare’ assignment throughout the analysis incase a more detailed breakdown of a pathology group was required. The pathology classifications were subdivided as far as possible in order to facilitate more detailed Raman modeling as the dataset is expanded.

Table 4.12: Numerical data for individual pathology coded specimens in larynx study.

Pathology Code	Description	Number of Patients	Number of Samples	Number of Spectra	Average Spectra per Sample	Average Spectra per patient
1	Laryngeal polyp	*1*	*2*	*63*	*31.5*	*63.0*
2	CT/Stroma	*1*	*3*	*59*	*19.7*	*59.0*
3	Muscle	*0*	*0*	*0*	*0.0*	*0.0*
4	Tonsil/Lymphoid Tissue	*3*	*6*	*185*	*30.8*	*61.7*
5	Papilloma	*1*	*1*	*28*	*28.0*	*28.0*
6	TB	*0*	*0*	*0*	*0.0*	*0.0*
7	Controls - Hyperplasia/Hyperkeratosis	*9*	*13*	*341*	*26.2*	*37.9*
8	V/C Dysplasia - mild	*1*	*1*	*26*	*26.0*	*26.0*
9	V/C Dysplasia - moderate	*1*	*1*	*11*	*11.0*	*11.0*
10	V/C Dysplasia - severe	*1*	*1*	*41*	*41.0*	*41.0*
11	Carcinoma in situ	*2*	*2*	*49*	*24.5*	*24.5*
12	SCC Poorly differentiated	*5*	*9*	*302*	*33.6*	*60.4*
13	SCC Moderate differentiated	*4*	*15*	*517*	*34.5*	*129.3*
14	SCC Well differentiated	*1*	*5*	*219*	*43.8*	*219.0*
15	Controls - Normal squamous epithelium	*4*	*10*	*251*	*25.1*	*62.8*
16	Not used	*0*	*0*	*0*	*0.0*	*0.0*
17	Reactive lymph node	*5*	*14*	*330*	*23.6*	*66.0*
		39	83	2422		

The number of laryngeal mucosal specimens is small compared to the number of specimens used in the lymph node study (83 to 159). In particular there is only one sample classified as showing each of the dysplasias and 5 samples from one patient which contained well differentiated SCC. Two patients gave one sample each of carcinoma in situ. This is a reflection of the throughput of patients requiring microlaryngoscopy and biopsy, time pressure on the operating lists and the nature of the operation meant only very small sample numbers could be obtained from a single patient. In the lymph node study larger neck dissection specimens often afforded the opportunity to retrieve multiple lymph nodes from a single patient. These specimens were generally larger and easier to handle affording less wastage during processing.

Matlab scripts were written to combine sets of pathology codes into study groups (SGs). For example pathology codes 12, 13 and 14 all define SCCs, however pathology code 12 is used to describe those specimens which are poorly differentiated; 13 moderately well differentiated and 14 well differentiated. Combined these three pathology codes make up study group 1 (SG1). A summary of the pathology codes which make up the sixteen study groups is contained in Table 4.13.

Table 4.13: Numerical data for combinations of pathology codes used to form larynx study groups.

Study Group	Description	Pathology Codes	Number of Patients	Number of Samples	Number of Spectra
1	SCC	12,13,14	*10*	*29*	*1038*
2	Mild Dysplasia	8	*1*	*1*	*26*
3	Controls - Hyperplasia Hyperkeratosis	7	*9*	*13*	*341*
4	Non-malignant	1,2,3,4,5,6,7,8,9, 10,11,15,17	*29*	*54*	*1384*
5	All Controls	7,15	*13*	*23*	*592*
6	Moderate Dysplasia	9	*1*	*1*	*11*
7	Abnormal Mucosa	8,9,10,11	*5*	*5*	*127*
8	Severe Dysplasia	10	*1*	*1*	*41*
9	Carcinoma in Situ	11	*2*	*2*	*49*
10	Controls - Normal squamous epithelium	15	*4*	*10*	*251*
11	SCC Poorly differentiated	12	*5*	*9*	*302*
12	SCC Moderately differentiated	13	*4*	*15*	*517*
13	SCC Well differentiated	14	*1*	*5*	*219*
14	Dysplasic Mucosa	8,9,10	*3*	*3*	*78*
15	Cleaned SCC Well differentiated	01	*1*	*5*	*212*
16	SCC + Abnormal Mucosa	12,13,14,8,9, 10,11	*15*	*34*	*1165*

A comparison between different study groups forms the basis of the larynx study mini-models, Table 4.14 summarises which SGs are used in each one. The models are used to work systematically through the different options for comparing pathology groups and the rational for investigating each one is summarised in the results section for that model.

Appendix D contains tables and figures relating to results from the larynx studies. A summary sheet of the makeup of the different mini-models can be found in *Appendix D.2*.

The organization of the lymph node study dataset has been done in a similar way as for the larynx.

Table 4.14: Laryngeal mini models – a comparison between different study groups.

Mini Model	Description	Study Group	Description	Study Group	Description	Study Group	Description	Study Group
L1	SCC	**1**	Non-malignant	**4**				
L1-1	SCC+Abnormal Mucosa	**16**	All Controls	**5**				
L2a	SCC	**1**	All Controls	**5**				
L2b	Controls - Hyperplasia Hyperkeratosis	**3**	Controls - Normal Sq epithelium	**10**				
L2c	SCC	**1**	All Controls	**5**	Abnormal Mucosa	**7**		
L2c-1	SCC	**1**	Controls - Hyperplasia Hyperkeratosis	**3**	Abnormal Mucosa	**7**		
L2c-2	SCC	**1**	Controls - Normal Sq epithelium	**10**	Abnormal Mucosa	**7**		
L2c-3	SCC	**1**	Controls - Normal Sq epithelium	**10**	Displastic Mucosa	**14**		
L3	Mild Dysplasia	**2**	Moderate Dysplasia	**6**	Severe Dysplasia	**8**	Carcinoma in Situ	**9**
L4	Carcinoma in Situ	**9**	SCC Poorly Differentiated	**11**	SCC Moderately Differentiated	**12**	SCC Well Differentiated	**13**
L4-1	SCC Well Differentiated	**13**	Controls - Hyperplasia Hyperkeratosis	**3**				
L4-2	Carcinoma in Situ	**9**	SCC Poorly Differentiated	**11**	SCC Moderately Differentiated	**12**	Cleaned SCC Well Differentiated	**15**

4.2.2 Pathology overview

4.2.2.1 Normal laryngeal tissue

The spectrum obtained from normal laryngeal mucosa is seen in Figure 4.5 and the main spectral peaks are summarised in Table 4.15. Many of the peak assignments are the same as those published previously (Stone, 2002). There are peaks which are present in both studies but which are very small (780, 1048, 1172, 1386 and 1617cm^{-1}). Peaks which cannot be seen in Figure 4.5 but are noted by Stone et al are positioned at 725, 899, 920, 1228, 1314, 1560, 1583, and 1601cm^{-1}. No clear pattern emerges to explain these omissions. The peaks may in the spectrum obtained during this work but better resolution of the SG10 mean normalised spectrum may be needed to see them, also some variations in the Controls - 'normal' squamous epithelium spectra are noted, this is more fully discussed in *Section*.4.2.3.4. One point is noted, the peak at 480 cm^{-1} attributed to glycogen is less prominent in the spectra of ' normal' laryngeal mucosa compared to that of normal oesophagus or cervix.

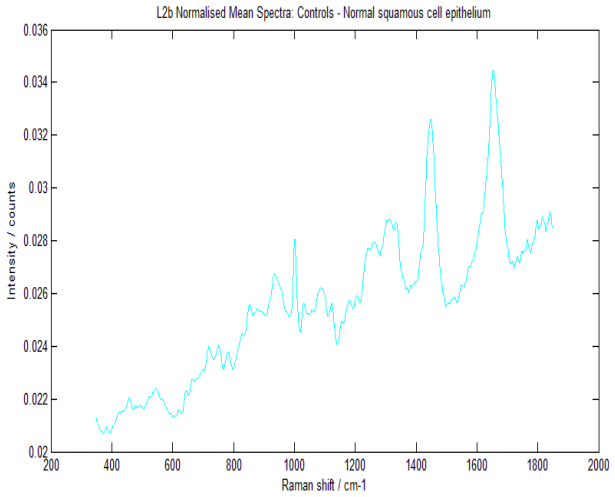

Figure 4.5:.Raman spectra of 'normal' laryngeal mucosa.

Table 4.15: Main spectral peak assignments for normal laryngeal mucosa (SG10).

SG10	Peak postion cm^{-1}	Major Assignments
Group10.1	421	δCCC
Group10.2	457	no assignment
Group10.3	547	Cholesterol
Group10.4	618	Phenylalanine (amino acid)
Group10.5	643	ν(C-S). Amine IV
Group10.5	643	Tyrosine
Group10.6	663	C-S stretching mode of cystine
Group10.7	719	Nucleotides
Group10.8	752	? Symmetric breathing of tryptophan
Group10.9	782	Cytosine ring breathing, ?Nucleotides
Group10.10	827	δ(CCH) aliphatic - (human strateum corneum)
Group10.11	851	Tyrosene (amino acid), δ(CCH) aromatic - (human strateum corneum)
Group10.12	878	Tryptophan (amino acid)
Group10.13	935	CH_3 rocking, C-C stretch α helix keratin - (strateum corneum)
Group10.14	1002	?(C-C) aromatic ring
Group10.14	1002	(C-C) skeletal vibrations, β sheet
Group10.14	1002	Tyrosene
Group10.14	1002	? ν(CC) aromatic ring stretch of phenylalanine residue in keratin
Group10.14	1002	Symmetric ring breathing mode of phenylalanine
Group10.15	1030	Collagen
Group10.15	1030	?ν(CC) skeletal cis conformation (human strateum corneum)
Group10.15	1030	?(C-C) keratin (strateum corneum)
Group10.16	1058	DNA backbone C-O stretch
Group10.17	1086	C-C stretch, PO_2 stretch (in phospholipids)
Group10.18	1124	C-N stretching mode of proteins
Group10.19	1154	C-N stretching mode of proteins (also carotenoid mode)
Group10.20	1180	Tyrosine
Group10.20	1180	Cytosine, guanine, adenine
Group10.21	1205	Tyrosine + Phenylalanine
Group10.22	1241	Amine III - ν(C-N) (β pleated sheet protein)
Group10.23	1304	CH_3CH_2 twisting
Group10.24	1337	Nucleic acid, purine bases (adenine, guanine)
Group10.25	1448	CH_2 deformation
Group10.25	1448	CH_2 scissoring (strateum corneum)
Group10.26	1529	Carotenoid
Group10.27	1547	Tryptophan
Group10.28	1572	? Nucleotides
Group10.29	1653	C=C vibrations (phospholipid membrane)
Group10.29	1653	Amine I, ν(C=O) (human skin)
Group10.29	1653	?(C-O) Amide I, α helix (strateum corneum)
Group10.30	1733	no assignment
Group10.31	1766	?ν(COO) (human strateum corneum)
Group10.32	1797	no assignment
Group10.33	1816	no assignment
Group10.34	1840	no assignment

4.2.2.2 Normalised spectra for single pathology codes

Figure 4.6 is a plot of all the normalised spectra for a single pathology code i.e. tissue type. In this case tissue classified histologically by majority consensus as showing features of severe dysplasia (pathology code 10). The corresponding plots for the other pathology codes can be found in *Appendix D.1*.

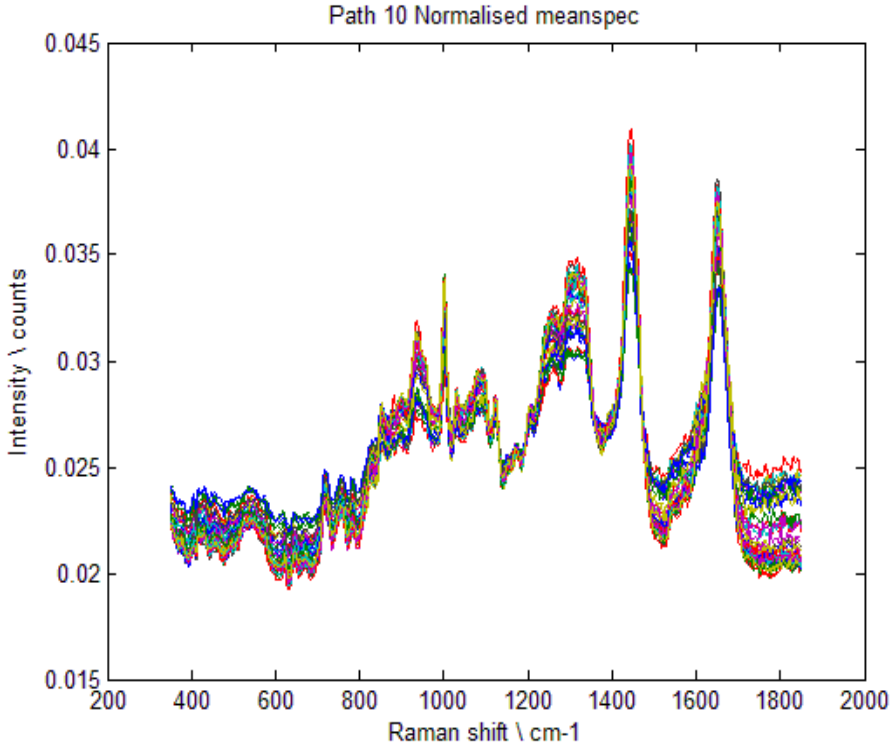

Figure 4.6:Normalised mean spectra for larynx study group 10 – normal vocal cord squamous epithelium.

There are some interesting simple features seen in these plots. Data sets containing small numbers of spectra become obvious and the degree to which the spectra vary across their mean can be seen. To the experienced reviewer the sharpness and overall shape of some peak groups can give an idea as to the proportion of certain molecular constituents within a sample. Some plots show spectra that do not appear to fit the norm; for example in the plot for pathology group 13 (*Appendix D.1*). Here a single spectrum (red) stands out but prompted by unexpected findings in mini model L4 a closer examination showed other features which are discussed in the results section for this mini model.

4.2.2.3 Normalised mean spectra for all study groups

Figure 4.7 shows the normalised mean spectra for each of the study groups on one graph. Figure 4.8 the same plot but for SGs 4, 8 and 12 only, a review of this figure allows a very general assessment of the variation between the spectra and some interesting features have been noted. Even taking into account variations in the spectra baseline the relative ratios of some peaks appear quite different. When the two most

prominent peaks at 1444cm^{-1} and 1650cm^{-1} are considered it can be seen that the spectra from study groups 4, 8 and 12 exhibit different peak intensity ratios.

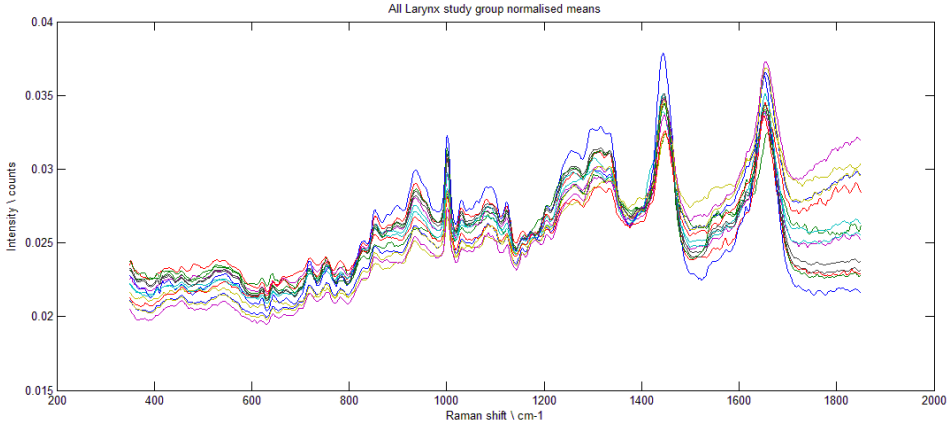

Figure 4.7:Normalised mean spectra for each larynx study group.

To clarify this section of the spectra has been magnified (Figure 4.9). The peak intensities at these wavenumbers for SG4 (non malignant tissue) appear to be very similar. For SG8 (severe dysplasia) the peak intensity at 1444cm^{-1} is greater than that for the peak at 1651cm^{-1} and this is reversed for SG12, poorly differentiated SCC. To be rigorous it is the difference in the PIRs that should be considered for each study group spectral pair. For each peak these are measured from a line between the two adjacent troughs rather than the x axes. The PIR values for these peaks are recorded in Table 4.16. Whilst the absolute peak intensities, read from the x axis in Figure 4.9, for SG4 appear almost equal the difference in the relative PIRs is quite large. This reemphasises the need to use PIRs for this type of paired comparison to minimise the error associated with factors such as baseline variation.

Table 4.16: Laryngeal mini models – a comparison between different study groups.

Column1	1444cm^{-1}	1651cm^{-1}
PIR - SG4	37.15	33.69
PIR - SG8	31.47	30.54
PIR - SG12	17.85	18.51

It can also be seen that the peaks in the spectra for SG 12(SCC) appear to be slightly shifted to the right, 1444cm^{-1} to 1446cm^{-1} and 1651 to 1655cm^{-1}. There can be slight variation in the placement of the peak wavenumber assignment cursor when attaining these wavenumbers but the value of simply looking at the spectra when magnified as in Figure 4.9 is that it is clear that the spectrum for SG12 is genuinely offset slightly to the right. This is interesting in that the tissue samples involved were not measured together but on different days and randomly selected for acquisition of their spectra. The change may be a reflection of a change in secondary structure form α helix to ß pleated sheet/random coil as might be expected in cancer cells.

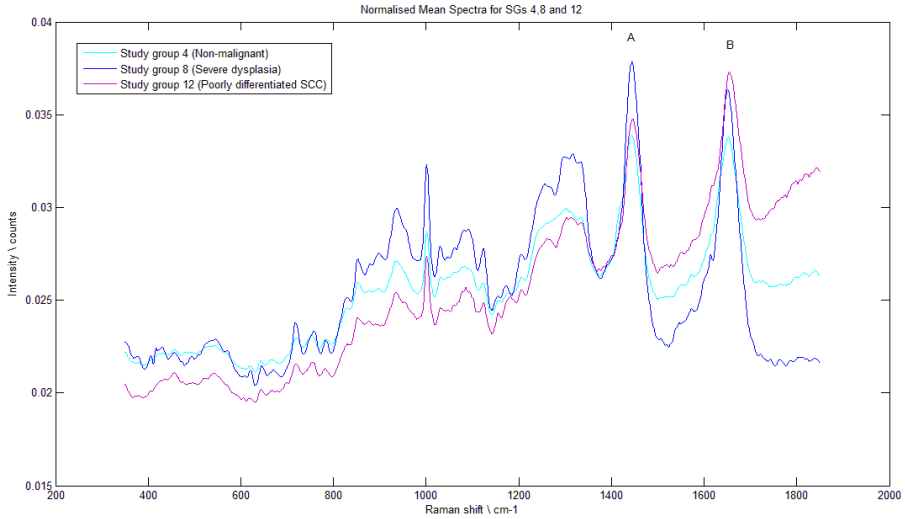

Figure 4.8:Normalised mean spectra for larynx study groups 4, 8 and 12.

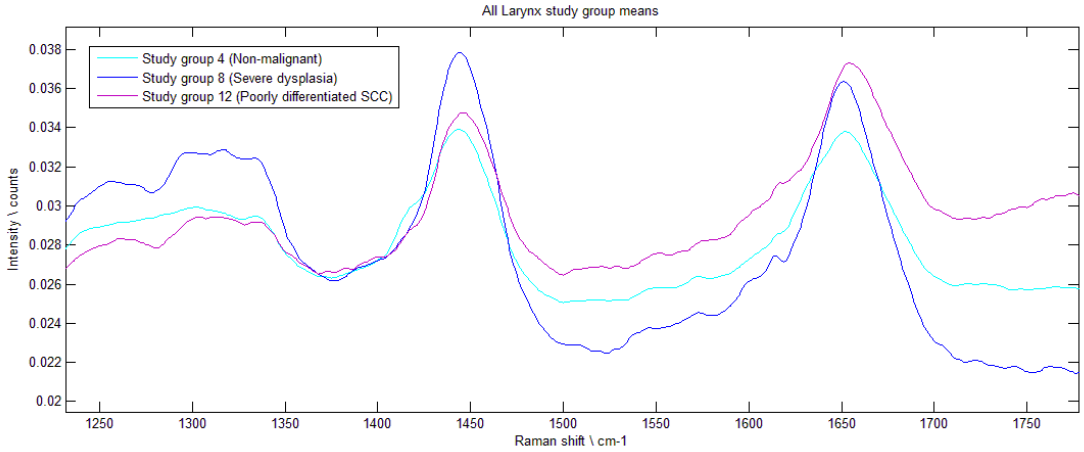

Figure 4.9:.Magnified normalised mean spectra for larynx study groups 4, 8 and 12.

4.2.3 Diagnostic models

4.2.3.1 L1 - SCC/Non-malignant tissue (SG1/SG4)

Empirical analysis

Figure 4.10 shows the normalised mean spectra for the two study groups examined in this model, their difference spectrum is shown beneath. Figure 4.11 contains two plots; the normalised mean spectra from both study groups overlaid and the difference spectra obtained from them is placed adjacent. Figure 4.11 has been included in addition to Figure 4.10 in order to show the development of the study from the simple normalised mean spectra. The difference spectra for all the larynx mini models can be found in *Appendix D.3.*

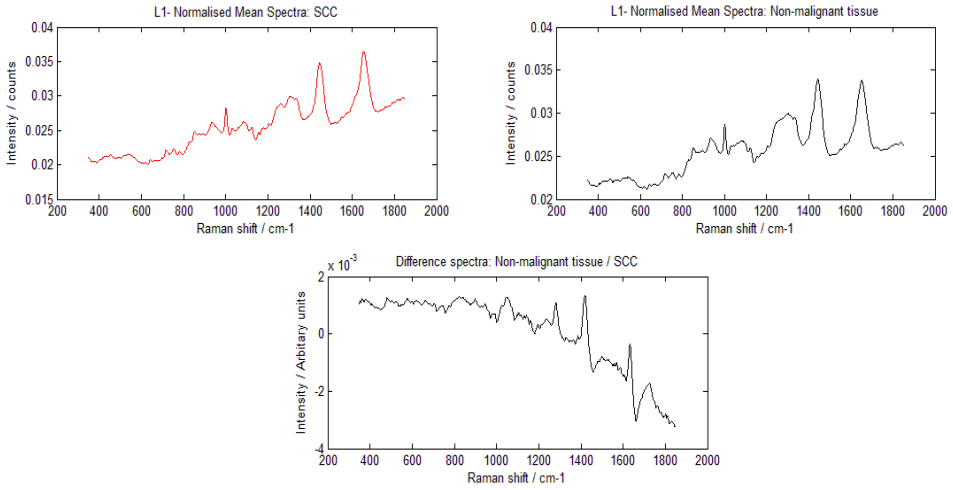

Figure 4.10: L1 - Normalised mean and difference spectra for SCC and non malignant tissue (SG1/SG4).

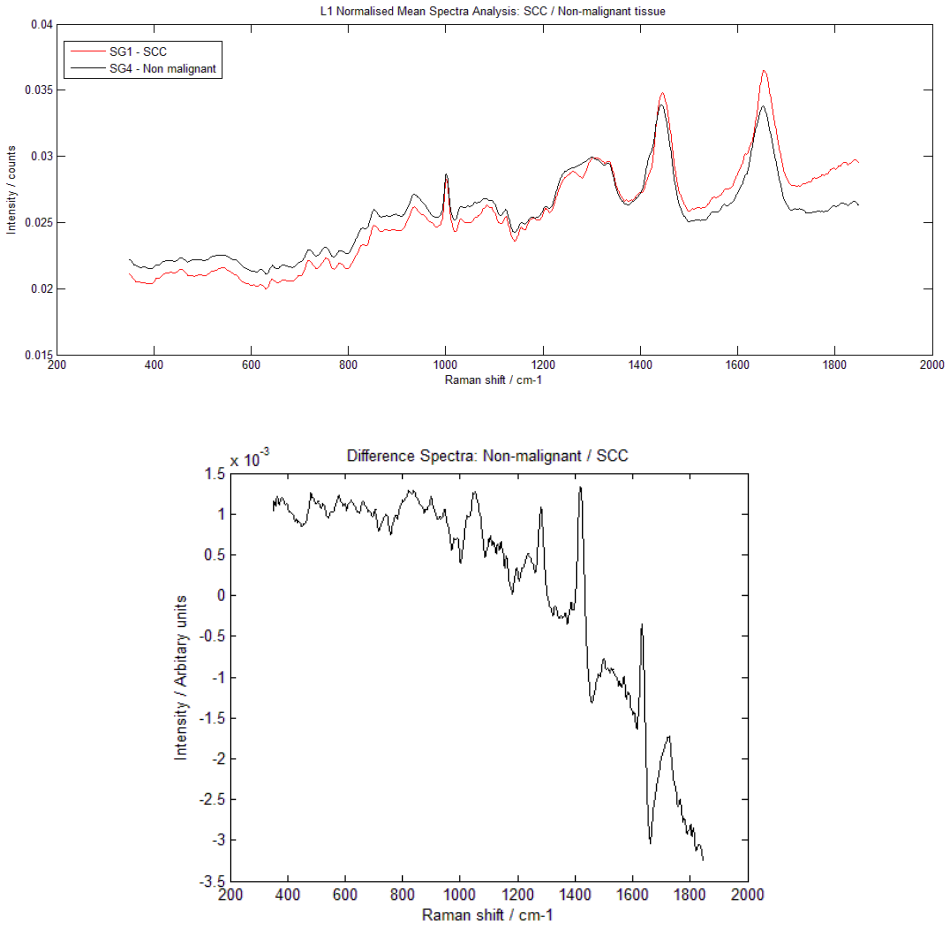

Figure 4.11: L1 – Overlaid normalised mean and difference spectra.

The wavenumbers of major peaks present in the normalised mean spectra of each study group were recorded with the corresponding peak intensities and areas, these data sets can be found in *Appendix D.5*. Those peaks which occurred in all study groups within a particular mini model where separated out and the ratios of their peak intensities and areas calculated. The peak with the lowest wavenumber was used as the reference point from which all ratios were calculated. For each shared peak the two PIRs were subtracted to examine the degree to which the peak intensities and areas differed across the groups. Figure 4.13 shows these results as a histogram.

Whilst the changes in the ratios of peaks is very interesting and gives objective evidence as to possible biochemical differences in the tissue samples from each group, of equal importance is the presence of isolated peaks not shared between study groups. This data is also recorded in *Appendix D.5.1*. Figure 4.14 records the difference in the area ratios superimposed on those of peak intensity and the same pattern is seen for both variables. This finding was consistent for all mini models and so only the variation in peak intensities ratios is discussed.

Biochemical assignments, based on wavenumber, were given to the peaks where differences in peak intensity ratio existed in order to investigate the possible biochemical differences that might exist between the study groups. The main spectral peaks for individual SGs can be found in *Appendix D.4* and a comparison between them for the SGs in each mini model, highlighting shared and unique peaks, in *Appendix D.5*.

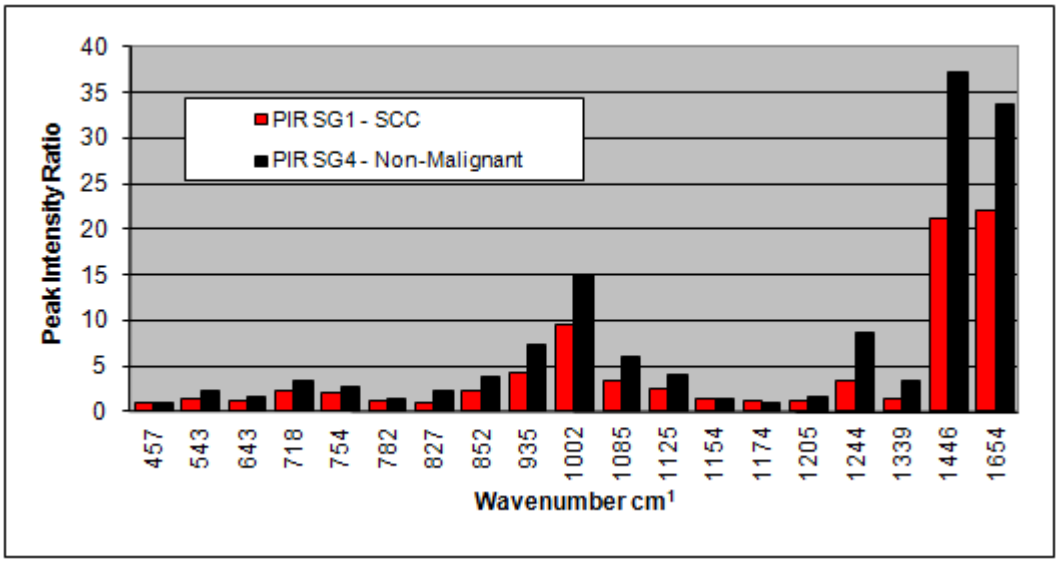

Figure 4.12: L1 – Peak intensity ratios for Study Groups 1 and 4.

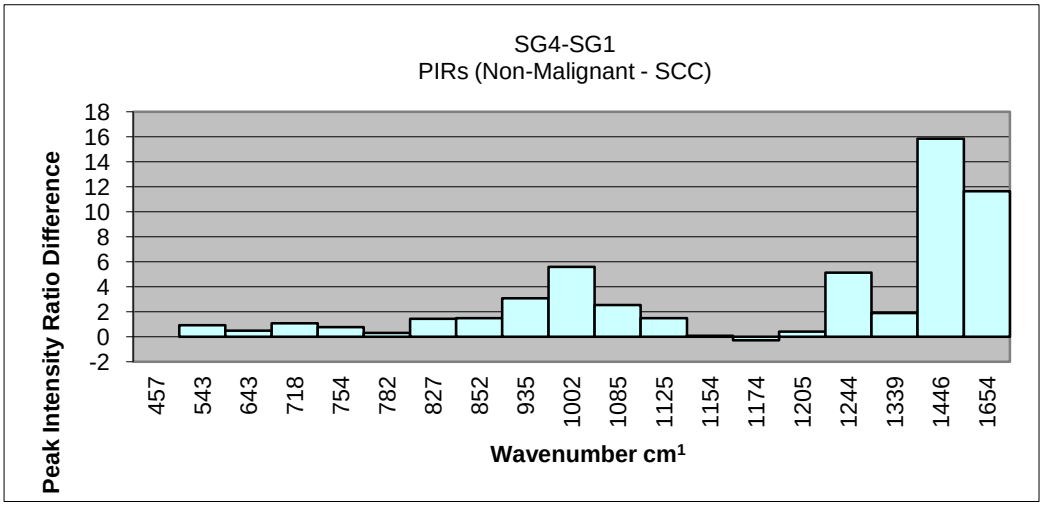

Figure 4.13: L1 – Differences in peak intensity ratios for Study Groups 1 and 4.

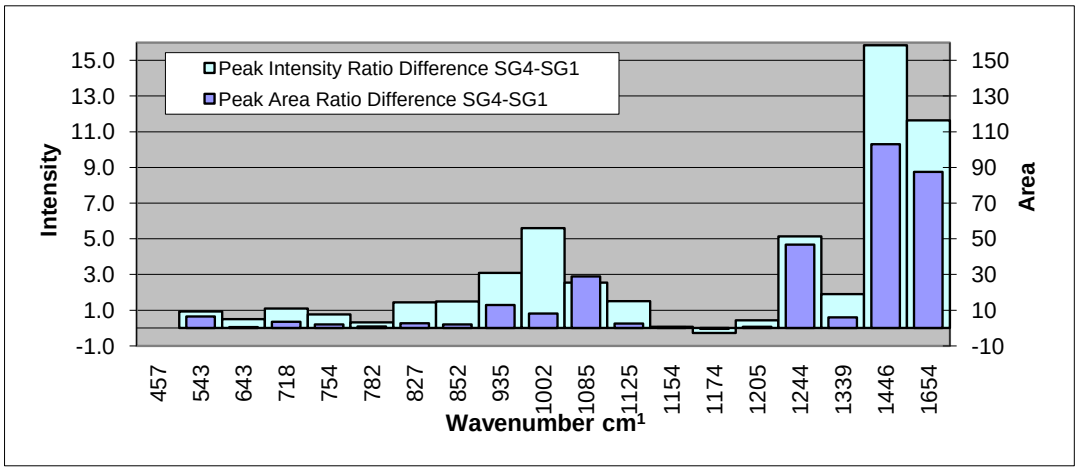

Figure 4.14: L1 – Differences in peak intensity and area ratios for Study Groups 1 and 4.

Multivariate analysis

The results for the L1 multivariate analysis are detailed below. Figure 4.15 shows the mean centred data, followed by a histogram demonstrating the separation between study groups using LDA (Figure 4.16). Figures 4.17 and 4.18 detail the percentage correct classification for each SG and show the calculated sensitivity and specificity

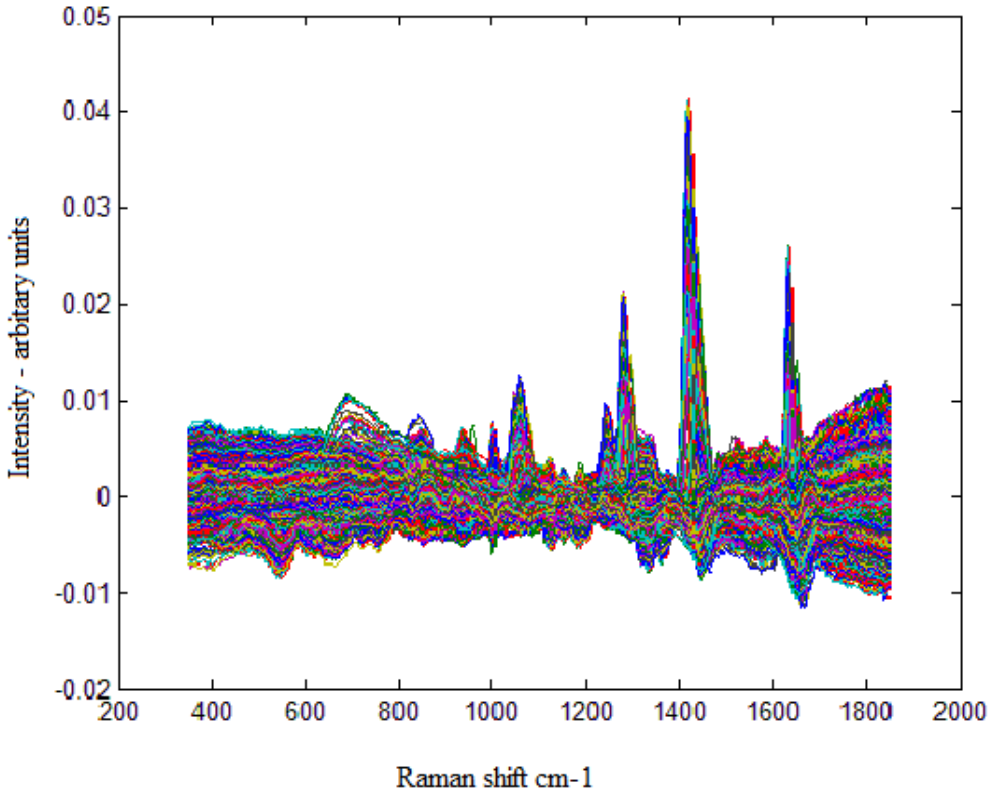

Figure 4.15: L1 –. Mean centred data set.

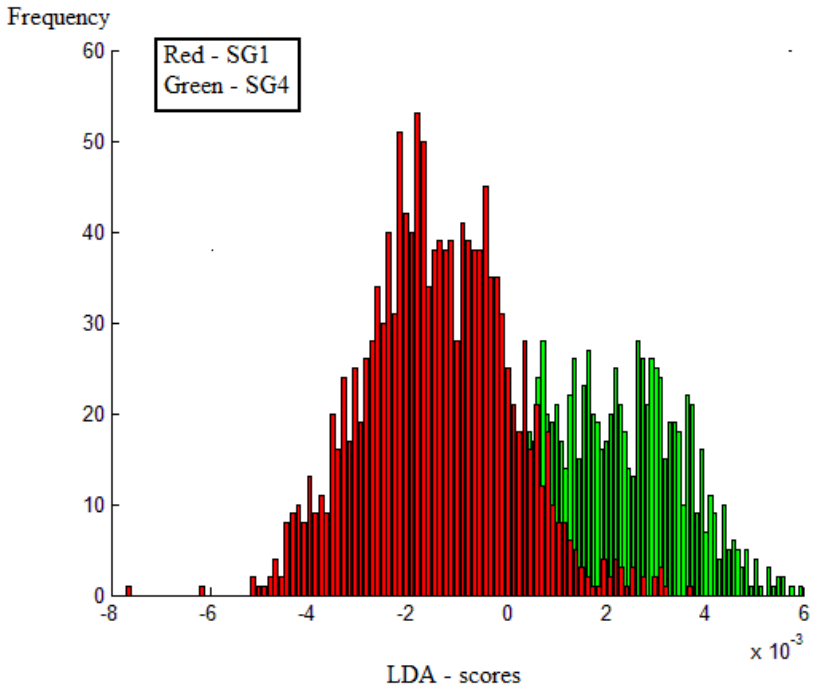

Figure 4.16: L1 – Histogram demonstrating the separation between study groups using LDA.

L1	% Correct
SG1	85.6
SG4	87.2

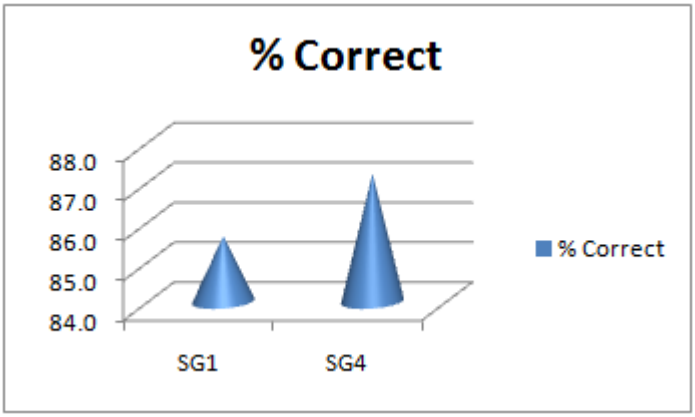

Figure 4.17: L1 – Classification of study group samples by multivariate analysis.

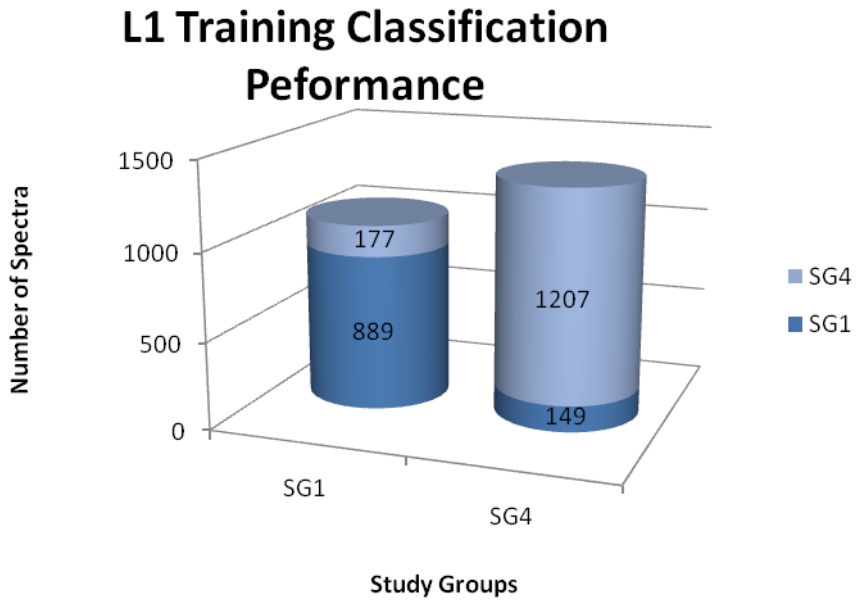

L1	SG1	SG4	Sensitivity	Specificity
SG1	889	149	85.6%	87.2%
SG4	177	1207	87.2%	85.6%

Figure 4.18: L1 – Training classification performance

Figure 4.19 is made up of the load plots for the 6 highest principal component scores out of a total of 25 PCs determined by ANOVA as statistically significant ($p>0.001$), and in addition the load plot for PC2 is also shown.

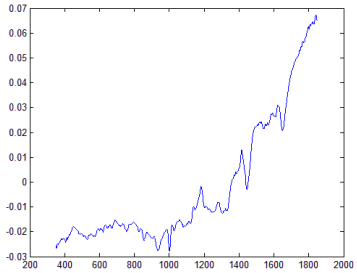

Load for PC1

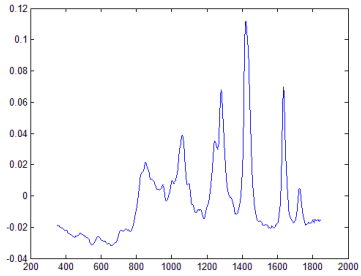

Load for PC2

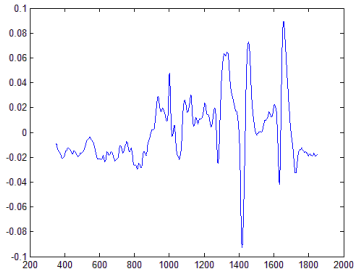

Load for PC3

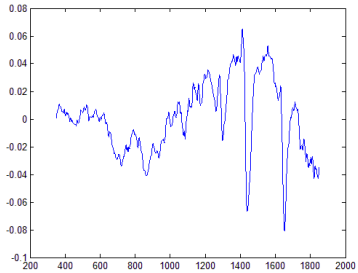

Load for PC4

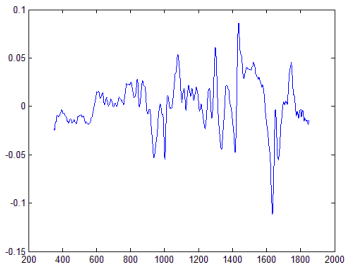

Load for PC 6

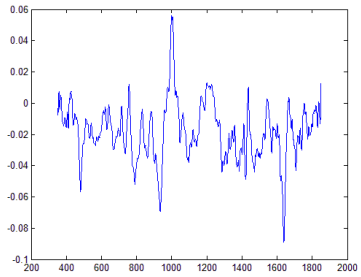

Load for PC10

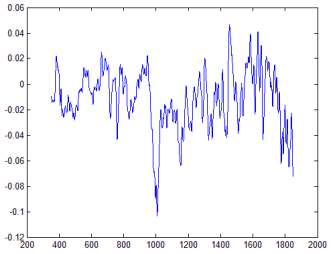

Loads for PC11

Figure 4.19: L1 – Plots of loads for 6 highest principal component scores out of a total of 25 PCs determined by ANOVA as statistically significant (p>0.001), and in addition the load plot for PC2.

Discussion

Within the larynx study this mini model contains the greatest number of tissue samples and compares groups with the broadest range of diseases. SG1 contains samples of SCC where as SG4 is made up of many types of tissue with a single unifying property; none were felt histologically to show features of malignant change. As a consequence of the heterogenicity of tissue samples in SG4 it was expected that there might be some difficulty in separating these study groups.

29 samples showing SCC were compared with 54 samples of non malignant tissue. From these samples 1038 spectra were obtained from the SCC tissue and 1384 from the non malignant tissue group. The non-malignant group includes a diverse range of tissue types including papilloma, muscle and connective tissue. Ideally small targeted mucosal biopsies would be sufficient to give a diagnosis without the need for removal of deeper vocal cord tissue or muscle but this can be very difficult and is not always possible.

The aim of surgery is to obtain an adequate biopsy to definitively secure the diagnosis with one surgical procedure in a group of patients who often have considerable co morbidity. The success of this is dependent on the extent and type of disease and in some cases surgical ability. Another factor to consider is the presence of benign conditions such as hyperplasia and hyperkeratosis. These can visually mimic SCC, the upper most layers of cells can be very thick and the depth to which a biopsy is taken is very much a matter of individual judgement. It was with all these factors in mind that it was felt that the analysis in this mini model was clinically relevant. The inclusion of the papilloma sample was felt valid as infection of the larynx with Human Papilloma Virus (HPV) is not uncommon and can be difficult to irradiate. The presence of papilloma

tissue can lead to voice dysfunction, both as a result of the disease and from treatment, respiratory distress and airway obstruction. However it is the relationship between HPV laryngeal infection and neoplastic changes leading to the development of SCCs that gave reason for inclusion of this sample in the study.

A simple visual inspection of Figure 4.11 was the first step in the analysis and shows that, even after variations in baseline intensity are taken into consideration, there are areas where peak intensity ratios (PIRs) e.g. 1444 and 1654 cm^{-1} and peak shapes are clearly very different. The different shapes of the spectra over the range 1220 to 1380 cm^{-1} are very interesting. The spectrum from tissue classified as SCC shows a trough and that from non-malignant samples a plateau at 1280 cm^{-1}. This wavenumber corresponds to Amide III/ phospholipid membrane. The phospholipid membrane is considered a basic building block for cell walls and a relative increase in this cellular constituent is more usually associated with the presence of cancer cells. However more generically it can be associated with an increase in any form of cell division, suggesting that SG 4 might contain cells which are either misclassified as non- malignant or that this study group might contain cells undergoing other types of proliferation. The peak at 1085 cm^{-1} seen in the spectra of both SGs has also been attributed to phospholipids, but reflecting the difficulty of this type of analysis it is also seen in the spectrum of the amino acid phenylalanine. In order to investigate these spectra more closely the relative peak intensity ratios were calculated and compared. A summary of peak assignments referred to in this work can be found in *Appendix E*.

Figures 4.12, 4.13 and 4.14 consider the peaks that are shared between the two study groups SG1 and SG4. The only peak showing a PIR greater in SG1 is the peak at 1174 cm^{-1}. Peaks at 1175 cm^{-1} and 1176cm^{-1} have been attributed to C-O stretching and the presence of amino acids tyrosine and phenylalanine.

The largest difference between the SGs for peaks common to both is the peak intensity ratios at 1446cm^{-1} and 1654 cm^{-1}. The peak at 1654 cm^{-1} has been assigned to Amide I (C=O stretch) with an α helix secondary structure and has also been seen in lipid. The peak at 1446 cm^{-1} represents δ (CH2) or δ (CH3) / deformation of CH3CH2 in collagen.

The peak at 1244cm^{-1}, common to both study groups, has a larger PIR in the SG4 spectrum. The peak assignment for this wavenumber is given as Amide III with a random coil secondary structure but it has also been shown to be present as Amide III in disordered collagen from keratin. A further peak for Amide III (random coil) would be expected at 1238 cm^{-1} but this is absent from both spectra. Other peaks are present that are associated with keratin such as that seen at 935 cm^{-1}. This peak is shared between SG1 and 4 but is again more prominent in the spectrum from SG4. It has been attributed to C-C skeletal vibrations in protein with an α helix secondary structure but also to C-C stretching within the backbone of collagen in skin and keratotic tissue. Peaks at 827, 852 and 1002 cm^{-1}have been found in spectra obtained from strateum corneum from skin and psoriatic plaques. 872cm^{-1} has been assigned to δ (CCH) aliphatic and 852cm^{-1} to δ (CCH) aromatic and it is noted that both these wavenumbers have also been assigned to the amino acid tyrosine as has the peak both SGs share at 1002cm^{-1}.

The peak at 1002cm-1 is sharp and consistent; it is seen in the spectra of phenylalanine and has been attributed to a ν (CC) aromatic ring stretch of the phenylalanine residue in keratin. The peak at 852cm^{-1} has also been found in the spectra of glycogen and there are some other peaks present that could be attributed to this compound (935, 1085, 1125cm^{-1}) but the majority usually seen are not present in significant intensities. There are tiny peaks at 1047 and 481 cm^{-1} that could be attributed to glycogen in the spectrum obtained from SG4 and these are not seen in the spectrum obtained from SCC tissue (SG1). Both tyrosine and phenylalanine are significant constituents of keratin.

Peaks are present at 1030, 1303 and 1339 cm^{-1}, those at 1303 cm^{-1} and 1339 cm^{-1} are both seen in the spectra obtained from adenine and in addition 1303 cm^{-1}is seen in CH_2 twisting, triglycerides and δ (CH_2) in phospholipid membrane. The empirical analysis in the wavenumber range (1217 to 1363 cm^{-1}) is very difficult to interpret particularly in SG4 as the shape of the plot becomes a plateau suggesting the confluence of several peaks resulting in considerable inaccuracies when peak baseline extremities are picked and hence in the calculation of intensity and area. A review of the difference spectra however show several large positive peaks suggesting SG4 has a proportionally greater amount of the molecular entities responsible for these Raman signals.

The peaks that appear only in the spectrum of SG4 can be attributed to thymine (666 cm^{-1}), proline (898cm^{-1}) and δ (CH_2) scissoring seen in the spectrum of strateum corneum (1438 cm^{-1}).

In histopathology an increase in the nuclear to cytoplasmic ratio is used as a marker of the progression of neoplastic change. The relative intensity ratios of peaks at 1336 cm^{-1} and 1250 cm^{-1} have been used in a similar way. The peak at 1336 cm^{-1} is a reflection of nucleic acid content and the one at 1250 cm^{-}1 the Amide III mode protein (random coil). The relative peak intensity ratios for the peaks with the wavenumbers closest to these in SGs4 and 1 (1339 and 1244 cm^{-1}) give ratios of 0.40 and 0.38 for SG1 and SG4 as would be expected.

The multivariate analysis of the data from this model confirms that there is a statistically significant ($p<0.001$) difference between the two study groups tested. ANOVA determined significant principal component scores with values greater than the F crit. The value of this parameter alters for each model and they are summarised in *Appendix D.5.11*. The most statistically significant of the first 25 PC scores were calculated by ANOVA and the combination describes 99.9% of the variance across the dataset. Figure 4.19 shows plots of the 6 most significant scores. ANOVA is a test to determine how well the PCs discriminate between the groups alone. Linear discriminate analysis, a multivariate technique, then uses a combination of the diagnostically significant PCs to create the model. A single PC will not adequately describe the spectra however a plot of an individual PC load may highlight peaks that help towards an understanding of the molecular differences between the groups. The load plot of PC1 shows the best representation of the variance across the dataset and as the PC number increases less variance of the dataset is described and more noise is seen (Figure 4.19). In the load plots for this model certain features stand out. The peaks that have been noted in the empirical analysis are also prominent in the load plots. However analysis of these plots can be of enormous help and an example is in the 1217 to 1363 cm^{-1} region.

This region was very difficult to analyse as it appeared in the normalised mean spectra as a confluence of peaks. In the PC load plots this area can be teased out. The load plots especially PC 2 show there to be peaks at1244 and 1280 cm^{-1} which can be attributed to proteins, 1244 cm^{-1} with a ß sheet secondary structure and 1280 cm^{-1} to Amide III. The peak seen at 1421 cm^{-1} may be due to δ (CH3) previous seen in keratin and those at 1060 and 1634 cm^{-1} lipids and protein respectively. The load plot for PC1 is inverted suggesting the presence of high levels of protein and the sharp change in orientation of the peaks at 1280, 1454 and 1632 cm^{-1} suggests a change in lipid and protein structure. The peak at 1280 can be assigned to Amide III in phospholipid and that at 1654cm^{-1} to Amide I in the α helix form whilst the peak at 1001cm^{-1} can be due to several molecular entities but it can be due to proteins with a ß sheet structure.

4.2.3.2 L1-1 – Controls – Normal squamous epithelium/Neoplastic tissue (SG5/SG16)

This extra mini model was performed to address the question as to whether Raman spectroscopy can differentiate a sample of squamous epithelium from a vocal cord that had been assessed histologically as not showing features of neoplasia from those that did.

Figures 4.20 and 4.21 show the overlaid mean normalised and difference spectra for the two study groups. These study groups are subdivided further in later mini models and a detailed empirical analysis has been done then. Figure 4.22 is a plot of the mean centred dataset and is followed by Figure 4.23 which is a histogram demonstrating the separation between SG5 (red – 'normals') and SG16 (green - neoplastic) using LDA. The overall results of the multivariate analysis are summarised in Figures 4.24 and 4.25 with those of the cross-validation found in Tables 4.17 and 4.18.

Empirical analysis

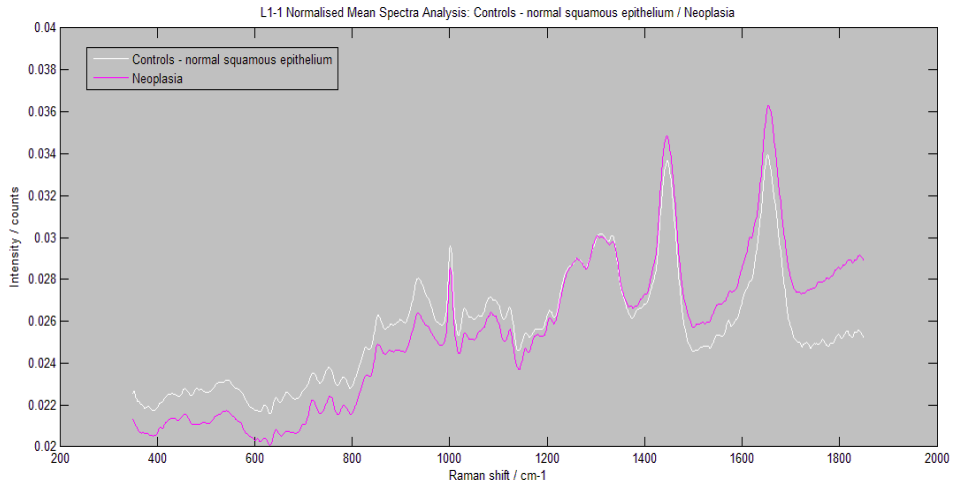

Figure 4.20: L1-1 – Overlaid normalised mean spectra.

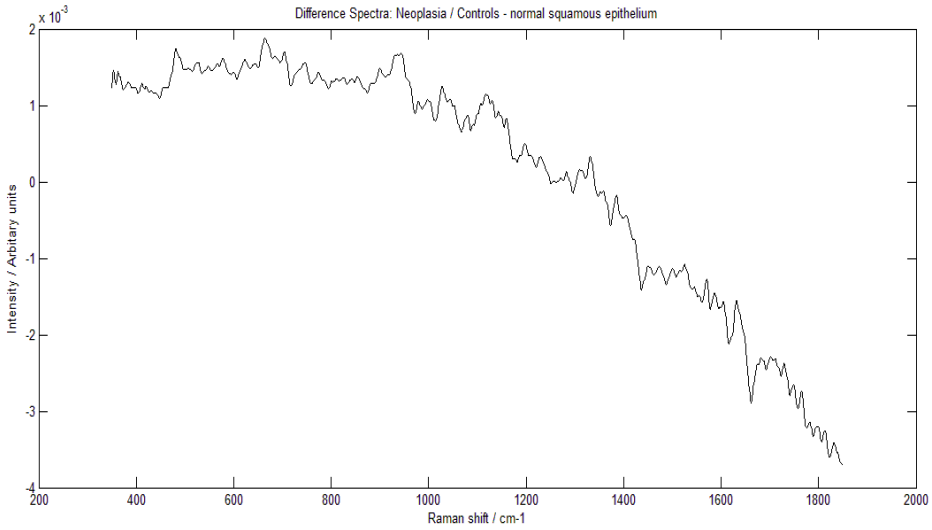

Figure 4.21: L1-1 –Difference spectra.

Multivariate analysis

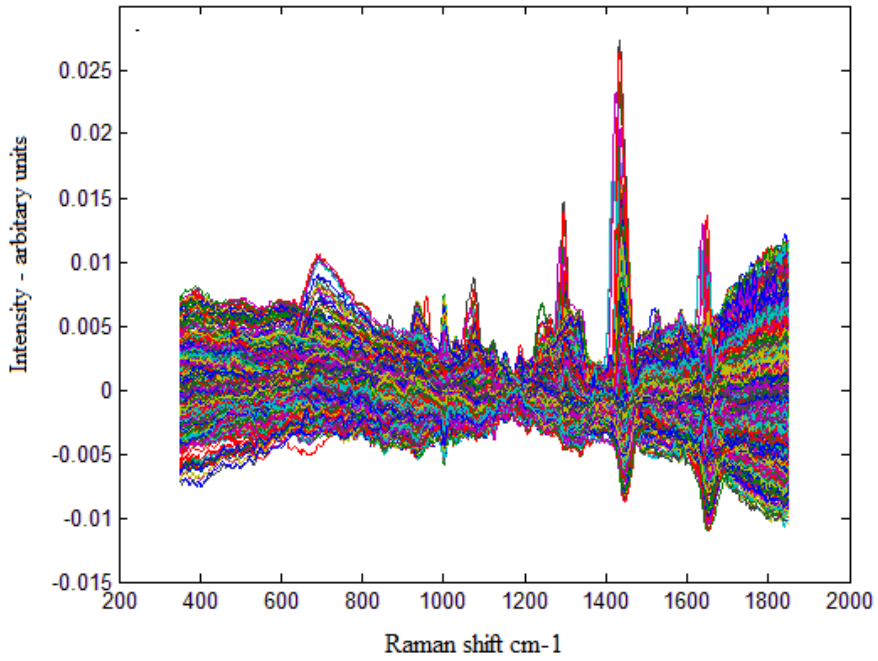

Figure 4.22: L1-1 – Mean centred data set.

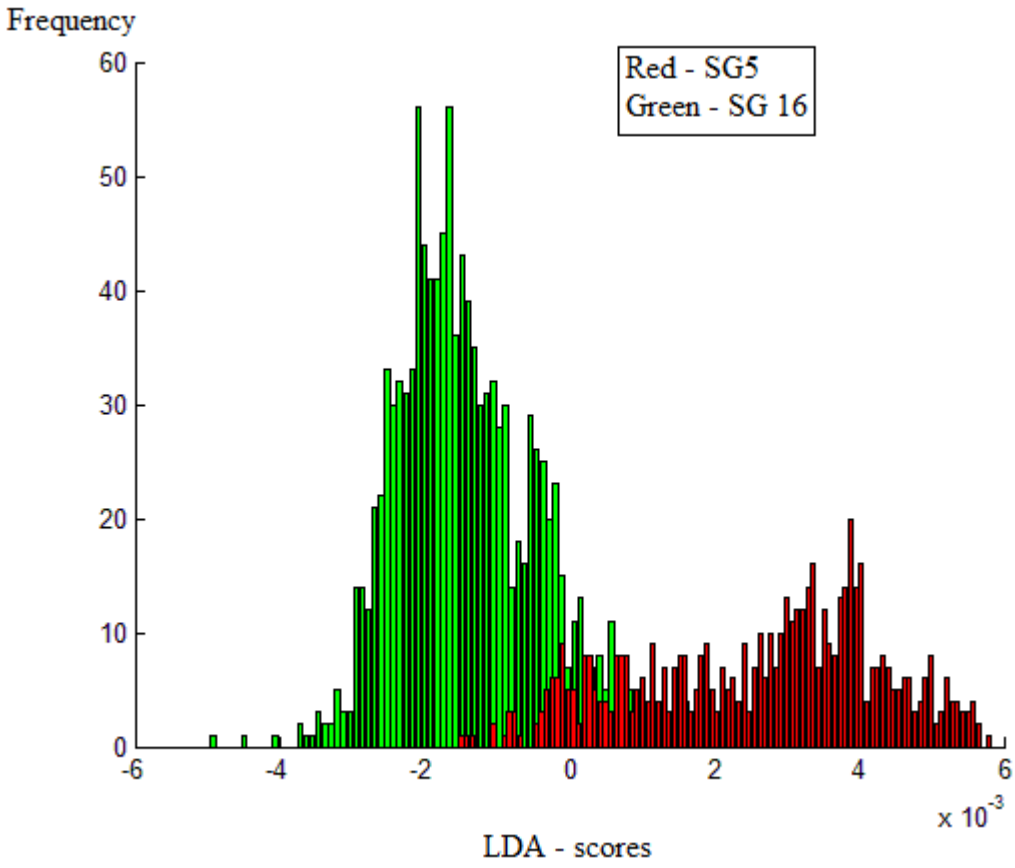

Figure 4.23: L1-1 – Histogram demonstrating the separation between SG5 (red) and SG16 (green).

L1-1	% Correct
SG16	95.2
SG5	84.6

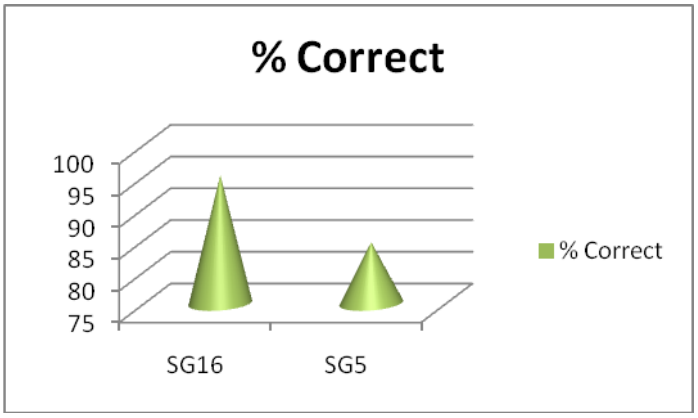

Figure 4.24: L1-1 – Classification of study group samples by multivariate analysis.

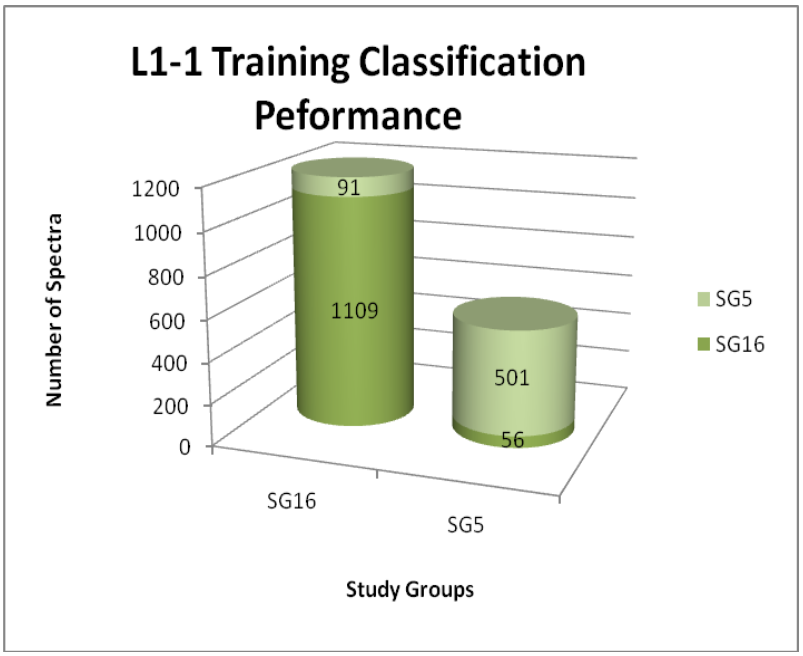

L1-1	SG16	SG5	Sensitivity	Specificity
SG16	1109	56	95.2%	84.6%
SG5	91	501	84.6%	95.2%

Figure 4.25: L1-1 – Training classification performance

Cross validation

Table 4.17:– L1-1 – Training performance.

Training Performance	91%
Neoplasia (SG16)	95%
Normal Sq Epithelium (SG5)	84%

Table 4.18:– L1-1 –Test performance.

Test performance	
Neoplasia (SG16)	73%
Normal Sq Epithelium (SG5)	89%

Discussion

Mini model L1-1 is a comparison of SG5 and SG16. SG5 is made up of those samples of vocal cord mucosa classified by histopathology not containing evidence of neoplastic change, those in SG the opposite. SG5 contains 23 specimens gathered from 13 patients and from these 592 spectra have been obtained. SG16 has 34 samples, from 15 patients and 1165 spectra have been measured.

The histogram demonstrating the separation between SG5 (red) and SG16 (green) shows the presence of a possible double peak in the plot for SG5 and this has been seen in other models e.g. L2a; it is investigated further in mini model L2b. This model predicts correctly for the neoplasia group (SG16 – 95.2%) better than the controls (SG5 - 84.6%). This may suggest the control group is not truly homogeneous.

In the cross-validation study (leave one sample out) the test performance for SG16 gives a sensitivity of 73% and for SG5 89%.

4.2.3.3 L2a - SCC/Controls – All (SG1/SG5)

Empirical analysis

Figure 4.26 demonstrates the normalised mean spectra overlaid for SG5 and SG1, the difference spectrum is adjacent. The PIRs for the shared spectral peaks and lists those peaks which occur in only one of the spectra can be found in *Appendix D5.2*. The histograms in Figures 4.27 and 4.28 are used to more clearly to display this data.

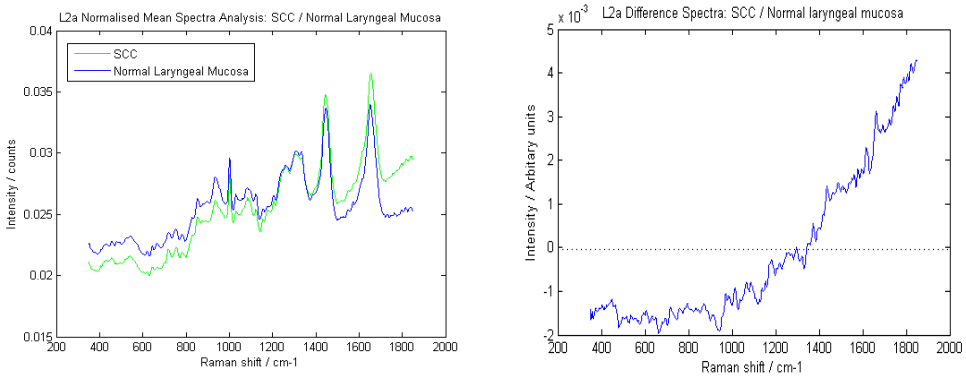

Figure 4.26: L2a – Overlaid normalised mean and difference spectra.

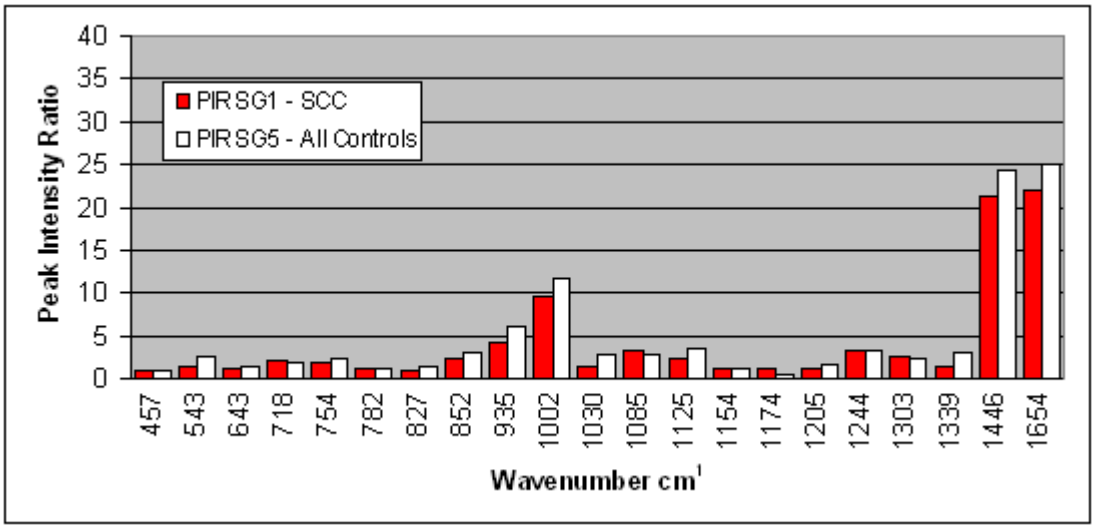

Figure 4.27: L2a – Peak intensity ratios for Study Groups 1 and 5.

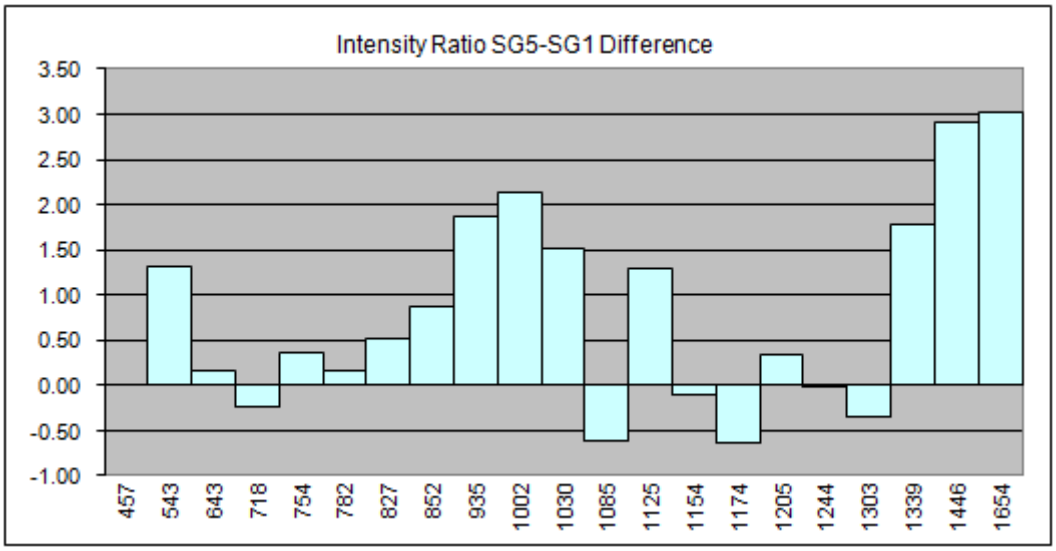

Figure 4.28: L2a – Differences in peak intensity ratios for Study Groups 1 and 5.

Multivariate analysis

Figure 4.29 shows the mean centred dataset and is followed by Figure 4.30 demonstrating the separation of the SGs with multivariate analysis using LDA. The numerical results are summarised in Figures 4.31 and 4.32.

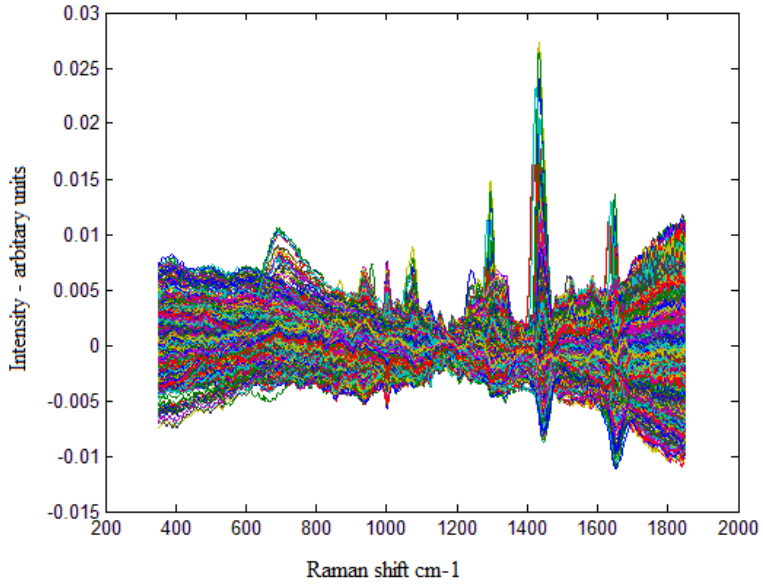

Figure 4.29: L2a – Mean centred data set.

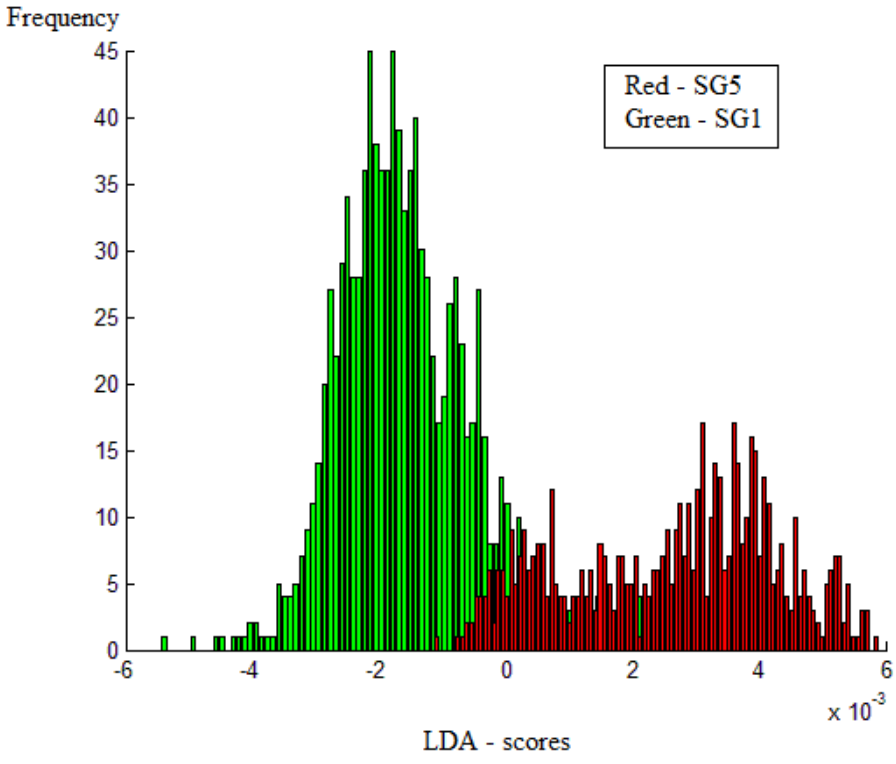

Figure 4.30: L2a – Histogram demonstrating the separation between study groups using LDA.

L2a	% Correct
SG1	94.6
SG5	83.4

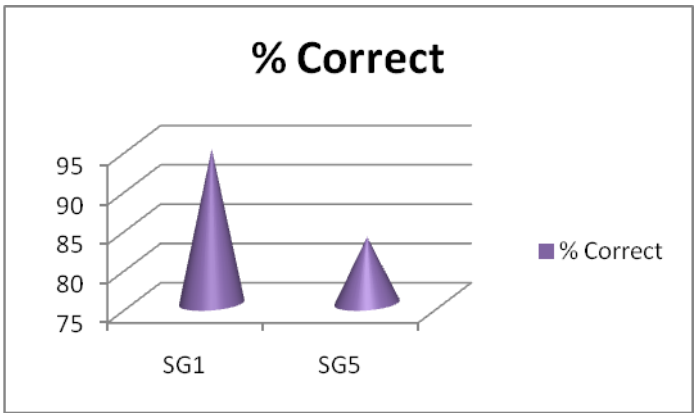

Figure 4.31: L2a – Classification of study group samples by multivariate analysis.

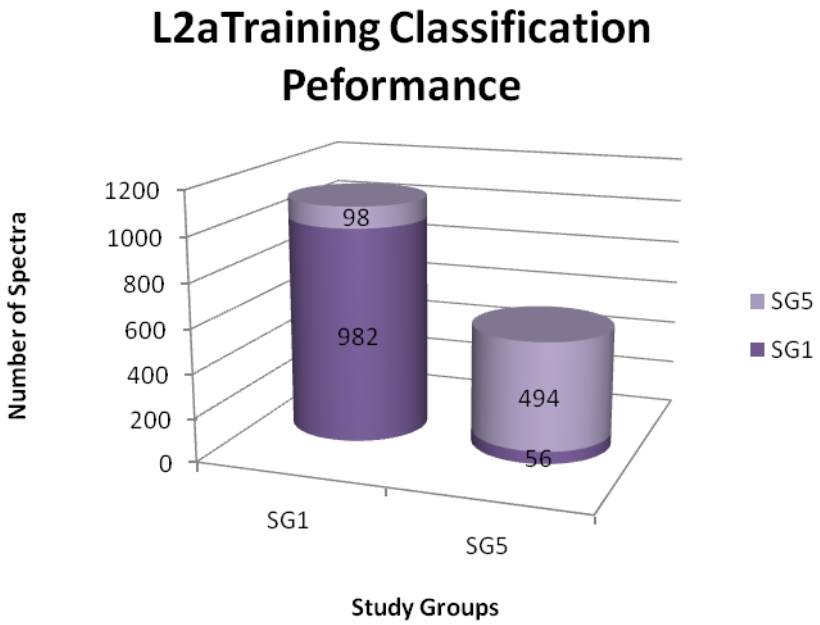

L2a	SG1	SG5	Sensitivity	Specificity
SG1	982	56	94.6%	83.4%
SG5	98	494	83.4%	94.6%

Figure 4.32: L2a – Training classification performance

Discussion

This mini model is a natural progression from L1 and compares the Raman spectra obtained from SCC against that of normal squamous cell epithelium. The inclusion criteria for the latter group were that tissue samples should be of squamous cell epithelium which exhibited no features of neoplastic change; SG5 – pathology codes 7 & 15.

Specimens in pathology groups 7 and 15 were taken as control specimens and to the naked eye appeared to be normal squamous epithelium. Initially classified together as non-neoplastic squamous epithelium certain features found within the analysis prompted a further review. This showed that the samples making up SG5 could be split into two. This prompted a review of the histopathology reports and further subdivision of the samples. Resulting in the formation of SG3; containing samples exhibiting hyperplasia or hyperkeratosis (pathology code 7) and SG10 containing samples felt to represent truly normal squamous cell epithelium (pathology group 15).

The striking feature of the empirical analysis in this mini model is that all the peaks shared in mini model L1 are also seen in this model however the pattern of difference in the peak intensity ratios is altered. The peaks seen at 1085, 1154, and 1030 cm^{-1}can all be attributed to the presence of phospholipids and are seen in relatively greater amounts in SG1 (SCC). The peak at 718$cm^{-1}$is associated with the presence of nucleotides and has a PIR greater for SG1. The peak at 1339 $cm^{-1}$is larger for SG4 and this peak is also a feature of tissue containing nucleotides but can also be attributed to collagen. The peaks that can be attributed to keratin or specific residues present within keratin predominate in the spectrum of SG4 as might be expected.

SG5 contains all the peaks that occur only in SG1, within the limits of the technique with which they can be selected. Peaks at 422 and 620 cm^{-1} are at wavenumbers similar to peaks attributed to δ (CCC) from strateum corneum and n(C-S) from phenylalanine in a psoriatic plaque. The peak occurring at 481 cm^{-1}suggests the presence of glycogen and those at 898, 1547 and 1572cm^{-1} proline, tryptophan and nucleotides.

The empirical analysis of such complex spectra is difficult and even more so when the cell populations exhibit similar properties and in cases such as this multivariate analysis comes into its' own and the findings seen on the PC load plots support those of the empirical analysis.

Multivariate analysis confirmed the finding above and showed that whilst the two main study groups separated well, and somewhat better that that seen in L1, there does appear to be a large distribution of values / variance in SG5 because of the mixed pathologies included. Plots of the PC loads supported the findings of the empirical analysis. The percentage of SCC samples correctly classified by LDA in this model is 83.4 % and for the All – controls group 94.6%.

4.2.3.4 L2b - Controls All / Control - Normal squamous epithelium (SG3/SG10)

Empirical analysis

The overlaid, normalized mean and difference spectra for this study are shown in Figure 4.33.

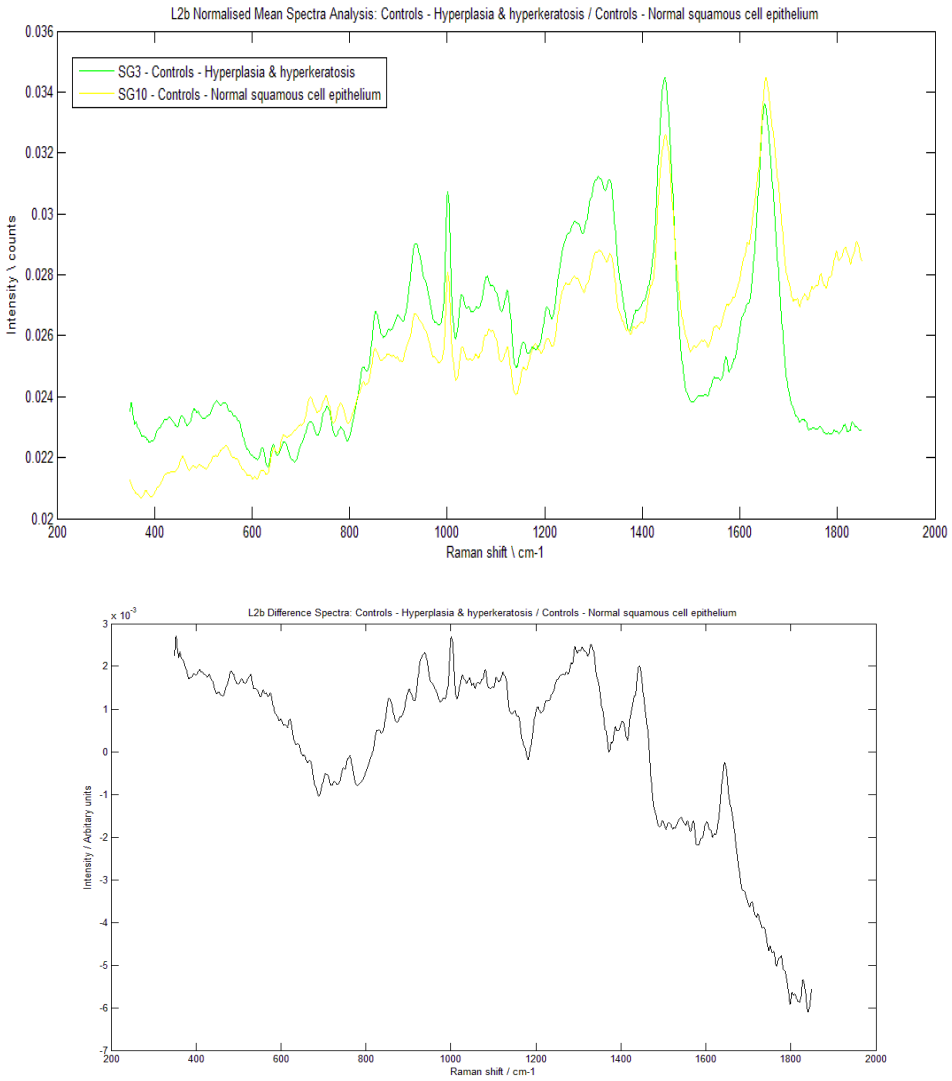

Figure 4.33: L2b – Overlaid normalised mean spectra and difference spectra (SG3/SG10).

PIR tables for the shared spectral peaks and details of unique peaks can be found in *Appendix D5.3*. Figures 4.34 and 4.35 show the data displayed as histograms for ease of analysis. For subsequent mini models tabulated PRI data and the corresponding histograms can be found in *Appendix D5*.

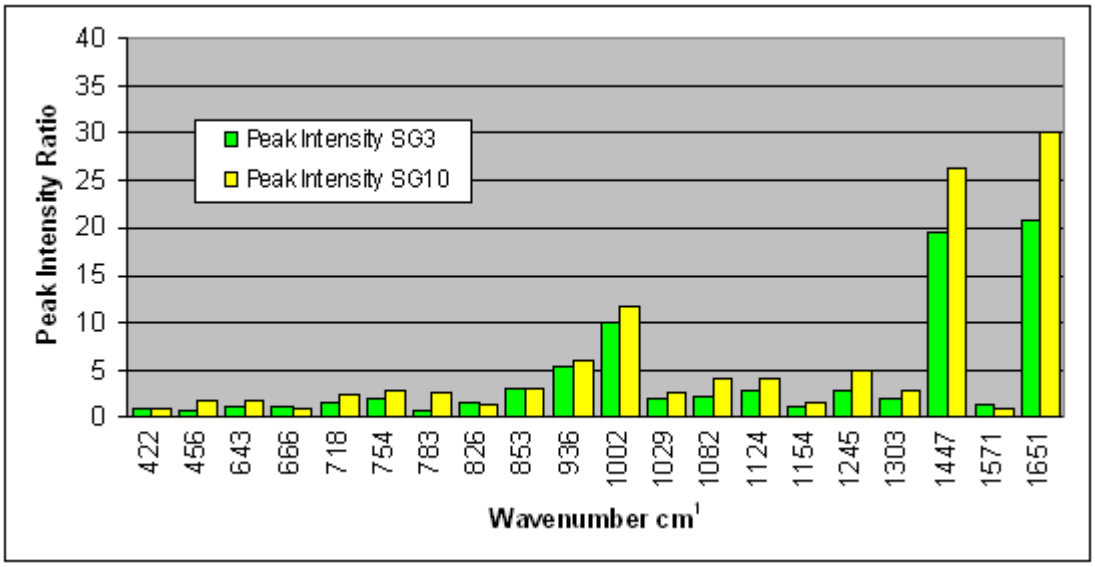

Figure 4.34: L2b – Peak intensity ratios for Study Groups 3 and 10.

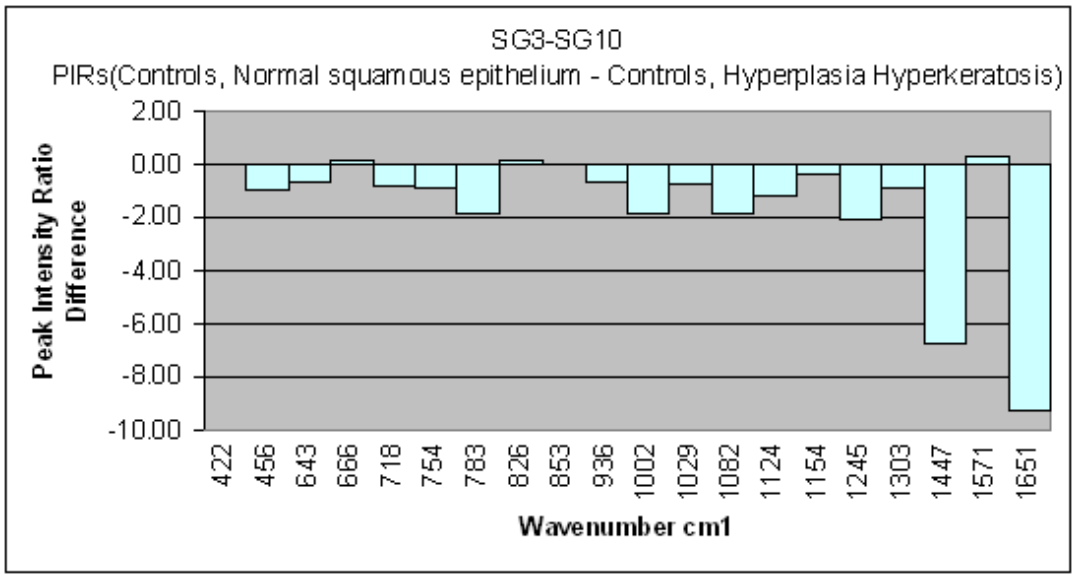

Figure 4.35: L2b – Differences in peak intensity ratios for Study Groups 3 and 10.

Multivariate analysis

Figure 4.36 shows the L2b mean centred data and the results of the multivariate analysis are summarised in Figures 4.37, 4.38 and 4.39.

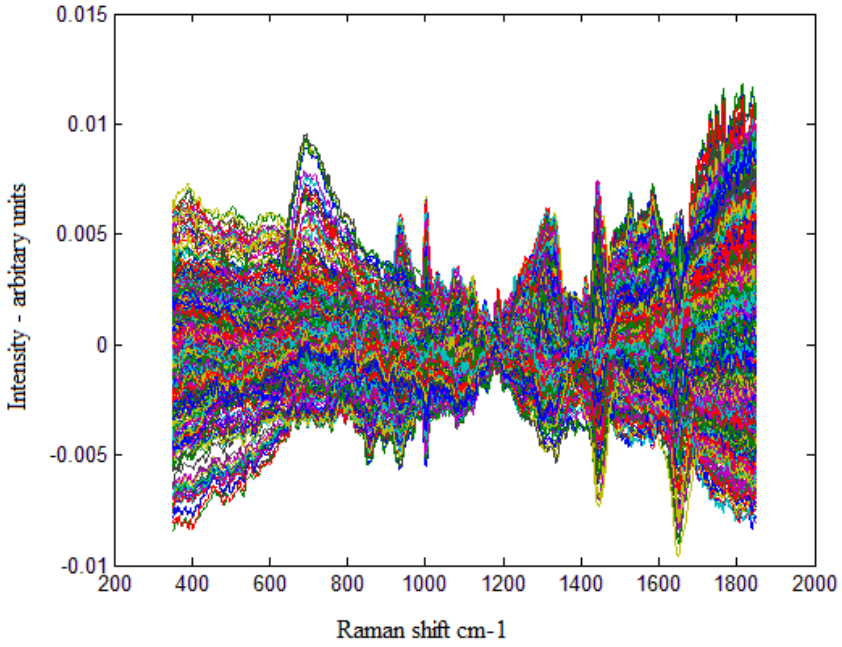

Figure 4.36: L2b – Mean centred data set.

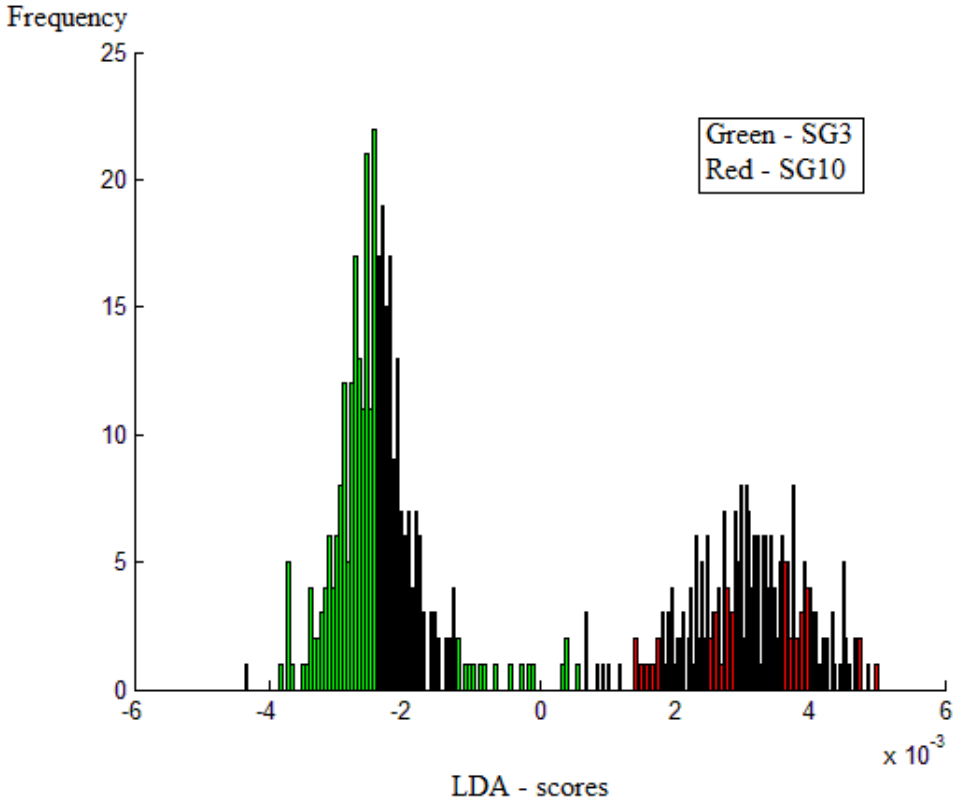

Figure 4.37: L2b – Histogram demonstrating the separation between study groups using LDA.

L2b	% Correct
SG3	97.9
SG10	100.0

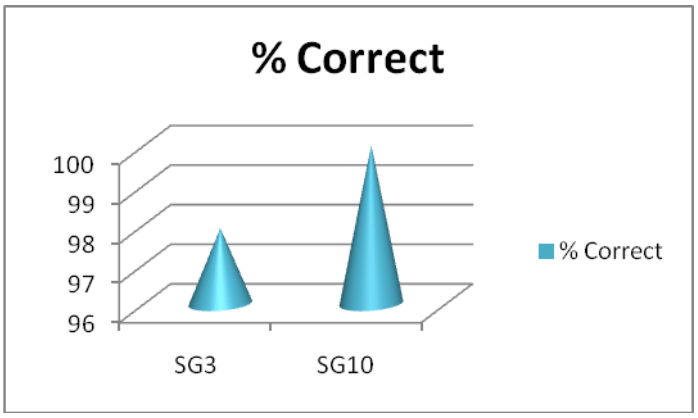

Figure 4.38: L2b – Classification of study group samples by multivariate analysis.

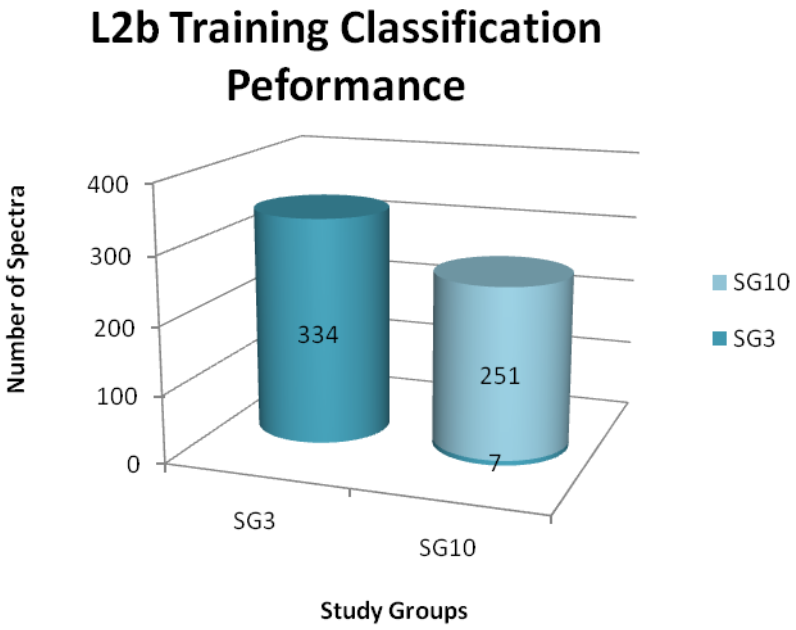

L2b	SG3	SG10	Sensitivity	Specificity
SG3	334	7	97.9%	100.0%
SG10	0	251	100.0%	97.9%

Figure 4.39: L2b – Training classification performance

Discussion

This study was undertaken as a result of the findings in mini model L2a and was to further assess the separation of samples with pathology codes 7 and 15 and to investigate any specific features that might help understand the differences between them.

SG3 (hyperkeratosis/hyperplasia) contains 13 samples obtained from 9 patients and these samples afforded 341 spectra. SG10 contains 10 samples classified histologically as truly normal vocal cord mucosa. These came from 4 patients and produced 251 spectra. The data from the two groups is reasonably well balanced. Specimens assigned to group 7 show either hyperplasia or hyperkeratosis. These specimens would not be considered as showing histological features of neoplastic change but their appearance to the eye and even under a microscope can be very similar to SCC. The clinical importance of this prompted mini-models L2c-1,-2 and -3 to be undertaken. The presence of hyperplasia implies that within the specimen there is a proliferation of normal squamous cells and where hyperkeratosis is seen layers of keratin have been deposited. The ability of Raman spectroscopy to differentiate non-neoplastic tissue and cancer relies on the presence and relative intensity of certain peaks for example peaks related to the presence of cellular constituents reflecting the expansion of a cell line in a neoplastic process. The Raman spectral features associated with this might also be seen in the presence of hyperplasia/hyperkeratosis and a more reliable interrogation strategy might prove to be the presence of Raman spectral changes associated with structural conformational changes in neoplastic tissue.

A visual inspection of the overlaid normalised mean spectra for these two SGs shows great variation between the two plots. This is confirmed by the difference spectra where the mean normalised spectrum of SG10 is subtracted from that of SG3 (Figure 4.33). Positive peaks therefore reflect an increase in the amount of the molecular entity producing the Raman signal at that wavenumber in the samples making up SG3. There are small glycogen peaks at 480cm^{-1} in both spectra, these are less prominent than might be expected compared to this peak in other normal tissue from the oesophagus and cervix. The difference spectra has strong negative signals at 689, 733, 717, 780 cm^{-1} and again over the range 1488 - 1617 cm^{-1}. There a large number of clearly positive peaks. The one at 620 cm^{-1} is noted as of possible particular significance in the L4 mini model analysis. Strong positive peaks at 826 and 854 cm^{-1} have been assigned to tyrosine and δ (CCH) aromatic determined from strateum corneum and interestingly the peak at 935, which is also positive is associated with CH3 rocking and C-C stretch in the α helix of keratin. The positive peak at 1122/1123 cm^{-1} may be due to glycogen or lipid but there is also a positive peak at 1372 that can be attributed to lipid. In the range 1470 to 1645 cm^{-1} the peaks are negative and confluent and are likely to be due to nucleic acid bases, carotenoids and protein. There is also a negative confluence of peaks over the 689 to 780 cm^{-1} range which is again likely to reflect the presence of nucleotides/DNA.

The PIRs for SG10 look higher on the histogram relative to those for SG3 (Figure 4.34) however care must be taken in drawing general conclusions as this histogram only shows a sample of the peaks that are present.

The multivariate analysis of this model gives an excellent separation of the two study groups with high scores over the lowest six PCs which agree with the findings of the empirical analysis. This mini model supports the findings from L2a; the presence of two separate groups with different biochemical spectral fingerprints within the All – controls (SG5) study group. It also shows there is some evidence that Raman spectroscopy can differentiate hyperkeratosis/hyperplasia of vocal cord mucosa but it would be helpful and important for the dataset relating to these findings to be expanded as the numbers

included in this study do not give data that is strong enough to support extensive cross-validation or full independent testing.

4.2.3.5 L2c mini model series

This is a series of models exploring the ability of Raman spectroscopy to evaluate the effect of a possible lack of homogenicity in a collection of samples all consider not to display features of neoplasia (All-controls). It will also try to evaluate if Raman spectroscopy can distinguish between SCC, different subgroups of 'normal' mucosa, tissue displaying dysplasia and carcinoma in situ.

Summary of L2c models

- L2c SCC/ Controls – All / Abnormal mucosa (SG1/SG5/SG7)
- L2c-1 SCC /Controls – hyperplasia & hyperkeratosis / Abnormal mucosa (SG1/SG3/SG7)
- L2c-2 SCC / Controls – normal squamous epithelium / Abnormal mucosa (SG1/SG10/SG7)
- L2c-3 SCC / Controls – Normal squamous epithelium / Dysplastic mucosa (SG1/SG10/SG14)

To avoid repetition the discussion relating to all the L2c models is done together after the results of the empirical and multivariate analyses for each mini model.

Empirical analyses

The overlaid, normalized mean spectra for these studies are shown in Figures 4.40 to 4.43 and the PIR histograms in Figures 4.44 to 4.47. The individual difference spectra are recorded in *Appendix D3.4* to *D.3.7* and the tabulated PIR data and difference histograms in *Appendix D.5.4* to *D.5.7.*

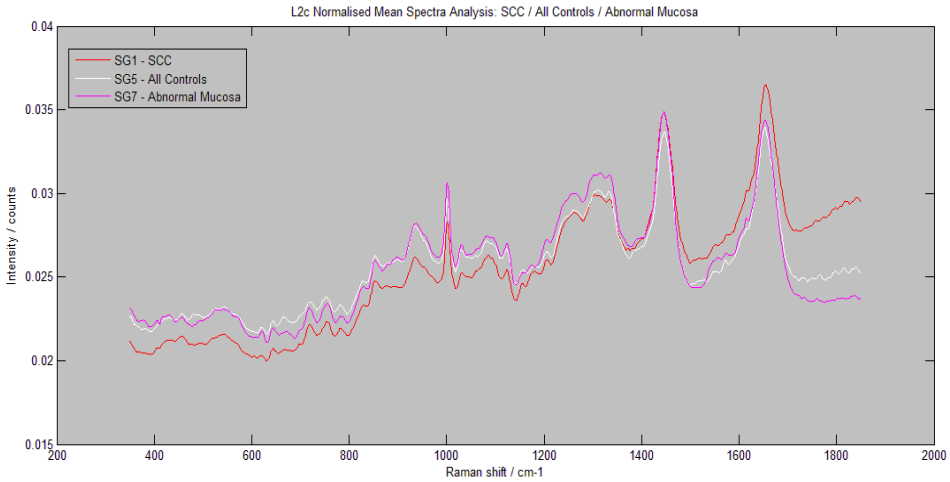

Figure 4.40: L2c – Overlaid normalised mean spectra.

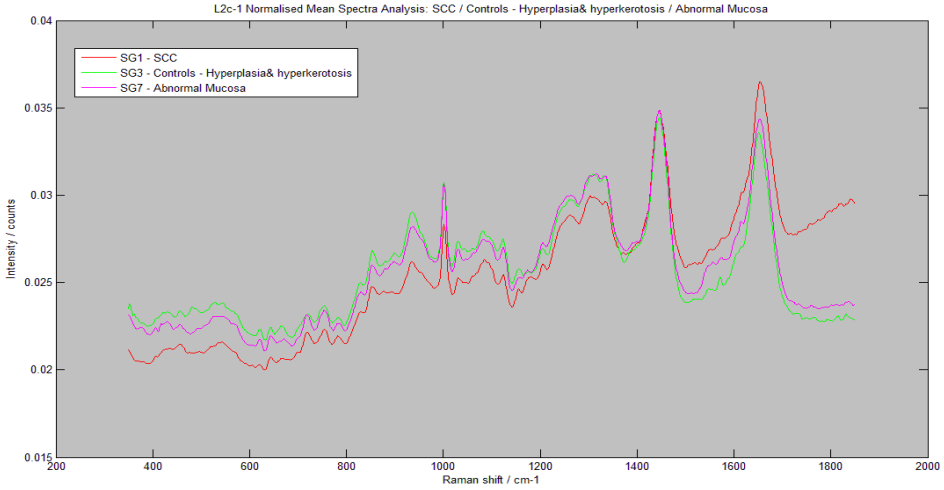

Figure 4.41: L2c-1 – Overlaid normalised mean spectra.

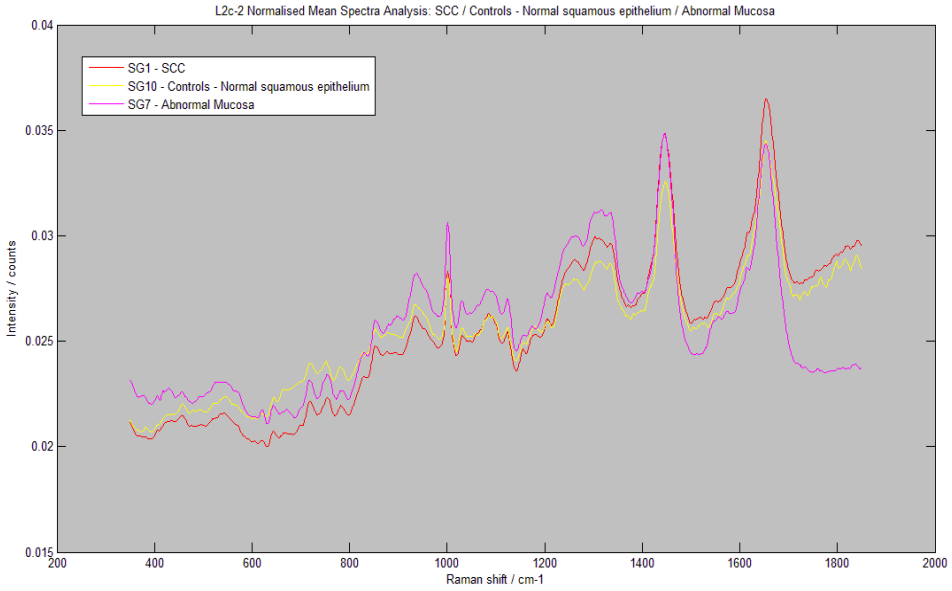

Figure 4.42: L2c-2 – Overlaid normalised mean spectra.

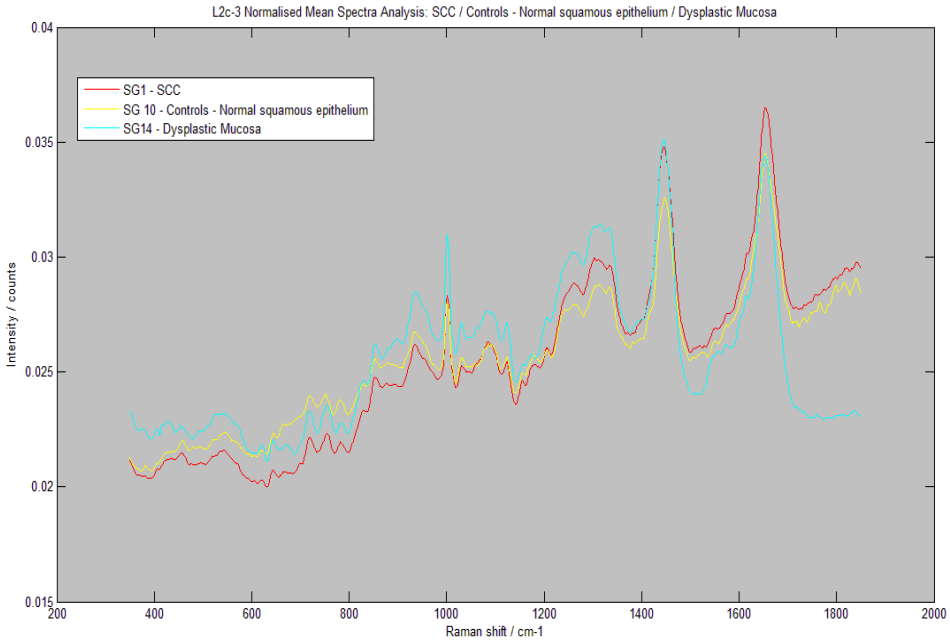

Figure 4.43: L2c-3 – Overlaid normalised mean spectra.

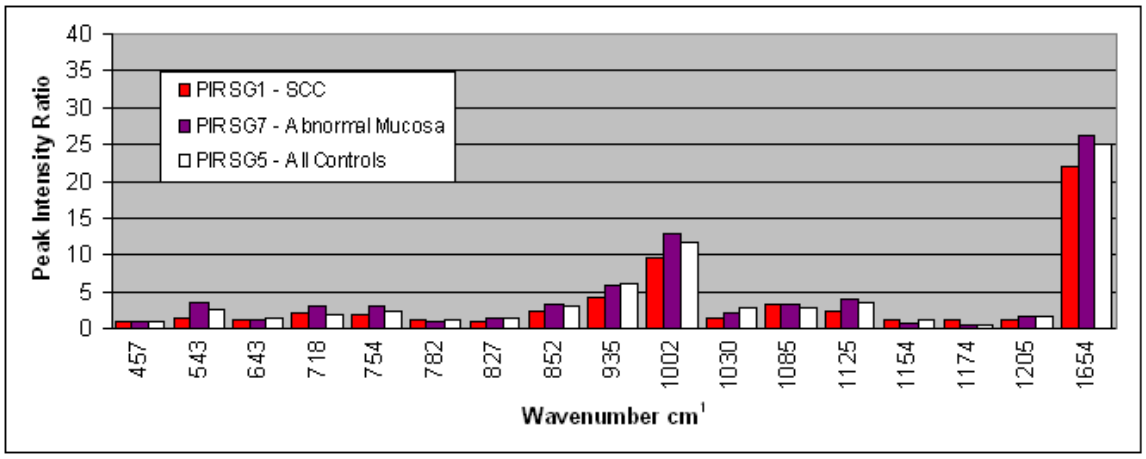

Figure 4.44: L2c – Peak intensity ratios for Study Groups 1, 5 and 7.

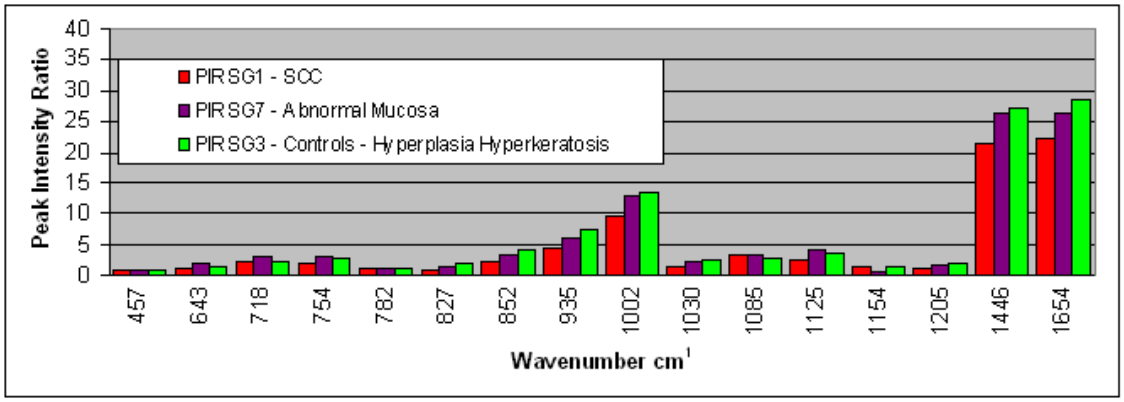

Figure 4.45: L2c-1 – Peak intensity ratios for Study Groups 1, 3 and 7.

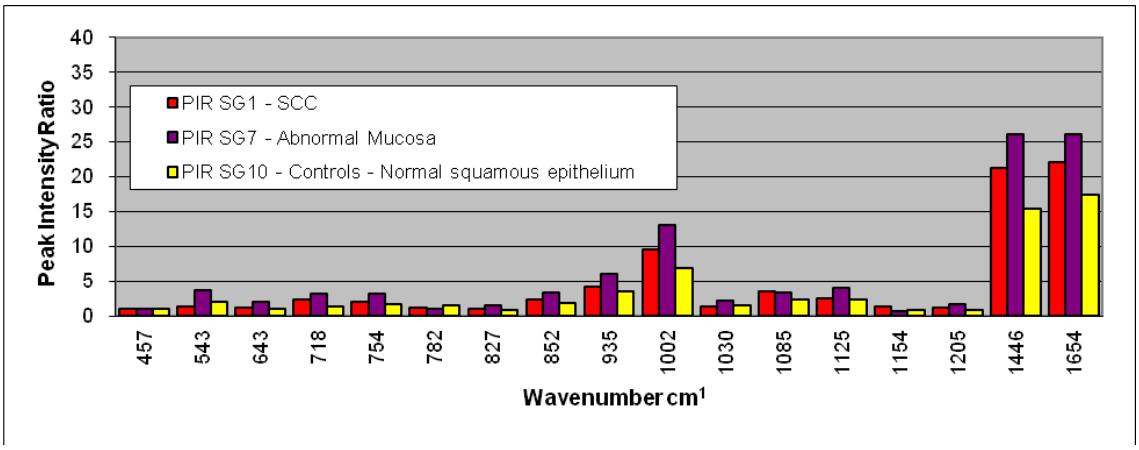

Figure 4.46: L2c-2 – Peak intensity ratios for Study Groups 1, 10 and 7.

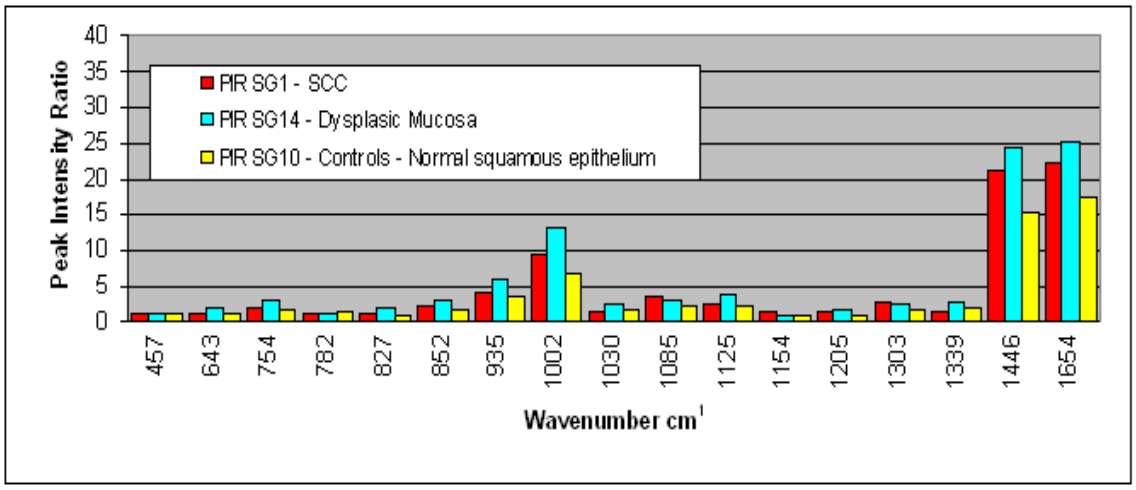

Figure 4.47: L2c-3 – Peak intensity ratios for Study Groups 1, 10 and 14.

Multivariate analysis

The mean centred data for these mini models are shown in Figures 4.48, 4.50 and 4.52. Examples of scatter plots for each mini model are given in Figures 4.49, 4.51, 4.53 and 4.54 the numerical results of the multivariate analysis are recorded, including sensitivities and specificities in Figures 4.55 to 4.62.

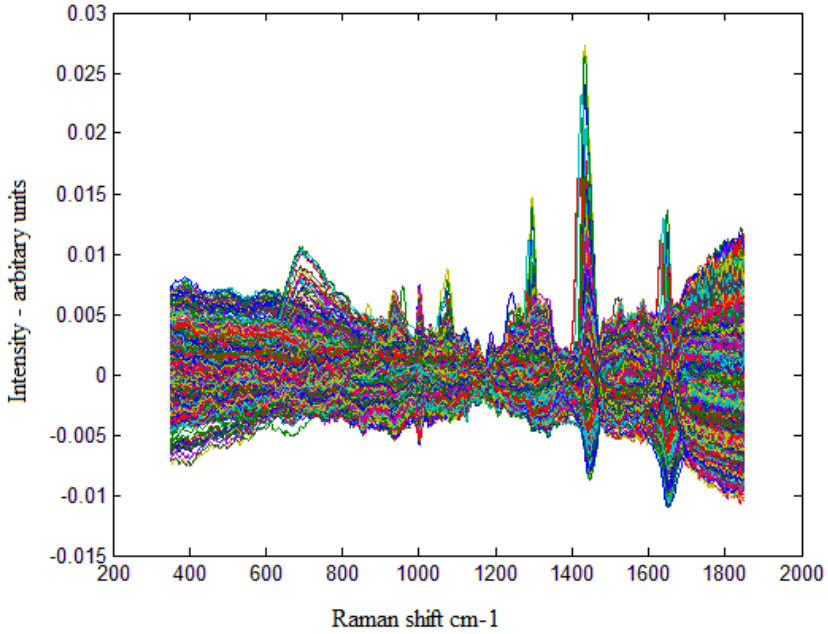

Figure 4.48: L2c - Mean centred data set.

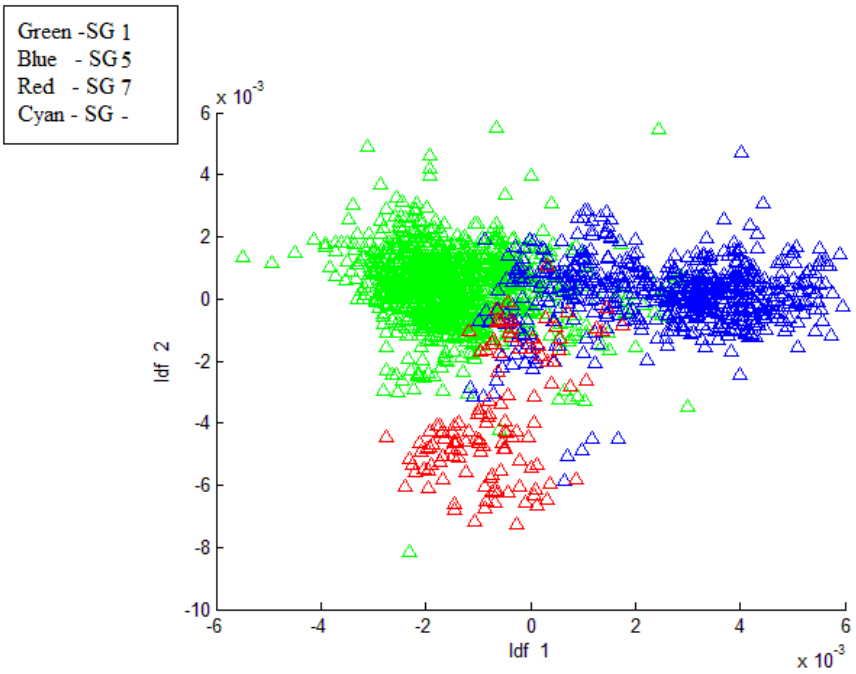

Figure 4.49: L2c – Scatter plot comparing linear discriminant functions 1 & 2.

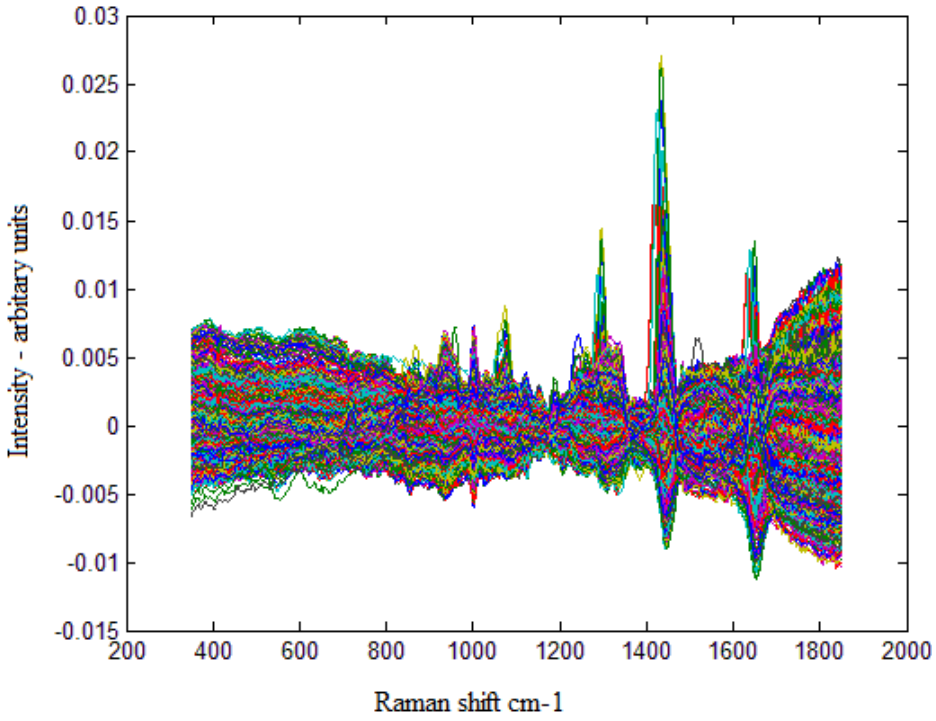

Figure 4.50: L2c-1 - Mean centred data set.

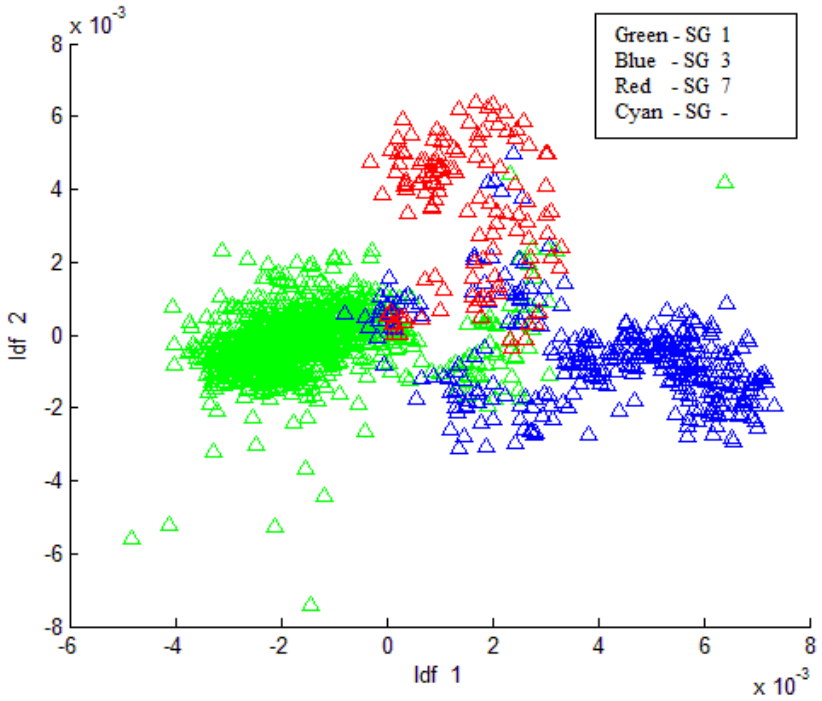

Figure 4.51: L2c-1 - Scatter plot comparing linear discriminant functions 1 & 2.

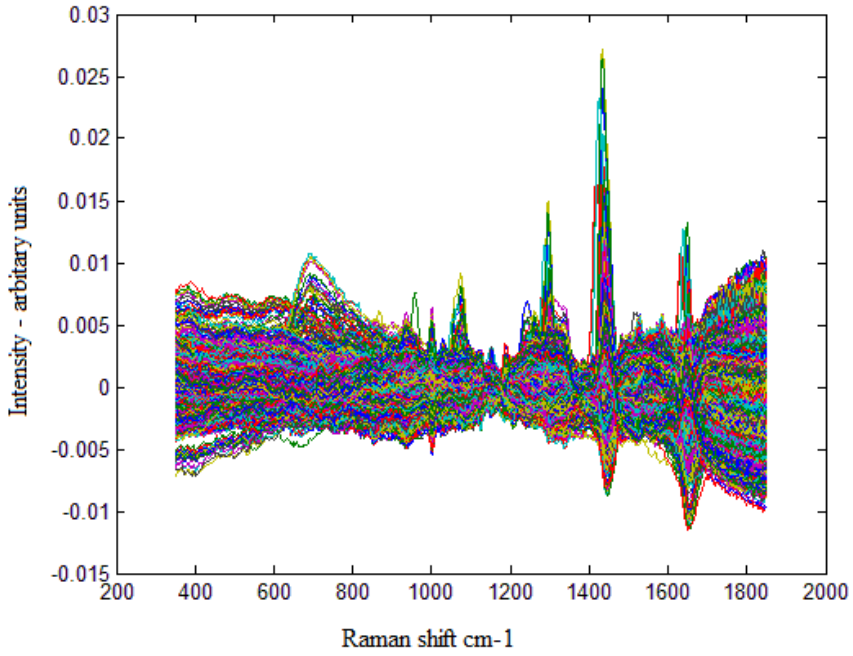

Figure 4.52: L2c-2 - Mean centred data set.

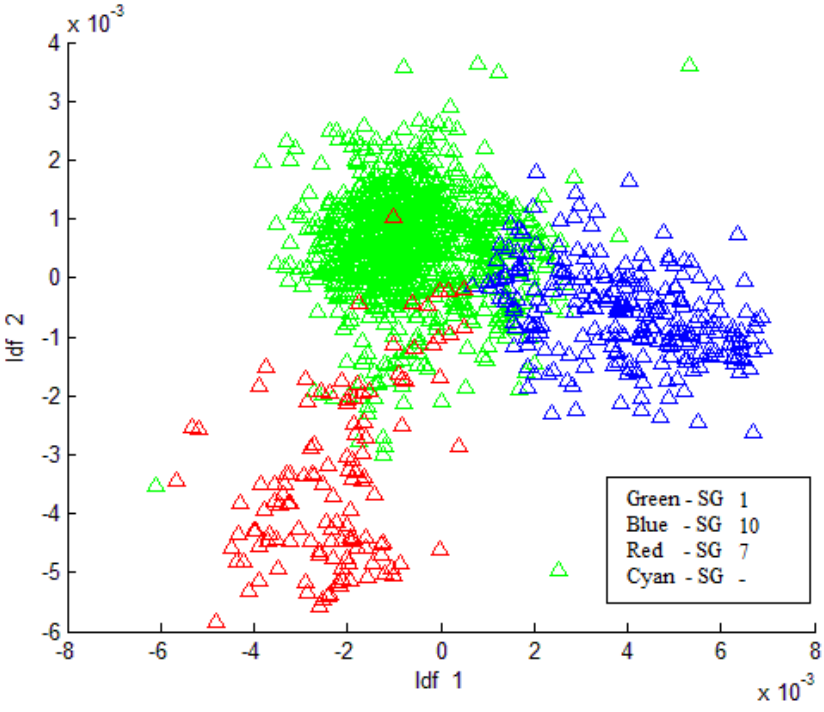

Figure 4.53: L2c-2 - Scatter plot comparing linear discriminant functions 1 & 2.

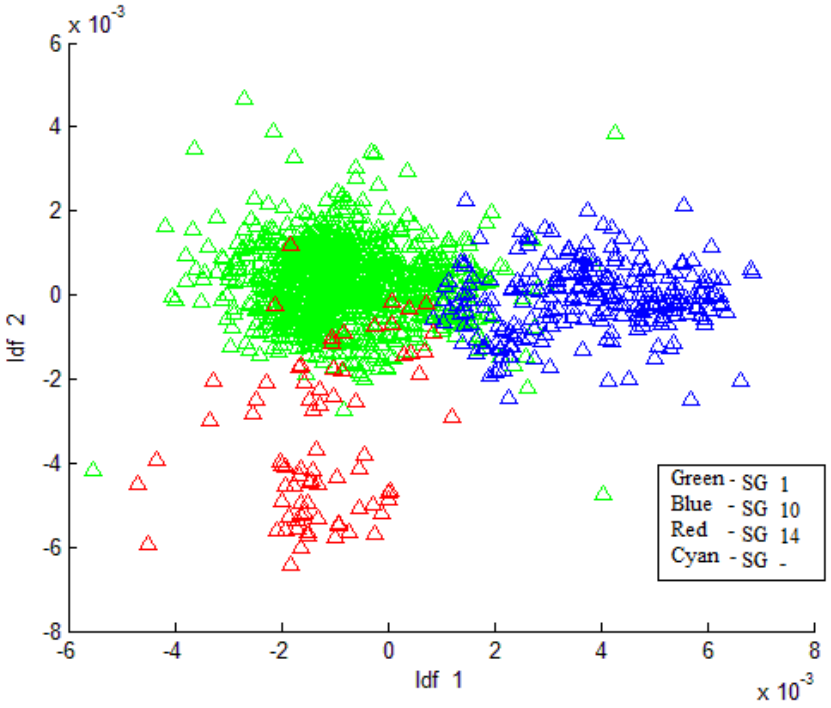

Figure 4.54: L2c-3 - Scatter plot comparing linear discriminant functions 1 & 2.

L2c	% Correct
SG1	91.8
SG5	84.3
SG7	77.2

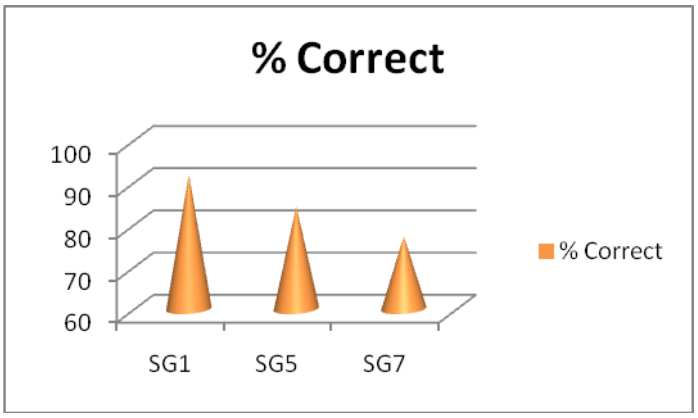

Figure 4.55: L2c - Classification of study group samples by multivariate analysis.

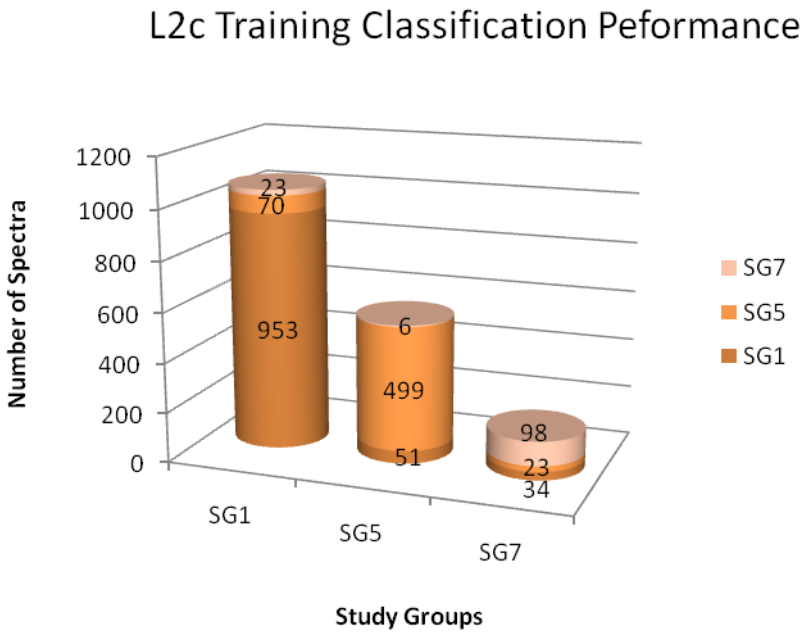

L2c	SG1	SG5	SG7	Sensitivity	Specificity
SG1	953	51	34	91.8%	87.1%
SG5	70	499	23	84.3%	95.1%
SG7	23	6	98	77.2%	96.5%

Figure 4.56: L2c – Training classification performance

L2c-1	% Correct
SG1	93.9
SG3	86.5
SG7	83.5

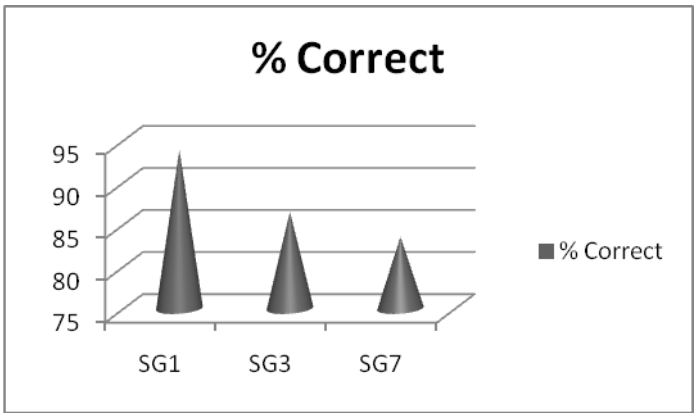

Figure 4.57: L2c-1 - Classification of study group samples by multivariate analysis.

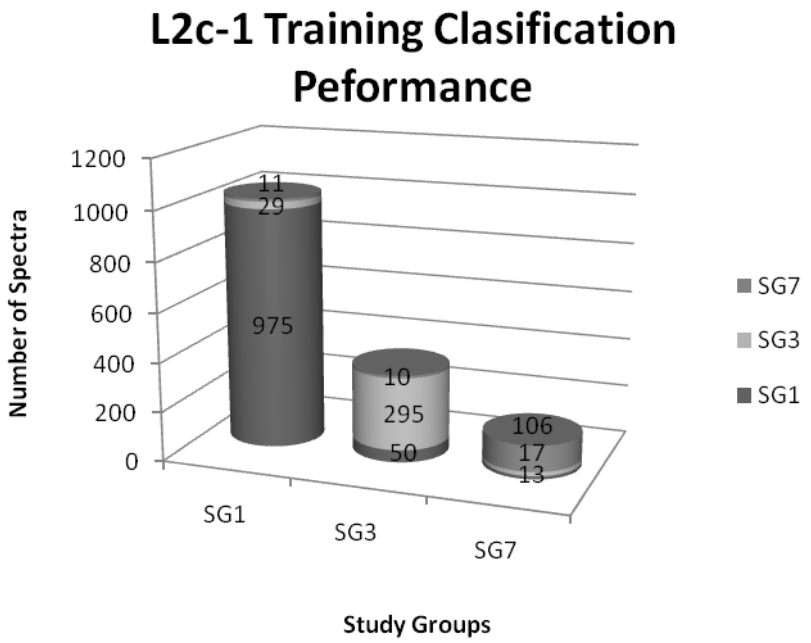

L2c-1	SG1	SG3	SG7	Sensitivity	Specificity
SG1	975	50	13	93.9%	91.5%
SG3	29	295	17	86.5%	94.8%
SG7	11	10	106	83.5%	97.8%

Figure 4.58: L2c-1 – Training classification performance

L2c-2	% Correct
SG1	93.7
SG10	90.4
SG7	89.0

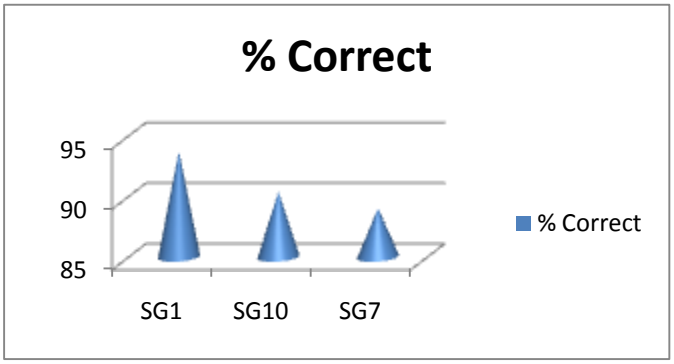

Figure 4.59: L2c-2 - Classification of study group samples by multivariate analysis.

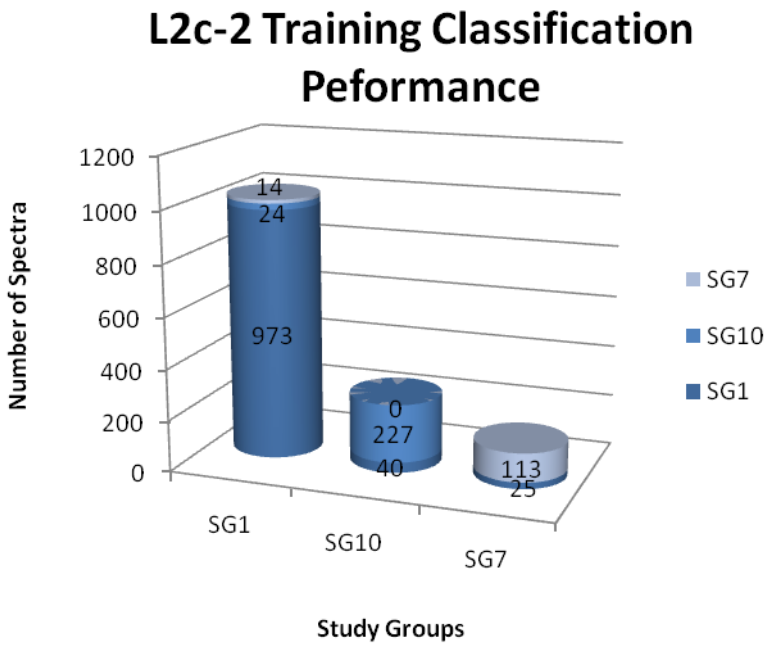

L2c-2	SG1	SG10	SG7	Sensitivity	Specificity
SG1	973	40	25	93.7%	89.9%
SG10	24	227	0	90.4%	96.6%
SG7	14	0	113	89.0%	98.1%

Figure 4.60: L2c-2 – Training classification performance

L2c-3	% Correct
SG1	94.7
SG10	94.8
SG14	82.0

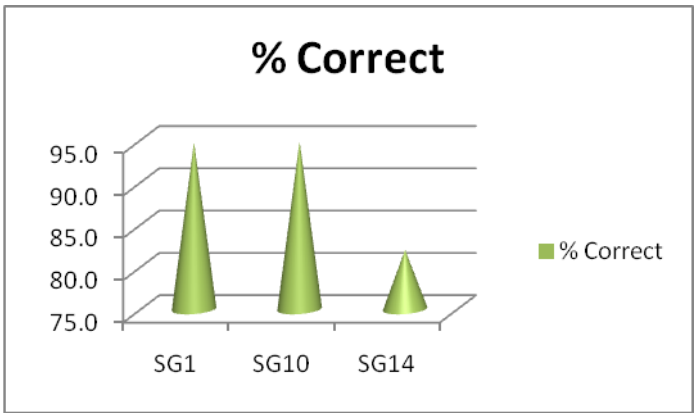

Figure 4.61: L2c-3 - Classification of study group samples by multivariate analysis.

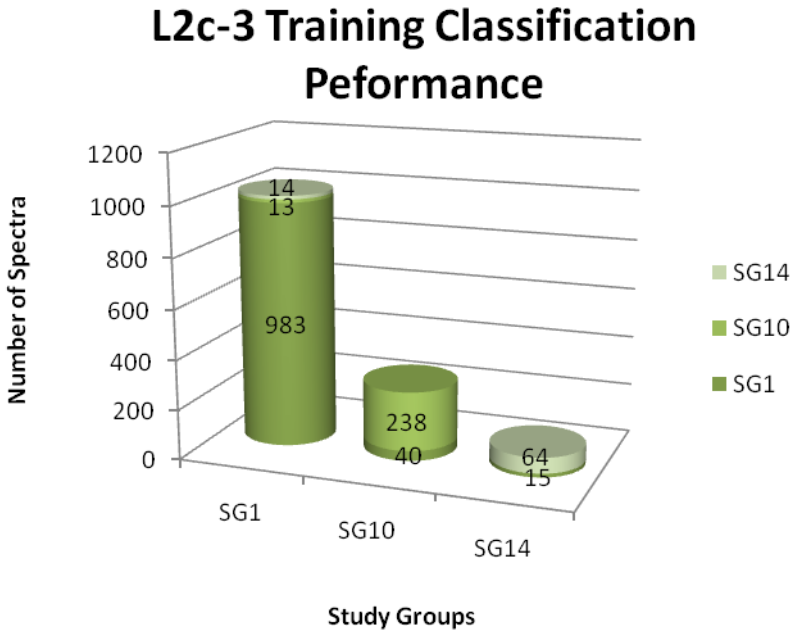

L2c-3	SG1	SG10	SG14	Sensitivity	Specificity
SG1	983	40	15	94.7%	91.8%
SG10	13	238	0	94.8%	96.4%
SG14	14	0	64	82.1%	98.8%

Figure 4.62: L2c-3 – Training classification performance

Discussion L2C / L2c-1 / L2c-2 / L2c-3

It is clear from the analysis of mini models L2a and L2b that pathology groups 7 and 15 can be separated by Raman spectroscopy however for completeness the L2c mini model was performed with SG5 – all controls as it can be very difficult clinically to distinguish between normal, and hyperplastic mucosa, hyperkeratotic mucosa, SCC and carcinoma in situ.

L2c compares SCC against all controls and also to the group labelled 'abnormal mucosa.' This group contains all samples classified as showing dysplastic changes and also those displaying carcinoma in situ. Other mini models related to this study, L2c-1, L2c-2 and L2c-3, subdivide this model to account for the discovery that the original control group contained two discreet types of tissue. L2c-3 investigates if Raman spectroscopy can differentiate between SCC, truly normal vocal cord mucosa and dysplastic tissue.

As the models are developed and the study groups subdivided, the numbers of specimens considered in each is reduced. The largest study group is SCC were 10 patients gave 29 samples and from these 1038 spectra were obtained. This is a large data set compared to the abnormal mucosa study group which contained 5 samples and 127 spectra. The number of spectra in the 'All controls' group lies between the two other study groups and forms a reasonably large dataset of 592 spectra. Interestingly these spectra were obtained from 23 samples whereas many more spectra were collected per sample for the SCC group. This reflects the size of the samples which were generally larger in the SCC group and these samples were much easier to process.

Visually inspecting the overlaid normalised mean spectra and taking into consideration the variation in the baselines, the plot for SCC still tends to sit alone in the L2c and L2c-1 mini models (Figures 4.40 & 4.41). The spectra for 'All controls' and 'Controls – hyperplasia & hyperkeratosis seem very similar to that of 'Abnormal mucosa'. In L2c-2 and 3 this trend is reversed with the spectra for SCC and Controls – normal squamous epithelium more closely associated (Figures 4.42 & 4.43).

When the overlaid normalised spectra for all the samples in SG10 (pathology group 15) are looked at in detail and with the spectra magnified as shown in Figure 4.63 three distinct features are noted; there appears to be two spectral shapes, one drawn in blue and labelled A, and a second that has a broad peak between 630 and 800cm^{-1} with irregularities that look like peak vertices, the most prominent at 720 $cm^{-1}$and labelled B. This range is most often attributed to Raman signal arising from DNA and in particular amino acids such as tyrosine and phenylalanine. The peak at 720 cm^{-1} has been assigned to nucleotides, the peak at 854cm^{-1}, in the spectra whose shape is highlighted in red, can be attributed to both tyrosine and δ (CCH) aromatic from strateum corneum . The peak at 937 cm^{-1} that can be seen in Figure 4.64 can arise from a protein with an α helix secondary structure and this has been seen in the analysis of nails. All these factors combined suggest the possibility of a rise in keratin content. There are several explanations that may account for this; some samples may have been misclassified, are heterogenous, or Raman spectroscopy is detecting features at a molecular level before they are obvious histologically.

The PRI trend in L2c (Figure 4.44) shows that for the shared peaks the PRI is generally smallest for the SCC samples and the PRIs for the other two groups again are generally larger with the greatest being in the lipid/protein range and at 1001cm^{-1}. The PIR histogram for L2c-1 (Figure 4.45) shows a consistent trend with the PIRs increasing

from SG1 (SCC) to SG7 (Abnormal mucosa) to SG3 (Controls – hyperplasia & hyperkeratosis). This is a trend that correlates well with our knowledge of the nature of the disease which is understood to be a progression from normal through dysplasia to carcinoma in situ and then to SCC; SCC subdividing into well, moderate and poorly differentiated. The latter having the worse prognosis and being made up of cells morphologically most distinct from normal squamous cells. The pattern seen in the PRI histogram for L2c-2 is similar to that seen in L2c. Suggesting that the differences in molecular structure associated with SG10, normal squamous epithelium, predominates over those resulting in the PRIs for SG3 (controls - hyperplasia/hyperkeratosis). The histogram for L2c-3 is almost identical to that of L2c-2. This is likely to be due to the fact that the only difference between the two models is that in L2c-2 a comparison is made between SG1 (SCC), SG10 (Controls – normal squamous epithelium) and SG7 (Abnormal mucosa) whereas in L2c-3 SG7 is replaced by SG14 (dysplastic mucosa). The latter, SG14, is the same as SG7 except that it does not contain the spectra from the carcinoma in situ samples.

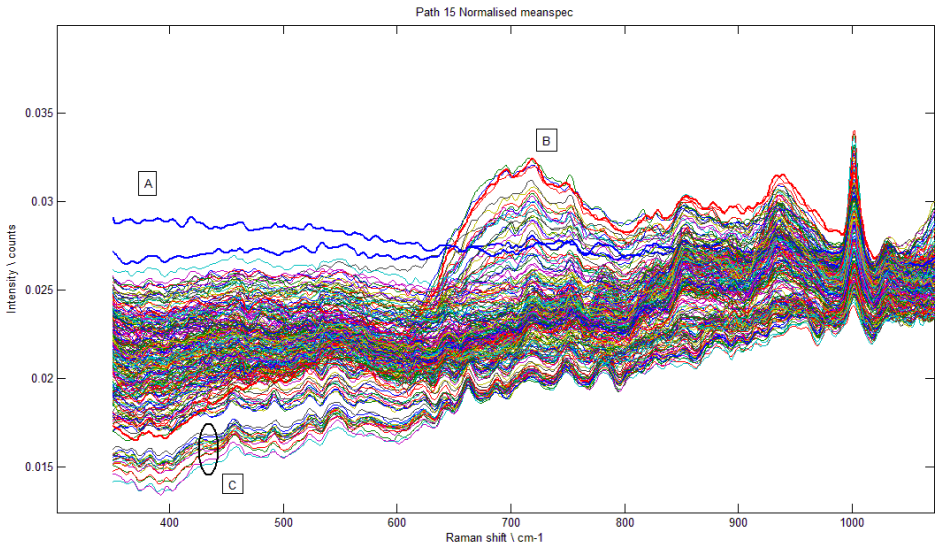

Figure 4.63: L2c-3 – Magnified section of normalised spectra for SG 10 (Controls - normal squamous epithelium).

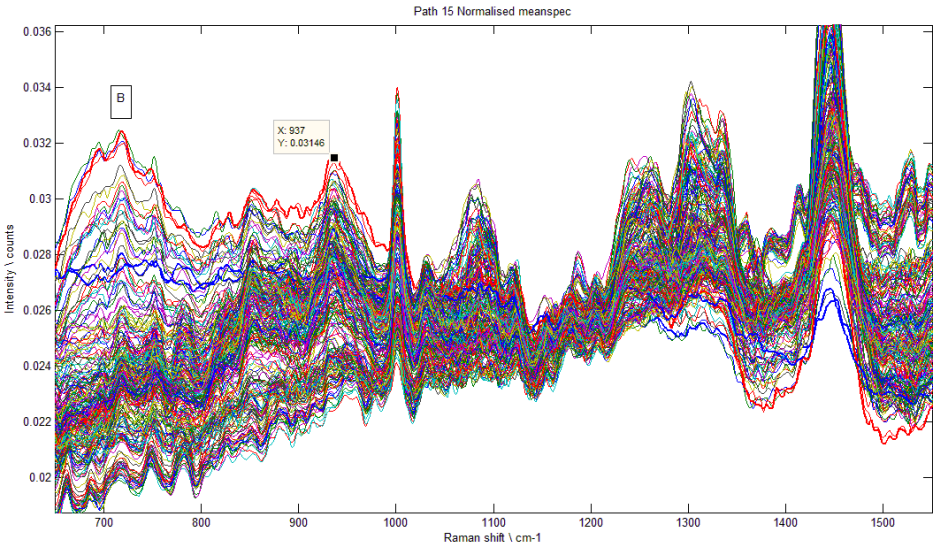

Figure 4.64: L2c-3 – Further magnified section of normalised spectra for SG 10 (Controls normal squamous epithelium).

The multivariate analysis of this series of mini models has been very useful in clarifying the advantages of further refining a model although this must be viewed in the light of a decreasing and more imbalanced dataset, the scatter plots do reemphasise these points. The colour coding of the data sets is consistent throughout with reference to the order the groups are compared, detailed in Table 4.14. The colours are assigned in the order green, blue, red and cyan for example in mini model L2c green codes SG1 (SCC), blue SG5 (All controls) and red SG7 (Abnormal mucosa). Reviewing the scatter plots even taking into account the discrepancy in spectra numbers SG5 (All controls) does again seem to be dividing into two (Figure 4.49). In Figure 4.51 the SCC group has a very definite area of maximal density but there is a distinct overlap group with the abnormal mucosa and hyperplasia/hyperkeratosis groups.

Comparing L2c to L2c-1 where the all-controls group is replaced by one of its subgroups, SG3 (hyperkeratosis/hyperplasia), there is an improvement in the percentage of correctly predicted spectra for all study groups. The largest improvement is seen in SG7. That is some of those spectra wrongly predicted in L2c as belonging to SG7 (Abnormal mucosa) are predicted correctly when SG5 (All controls) is replaced by SG3 (hyperkeratosis/hyperplasia).

Comparing L2c-1 and L2c-2; the difference between these is that SG3 (hyperkeratosis/hyperplasia) is replaced by SG10 (Normal squamous epithelium). A significant improvement is seen in the ability of the model to predict both SG7 (Abnormal mucosa) and also SG10 (Normal squamous epithelium) with very little change in the result for SG1 (SCC).

The final mini model in this series replaces SG7 (Abnormal mucosa) with SG14 (Dysplastic mucosa). Spectra of samples classified as carcinoma in situ have been

removed leaving only dysplastic mucosa spectra in SG14. Again there a further improvement in the prediction of samples classified as SG10 (Normal squamous epithelium) and a slight improvement in the result for SG1 (SCC). The ability of this model to predict SG14 (Dysplastic mucosa) is reduced compared to the prediction for SG7 (Abnormal mucosa) in mini-model L2c-2 however the imbalance in spectra numbers is the worst for this model

4.2.3.6 L3 - Mild dysplasia / Moderate dysplasia / Severe dysplasia / Carcinoma in situ (SG2/SG6/SG8/SG9)

Empirical analysis

Figure 4.65 is a plot of the overlaid, normalized mean spectra for this model. With 4 study groups there are 12 possible difference spectra and examples of these can be found in *Appendix D.3.8.* Figure 4.66 is the corresponding PIR histogram.

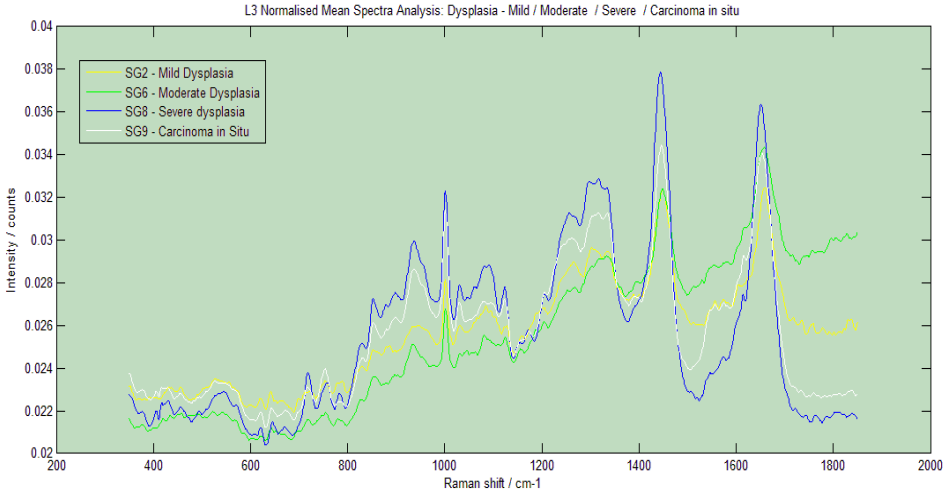

Figure 4.65: L3 – Overlaid normalised mean spectra.

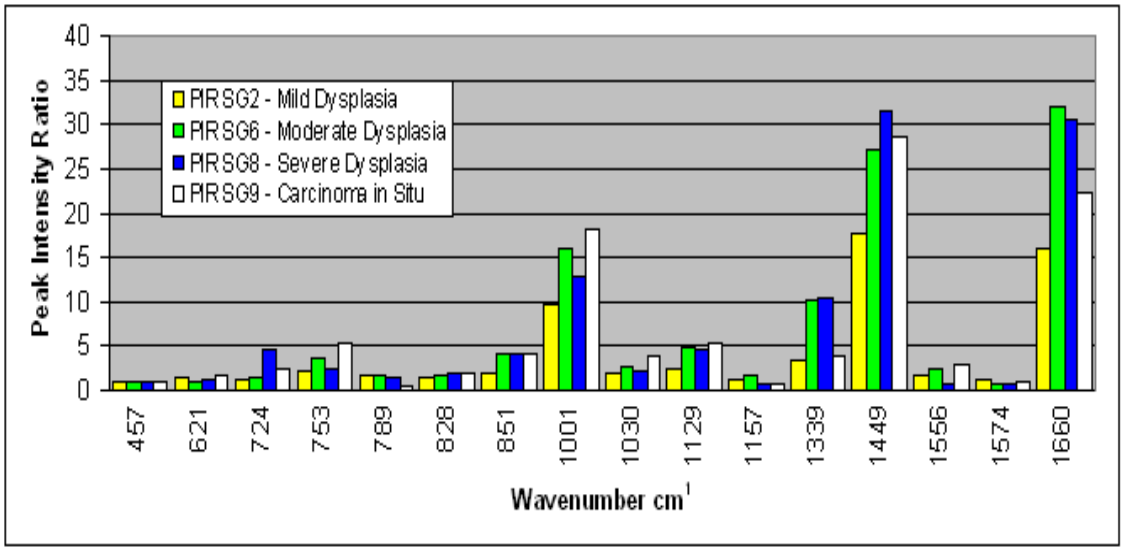

Figure 4.66: L3 – Peak intensity ratios for Study Groups 2, 6, 8 and 9.

Multivariate analysis

Figure 4.67 shows the mean centred dataset for mini model L3 and Figures 4.68 to 4.72 the results of the multivariate analysis.

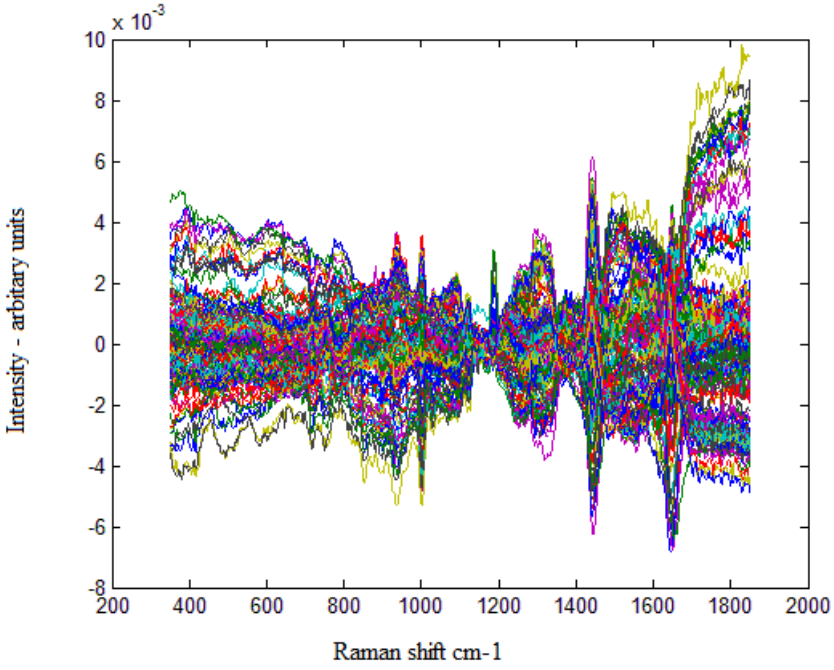

Figure 4.67: L3 – Mean centred data set.

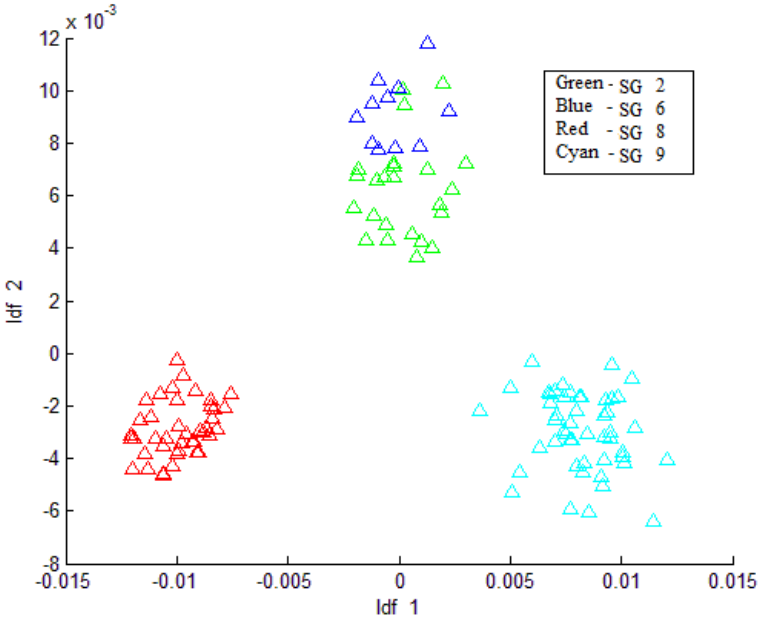

Figure 4.68: L3 – Scatter plot comparing linear discriminant functions 1 & 2.

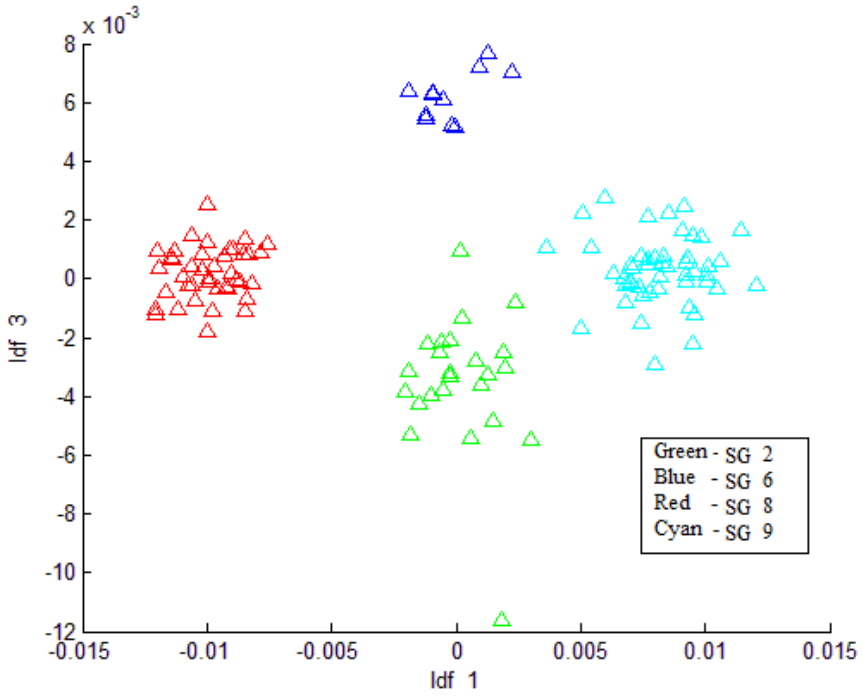

Figure 4.69: L3 – Scatter plot comparing linear discriminant functions 1 & 3.

L3	% Correct
SG2	96.1
SG6	100.0
SG8	100.0
SG9	100.0

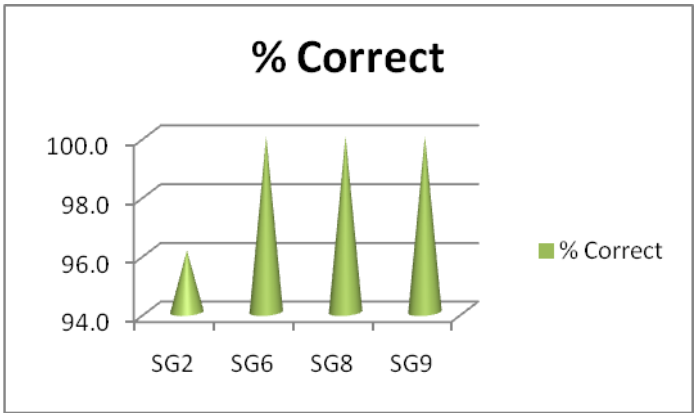

Figure 4.70: L3 – Classification of study group samples by multivariate analysis.

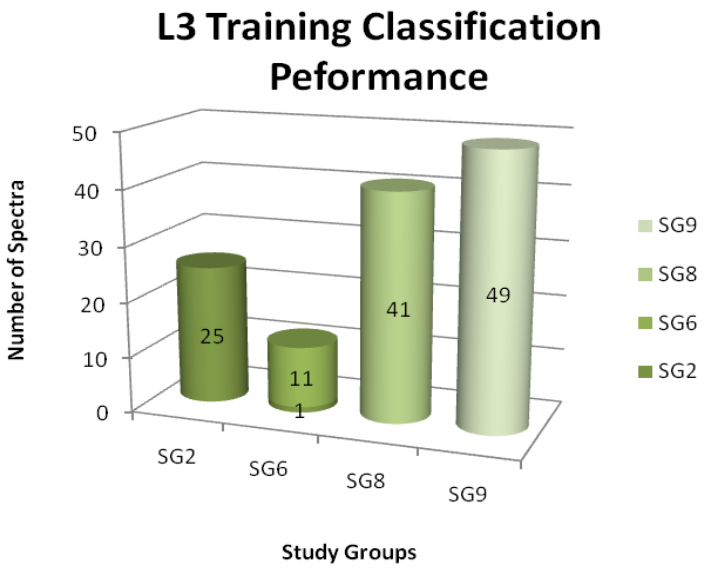

L3	SG2	SG6	SG8	SG9	Sensitivity	Specificity
SG2	25	1	0	0	96.2%	91.8%
SG6	0	11	0	0	100.0%	96.3%
SG8	0	0	41	0	100.0%	98.8%
SG9	0	0	0	49	100.0%	100.0%

Figure 4.71: L3 – Training classification performance

ID	Group	Group2	Dot Product
A	Mild dysplasia (SG2)	Moderate dysplasia (SG6)	0.994
B	Mild dysplasia (SG2)	Severe dysplasia (SG8)	0.9925
C	Mild dysplasia (SG2)	Carcinoma in Situ (SG9)	0.991
D	Moderate dysplasia (SG6)	Severe dysplasia (SG8)	0.9933
E	Moderate dysplasia (SG6)	Carcinoma in Situ (SG9)	0.9916
F	Severe dysplasia (SG8)	Carcinoma in Situ (SG9)	0.9931

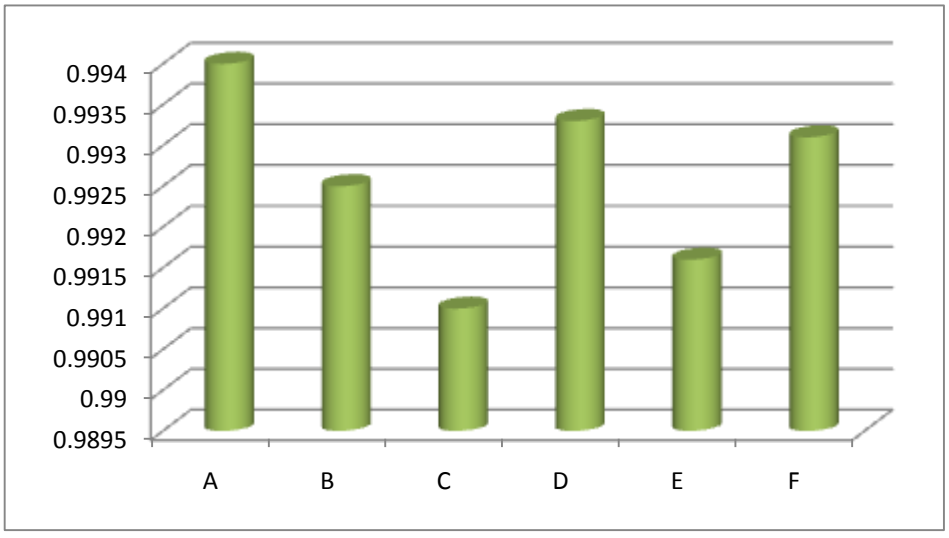

Figure 4.72: L3 – Results of dot product analysis.

Discussion

Differentiation between these groups is notoriously difficult both clinically and histologically and so it was felt that despite the small number of samples available it was important to begin the analysis of this dataset and use it as a pilot study on which to base future work.

The main difficulty in this study is that the numbers of patients, samples and spectra are extremely small. Each of the dysplasia groups contains one patient and there are two in the carcinoma in situ group. 1 sample was obtained for both the mild and moderate dysplasia groups and from these 26 spectra obtained from the former and 11 from the latter. 41 spectra were obtained from the single sample showing severe dysplasia and 49 from the two samples of carcinoma in situ.

The carcinoma in situ overlaid normalised spectra show some unusual features, for example those labeled in Figure 4.73 and also shown in Figure 4.74, the latter has been magnified.

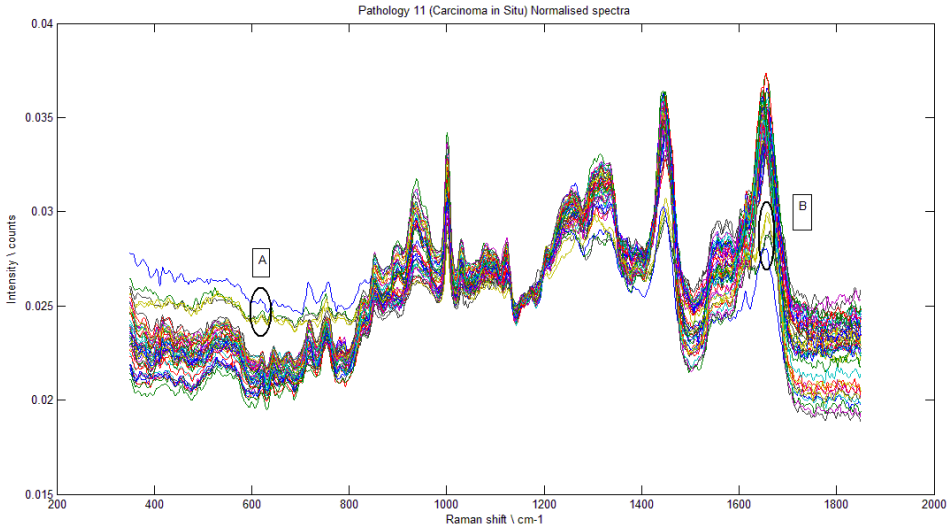

Figure 4.73: L3 – Normalised spectra for pathology 11 (SG9) - Carcinoma in Situ.

It is important when assessing a group of spectra that appear to vary significantly from the mean to appreciate the features that set them apart may simply be a reflection of the variance across the dataset. In this case there does appear to be distinct differences in the spectra shape and this can be seen in the 716 to 757cm^{-1} range.

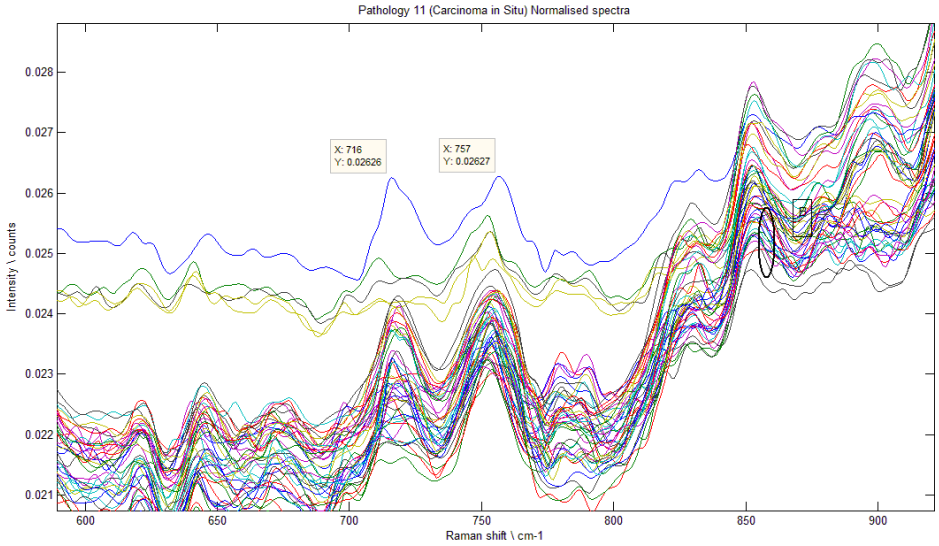

Figure 4.74: L3 – Normalised spectra magnified for pathology 11 (SG9) - Carcinoma in Situ.

Limited conclusions can be drawn from this data but it is interesting to note that the main shared peaks can be attributed to DNA (724cm^{-1}), tyrosine (851 cm^{-1}), lipids (1129 cm^{-1}), nucleic acids (1339 cm^{-1}) and protein (1660 cm^{-1}) with the largest PIRs in the lipid and protein ranges. The mild dysplasia group consistently has the lowest PIRs and those of moderate and severe dysplasia tend to be similar. The PIRs for dysplastic tissue at 1449cm^{-1} vary in a way that would be expected from our knowledge of the disease process to date as do those at 1339 cm^{-1}, a peak which is related to nucleic acid content.

Very little can be drawn conclusively from the results of the multivariate analysis in this mini model however the scatter plot Figures 4.68 does seem to show that in this model the spectra represented by green (mild dysplasia) and blue (moderate dysplasia) seems to relate to each other.

An additional piece of data analysis was performed on the dataset from this model. Knowledge of the disease process would suggest that the molecular configuration of the tissue should change in a way that reflects the progression of disease from mild through moderate to severe dysplasia and finally to carcinoma in situ. Empirical analysis did not uphold this but only specific peaks were considered and a great deal of information from the spectra was not used. Whilst multivariate analysis improves on this it still breaks down the spectra into a limited number of PCs. In view of this a dot product analysis was applied to the data set after the background signal had been removed. This analysis calculates the cosine of the angle between the two datasets, in this case the normalised mean spectra. The cosine of the angle is the result of the dot product of the two spectra divided by the product of their size vectors. If the spectra are identical the angle between them will be 0 and the cosine of this is 1. If the spectra are maximally different the angle will be 90 degrees and the cosine of this is 0. In summary the closer the spectra are to each other the nearer the dot product will be to 1. The results of this analysis is summarised in Table 4.72. It can be seen that when the data is analysed in

this way the spectra that are most similar are mild dysplasia (SG2) and moderate dysplasia (SG6), moderate and severe dysplasia (SG6 & SG8) and severe dysplasia and carcinoma in situ (SG8 & SG9) which would agree with our knowledge of the disease and suggests that Raman spectroscopy may be used to differentiate these conditions but that studies containing larger sample numbers are required.

4.2.3.7 L4 - Carcinoma in Situ / Poorly differentiated SCC / Moderately differentiated SCC / Well differentiated SCC (SG9/SG11/SG12/SG13)

Empirical analysis

This mini model utilises the relatively large number of spectra from SCC samples and begins to assess the ability of Raman spectroscopy to differentiate between different grades of SCC and carcinoma in situ. Figure 4.75 shows the overlaid, normalised mean spectra from the SGs, Figures 4.76 and 4.77 the PIR histograms for both L4 and L4-2 models. Figure 4.78 shows the PIRs at two specific peaks and assesses their relationship to each other. Figure 4.79 shows the separation of the study groups in L4_1 and Figure 4.80 demonstrates the mean centred data for L4. Scatter plots are demonstrated for both the L4 and L4-2 models in Figures 4.81 to 4.85 and the results of training classification performance for both are recorded in Figures 4.86 to 4.89.

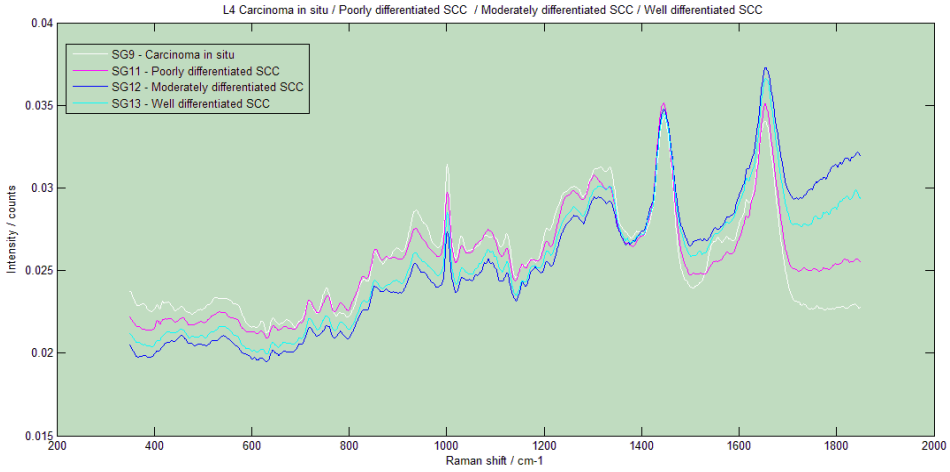

Figure 4.75: L4 – Overlaid normalised mean spectra.

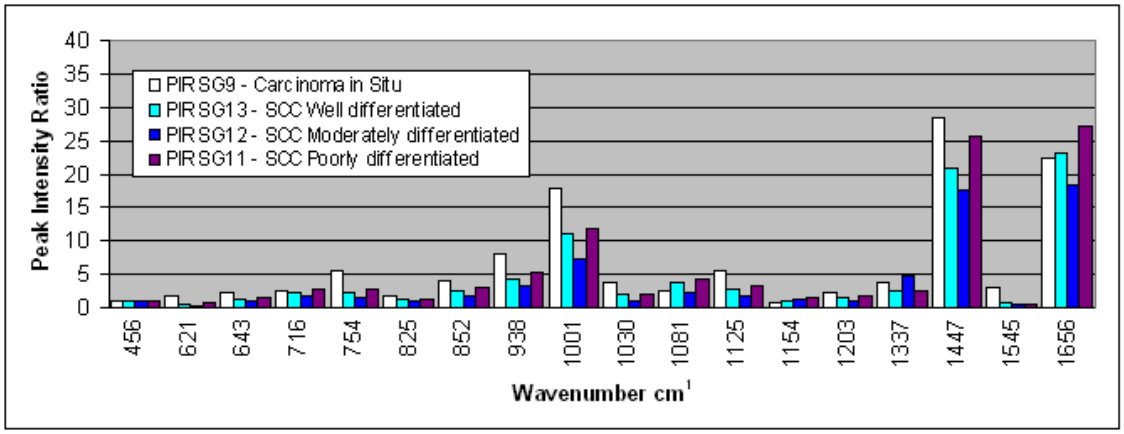

Figure 4.76: L4 – Peak intensity ratios for Study Groups 9, 11, 12 and 13.

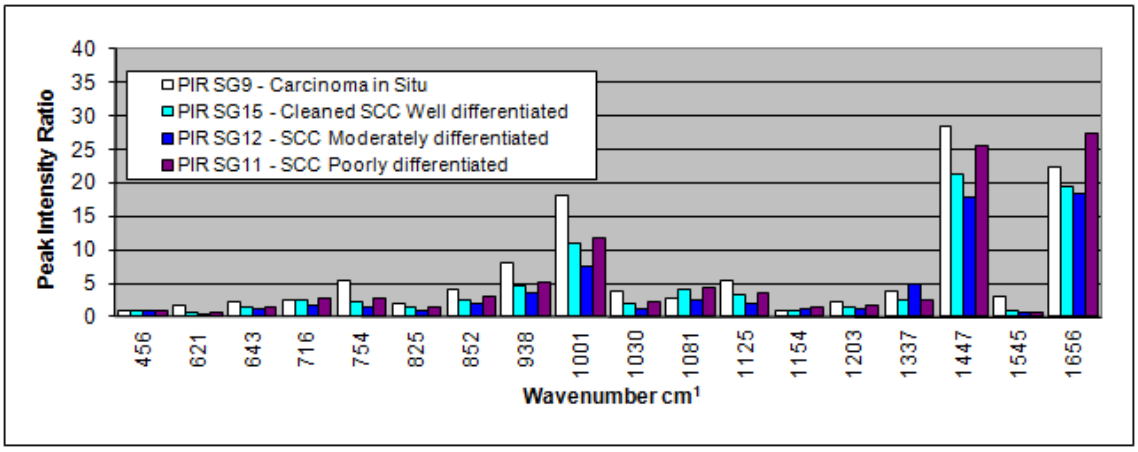

Figure 4.77: L4-2 – Peak intensity ratios for Study Groups 9, 11, 12 and 15.

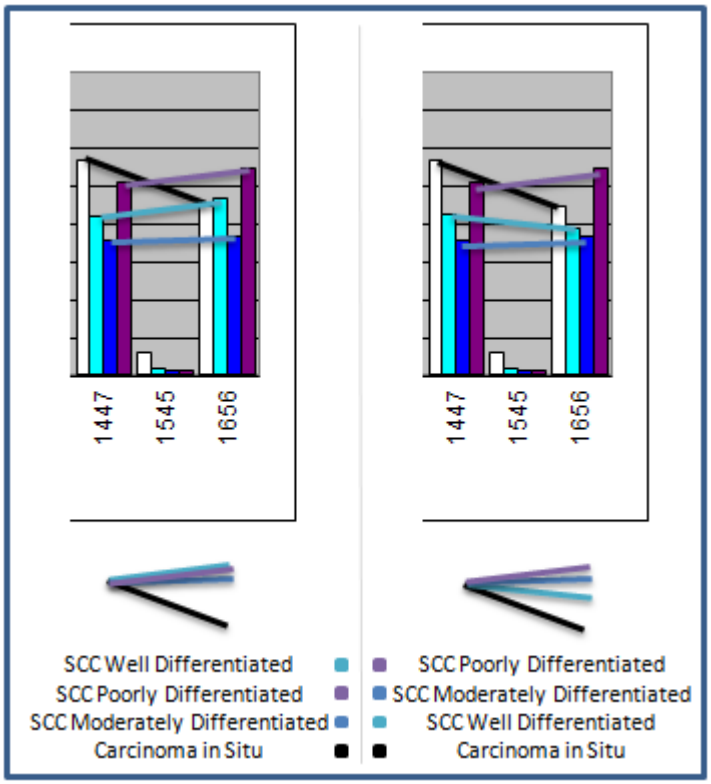

Figure 4.78: L4-2 – Peak intensity ratio comparison for Study Groups 9, 11, 12 and 13 at peak positions 1447 and 1656 cm^{-1}.

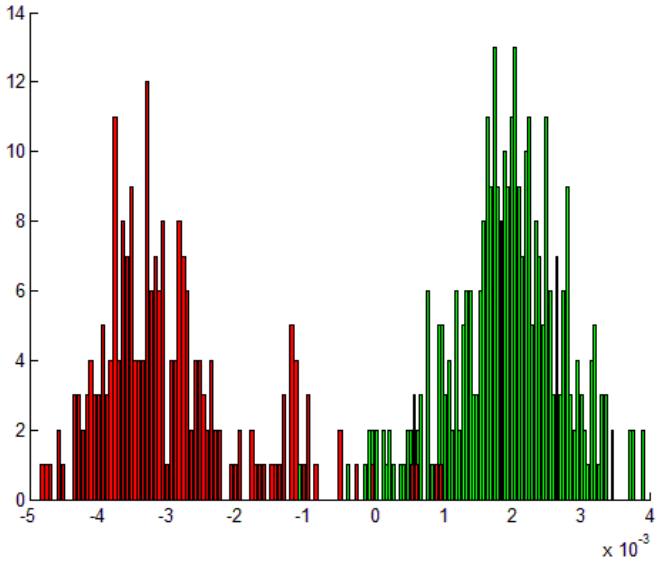

Figure 4.79: L4_1 – Histogram demonstrating the separation between SG3 and SG13.

Multivariate analysis

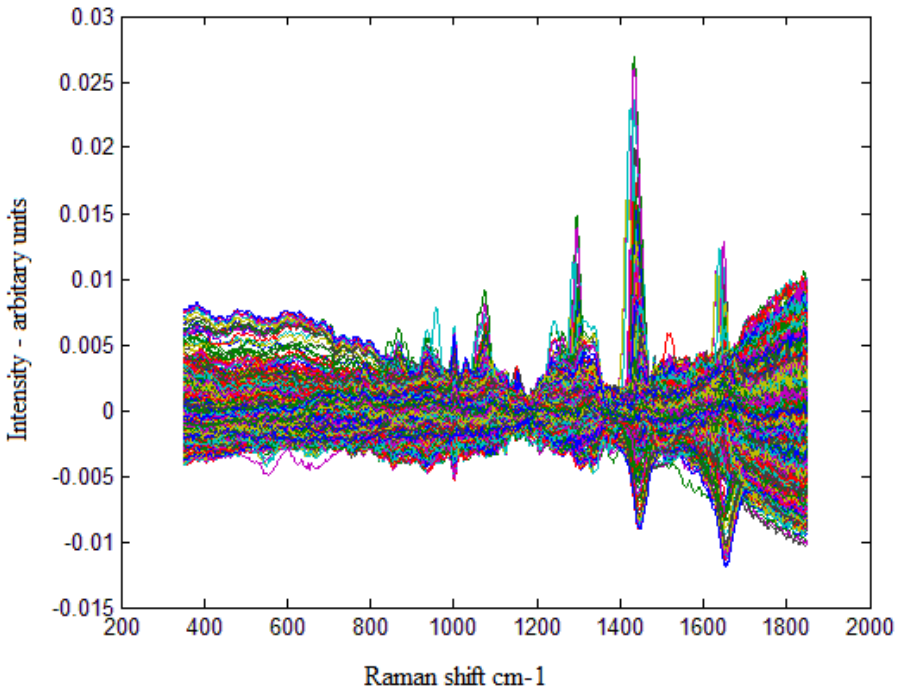

Figure 4.80: L4 - Mean centred data set.

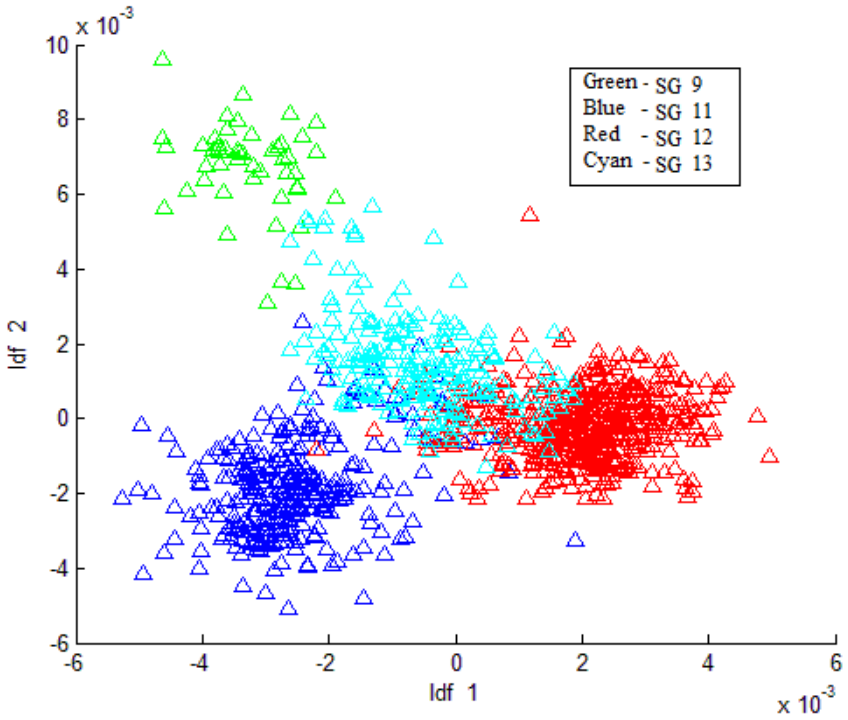

Figure 4.81: L4 – Scatter plot comparing linear discriminant functions 1 & 2.

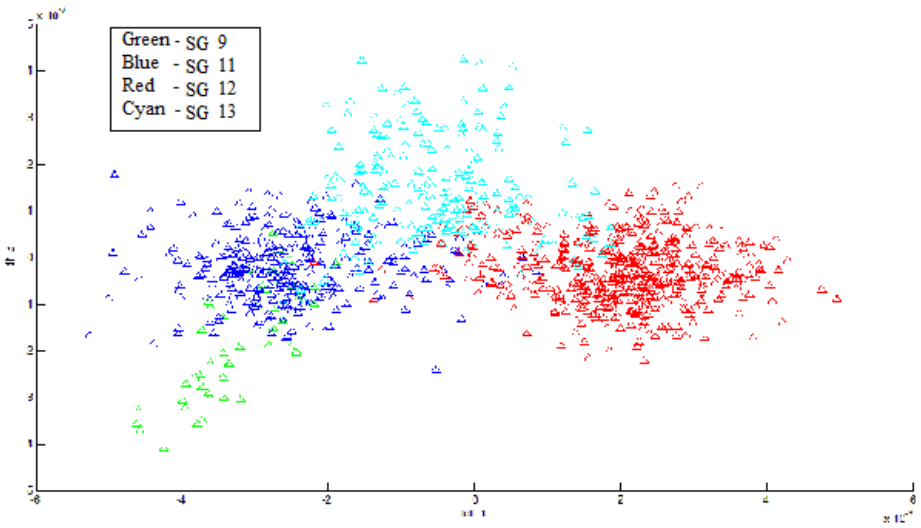

Figure 4.82: L4 - Scatter plot comparing linear discriminant functions 1 & 3.

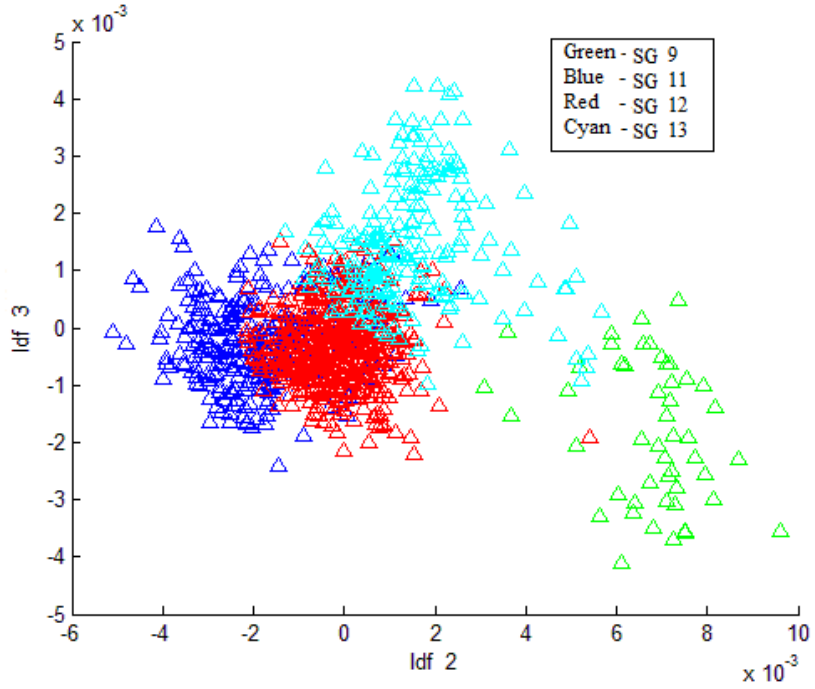

Figure 4.83: L4 - Scatter plot comparing linear discriminant functions 2 & 3.

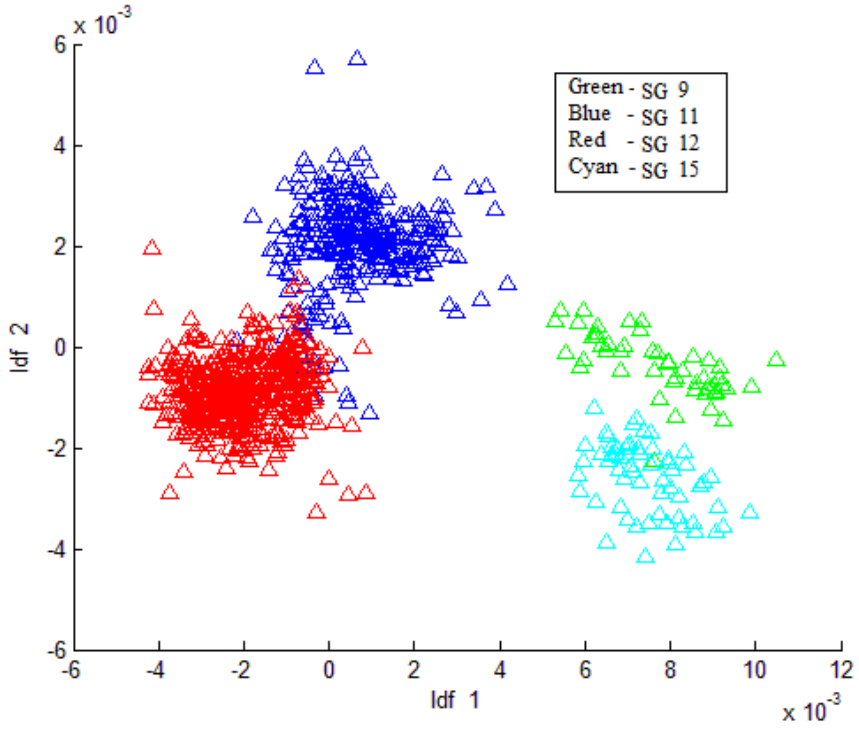

Figure 4.84: L4-2 - Scatter plot comparing linear discriminant functions 1 & 2.

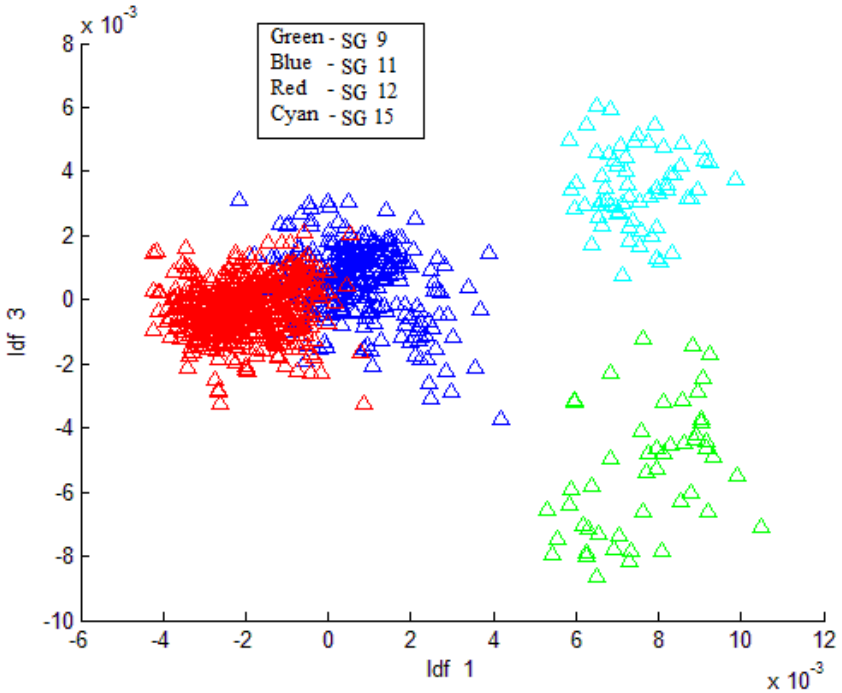

Figure 4.85: L4-2 - Scatter plot comparing linear discriminant functions 1 & 3.

L4	% Correct
SG9	98
SG11	90.7
SG12	94.2
SG13	87.2

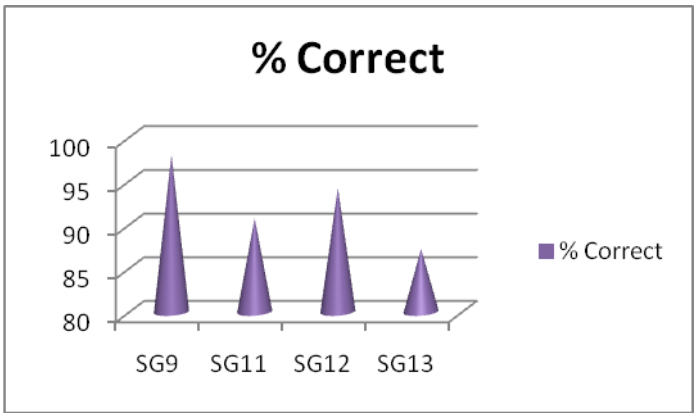

Figure 4.86: L4 - Classification of study group samples by multivariate analysis.

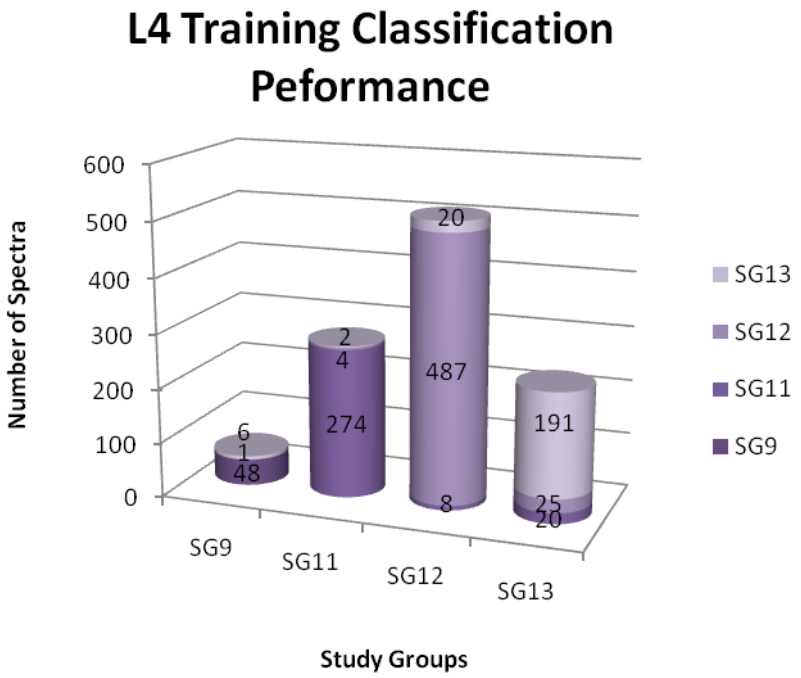

L4	SG9	SG11	SG12	SG13	Sensitivity	Specificity
SG9	48	0	0	1	98.0%	99.3%
SG11	0	274	8	20	90.7%	99.2%
SG12	1	4	487	25	94.2%	95.1%
SG13	6	2	20	191	87.2%	94.7%

Figure 4.87: L4 – Training classification performance

L4-2	% Correct
SG9	98.0
SG11	90.7
SG12	94.4
SG15	87.3

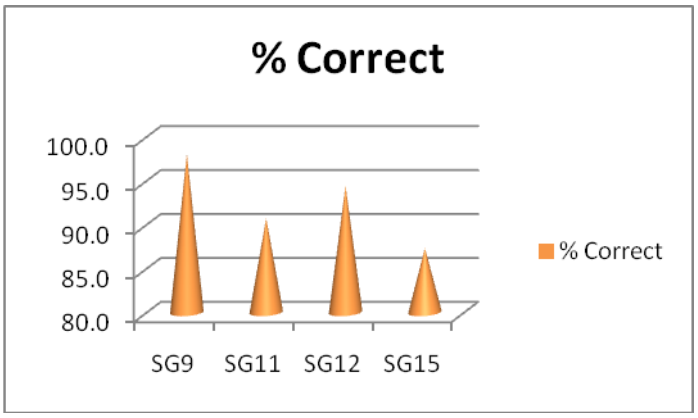

Figure 4.88: L4-2 - Classification of study group samples by multivariate analysis.

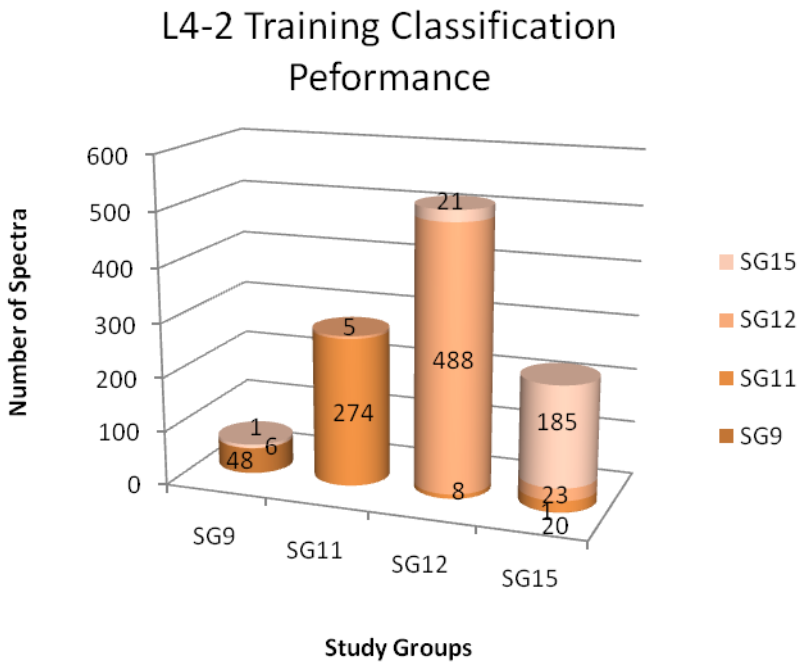

L4-2	SG9	SG11	SG12	SG15	Sensitivity	Specificity
SG9	48	0	0	1	98.0%	99.3%
SG11	0	274	8	20	90.7%	99.4%
SG12	1	5	488	23	94.4%	94.8%
SG15	6	0	21	185	87.3%	94.9%

Figure 4.89: L4-2 – Training classification performance

Discussion

L4 investigates the ability of Raman spectroscopy to differentiate between subgroups of SCC and also begins to assess if Raman spectroscopy can be used to solve the important clinical problem of differentiation of carcinoma in situ from SCC.

This mini model is very limited by small sample numbers particularly in the carcinoma in situ and well differentiated SCC groups. 49 spectra were obtained from 2 samples, provided by two patients for carcinoma in situ and 4 patients provided 15 tissue samples for the moderately differentiated SCC group. 219, 517 and 302 spectra were obtained from the well, moderately and poorly differentiated SCC samples There is a much better balance in the spectral data numbers when only the SCC specimens are included but it is important to note again that the number of patients providing these specimens varies with only one in the well differentiated group and 4 and 5 in the moderately and poorly differentiated groups respectively. Overall there is a large number of spectra from samples containing SCC and these are reasonably evenly spread between the three subgroups. Should the SCC subgroups separate this would help lend some confidence in that result. All these factors must be considered and must limit confidence in the results of the complete model however it is included as it shows the successful application of the empirical and multivariate analytical tools in directing the interrogation of the results as is noted further on in the discussion.

The use of empirical techniques based on visualization of the overlaid spectra is difficult when there are four spectra however there appears to be differences between the spectra for carcinoma in situ and those of SCC at 1096 cm^{-1} a region associated with phosphate and DNA. There also appears to be a prominent shoulder in the carcinoma in situ spectra over the range 1510 to 1600 cm^{-1} and this may be attributed to amino acids such as tyrosine but interestingly it has also been shown to be present in heme. There is a broad set of positive peaks between 400 cm^{-1} and 500 cm^{-1} which may have a significant contribution from glycogen as there are also peaks attributable to this compound in the same orientation at1122 cm^{-1} and 1380 cm^{-1}.The two positive peaks at 1029 cm^{-1} and 1166 cm^{-1} are seen in the spectra of collagen.

This model generates six difference spectra. The difference spectra resulting from poorly differentiated SCC subtracted from carcinoma in situ shows the most obvious differences (*Appendix D.3.9*). This is as would be expected as these two pathologies are the furthest apart in severity. A positive peak is present in the difference spectra at 1274 and this wavenumber has been assigned to a Raman signal from heme. This combined with the finding noted from review of the overlaid spectra suggests the possibility that the carcinoma in situ sample may contain heme as a contaminant. There are negative signals over the 770-880 and 1410 to 1530 cm^{-1} ranges, the former is a range where DNA produces Raman signals and the latter mainly lipid and protein.

A comparison of the PIRs for these study groups produced patterns that did not intuitively trend suggesting the possibility that the spectra from the well differentiated SCC group (SG 13) might be slightly unusual. This prompted a closer look at the original data. The data from SG13 was analysed against that from SG3 (mini model L4-1), the latter group was arbitrarily chosen in order to assess if a histogram might show a double peak for the SG13 data as per the discovery made in L2a. Figure 4.79 shows that there might be the possibility of a double peak in the red histogram i.e. that of SG13 but this was by no means definitive and may be just indicative of missing data in a normal distribution.

The next step was that the plot containing all the normalised spectra for SG13 (pathology group 14 – Well differentiated SCC) was carefully examined and there was a band of 7 spectra seen to be clearly different. All these spectra came from the same sample which had 35 spectra in total. The spectra were all collected on same day and were not recorded consecutively These seven spectra were removed from the data set and a new amended data set produced in addition to the original, this was called SG15. The normalised mean spectra from this new group (SG15/path 01) was subtracted from that of SG13 in the hope that the difference spectra might give some idea as to the areas in which the differences arose however this was unsuccessful. It is felt that the imbalance in spectra numbers and more importantly the fact that mean spectra were compared is likely to be the reason for this.

The new data set was then used to rerun the model and the PIRs recalculated. The pattern of the PRIs altered to one that showed a gradation smoothly through carcinoma in situ, well, and moderate and poorly differentiated SCC as would be expected. The multivariate analysis also showed a marginal improvement. In this study PIRs histograms proved useful in detecting subtleties in sets of spectra and the detailed look at the histogram for L4-2 between 1447 and 1656cm^{-1}shows a trend in PIRs that would be expected for these diseases and agrees with the findings noted by other authors (Stone, 2000)

The multivariate analysis on the original data set of mini model L4 gives a scatter plot, when linear discriminant functions (ldf) 1 and 2 are compared, that shows a separation of the four groups (Figures 4.81, 4.82 & 4.83). Whilst the group containing specimens of carcinoma in situ (green) contains fewer spectra this group does appear to sit apart from those of SCC. In Figure 4.83 there is one spectrum from the moderately differentiated group that sits within the carcinoma in situ group but considering the great difficulty in consistently differentiating between these groups histologically it is encouraging that there is so little overlap and incongruous spectrum positions. The L4-2 model has been shown to have better PRI correlation with disease and also shows better group separation on multivariate analysis scatter plots (Figures 4.84 & 4.85). These plots also show moderate and poorly differentiated SCC and well differentiated and carcinoma in situ groups sitting closer together again this would agree with our understanding of the spectrum of this disease. The percentage of spectra correctly predicted by model L4-2 is the same for carcinoma in situ and marginally better for all the SCC subgroups compared to the results for the basic L4 model.

4.3 Lymph Node Study

The variety of tissue samples collected and the range of diseases present necessitated a slightly different and simplified approach to the lymph node study work. The primary question of whether Raman spectroscopy is capable of differentiating lymph nodes within the neck that showed reactive changes from those which contained tissue exhibiting features of neoplastic change was addressed. The second question, which has equal importance to the clinician, is whether Raman spectroscopy can differentiate between SCC, lymphoma and adenocarcinoma.

4.3.1 Data summary

Tables 4.19, 4.20 and 4.21 summarise the data organisation for these mini models in total 48 patients were recruited to take part in this work and from these patients 159 tissue samples and 4549 spectra obtained. The mean number of spectra per patient was 95 (range 15 to 242) and the mean number of spectra per sample 29 (range 15 to 44). The samples were generally much larger and. the range of diseases seen wider in the lymph node study compared to the larynx study. For studies N1 and N2 only part of the dataset was used; 86 spectra from the reactive lymph node (SG1) and 4 from the SCC (SG3) group, this resulted in two samples being lost from (SG1). This was due to a lack of phenylalanine peaks in these spectra meaning that they could not be corrected in the same way as the other spectra so were put to one side and will be looked at separately at another time to check they are not representing a subgroup of disease not accommodated for in the classification. For the four group model only spectra from samples containing Hodgkin's lymphoma (pathology codes16, 17, 19) were used for the main analysis, more samples are now available as detailed in the specimen summary (Table 4.19) and these will be used in the future to expand the spectra dataset and begin work on assessing the efficacy of Raman spectroscopy in differentiating subgroups of the disease. During empirical analysis it was noted that the spectra for Non-Hodgkin's lymphoma shows some subtle but clear differences from both Hodgkin's lymphoma and the other study groups, this would also warrant further work in the future.

Table 4.19: Numerical data for individual pathology coded specimens in lymph node studies.

Pathology Code	Description	Number of Patients	Number of Samples	Number of Spectra	Average Spectra per Sample	Average Spectra per patient
1	Reactive Lymph node	*18*	*55*	*1475*	*27*	*82*
2	Branchial cyst	*1*	*1*	*15*	*15*	*15*
3	Fibrous connective tissue	*3*	*6*	*134*	*22*	*45*
4	Normal squamous epithelium	*3*	*8*	*202*	*25*	*67*
5	Fat	*0*	*0*	*0*	*0*	*0*
6	Parotid salivary tissue	*1*	*8*	*226*	*28*	*226*
7	Normal thyroid tiassue	*1*	*5*	*78*	*16*	*78*
8	SCC - Poorly differenciated	*3*	*6*	*170*	*28*	*57*
9	SCC - Moderately differentiated	*4*	*18*	*622*	*35*	*156*
10	SCC - well differentiated	*0*	*0*	*0*	*0*	*0*
11	Adenocarcinoma	*1*	*8*	*242*	*30*	*242*
12	Pleomorphic adenoma	*2*	*3*	*132*	*44*	*66*
13	Poorly differentiated carcinoma	*2*	*8*	*251*	*31*	*126*
14	Thyroid - papillary carcinoma	*2*	*5*	*165*	*33*	*83*
15	Thyroid - follicular carcinoma	*1*	*7*	*187*	*27*	*187*
16	Hodgkin's lymphoma (HL) - mixed cellularity	*1*	*2*	*60*	*30*	*60*
17	HL - nodular sclerosing	*1*	*4*	*113*	*28*	*113*
18	HL - follicular cell	*1*	*1*	*34*	*34*	*34*
19	HL - classical lymphocyte predominant	*1*	*4*	*149*	*37*	*149*
20	HL - Non-classical	*1*	*2*	*62*	*31*	*62*
21	Non-Hodgkin's lymphoma (NHL) - diffuse large B cell	*1*	*8*	*232*	*29*	*232*
22	NHL - Low grade malignant	*0*	*0*	*0*	*0*	*0*
23	NHL - MALT type	*0*	*0*	*0*	*0*	*0*

The numerical data and combinations of pathology codes used to make up the lymph node study groups are detailed in Table 4.20 and 4.21. The best balance of data is for

mini model N1. The balance of data for N2 is less good and adenocarcinoma is the least well represented.

Table 4.20: Numerical data for combinations of pathology codes used to form lymph node study groups.

Study Group	Description	Pathology Codes	Number of Patients	Number of Samples	Number of Spectra
1	Reactive Lymph node	1	*18*	*53*	*1389*
2	Cancer	8,9,11,16,17,19, 21	*12*	*50*	*1584*
3	SCC	8,9	*7*	*24*	*788*
4	Adenocarcinoma	11	*1*	*8*	*242*
5	Hodgkin's Lymphoma	16,17,19	*3*	*10*	*322*

Table 4.21: Lymph node mini models – a comparison between different study groups.

Mini Model	Description	Study Group	Description	Study Group	Description	Study Group	Description	Study Group
L1	Reactive Lymph node	**1**	Cancer	**2**				
L2	Reactive Lymph node	**1**	SCC	**3**	Adenocarcinoma	**4**	Hodgkin's Lymphoma	**5**

4.3.2 Diagnostic models

4.3.2.1 N1 Reactive tissue/Neoplastic tissue

There can be difficulties in interpreting the spectral differences between two groups were one contains such a diverse range of tissue samples as the cancer group in this study so a simple two group model was formulated which aimed to address the question as to whether Raman spectroscopy could differentiate reactive lymph nodes from those containing cancer.

A more detailed empirical look at the mean normalised spectra is discussed in *Section 4.3.2.2.*

25 statistically significant principal components determined by ANOVA were examined and Figures 4.91, 4.92 & 4.93 shows the load plots with those for PCs 5 and 6 shown in more detail. Linear discriminant analysis exhibited a clear separation between the study groups as is demonstrated in Figure 4.90.

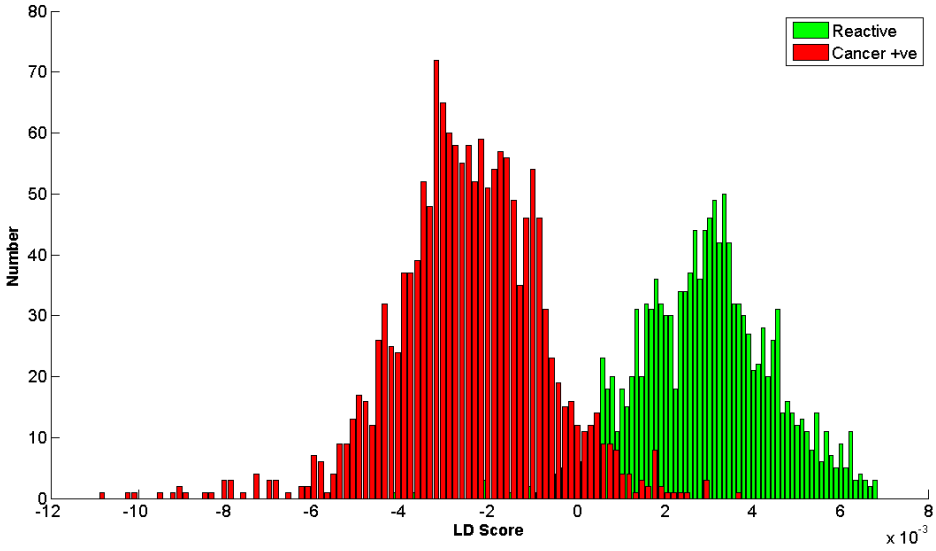

Figure 4.90:.N1 – Histogram of lymph node two group model showing separation of reactive lymph nodes from those containing cancer.

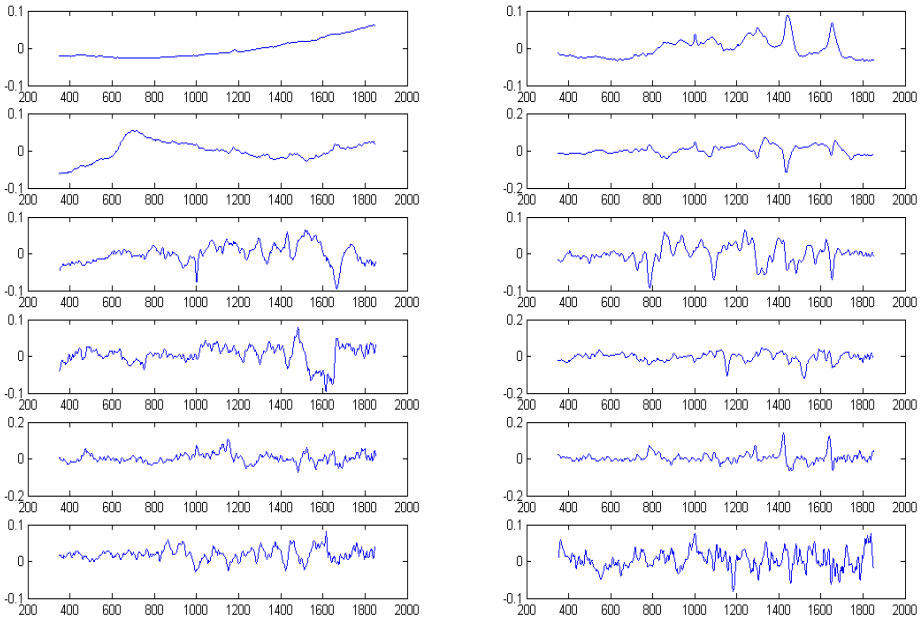

Figure 4.91:.N1 – LDA loads.

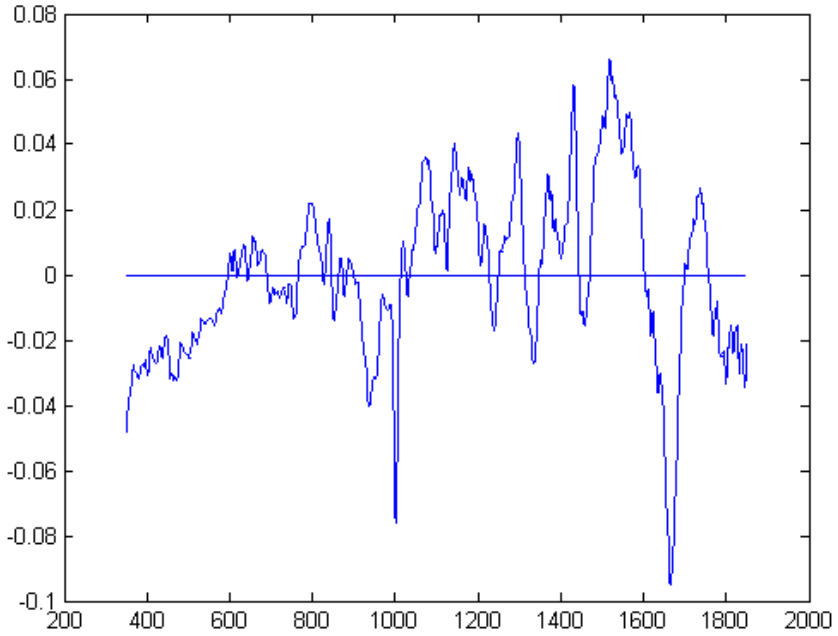

Figure 4.92:.N1 – PC load 5.

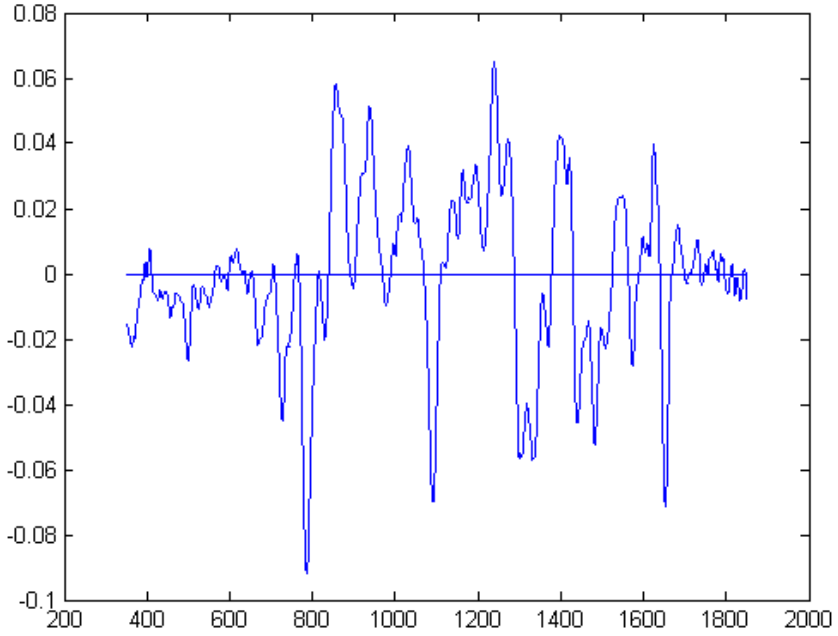

Figure 4.93:.N1 – PC load 6.

These load plots can help tease out significant differences between study group spectra which may be obscured in the overlaid normalised mean spectra plot for example PC 6 looks positive for the presence of collagen.

This model was cross-validated and the results of this are summarised in Tables 4.22 and 4.23. The results are very encouraging, for the two group model the cross-validated result showed 90% specificity for cancer and 88% for reactive nodes and the reverse for sensitivity.

Table 4.22:– N1 – Spectral prediction performance for 2 group model (leave one sample out - cross validation).

Spectral Prediction		
Histopathology	**Reactive**	**Cancer +ve**
Reactive	1245	144
Cancer +ve	192	1392
Sensitivity	90	88
Specificity	88	90

It was interesting to note that cross-validation assessing spectral performance by node showed even better results. Assessment of the model by node could be viewed as somewhat closer to the clinical scenario and a help in negating somewhat the effects of aberrant spectra.

Table 4.23:- N1 – Spectral prediction performance by node for 2 group model (leave one sample out - cross validation).

Spectral Prediction		
Histopathology	**Reactive**	**Cancer +ve**
Reactive	49	4
Cancer +ve	7	43
Sensitivity	92	86
Specificity	86	92

4.3.2.2 N2 Reactive Lymph nodes/ SCC/Adenocarcinoma/Lymphoma

This mini model is a natural progression from N1. In the past it has been difficult to balance sample numbers in this type of study because of the paucity of reactive lymph node specimens. In this work the reverse is true and the numbers of samples from adenocarcinoma and lymphoma could be improved. The figures did allow cross-validation on a leave one sample out basis to be performed. The results of the cross-validation studies are summarised in Tables 4.24 and 4.25.

Figures 4.94 and 4.95 show the normalised mean spectra for the study groups in this mini model with SG5 split into two; Hodgkin's and Non-Hodgkin's lymphoma. This split was prompted by knowledge of the difficulties that exist in the classification of

lymphomas. The thought being that Raman spectroscopy might be able to differentiate between the two types of lymphoma and in the future as the data set is expanded perhaps be able to subdivide them even further.

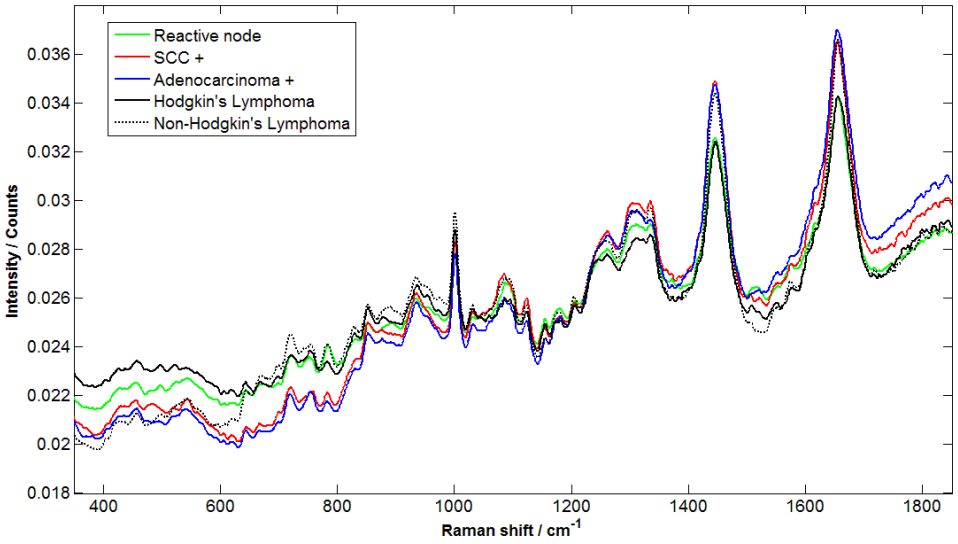

Figure 4.94:.N1 – PC:Overlaid mean normalised spectra for individual pathology groups.

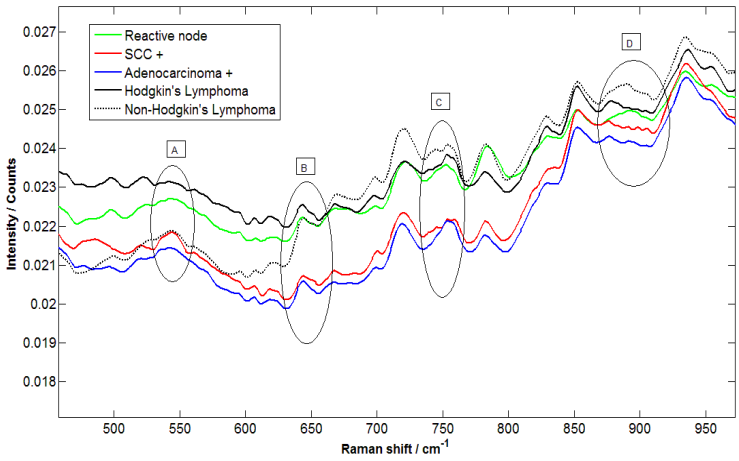

Figure 4.95:.N2 – Normalised spectra for individual pathology groups

The areas enclosed in the ovals show subtle differences in the spectra between the five different groups. In the mini model N2 Hodgkin and non-Hodgkin lymphoma groups are combined however it is interesting to note that there are distinct features within the spectrum for Non- Hodgkin's that distinguish it from the other groups. Even accounting for the variation in the baseline the feature labelled A shows that for SCC there appears to be a more prominent peak at 540cm^{-1}. At B and just beyond there are some unusual features in the plot for Non-Hodgkin's lymphoma were it crosses those of Hodgkin's lymphoma and reactive lymph nodes (670cm^{-1}). At 744cm^{-1} there is a small peak that is

seen in the spectrum for Non-Hodgkin's lymphoma and possibly in SCC but appears absent in the plot for adenocarcinoma. At 895cm^{-1} there is a broad peak that again is present in Non-Hodgkin's lymphoma and the spectrum for reactive lymph nodes. The feature at 540 cm^{-1} is likely to be a protein peak and that at 670 cm^{-1} can be attributed to the breathing of aromatic rings in purine bases (DNA). The peaks at 744 and 895 cm^{-1} can be assigned to phosphate bonds in DNA and DNA backbone.

Figure 4.96 shows the different linear discriminant functions for this model and Figure 4.97 is a 3D representation of the separation of the study groups achieved.

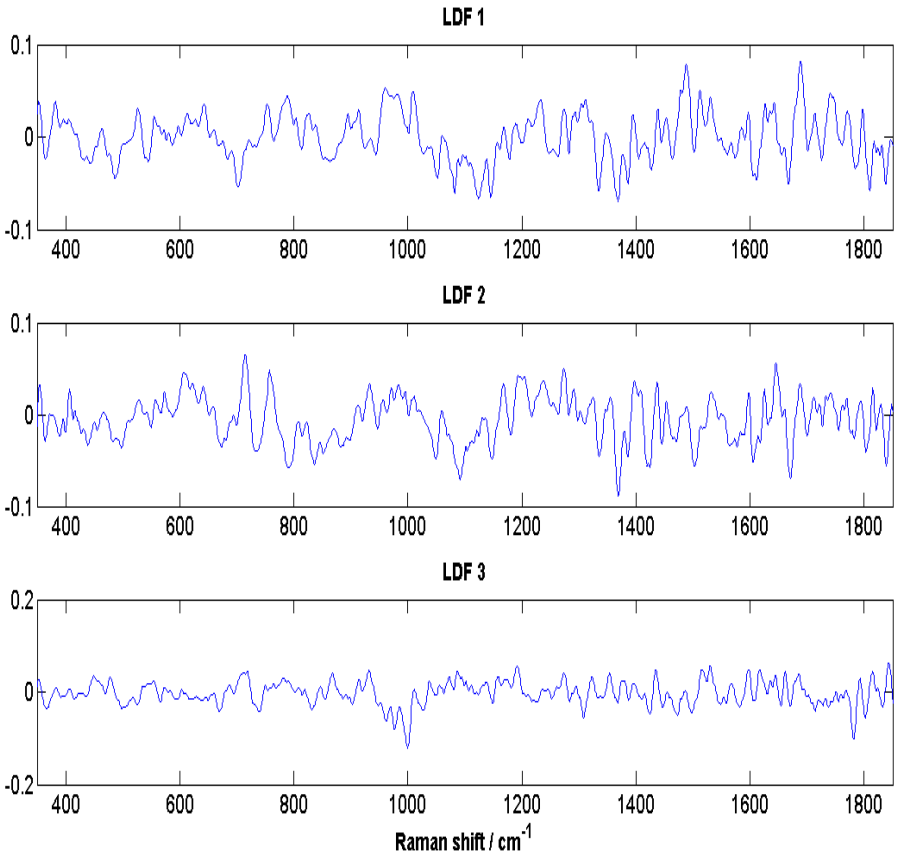

Figure 4.96:.N2 – Linear discriminate functions.

The 3D plot of the linear discriminant functions shows diagrammatically that the separation of the groups is excellent and to further assess the dataset a cross-validation study was performed.

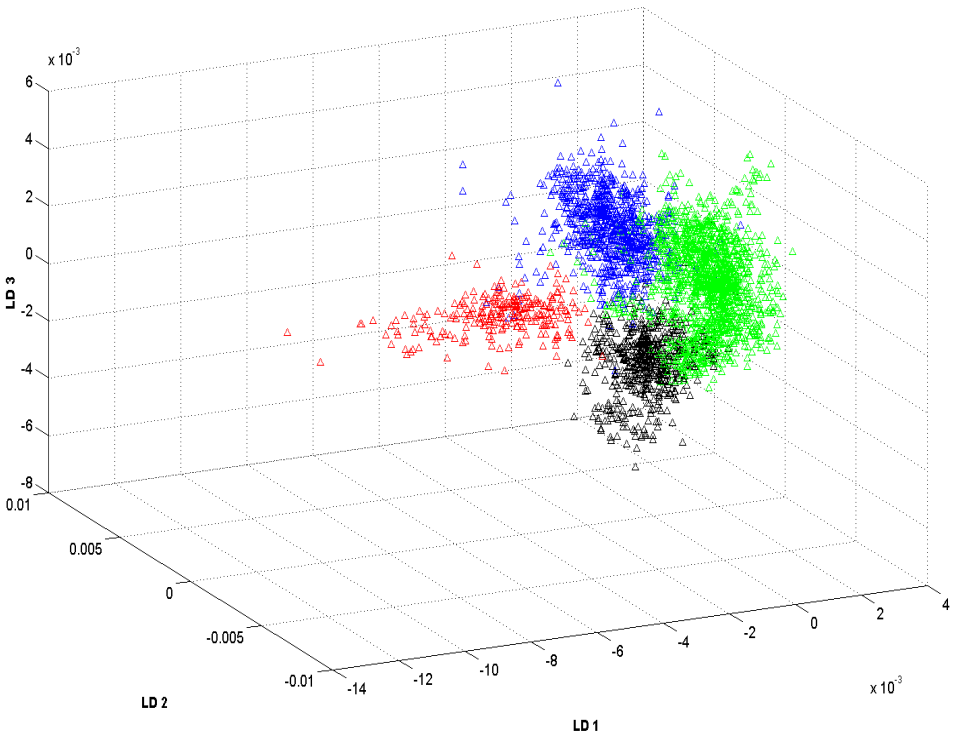

Figure 4.97:.N2 – 3D linear discriminate plot for 4 group model.

Cross-validation

Tables 4.24 and 4.25 summarise the results for the 4 group model (cross–validated). The model sensitivity is best for adenocarcinoma and worst for SCC with similar values for reactive nodes and lymphoma. Whilst no misdiagnoses, in particular false negatives, are acceptable the results show that the specificity of the model is very good for cancer, 99, 95 and 90% respectively for adenocarcinoma, SCC and Hodgkin's lymphoma (Table 4.24)

Table 4.24:– N2 – Spectral prediction performance for 4 group model (cross validation - leave one sample out).

	Spectral Prediction			
Histopathology	**Reactive**	**Adenocarcinoma**	**SCC**	**Lymphoma**
Reactive	1130	20	76	163
Adenocarcinoma	0	225	8	9
SCC	107	2	598	81
Lymphoma	86	0	23	445
Sensitivity %	81	93	76	80
Specificity %	88	99	95	90

Table 4.25:– N2 – Spectral prediction performance by node for 4 group model (cross validation - leave one sample out.

	Spectral Prediction			
Histopathology	**Reactive**	**Adenocarcinoma**	**SCC**	**Lymphoma**
Reactive	45	1	2	5
Adenocarcinoma	0	8	0	0
SCC	4	0	18	2
Lymphoma	3	0	0	15
Sensitivity %	85	100	75	83
Specificity %	86	99	97	92

In the cross-validation of the spectral performance by node the sensitivity is improved for reactive nodes, adenocarcinoma and lymphoma and is reduced by 1% for SCC. The specificity of the model for cancer improves to give even better result; 92% (lymphoma), 99% (adenocarcinoma) and 97% SCC.

4.4 Discussion summary

4.4.1 Consensus studies

The consultant consensus histology classification for both studies was excellent with complete agreement achieved for 89.1% of samples in the larynx study and 86.8% in the lymph node study. In no cases did all three consultants disagree. This level of concordance is unusual considering the inherent difficulties in the assessment of H&E slides derived from frozen sections and increases confidence in the results of the models developed in the larynx and lymph node studies. The comparison of the consultant consensus and the histopathology report from the main operative specimen showed lower levels of agreement as would be expected, 75.5% and 72.3% for the larynx and lymph node studies respectively; this is fully discussed in *Section 4.1.2.* The importance of this finding is that the study has sought where ever possible to reference experimental procedure to the clinical setting and it highlights a difficulty in the future development of Raman spectroscopy as a real time useful in vivo tool. It will be imperative that in heterogenous samples where foci of disease exists Raman spectroscopy is able to pick up the presence of disease either through the detection of field changes or by use in combination with other imaging techniques. The consultant consensus and consultant/histopathology report studies were also small enough that data could be looked at in great detail. Individual histopathology opinions were compared and if a discrepancy was noted this was thoroughly investigated by reference to the original patient notes and history. This ensured no adverse clinical decisions were made on the basis of the main operative specimen histopathology report where a different diagnosis had been assigned through consultant consensus of the experimental sample.

4.4.2 Larynx studies

The development of the diagnostic models created in the main larynx study was based on the need to investigate the efficacy of Raman spectroscopy in answering key clinical questions. Each step in the development of the studies aimed to push further the assessment of the ability of Raman spectroscopy to differentiate ever more specific disease entities. Table 4.14 details the different types of tissue samples compared in

each of the mini-models. This table is further expanded in *Appendix D.2* to summarise the nomenclature used for pathology groups (tissue classified as one histopathological entity), study groups (different combinations of pathology groups) and also records the number of spectra obtained from each study group. A full break down of the numbers of patients, samples and spectra obtained from samples in each pathology group is recorded in Table 4.13.

The first, most basic question addressed in mini model L1 was could Raman spectroscopy differentiate between tissue containing malignancy (SCC) and tissue that did not? Whilst the tissue in the latter group did not contain malignancy it did contain samples where neoplastic change such as dysplasia and carcinoma in situ had occurred. No tissue samples, other than those containing TB, where removed from this study in order assess Raman spectroscopy in as clinically relevant way as possible. L1-1 refined this basic but fundamental assessment further by interrogating tissue that exhibited neoplasia (SCC) or neoplastic changes, such as dysplasia and carcinoma in situ, against tissue from vocal cords that had been assessed as showing no evidence of any form of neoplastic change (All controls) histologically. The results for L1 showed 85.6/ 87.2% (sensitivity/specificity) for SCC and 87.2/85.6%% for tissue containing no evidence of true malignancy. In the L1-1study when Raman spectroscopy was used to identify tissue showing neoplastic change it did so with 95.2% sensitivity and 84.6% specificity which gave an overall training performance of 91%. This reduced to 81% after independent testing by cross-validation. The specificities obtained for this model where 84.6% for the tissue showing neoplastic change and 95.2% for the tissue that did not. The refinement of the model giving improved results for sensitivity in diagnosis of tissue exhibiting neoplastic change of all types compared to SCC alone and an improvement in the specificity of diagnosis for vocal cord tissue that did not exhibit any neoplastic change compared to the non-malignant group in L1. The latter result is encouraging and would be as predicted as the samples in the corresponding group in the L1 study where completely heterogenous in nature. L1-1 compares groups that correlate very closely to those that would be obtained during surgical biopsy for the investigation of a vocal cord lesion and answer positively the key clinical question ‘ To what extent can Raman spectroscopy differentiate between normal vocal cord tissue and tissue showing degrees of neoplastic change?’

The L2 series of mini-models followed on initially as a refinement to the L1 study. L2a compared tissue containing SCC against ‘All controls’; vocal cord tissue assessed histologically as showing no evidence of any form of neoplastic change. The results from L2a showed 94.6% sensitivity for SCC and 83.4% for ‘All controls’. The specificity results were 83.4% for SCC and 94.6% for ‘All controls.’ These results were rather disappointing but multivariate analysis results highlighted the possibility that the ‘All controls group might be significantly heterogenous. This was confirmed by a closer look at the histology which showed that in fact this group contained samples exhibiting hyperplasia and perhaps more significantly hyperkeratosis. L2b was a study borne out of this observation and assessed if Raman spectroscopy could identify hyperkeratosis and separate it from genuinely normal vocal cord tissue. This study contained moderate numbers of samples and a reasonably well balanced number of spectra between groups. It gave excellent results with 97.9/100% (sensitivity/specificity) for hyperkeratosis and 100/97.9% for normal squamous cell epithelium. As clinically hyperkeratosis can look

very similar to SCC this is a very positive finding and supports the eventual use of Raman spectroscopy as a diagnostic tool.

The 3 group mini-models in the L2c study series work in a logical way through refinements to the L1-1 study by taking into account the findings of L2b that the original 'All controls' group could be divided into two; tissue showing hyperkeratosis/hyperplasia and tissue exhibiting normal squamous cell epithelium. This series of mini-models also subdivides the L1-1 group which contains tissue classified as showing any neoplastic change into two further groups; tissue containing SCC and a second group in which the tissue exhibited dysplasia or carcinoma in situ (abnormal mucosa). The last mini-model in this series removes the tissue containing carcinoma in situ from the 'abnormal mucosa 'group and assesses the Raman spectroscopy classification of SCC/normal squamous cell epithelium and dysplastic mucosa (L2c-3). With the caveat that as the mini-models become more refined the number of samples used reduces and this will reduce confidence in results this series that the general trend is an increase in the sensitivity and specificity of results as the study groups used become more specific for one pathology. This is discussed in much more detail in *Section 4.2.3.5*. Multivariate analysis also shows very clearly that the separation between study groups agrees with that expected from our knowledge of the natural history of these diseases. This again supports the development of a clinical diagnostic application for this technique within the larynx in the future.

There is considered to be a continuum of vocal cord neoplastic disease from normal through mild, moderate to severe dysplasia and from there to carcinoma in situ. From carcinoma in situ there is a key point where SCC develops, this is generally considered to progress in severity from well to moderately well and finally poorly differentiated SCC which has the worst prognosis. The mini- models in L3 and in the L4 series aim to investigate if Raman spectroscopy can differentiate between different grades of diseases such as the three grades of dysplasias (L3) and the three grades of SCC (L4) but they are also designed to investigate the degree to which carcinoma in situ can be separated from dysplasia (L3) and from SCC (L4). This latter point has great clinical significance as it is both histologically challenging and a key point at which treatment regimes change. The grades of dysplasia and SCC are notoriously difficult to consistently classify and particularly for SCC it can be of help in assessing patient prognosis.

L3 assesses the differentiation between tissue showing the three degrees of dysplastic change and that showing carcinoma in situ. Patients with vocal cord dysplasia and carcinoma in situ are followed up in the outpatient clinic often every few weeks/months with biopsy under general anaesthetic periodically if the disease is thought to be progressing. The assessment of vocal cords in outpatients is purely subjective, this study was designed to assess if Raman spectroscopy could do this objectively. The results for sensitivity and specificity obtained in this study cannot be validated because of the small number of samples however the multivariate results from this study again correlate well with our knowledge of the progression of this disease and the group separation shown graphically is striking. In order for this study to be validated it will need to be expanded however this work shows that Raman spectroscopy is likely to be able to differentiate these disease states and for the first time that Raman spectroscopy

might in time be a viable outpatient screening tool for the different grades of pre-malignant change seen in vocal cord tissue.

The series of mini- models in L4 are designed to look at the ability of Raman spectroscopy to differentiate the different grades of SCC and carcinoma in situ. Inspection of the mean centred data for this model and the empirical analysis highlighted the possibility that some of the spectra in the well differentiated SCC study group might be unusual. L4-1 selected the hyperplasia/hyperkeratosis group to nominally compare to the SCC – well differentiated group to assess if on multivariate analysis a 'double peak' could be seen in the LDA histogram for the SCC. This could not be seen and in retrospect this should have been expected as the number of spectra was small and the differences when averaged out would have made only a nominal difference. The spectra were so clearly different that they were removed and the model re-run (L4-2). This model would benefit enormously from increased numbers but the multivariate analysis clearly shows graphically in figures 4.81 to 4.85 that the groups separate and that they do so in a way that correlates well with our understanding of the disease.

4.4.3 Lymph node study

These two studies are used to assess for the first time the efficacy of Raman spectroscopy to differentiate between malignancies in lymph nodes obtained from the neck. Table 4.19 summarises the different tissues types by pathology codes, the numbers of patients from which they were obtained along with details of the corresponding number of samples and spectra. Table 4.20 details the combinations of pathology groups that are used to make up study groups which were then compared (Table 4.21). The results obtained for the mini-models in these studies are the best considered in this work and the large size of the dataset allowed for rigorous independent validation.

N1 compares the Raman spectra obtained from samples of lymph nodes considered to show only reactive changes against those considered to show changes indicative of malignancy done with a similar rational to that of the L1 study. N2 develops the model further by breaking down the cancer group into SCC, adenocarcinoma and Hodgkin's disease. This has great clinical significance as the removal of an undiagnosed SCC from the neck by simple lymph node excision is a disaster and has enormous consequences for the patient, yet this may be all that is required for the diagnosis and selection of a treatment regime for lymphoma. There were a larger number of specimens and spectra used in these studies and the results have been fully cross-validated. The spectral performance for N1 showed that Raman spectroscopy could clearly differentiate between reactive lymph nodes and those containing cancer (Tables 4.22 and 4.23). The results for N2 show for the first time that Raman spectroscopy can differentiate superbly between reactive lymph nodes, SCC, adenocarcinoma and Hodgkin's disease; cross-validated both by sample and by node (Tables 4.24 and 4.25).

The work on the analysis of the lymph node study data has only really been touched upon but it has given excellent results for the groups compared to date and the initial empirical analysis for Non- Hodgkin's disease is also very exciting. The development of

this work to consider the ability of Raman spectroscopy to identify different subgroups of cancer with further modelling and data analysis is ongoing.

Chapter 5: Conclusions and Future Work

5.1 Conclusions

This work differs from that previously published in that the reasoning for the studies themselves and importantly the way in which these studies were developed was driven by clinical pragmatism. Throughout the needs of the clinician to make a diagnosis and those of the patient to have this done in an accurate and timely fashion have been the priority in the assessment of Raman spectroscopy as a diagnostic technique. The conclusions drawn from the results of the three main studies, particularly those for the larynx and lymph node studies are detailed in this context.

5.1.1 Consensus studies

In this work the consensus between histopathologists as to the classification of disease in the samples used for spectral analysis was good; 89.1% complete agreement for the larynx study and 86.8% for lymph node study samples. These results showed excellent concordance however it was felt unusual for the results for consultant consensus in the lymph node study to be poorer than those for the larynx as the larynx study specimens were generally smaller and more heterogeneous. There are several reasons this might have occurred, one of which is the fact that no specimens were removed from the analysis because of heterogenicity. This was felt to be imperative as a surgeon has no way of telling intra-operatively whether the biopsy or resection obtained is homogeneous or heterogenous. The tissue samples used in the lymph node study were generally larger than those of the larynx study and so the potential for mixed disease states coexisting was greater. In likely hood more importantly is the fact that diseases such as lymphoma are very poorly diagnosed from H&E slides of frozen sections.

The possibility that one consultant histopathologist tended to grade the severity of disease slightly lower than the other consultants did arise. This was carefully examined and no changes in the clinical management of the patients would have resulted from the minor alterations in disease classification that could have ensued. Interestingly the classification afforded by this histopathologist generally agreed with that of the main operative specimen, suggesting that possibility that the other histopathologists might have tended to over-grade, again no material change in treatment would have occurred as a result.

5.1.2 Laryngeal studies

The spectra obtained during this work are consistent and reproducible. There are only a small number of studies to date that have investigated the use of Raman spectroscopy in the diagnosis of laryngeal disease and in particular to investigate the ability of Raman spectroscopy to differentiate between tissue showing neoplastic change and laryngeal mucosa which does not. This question was addressed in the two group mini model L1-1 and the results, which were subjected to cross-validation, support the finding of other studies that Raman spectroscopy shows great promise as a diagnostic tool in this area provided that the practical problems relating to its' use can be overcome.

The importance of empirical analysis cannot be over-emphasised. Whilst this technique uses only part of the data gathered in any one study it still allowed the pattern of change

between the spectra of different study groups to be assessed. This was used as the 'step off' point in the development of the early hypotheses as to the biochemical changes that may exist between study groups, for example in the secondary structure of some proteins (L1). The main study published to date in this area by Stone et al (Stone, 2002) is discussed in the literature review; the findings in this work are very similar for SCC, dysplasia and normal laryngeal mucosa sensitivity and specificity. They are detailed in full in the discussion section for the L1 and L2 mini models. An improvement is present in some results however the drawback of this work, as it was in the previous study, is the small number of specimens/patients in some arms of the mini models. The results are encouraging but for the work to be validated a larger data set is required so that cross-validation can be done initially with a leave one sample out technique but in time ideally a leave one patient out technique should be used leading to optimized models and full independent testing. The difficulties in obtaining samples means that further work would be most successful if a multicentre approach was taken. It might also prove interesting to trace back the few spectra that appear to be misclassified and review their notes to see the progression if any of their disease.

No tissue specimens were discarded and the power of this work is in its pragmatic approach; striving to keep the work as near to the clinical scenario as possible. It can be extremely difficult to target biopsies in the larynx and targeting tissue with the Raman probe in the future is likely to encounter many similar problems. It is hoped that by accepting all specimens into the study the validity of results supporting the effectiveness of Raman spectroscopy as a clinical tool will be upheld. Furthermore, it removes any errors introduced into studies where the full pathology mix is not included and real-world performance therefore not tested.

Yang (Yang, 1998) has investigated the use of Raman spectroscopy in the larynx where there is infection with Human Papilloma Virus. This is a very interesting area of study as prognosis in this disease can be very variable and there is an increased risk of the development of neoplastic change. Coupled with interest in vaccine development towards different HPV strains there maybe value in further work in this area. Whilst the disease is not common patients often require multiple debridements's affording the opportunity to harvest multiple samples and possibly map disease remission and progression and explore the reasons they occur.

Accurate visual or microscopic assessment of diseased laryngeal tissue is very difficult, for example hyperkeratosis can be extremely difficult to differentiate from SCC. At present accurate intra-operative assessment of diseased laryngeal tissue is not possible and in this work Raman spectroscopy has been shown to be a highly sensitive tool in the detection of non-neoplastic variations in the normal structure of vocal cords. Samples exhibiting hyperplasia and hyperkeratosis can be separated from samples considered to be 'true' normal histologically and this finding strongly supports the use of Raman spectroscopy as a clinical tool.

It was hoped that mini model L3 would answer the question as to whether Raman spectroscopy could differentiate carcinoma in situ from dysplasia. The small sample numbers make it very difficult to draw any definitive conclusions however the results again look promising and further work is needed to increase the dataset. On the other

hand study L4 has shown that Raman spectroscopy is likely to be able to discriminate well between SCC and carcinoma in situ. This study would be improved by increasing the number of patients and in particular the number of samples in the carcinoma in situ group, however the results strongly support the conclusion that Raman spectroscopy can differentiate between different grades of SCC. Once again these studies where designed to assess the ability of Raman spectroscopy to act as a diagnostic tool in areas where there is currently great diagnostic difficulty such as in the discrimination between SCC, dysplasia and carcinoma in situ and the results to date are extremely encouraging.

5.1.3 Lymph node studies

This work is the first to undertake a rigorous investigation into the efficacy of Raman spectroscopy as a diagnostic tool in neoplastic diseases of lymph nodes within the head and neck. Some work has been published in the past but primarily relating to metastatic deposits from breast disease (Smith, 2003 & 2005). The dataset for this study is much larger and whilst ideally a more even distribution of samples and increase in the number of patients in the adenocarcinoma and lymphoma groups would be good the number of reactive nodes harvested provides a good basis for future work. This work shows that Raman spectroscopy can differentiate between SCC, adenocarcinoma, lymphoma and reactive lymph nodes in the head and neck with excellent specificity and sensitivity. Sections of the remaining lymph node samples have been analysed with a Raman probe and early results are very encouraging it is hoped that this work will be continued within the research group and a comparison made between it and the static Raman system results. This study has been well tested and that the results are likely to be rapidly implemented. Our research group has recently secured funding to explore needle Raman probes for identification of suspicious nodes in the head and neck, the remaining lymph node specimens will be used to forward this work

5.2 Future work

A study into the degree to which histopathological classification varies between the participating consultants using carefully selected slides that optimise discrimination would be helpful in giving confidence to the experimental classification results. These results suggest that ‘histopathology panels’ for the classification of these types of samples might reduce the degree to which individual subjectivity influences outcome.

The development of a spectral library for ‘normal tissues’, in addition to those for single biochemical entities, would be extremely useful. During the collection of spectra the inclusion of a reference peak for the calculation of PIRs would be of help.

For Raman spectroscopy to be a genuinely useful tool it must be able to differentiate between neoplastic and non-neoplastic tissue in the real clinical setting. The use of lasers in the operating theatre is increasing and this is particularly true within oto-rhino-laryngology where the treatment of early vocal cord neoplasia has moved away from radiotherapy to primary laser resection. Operative margins are currently visually assessed by the surgeon with the use of a microscope and biopsies at the resection margin taken and send for analysis. These frozen sections are reported whilst the patient is in theatre anaesthetised, if positive further resection is undertaken and the process repeated. The development of Raman spectroscopy for intra-operative use in the delineation of resection margins would be a huge a step forward. In order for this to be

achieved data acquisition and processing time must be improved enormously and the development of systems such as those reliant on neural networks may be the way forward.

The laryngeal studies undertaken in this work assessed tissue taken from patients who had all smoked. Smoking is such a strong aetiological factor in the development of laryngeal cancer further work to elucidate the affect of this carcinogen using Raman spectroscopy would be very helpful particularly if, as has been shown, Raman spectroscopy may be picking up biochemical changes in tissue before it is evident using conventional histological techniques. A difficulty inherent within these studies is that the vocal cords we consider normal have also been exposed to the same chemical carcinogen as the visually affected cords. Ideally a spectral data base from laryngeal tissue not exposed to smoke should be developed however biopsying the vocal cords of non-smokers in whom there is no indication for microlaryngoscopy is ethically questionable. As such this may be an area in the future where an animal model might be useful, not as a means of further supporting the aetiological connection but in assessing the ability of Raman spectroscopy to show the spectroscopic changes, and hence the possible biochemical changes present in the vocal cord tissue of smokers before a neoplasia becomes clinically evident.

The maximum depth at which Raman spectroscopy can be used to probe diseased laryngeal tissue and still retain excellent sensitivity and specificity must be further assessed. This work could be usefully combined with the ongoing development of 'deep Raman probing.' Validation of the use of the Raman probe in the larynx has already started but in order to acquire enough tissue to expand the spectral data base of samples analysed in vitro, prior to an in vivo study, a multicentre trial is required. This should concentrate on the assessment of Raman spectroscopy in areas where difficulty exists in clinical decision making and where there is histological debate with reference to the classification of diseased laryngeal tissue.

One of the major challenges faced by Raman spectroscopy is its' use in the assessment of tissue which is not uniformly affected by disease such as in lymph nodes. This work clearly shows the excellent sensitivity and specificity with which Raman spectroscopy can be used to differentiate between SCC, adenocarcinoma and lymphoma in lymph nodes. This work would benefit for being expanded to include more adenocarcinoma. The practical question is how can Raman spectroscopy, which realistically can only sample limited volumes of tissue over real time guarantee to pick up the foci of disease within lymph nodes as well if not better than histopathology. It would seen unrealistic in the short term for Raman spectroscopy to be developed to the point where it can do this alone but in combination with image guidance systems to place the Raman probe accurately in areas of suspicion this problem may yet be overcome. Should Raman spectroscopy be shown to pick up early biochemical changes that affect whole lymph nodes in the presence of foci of disease this would add greatly to the potential for Raman spectroscopy to be a useful clinical tool in this area.

Vibrational spectroscopy applied to disease diagnosis is a rapidly expanding field and many new devices for signal collection and methods of data analysis are making this approach easier to perform, more rapid and likely to be more accurate at making a

molecular diagnosis of disease in the future. The number and variety of tissue types and diseases represented within the lymph node study dataset means that much more work could be done on data analysis and with time many other areas in the head and neck where Raman spectroscopy may be of use could be explored.

References

1. **Abou-Elhamd, K. A., Habib, T. N. (2007).** The flow cytometric analysis of premalignant and malignant lesions in head and neck squamous cell carcinoma. *Oral Oncology,* **43**(4), p.366-372.
2. **Abraham, J. L., Etz, E. S. (1979).** Molecular microanalysis of pathological specimens in situ with a laser-Raman microprobe. *Science*, **206**, p.716-718.
3. **Ager III, J. W., Nalla, R. K., Balooch, G., Kim, G., Pugach, M., Habelitz, S., et al. (2006).** On the increasing fragility of human teeth with age: A deep-UV resonance Raman study. *Journal of Bone and Mineral Research***, 21**(12), p.1879-1887.
4. **Agrawal, N., Morrison, G. A. (2006).** Laryngeal cancer after topical *mitomycin C* application. *Journal of Laryngology and Otology,* **120**(12), p.1075-1076.
5. **Alfano, R. R., Lui, C. H., Glassman, W. S. (1993).** US Pat. 5 261 410.
6. **Arens, C., Dreyer, T., Glanz, H., Malzahn, K. (2003).** Compact endoscopy of the larynx. *Annals of Otology, Rhinology and Laryngology,* **112**(2), p.113-119.
7. **Arens, C., Dreyer, T., Glanz, H., Malzahn, K. (2004).** Indirect autofluorescence laryngoscopy in the diagnosis of laryngeal cancer and its precursor lesions. *European Archives of Oto-Rhino-Laryngology,* **261**(2), p.71-76.
8. **Arens, C., Eistert, B., Glanz, H., Waas, W. (1998).** Endolaryngeal high-frequency ultrasound. *European Archives of Oto-Rhino-Laryngology,* **255**(5), p.250-255.
9. **Arens, C., Glanz, H., Wönckhaus, J., Hersemeyer, K., Kraft, M. (2007).** Histologic assessment of epithelial thickness in early laryngeal cancer or precursor lesions and its impact on endoscopic imaging. *European Archives of Oto-Rhino-Laryngology,* **264**(6), p.645-649.
10. **Armstrong, W. B., Ridgway, J. M., Vokes, D. E., Guo, S., Perez, J., Jackson, R. P., et al. (2006).** Optical coherence tomography of laryngeal cancer. *Laryngoscope,* **116**(7), p.1107-1113.
11. **Bakker Schut, T. C., Van Dekken, H, Tilanus, H. W., Bruining, H. A., Puppels, G. J. (1997).** Raman Spectrosopy of Healthy and Diseased Oesophagus. In: *Spectroscopy of Biological Molecules: Modern Trends, Edited by Carmona, P., Navarro, R., Hernanz, A. Kluwer Academic Publishers*, p.455-456.
12. **Baldwin K. J., Batchelder D., Webster S. (2001)**. Raman microscopy: Confocal and scanning near-field. In: *Handbook of Raman Spectroscopy. Practical Spectroscopy Series, Edited by Lewis I.R., Edwards H.G.M*, **28**, p.145-187.
13. **Bergbauer, K. L., Su, K. C., & Yu, N. (1993)**. Use of Raman spectroscopy to monitor UV-blocking contact lens efficacy. *Proc* SPIE, **69**, .222-223.
14. **Bernard, G., Auger, M., Soucy, J., Pouliot, R. (2007).** Physical characterization of the stratum corneum of an in vitro psoriatic skin model by ATR-FTIR and Raman spectroscopies. *Biochimica et Biophysica Acta - General Subjects,* **1770**(9), p.1317-1323.
15. **Bernstein, P. S., Zhao, D., Sharifzadeh, M., Ermakov, I. V., Gellermann, W. (2004).** Resonance Raman measurement of macular carotenoids in the living human eye. *Archives of Biochemistry and Biophysics,* **430**(2), p.163-169.
16. **Bertoluzza, A., Fagnano, C., Monti, P., Simoni, R., Tinti, A., Tosi, M. R., et al. (1992).** Raman spectroscopy in the study of biocompatibility. *Clinical Materials,* **9**(1), p.49-68.

17. **Bigenzahn, W., Steiner, E., Denk, D., Turetschek, K., Frühwald, F. (1998).** Stroboscopy and imaging in interdisciplinary diagnosis of early stages of carcinoma of the larynx. *Radiologe*, **38**(2), p.101-105.
18. **Boere, I. A., Bakker Schut, T. C., Van den Boogert, J., De Bruin, R. W. F., Puppels, G. J. (2003).** Use of fibre optic probes for detection of Barrett's epithelium in the rat oesophagus by Raman spectroscopy. *Vibrational Spectroscopy*, **32**(1 SPEC.), p.47-55.
19. **Boffetta, P., Gridley, G., Gustavsson, P., Brennan, P., Blair, A., Ekström, A. M., et al. (2000).** Employment as butcher and cancer risk in a record-linkage study from Sweden. *Cancer Causes and Control*, **11**(7), p.627-633.
20. **Boppart, S. A., Oldenburg, A. L., Xu, C.,Marks, D. L. (2005)**. Optical probes and techniques for molecular contrast enhancement in coherence imaging. *J Biomed Opt*, **10**(4), p.41208.
21. **Bosetti, C., Gallus, S., Trichopoulou, A., Talamini, R., Franceschi, S., Negri, E., et al. (2003).** Influence of the Mediterranean diet on the risk of cancers of the upper aerodigestive tract. *Cancer Epidemiology Biomarkers and Prevention*, **12**(10), p.1091-1094.
22. **Bosetti, C., La Vecchia, C., Talamini, R., Negri, E., Levi, F., Dal Maso, L., et al. (2002)**. Food groups and laryngeal cancer risk: A case-control study from Italy and Switzerland. *International Journal of Cancer*, **100**(3), p.355-360.
23. **Boustany, N. N., Crawford, J. M., Manoharan, R., Dasari, R. R., Feld, M. S. (1999).** Analysis of nucleotides and aromatic amino acids in normal and neoplastic colon mucosa by ultraviolet resonance Raman spectroscopy. *Laboratory Investigation*, **79**(10), p.1201-1214.
24. **Brennan, J. A., Mao, L., Hruban, R. H., et al (1995).** Molecular assessment of histopathological staging in squamous cell carcinoma of the head and neck. *N Engl J Med*, **332**, p.429-435.
25. **British Standards Institue. (2007)**. *Safety of laser products. Equipment classification and requirements***, BS EN 60825-1**, p.56 - 89.
26. **Burch, J. D., Howe, G. R., Miller, A. B., Semenciw, R. (1981).** Tobacco, alcohol, asbestos, and nickel in the aetiology of cancer of the larynx: A case-control study. *Journal of the National Cancer Institute*, **67**(6), p.1219-1224.
27. **Buschman, H. P., Motz, J. T., Deinum, G., Romer, T. J., Fitzmaurice, M., Kramer, J. R., Van der Laarse, A., Bruschke, A. V., Feld, M. S. (2001).** Diagnosis of human coronary atherosclerosis by morphology based Raman spectroscopy. *Cardiovasc Pathol*, **10**, p.59-68.
28. **Cancer Incidence Projections for Scotland. (2001-2020).** Cancer in Scotland: Sustaining Change. http://www.scotland.gov.uk/Publications/2004/12/20257/46699 (accessed 28 th September 2006).
29. **Cancer Research U K, Cancer Incidence Statistics. (2007).**
30. **Carbone, P. P., Kaplan, H. S., Musshoff, K., et al. (1971).** Report of the Committee on Hodgkin's Disease Staging Classification. *Cancer Res*, **31**, p.1860-1861.
31. **Carde, P., Hagenbeek, A., Hayat, M., et al. (1993).** Clinical staging versus laparotomy and combined modality with MOPP versus ABVD in early stage Hodgkin's disease. *J Clin Oncol*, **11**, p.2258-72.

32. **Carden, A., Morris, M. D. (2000).** Application of vibrational spectroscopy to the study of mineralized tissues (review). *Journal of Biomedical Optics*, **5**(3), p.259-268.
33. **Caspers, P. J., Lucassen, G. W., Carter, E. A., Bruining, H. A., Puppels, G. J. (2001).** In vivo confocal Raman microspectroscopy of the skin: Noninvasive determination of molecular concentration profiles. *Journal of Investigative Dermatology*, **116**(3), p.434-442.
34. **Casselman, J. W., Biebau, G. (1992).** Imaging of laryngeal cancer. *Acta Oto-Rhino-Laryngologica Belgica*, **46**(2), p.161-174.
35. **Cattaruzza, M. S., Maisonneuve, P., Boyle, P. (1996).** Epidemiology of laryngeal cancer. *European Journal of Cancer Part B: Oral Oncology*, **32**(5), p.293-305.
36. **Chang, S. K., Dawood, M. Y., Staerkel, G., Utzinger, U., Atkinson, E. N., Richards-Kortum, R. R., et al. (2002).** Fluorescence spectroscopy for cervical precancer detection: Is there variance across the menstrual cycle? *Journal of Biomedical Optics*, **7**(4), p.595-602.
37. **Chang. H., Qu, J. Y., Yuen, P., Sham, J., Kwong, D., Wei, W.I. (2002).** Light-induced autofluorescence spectroscopy for detection of nasopharyngeal carcinoma in vivo. *Applied Spectroscopy*, **56**(10), p.1361-1367.
38. **Chantry, G. W., Gebbie, H. A., Hilsum, C. (1964)**. Interferometric Raman spectroscopy using infra-red excitation. *Nature*, **203** (4949): p.1052-1053.
39. **Charlin, B., Brazeau-Lamontagne, L., Guerrier, B., Leduc, C. (1989).** Assessment of laryngeal cancer: CT scan versus endoscopy. *Journal of Otolaryngology*, **18**(6), p.283-288.
40. **Chatrath, P., Scott, I. S., Morris, L. S., Davies, R. J., Rushbrook, S. M., Bird, K., et al. (2003).** Aberrant expression of minichromosome maintenance protein-2 and Ki67 in laryngeal squamous epithelial lesions. *British Journal of Cancer*, **89**(6), p.1048-1054.
41. **Chen, M. Y. M., Ott, D. J., Casolo, B. J., Moghazy, K. M., Koufman, J. A. (1998).** Correlation of laryngeal and pharyngeal carcinomas and 24-hour pH monitoring of the esophagus and pharynx. *Otolaryngology - Head and Neck Surgery*, **119**(5), p.460-462.
42. **Choi, S. Y., Kahyo, H. (1991).** Effect of cigarette smoking and alcohol consumption in the aetiology of cancer of the oral cavity, pharynx and larynx. *International Journal of Epidemiology*, **20**(4), p.878-885.
43. **Coohill T. P., Peak M. J., Peak J. G. (1987).** The effects of the ultraviolet wavelengths of radiation present in sunlight on human cells *in vitro*. *Photochem. Photobiol*, **46**(6**)**, p.1043-1050.
44. **Crow, P., Uff, J. S., Farmer, J. A., Wright, M. P., Stone, N. (2004).** The use of Raman spectroscopy to identify and characterize transitional cell carcinoma in vitro. *BJU International***, 93**(9), p.1232-1236.
45. **Da Costa, R, S., Wilson, B.C., Marcon, N.E. (2007).** Fluorescence and spectral imaging. *Scientific World Journal*, **7**, p.2046-2071.
46. **DaCosta, R. S., Wilson, B. C., Marcon, N. E. (2005).** Optical techniques for the endoscopic detection of dysplastic colonic lesions. *Current Opinion in Gastroenterology*, **21**(1), p.70-79.
47. **Darvin, M. E., Gersonde, I., Albrecht, H., Steny, W., & Lademann, J. (2007).** Non-invasive in-vivo raman spectroscopic measurement of the dynamics of the

antioxidant substance lycopene in the human skin after a dietary supplementation. *Proc. Spie* **6535**, 176-184.

48. **Darvin, M. E., Gersonde, I., Albrecht, H., Sterry, W., Lademann, J. (2006).** In vivo Raman spectroscopic analysis of the influence of UV radiation on carotenoid antioxidant substance degradation of the human skin. *Laser Physics,* **16**(5), p.833-837.
49. **De Bree, R., Van der Putten, L., Hoekstra, O. S., Kuik, D. J., Uyl-de Groot, C. A., Van Tinteren, H., et al. (2007).** A randomized trial of PET scanning to improve diagnostic yield of direct laryngoscopy in patients with suspicion of recurrent laryngeal carcinoma after radiotherapy. *Contemporary Clinical Trials,* **28**(6), p.705-712.
50. **De Jong, B. W. D., Bakker Schut, T. C., Wolffenbuttel, K. P., Nijman, J. M., Kok, D. J., Puppels, G. J. (2002).** Identification of bladder wall layers by Raman spectroscopy. *Journal of Urology,* **168**(4 II), p.1771-1778.
51. **de Korte, C. L., Buschman, H. P. J., Van de Poll,Sweder W. E., Van der Steen, A. F. W., Puppels, G. J., Van der Laarse, A. (2000).** Vascular plaque characterization using intravascular ultrasound elastography and NIR Raman spectroscopy in vitro. *Proc SPIE,* **3982**, 180-186.
52. **De Stefani, E., Correa, P., Oreggia, F., Leiva, J., Rivero, S., Fernandez, G., et al. (1987).** Risk factors for laryngeal cancer. *Cancer,* **60**(12), p.3087-3091.
53. **De Stefani, E., Oreggia, F., Boffetta, P., Deneo-Pellegrini, H., Ronco, A., Mendilaharsu, M. (2000).** Tomatoes, tomato-rich foods, lycopene and cancer of the upper aerodigestive tract: A case-control in Uruguay. *Oral Oncology***, 36**(1), p.47-53.
54. **De Stefani, E., Oreggia, F., Rivero, S., Ronco, A., Fierro, L. (1995).** Salted meat consumption and the risk of laryngeal cancer. *European Journal of Epidemiology*, **11**(2), p.177-180.
55. **Dekker, E., Fockens, P. (2005).** Advances in colonic imaging: New endoscopic imaging methods. *European Journal of Gastroenterology and Hepatology,* **17**(8), p.803-808.
56. **Delahaye, M., Dhamelincourt, P. (1974).** Raman microprobe and microscope with laser excitation. *Journal of Raman Spectroscopy*, **3**, p.33-43.
57. **Dietz, A., Ramroth, H., Urban, T., Ahrens, W., Becher, H. (2004).** Exposure to cement dust, related occupational groups and laryngeal cancer risk: Results of a population based case-control study. *International Journal of Cancer,* **108**(6), p.907-911.
58. **Dippel, B., Mueller, R. T., Pingsmann, A., Schrader, B. (1998).** Composition, constitution, and interaction of bone with hydroxyapatite coatings determined by FT Raman microscopy. *Biospectroscopy,* **4**(6), p.403-412.
59. **Du Bois d'Aische, A., Craene, M. D., Geets, X., Gregoire, V., Macq, B., Warfield, S. K. (2005).** Efficient multi-modal dense field non-rigid registration: Alignment of histological and section images. *Medical Image Analysis,* **9**(6), p.538-546.
60. **Duindam, J. J., Vrensen, G. F. J. M., Otto, C., Greve, J. (1998).** Cholesterol, phospholipid and protein changes in focal opacities in the human eye lens. *Invest Ophthalmol Vis Sci*, **39,** p.94-103.

61. **Eberl, T., Jechart, G., Probst, A., Golczyk, M., Bittinger, M., Scheubel, R. et al. (2007)**. Can an endocytoscope system (ECS) predict histology in neoplastic lesions? *Endoscopy*, **39**(6), p.497-501.
62. **Edwards, H. G. M., Wilson, A. S., Nik Hassan, N. F., Davidson, A., Burnett, A. (2007).** Raman spectroscopic analysis of human remains from a seventh century cist burial on Anglesey, UK. *Analytical and Bioanalytical Chemistry*, **387**(3), p.821-828.
63. **Elwood, J. M., Pearson, J. C. G., Skippen, D. H., Jackson, S. M. (1984).** Alcohol, smoking, social and occupational factors in the aetiology of cancer of the oral cavity, pharynx and larynx. *International Journal of Cancer*, **34**(5), p.603-612.
64. **Ermakov, I. V., Ermakova, M. R., Gellermann, W. (2005)**. Simple Raman instrument for in vivo detection of macular pigments. *Applied Spectroscopy*, **59**(7), p.861-867.
65. **Estève, J., Riboli, E., Péquignot, G., Terracini, B., Merletti, F., Crosignani, P., et al. (1996).** Diet and cancers of the larynx and hypopharynx: The IARC multi-centre study in south-western Europe. *Cancer Causes and Control*, **7**(2), p.240-252.
66. **Farraro, J., Nakamoto, K., Brown, C.W. (2003a).** Origin of Raman Spectroscopy. In: *Introductory Raman Spectroscopy*, *2nd edn*. *Elsevier Science (USA)*, p.7.
67. **Farraro, J., Nakamoto, K., Brown, C.W. (2003b).** Origin of Raman Spectroscopy. In: *Introductory Raman Spectroscopy*, *2nd edn*. *Elsevier Science (USA)*, p.96-117**.**
68. **Farraro, J., Nakamoto, K., Brown, C.W. (2003c).** Origin of Raman Spectroscopy. In: *Introductory Raman Spectroscopy*, *2nd edn*. *Elsevier Science (USA)*, p.13-14.
69. **Fattori, B., Grosso, M., Nacci, A., Bianchi, F., Cosottini, M., Ursino, F., et al. (2005).** The role of 99mTc-tetrofosmin scintigraphy for staging patients with laryngeal cancer. *Cancer Biotherapy and Radiopharmaceuticals*, **20**(1), p.27-35.
70. **Feld, M. S., Manoharan, R., Salenius, J., Orenstein-Carndona, J., Roemer, T. J., Brennan III, J. F., et al. (1995).** Detection and characterization of human tissue lesions with near infrared Raman spectroscopy. Proc SPIE, 2388 99-104.
71. **Feng, Z. C. (2004)**. Raman spectroscopic detection of silicone leakage in human breast and lymph node tissues. *Proceedings of the Second Asian and Pacific Rim Symposium on Biophotonics*, p.69-74.
72. **Foehrenbach, H., Conessa, C., Maszelin, P., Kossowski, M., Poncet, J. L., Gaillard, J. F. (2001).** Positron emission tomography in head and neck oncology. *Annales d'Oto-Laryngologie Et De Chirurgie Cervico-Faciale*, **118**(6), p.365-372.
73. **Freije, J. E., Beatty, T. W., Campbell, B. H., Woodson, B. T., Schultz, C. J., Toohill, R. J. (1996).** Carcinoma of the larynx in patients with gastroesophageal reflux. *American Journal of Otolaryngology - Head and Neck Medicine and Surgery*, **17**(6), p.386-390.
74. **Furić, K., Mohaček-Grošev, V., Hadžija, M. (2005)**. Development of cataract caused by diabetes mellitus: Raman study. *Journal of Molecular Structure*, **744-747**(SPEC. ISS.), p.169-177.
75. **Gallivan, R. P., Nguyen, T. H., Armstrong, W. B. (1999).** Head and neck computed tomography virtual endoscopy: Evaluation of a new imaging technique. *Laryngoscope*, **109**(10), p.1570-1579.
76. **Gellermann, W., Ermakov, I. V., Ermakova, M. R., McClane, R. W., Zhao, D., Bernstein, P. S. (2002)**. In vivo resonant Raman measurement of macular carotenoid pigments in the young and the aging human retina. *Journal of the Optical Society of America A: Optics and Image Science, and Vision*, **19**(6), p.1172-1186.

77. **Gniadecka, M., Nielsen, O. F., Christensen, D. H., Wulf, H. C. (1998).** Structure of water, proteins, and lipids in intact human skin, hair, and nail. *Journal of Investigative Dermatology*, **110**(4), p.393-398.
78. **Gniadecka, M., Nielsen, O. F., Wessel, S., Heidenheim, M., Christensen, D. H., Wulf, H. C. (1998)**. Water and protein structure in photo aged and chronically aged skin. *Journal of Investigative Dermatology*, **111**(6), p.1129-1133.
79. **Goheen, S. C., Lis, L. J., Kauffman J. W. (1978)**. Raman spectroscopy of intact feline corneal collagen. *Biochim Biophys Acta*, **536**(1), p.197-204.
80. **Graham, S., Mettlin, C., Marshall, J. (1981).** Dietary factors in the epidemiology of cancer of the larynx. *American Journal of Epidemiology*, **113**(6), p.675-680.
81. **Griffiths, H., Malony, N. C. (2003).** Does asbestos cause laryngeal cancer? *Clinical Otolaryngology and Allied Sciences*, **28**(3), p.177-182.
82. **Harris, N. L., Jaffe, E. S., Diebold, J., et al. (1999).** World Health Organisation Classification of Neoplastic Diseases of the Haemopoietic and Lymphoid Tissues – A Progress Report. *Am J Clin Path*, **111**, S8-S12.
83. **Harris, N. L., Jaffe, E. S., Stein, H., et al. (1994).** A Revised European-American Classification of Lymphoid Neoplasms: A Proposal From the International Lymphoma Study Group. *Blood*, **85**, p.1361-92.
84. **Hartman, K. A., Clayton, N. W., Tomas, G. J. (1973)**. Studies of virus structure by Raman spectroscopy. *Biochemical and Biophysical Research Communications*, **50** (3), p.942-949.
85. **Hata, T. R., Scholz, T. A., Ermakov, I. V., McClane, R. W., Khachik, F., Gellermann, W., et al. (2000).** Non-invasive Raman spectroscopic detection of carotenoids in human skin. *Journal of Investigative Dermatology*, **115**(3), p.441-448.
86. **Haußinger, K., Becker, H., Stanzel, F., Kreuzer, A., Schmidt, B., Strausz, J., et al. (2005).** Autofluorescence bronchoscopy with white light bronchoscopy compared with white light bronchoscopy alone for the detection of precancerous lesions: A European randomised controlled multicentre trial. *Thorax*, **60**(6), p.496-503.
87. **Hendra, P. J., Ellis, G., & Cutler, D. J. (1988)**. Use of optical fibres in Raman **spectroscopy**, *Journal of Raman Spectroscopy*, **19**, p.413-418.
88. **Herity, B., Moriarty, M., Bourke, G. J., Daly, L. (1981).** A case-control study of head and neck cancer in the republic of Ireland. *British Journal of Cancer*, **43**(2), p.177-182.
89. **Herkenne, C., Alberti, I., Naik, A., Kalia, Y. N., Mathy, F., Préat, V., et al. (2008).** In vivo methods for the assessment of topical drug bioavailability. *Pharmaceutical Research*, **25**(1), p.87-103.
90. **Hill, W., Petrou, V. (1997).** Detection of caries and composite resin restorations by near-infrared Raman spectroscopy. *Applied Spectroscopy*, **51**(9), p.1265-1275.
91. **Hill, W., Petrou, V. (2000).** Caries detection by diode laser Raman spectroscopy. *Appl Spectrosc*, **54**, p.795-799.
92. **Hirschfield T., Chase B. (1998)**. Development and justification. *Appl Spectrosc*, **40**, p.133-137.
93. **Hirshfield, K. M., Toptygin, D., Grandhige, G., Kim, H., Packard, B. Z. Brand, L. (1996)**. Steady-state and time-resolved fluorescence measurements for studying molecular interactions: interaction of a calcium-binding probe with proteins. *Biophys Chem*, **62**(1-3), p.25--38.

94. **Hittelman, W. N. (2001).** *Genetic instability in epithelial tissues at risk for cancer. Annals of the New York Academy of Sciences.* **952**, p.1-12.
95. **Hoffbrand, A. V., Moss, P. A. H., Pettit, J. E. (2006a).** Hodgkin's Lymphoma. In: *Essential Haematology, 5th ed: Backwell Publishing*, p197-202.
96. **Hoffbrand, A. V., Moss, P. A. H., Pettit, J. E. (2006b).** The Aetiology and genetic of haematological malignancies. In: *Essential Haematology, 5th ed: Backwell Publishing*, p129-131
97. **Hoffbrand, A.V., Moss, P.A.H., Pettit, J.E. (2006c).** Non-Hodgkin's lymphoma. In: *Essential Haematology, 5th ed: Backwell Publishing*, p.203-215
98. **Hsieh, T., Yu, K., Lin, S. (2007).** Possible application of Raman microspectroscopy to verify the interstitial cystitis diagnosis after potassium sensitivity test: Phenylalanine or tryptophan as a biomarker. *Disease Markers*, **23**(3), p.147-152.
99. http://info.cancerresearchuk.org/cancerstats/types/hodgkinslymphoma/incidence/ (accessed 21st November 2007).
100. http://info.cancerresearchuk.org/cancerstats/types/nhl/incidence/ (accessed 21st November 2007).
101. http://www.info.cancerresearchuk.org/cancerstats/types/larynx/incidence/ (accessed 17 th November 2007).
102. **Huang, D., et al (1991).** Optical coherence tomography. *Science*, **254**, p.1178-1181.
103. **Huang, D., Swanson, E. A., Lin, C. P., Schuman, J. S., Stinson, W. G., Chang, W., Hee, M. R., Flotte, T., Gregory, K., Puliafito, C. A., Fujimoto, J. G. (1991),** Optical coherence tomography. *Science*, **254**, p.1178-1181.
104. **Huang, Q., Yu, G. P., McCormick, S. A., Mo, J., Datta, B., Mahimkar, M., et al. (2002).** Genetic differences detected by comparative genomic hybridization in head and neck squamous cell carcinomas from different tumour sites: Construction of oncogenetic trees for tumour progression. *Genes Chromosomes and Cancer*, **34**(2), p.224-233.
105. **Information Services Division, Scottish Executive. (2007).** Cancer in Scotland 2007. http://www.isdscotland.org/isd/1508.html (accessed 21st November 2007).
106. **Information Services Division, Scottish Executive. (2007).** Summary of Data Analyses and Reports, Head and Neck Cancers. http://www.isdscotland.org/isd/1446.html (accessed 29th May 2007).
107. **Inscore, F., Shende, C., Gift, A., Maksymiuk, P., & Farquharson, S. (2006).** Astronaut health monitoring. Proc SPIE, **6380.**
108. **Israel, O., Kuten, A. (2007).** Early detection of cancer recurrence: 18F-FDG PET/CT can make a difference in diagnosis and patient care. *Journal of Nuclear Medicine*, **48**(1 SUPPL.), p.28S-35S.
109. **Jahnke, V., Matthias, C., Fryer, A., Strange, R. (1996).** Glutathione S-transferase and cytochrome-P-450 polymorphism as risk factors for squamous cell carcinoma of the larynx. *American Journal of Surgery*, **172**(6), p.671-673.
110. **Jerjes, W., Swinson, B., Pickard, D. K. S., Thomas, G. J., Hopper, C. (2005).** Detection of cervical intranodal metastasis in oral cancer using elastic scattering spectroscopy: a study on archival material. *Arch Oral Biol*, **50**(3), p.361-366.
111. **Jess, P. R. T., Smith, D. D. W., Mazilu, M., Dholakia, K., Riches, A. C., Herrington, C. S. (2007).** Early detection of cervical neoplasia by Raman spectroscopy. *International Journal of Cancer*, **121**(12), p.2723-2728.

112. **Kast, R. E., Serhatkulu, G. K., Cao, A., Pandya, A. K., Dai, H., Thakur, J. S., et al. (2008)**. Raman spectroscopy can differentiate malignant tumours from normal breast tissue and detect early neoplastic changes in a mouse model. *Biopolymers,* **89**(3), p.235-241.

113. **Katzin, W. E., Centeno, J. A., Feng, L., Kiley, M., Mullick, F. G. (2005)**. Pathology of lymph nodes from patients with breast implants: A histological and spectroscopic evaluation. *American Journal of Surgical Pathology,* **29(**4), p.506-511.

114. **Keller, S., Schrader, B., Hoffman, A., Schrader, W., Metz, K., Rehlaender, J., Pahnke, J., Ruwe, M., Budach, W. (1994)**. Application of near infrared Fourier transform Raman spectroscopy in medical research. *J Raman Spectrosc*, **25**, p.663-671.

115. **Kendall, C., Schut, T. B., Stone, N., Stravroulaki, P., Puppels, G., Barr, H. (2000)**. Raman spectroscopy for the diagnosis of dysplasia in columnar and squamous epithelium. *Proc SPIE,* **4161**, 131-137.

116. **Kendall, C., Stone, N., Shepherd, N., Geboes, K., Warren, B., Bennett, R., et al. (2003).** Raman spectroscopy, a potential tool for the objective identification and classification of neoplasia in Barrett's oesophagus. *Journal of Pathology,* **200**(5), p.602-609.

117. **Kendall, C.A. (2002a).** A Study of Raman Spectroscopy for the early Detection and Classification of Malignancy in Oesophageal Tissue. *PhD Thesis*, p.119-121.

118. **Kendall, C.A. (2002b).** A Study of Raman Spectroscopy for the early Detection and Classification of Malignancy in Oesophageal Tissue. *PhD Thesis*, p.64.

119. **Kendall, C.A. (2002c).** A Study of Raman Spectroscopy for the early Detection and Classification of Malignancy in Oesophageal Tissue. *PhD Thesis*, p.67.

120. **Kendall, C.A. (2002d).** A Study of Raman Spectroscopy for the early Detection and Classification of Malignancy in Oesophageal Tissue. *PhD Thesis*, p.66.

121. **Kendall, C.A. (2002e).** A Study of Raman Spectroscopy for the early Detection and Classification of Malignancy in Oesophageal Tissue. *PhD Thesis*, A.1-A.26.

122. **Kiesslich, R., Gossner, L., Goetz, M., Dahlmann, A., Vieth, M., Stolte, M., et al. (2006**). In vivo histology of Barrett's oesophagus and associated neoplasia by confocal laser endomicroscopy. *Clinical Gastroenterology and Hepatology,* **4**(8), p.979-987.

123. **Ko, A. C., Choo-Smith, L., Zhu, R., Hewko, M., Dong, C., Cleghorn, B., et al. (2006).** Application of NIR Raman spectroscopy for detecting and characterizing early dental caries. *Proc SPIE, 6093.*

124. **Koufman, J. A., Burke, A. J. (1997).** The aetiology and pathogenesis of laryngeal carcinoma. *Otolaryngologic Clinics of North America,* **30**(1), p.1-19.

125. **Krishna, C. M., Prathima, N. B., Malini, R., Vadhiraja, B. M., Bhatt, R. A., Fernandes, D. J., et al. (2006)**. Raman spectroscopy studies for diagnosis of cancers in human uterine cervix. *Vibrational Spectroscopy,* **41**(1), p.136-141.

126. **Kundu, L. M., Loppnow, G. R. (2007**). Direct detection of 8-oxo-deoxyguanosine using UV resonance Raman spectroscopy. *Photochemistry and Photobiology,* **83**(3), p.600-602.

127. **La Via, W. V., Lambert, J. L., Pelletier, M. J., Morookian, J. M., Sirk, S. J., Mickiene, D., et al. (2006)**. Measurement of Amphotericin B concentration by resonant Raman spectroscopy - A novel technique that may be useful for non-invasive monitoring. *Medical Mycology,* **44**(2), p.169-174.

128. **Lademann, J., Weigmann, H. J., Rickmeyer, C., Barthelmes, H., Schaefer, H., Mueller, G., Sterry, W. (1999).** Penetration of titanium dioxide microparticles in a sunscreen formulation into the horny layer and the follicular orifice. *Skin Pharmacology and Applied Skin Physiology*, **12**(5), p.247-256.
129. **Laforest, L., Luce, D., Goldberg, P., Begin, D., Gerin, M., Demers, P. A., et al. (2000).** Laryngeal and hypopharyngeal cancers and occupational exposure to formaldehyde and various dusts: A case-control study in France. *Occupational and Environmental Medicine*, **57**(11), p.767-773.
130. **Lambert, J. L., Pelletier, C. C., Borchert, M. (2005).** Glucose determination in human aqueous humor with Raman spectroscopy. *Journal of Biomedical Optics*, **10**(3), p.1-8.
131. **Landini, L., Santarelli, M. F., Pingitore, A., Positano, V. (2003).** New technological developments in the clinical imaging of atherosclerotic plaque. *Current Pharmaceutical Design*, **9**(29), p.2403-2415.
132. **Lane, D. P. (1992)**.Guardian of the genome. *Nature*, **358**, no. 6381(15-16) p53.
133. **Lau, D. P., Huang, Z., Lui, H., Anderson, D. W., Berean, K., Morrison, M. D., et al. (2005)**. Raman spectroscopy for optical diagnosis in the larynx: Preliminary findings. *Lasers in Surgery and Medicine*, **37**(3), p.192-200.
134. **Lawson, E. E., Edwards, H. G. M., Barry, B. W., Williams, A. C. (1998).** Interaction of salicylic acid with verrucae assessed by FT-Raman spectroscopy. *Journal of Drug Targeting*, **5**(5), p.343-351.
135. **Leroy, G., Penel, G., Leroy, N., Brès, E. (2002).** Human tooth enamel: A Raman polarized approach. *Applied Spectroscopy*, **56(**8), p.1030-1034.
136. **Leuwer, R. M., Westhofen, M., Schade, G. (1997).** Colour duplex echography in head and neck cancer. *American Journal of Otolaryngology - Head and Neck Medicine and Surgery*, **18**(4), p.254-257.
137. **Lewensohn-Fuchs, I., Munck-Wikland, E., Berke, Z., Magnusson, K. P., Pallesen, G., Auer, G., et al. (1994).** Involvement of aberrant p53 expression and human papilloma virus in carcinoma of the head, neck and oesophagus. *Anticancer Research*, **14**(3 B), p.1281-1285.
138. **Li, X., Wang, D., & Wang, Y. (2007).** Discrimination of normal and colorectal cancer using Raman spectroscopy and fluorescence. *Proc SPIE* , 6633.
139. **Lieber, C. A., Ellis, D. L., Billheimer, Dean, D., Mahadevan-Jansen, A. (2004**). Handheld confocal Raman microspectrometer for in-vivo skin cancer measurement. *Proc SPIE*, **5321**, 10-16.
140. **Lister, T. A., Crowther, D., Sutcliffe, S.B., et al. (1989).** Report of a committee convened to discuss the evaluation and staging of patients with Hodgkin's disease: Cotswold meeting. *J Clin Oncol*, **7**, p.1630-6.
141. **Liu, G., Liu, J., Zhang, L., Yu, F., Sun, S. (2005)**. Raman spectroscopic study of human tissues. *Spectroscopy and Spectral Analysis*, **25**(5), p.723-725.
142. **Lončar, B., Pajtler, M., Miličić-Juhas, V., Kotromanović, Z., Staklenac, B., Pauzar, B. (2007).** Imprint cytology in laryngeal and pharyngeal tumours. *Cytopathology*, **18**(1), p.40-43.
143. **Lundgren, J., Olofsson, J., Hellquist, H., Strandh, J. (1982).** The role of smear cytology in laryngeal diagnosis. *Journal of Otolaryngology*, **11**(6), p.371-378.
144. **Lyng, F. M., Faoláin, E. O., Conroy, J., Meade, A. D., Knief, P., Duffy, B., et al. (2007).** Vibrational spectroscopy for cervical cancer pathology, from

biochemical analysis to diagnostic tool. *Experimental and Molecular Pathology*, **82**(2), p.121-129.

145. **Mahadevan-Jansen, A., Mitchell, M. F., Ramanujam, N., Malpica, A., Thomsen, S., Utzinger, U., et al. (1998).** Near-infrared Raman spectroscopy for in vitro detection of cervical precancers. *Photochemistry and Photobiology*, **68**(1), p.123-132.

146. **Maier, H., Tisch, M. (1997).** Epidemiology of laryngeal cancer: Results of the Heidelberg case- control study. *Acta Oto-Laryngologica, Supplement*, (**527**), p.160-164.

147. **Maier, H., Dietz, A., Gewelke, U., Heller, W., Weidauer, H. (1992).** Tobacco and alcohol and the risk of head and neck cancer. *Clinical Investigator*, **70**(3-4), p.320-327.

148. **Maiman, T.H. (1960)**. Stimulated optical radiation in ruby. *Nature*, **187**, p.493-494.

149. **Major, T., Szarka, K., Sziklai, I., Gergely, L., Czeglédy, J. (2005).** The characteristics of human papillomavirus DNA in head and neck cancers and papillomas. *Journal of Clinical Pathology*, **58**(1), p.51-55.

150. **Manfait, M., Lamaze, P., Lamfarraj, H., Pluot, M., Sockalingum, G. D. (2000)**. Diagnosis and prognosis of tissue pathologies by Raman microspectroscopy: An application to human thyroid tumours. *Proc SPIE*, **3918**,153-160.

151. **Manoharan, R., Wang, Y., Feld, M. S. (1996)**. Histochemical analysis of biological tissues using Raman spectroscopy. *Spectrochimica Acta - Part A Molecular Spectroscopy*, **52**(2 PART A), p.215-249.

152. **Manoharan, R., Wang, Y., Dasari, R. R., Singer, S. S., Rava, R. P., Feld, M. S. (1995).** Ultraviolet resonance Raman spectroscopy for detection of colon cancer. *Lasers in the Life Sciences*, **6**(4), p.217-227.

153. **Maquelin, K., Choo-Smith, L. P., Van Vresswijk, T., Endtz, H. P., Smith, B., Bennett, R., Bruining, H. A., Puppels, G. J**. Raman spectroscopic method for identification of clinically relevant micro organisms growing on solid culture medium. *Anal Chem*, **72**, p.12-19.

154. **Marioni, G., Marchese-Ragona, R., Cartei, G., Marchese, F., Staffieri, A. (2006).** Current opinion in diagnosis and treatment of laryngeal carcinoma. *Cancer Treatment Reviews*, **32**(7), p.504-515.

155. **Masui, T., Tategaki, H., Furukawa, S., & Imanaka, N. (2004)**. Synthesis and characterization of new environmentally-friendly pigments based on cerium phosphate. *Nippon Seramikkusu Kyokai Gakujutsu Ronbunshi/Journal of the Ceramic Society of Japan*, **112**(1312), p.646-649.

156. **Matthias, C., Bockmühl, U., Jahnke, V., Harries, L. W., Wolf, C. R., Jones, P. W., et al. (1998).** The glutathione S-transferase GSTP1 polymorphism: Effects on susceptibility to oral/pharyngeal and laryngeal carcinomas. *Pharmacogenetics*, **8**(1), p.1-6.

157. **McMinn, R. M. H. (1995)**. Head, Neck and Spine. In: *Last's Anatomy – Regional and Applied, 9th Ed, Published by Churchill Livingstone*, **6**, p.486-505.

158. **Medina-Gutiérrez, C., Quintanar, J. L., Frausto-Reyes, C., Sato-Berrú, R. (2005)**. The application of NIR Raman spectroscopy in the assessment of serum thyroid-stimulating hormone in rats. *Spectrochimica Acta : Molecular and Biomolecular Spectroscopy*, **61**(1-2), p.87-91.

159. **Michelson, A. A. (1920).** The Vertical Interferometer. *Proc Natl Acad Sci U.S.A*, **6**, p.473-474.

160. **Molckovsky, A., Wong Kee Song, L., Shim, M. G., Marcon, N. E., Wilson, B. C. (2003).** Diagnostic potential of near-infrared Raman spectroscopy in the colon: Differentiating adenomatous from hyperplastic polyps. *Gastrointestinal Endoscopy,* **57**(3), p.396-402.

161. **Morrison, M. D. (1988).** Is chronic gastroesophageal reflux a causative factor in glottic carcinoma? *Otolaryngology - Head and Neck Surgery,* **99**(4), p.370-373.

162. **Muller, M. G., Valdez, T. A., Georgakoudi, I., Backman, V., Fuentes, S., Kabani, S. (2003).** Spectroscopic detection and evaluation of morphological and biochemical changes in early human oral cancer. Cancer. **97**(7), p.1681-92.

163. **Nafie, L. A. (2001).** Theory of Raman Spectroscopy. In: *Handbook of Raman Spectroscopy*, *Edited by Lewis, I. R., Edwards, H. G. M. Marcel Dekker, New York*, p.1.

164. **Naghavi, M., Madjid, M., Khan, M. R., Mohammadi, R. M., Willerson, J. T., Casscells, S. W. (2001**). New developments in the detection of vulnerable plaque. *Current Atherosclerosis Reports,* **3**(2), p.125-135.

165. **National Statistics Online. (2006).** – Health. http://www.statistics.gov.uk (accessed 28 th September 2006).

166. **Nelson, D. B., Block, K. P., Bosco, J. J., Burdick, J. S., Curtis, W. D., et al (2000)**. High resolution and high magnification endoscopy. *Gastrointest. Endosc*. **52**, p.864-866.

167. **Nie, S., Castillo, C. G., Bergbauer, K. L., Kuck Jr., J. F. R., Nabiev, I. R., Yu, N. (1990).** Surface-enhanced Raman spectra of eye lens pigments. *Applied Spectroscopy,* **44**(4), p.571-575.

168. **Nijssen, A., Maquelin, K., Santos, L. F., Caspers, P. J., Bakker Schut, T. C., den Hollander, J. C., et al. (2007).** Discriminating basal cell carcinoma from perilesional skin using high wave-number Raman spectroscopy. *Proc SPIE,* **12,** 3

169. **Nishiyama, Y., Yamamoto, Y., Yokoe, K., Miyabe, K., Iwasaki, T., Toyama, Y., et al. (2004).** Superimposed dual-isotope SPECT using 99mTc-hydroxymethylene diphosphonate and 201Tl-chloride to assess cartilage invasion in laryngohypopharyngeal cancer. *Annals of Nuclear Medicine,* **18**(6), p.527-532.

170. **Obana, A., Hiramitsu, T., Gohto, Y., Ohira, A., Mizuno, S., Hirano, T., et al. (2008)**. Macular carotenoid levels of normal subjects and age-related maculopathy patients in a Japanese population. *Ophthalmology,* **115**(1), p.147-157.

171. **Olsen, J., Sabroe, S. (1984).** Occupational causes of laryngeal cancer. *Journal of Epidemiology and Community Health***, 38**(2), p.117-121.

172. **Olszewski, J., Latusiński, J., Kita, A., Pietkiewicz, P., Starostecka, B., Majak, J. (2006).** Comparative assessment of aluminum and lead concentrations in serum and tissue bioptates in patients with laryngeal papilloma or cancer. *B-ENT***, 2**(2), p.47-49.

173. **Ozaki, Y. (1988).** Medical Applications of Raman Spectroscopy. *Applied Spectroscopy Reviews*, **24**(3-4**)**, p.259-312.

174. **Ozaki, Y., Iriyama, K., Hamaguchi, H. (1987).** Multchannel Raman spectroscopy of an intact lens: Raman measurement with laser irradiation below the threshold for retinal damage. *Applied Spectroscopy*, **41**(7), p.1245-1247.

175. **Ozer, K., Cilingiroglu, M. (2005).** Vulnerable plaque: Definition, detection, treatment, and future implications. *Current Atherosclerosis Reports*, **7**(2), p.121-126.
176. **Paczona, R., Temam, S., Janot, F., Marandas, P., Luboinski, B. (2003).** Autofluorescence videoendoscopy for photodiagnosis of head and neck squamous cell carcinoma. *European Archives of Oto-Rhino-Laryngology*, **260**(10), p.544-548.
177. **Palasz, Z., Grobelny, A., Pawlik, E., Fraczek, M., Zalesska-Krecicka, M., Klimczak, A., et al. (2003).** Investigation of normal and malignant laryngeal tissue by autofluorescence imaging technique. *Auris Nasus Larynx*, **30**(4), p.385-389.
178. **Pellicano, R. (2000).** Gastroesophageal reflux disease in laryngology. [Malattia da reflusso gastro-esofageo e patologie faringo-laringee] *Otorinolaringologia*, **50**(1), p.13-26.
179. **Pfeifer, G. P., Denissenko, M. F., Olivier, M., Tretyakova, N., Hecht, S. S., & Hainaut, P. (2002).** Tobacco smoke carcinogens, DNA damage and p53 mutations in smoking-associated cancers. *Oncogene*, **21**(48 Rev. ISS. 6), p.7435-7451.
180. **Pfeifer, G. P., You, Y., Besaratinia, A. (2005)**. Mutations induced by ultraviolet light. *Mutation Research - Fundamental and Molecular Mechanisms of Mutagenesis*, **571**(1-2): SPEC. ISS. P.19-31.
181. **Pradier, R., Gonzalez, A., Matos, E., Loria, D., Adan, R., Saco, P., et al. (1993).** Prognostic factors in laryngeal carcinoma: Experience in 296 male patients. *Cancer*, **71**(8), p.2472-2476.
182. **Profio, A. E., Doiron, D. R. (1977).** A feasibility study of the use of fluorescence bronchoscopy for localization of small lung tumours. *Physics in Medicine and Biology*, **22**(5), p.949-957.
183. **Puppels, G. J., Baker-Schut, T. C., Caspers, P. J., Wolthuis, R., Van Aken, M., Van Laarse, A., Bruining, H. A., Buschman, H. P. J., Shim, M. G., Wilson, B. C. (2001).** *In vivo* Raman spectroscopy. In: *Handbook of Raman Spectroscopy, Practical Spectroscopy Series, Edited by Lewis, I. R., Edwards, H. G. M., Marcel Dekker*. ***28***, p.549-574.
184. **Rady, P. L., Schnadig, V. J., Weiss, R. L., Hughes, T. K., Tyring, S. K. (1998).** Malignant transformation of recurrent respiratory papillomatosis associated with integrated human papillomavirus type 11 DNA and mutation of p53. *Laryngoscope*, **108**(5), p.735-740.
185. **Raman, C. V., Krishnan, K. S. (1928).** A New Type of Secondary Radiation. *Nature*, **121**, p.501-502.
186. **Ridgway, J. M., Ahuja, G., Guo, S., Su, J., Mahmood, U., Chen, Z., Wong, B. (2007**). Imaging of the paediatric airway using optical coherence tomography. *Laryngoscope*, **117**(12), p.2206-2212.
187. **Rimai, L., Kilponen, R. G., Gill, D. (1970).** Resonance-enhanced Raman spectra of visual pigments in intact bovine retinas at low temperatures. *Biochemical and Biophysical Research Communications*, **41**(2), p.492-497.
188. **Robbins, S. L., Cotran, R. S., Kumar, V. (1989a)**. Pathogenesis of Karposi's sarcoma, In: *Pathologic, Basis of Disease, 4th Ed, Published by W.B. Saunders*, **12**, p.592.
189. **Robbins, S. L., Cotran, R. S., Kumar, V. (1989b)**. Pathogenesis of Karposi's sarcoma, In: *Pathologic, Basis of Disease, 4th Ed, Published by W.B. Saunders*, **6**, p.272.

190. **Robbins, S. L., Cotran, R. S., Kumar, V. (1989c)**. Pathogenesis of Karposi's sarcoma, In: *Pathologic, Basis of Disease, 4th Ed, Published by W.B. Saunders*, **6**, p.239-306.
191. **Robbins, S. L., Cotran, R. S., Kumar, V. (1989d)**. Pathogenesis of Karposi's sarcoma, In: *Pathologic, Basis of Disease, 4th Ed, Published by W.B. Saunders*, **6**, p.291.
192. **Robichaux, A., Lieber, C., Shappell, H., Huff, B., Jones III, H., Mahadevan-Jansen, A. (2002).** In vivo detection of cervical dysplasia with near infrared Raman spectroscopy. *Proc SPIE*, **4614**, 145-151.
193. **Rogers, M. A. M., Thomas, D. B., Davis, S., Vaughan, T. L., Nevissi, A. E. (1993).** A case-control study of element levels and cancer of the upper aerodigestive tract. *Cancer Epidemiology Biomarkers and Prevention*, **2**(4), p.305-312.
194. **Rohr, T. E., Cotton, T., Fan, N., Tarcha, P. J. (1989)**. Immunoassay employing surface-enhanced Raman spectroscopy. *Analytical Biochemistry*, **182**(2), p.388-398.
195. **Römer, T. J., Brennan III, J. F., Bakker Schut, T. C., Wolthuis, R., Van Den Hoogen, R. C. M., Emeis, J. J., et al. (1998).** Raman spectroscopy for quantifying cholesterol in intact coronary artery wall. *Atherosclerosis*, **141**(1), p117-124.
196. **Rosasco, G. J., Etz, E.S., Cassatt, W.A. (1975**).Analysis of discrete fine particles by Raman spectroscopy. *Applied Spectroscopy*, **29**(5), p.396-404.
197. **Rosasco, G. J. (1980).** Raman microprobe spectroscopy. In: *Advances in infrared and Raman spectroscopy,Edited by Clarke R.J.H, Hester R.E, Publishers, Heyden and Sons Ltd*, p7.
198. **Rünger, T. M., U. P. Kappes. (2008)**. Mechanisms of mutation formation with long-wave ultraviolet light (UVA). *Photodermatology Photoimmunology and Photomedicine* **24**(1), p. 2-10.
199. **Sadri, M., McMahon, J., Parker, A. (2006).** Laryngeal dysplasia: Aetiology and molecular biology. *Journal of Laryngology and Otology*, **120**(3), p.170-177.
200. **Sajid, J., Ellhaddaoui, A., Turrell, S. (19997)**. Fourier transform vibrational spectroscopic analysis of human cerebral tissue. *J Raman Spectrosc*, **28**, p.165-169.
201. **Salenius, J. P., Brennan III, J. F., Miller, A., Wang, Y., Aretz, T., Sacks, B., et al. (1998)**. Biochemical composition of human peripheral arteries examined with near- infrared Raman spectroscopy. *Journal of Vascular Surgery*, **27**(4), p.710-719.
202. **Sanuki, T. (1997).** Endoscopic mode for three-dimensional CT display of normal and pathologic laryngeal structures. *Otolaryngology - Head and Neck Surgery (Tokyo)*, **69**(3), p.211-216.
203. **Sasiadek, M., Stembalska-Kozlowska, A., Smigiel, R., Krecicki, T., Blin, N., & Mirghomizadeh, F. (2001).** Microsatellite and chromosome instability in squamous cell laryngeal carcinoma. *International Journal of Oncology*, **19**(2), p.401-405.
204. **Schallreuter, K. U., Rübsam, K., Gibbons, N. C. J., Maitland, D. J., Chavan, B., Zothner, C., et al. (2008).** Methionine sulfoxide reductases A and B are deactivated by hydrogen peroxide (H2O2) in the epidermis of patients with vitiligo. *Journal of Investigative Dermatology*, **128**(4), p.808-815.
205. **Scheifele, C., Reichart, P. A., Hippler-Benscheidt, M., Neuhaus, P., Neuhaus, R. (2005).** Incidence of oral, pharyngeal, and laryngeal squamous cell

carcinomas among patients after liver transplantation. *Oral Oncology*, **41**(7), p.670-676.

206. **Schlecht, N. F., Franco, E. L., Pintos, J., Negassa, A., Kowalski, L. P., Oliveira, B. V., et al. (1999)**. Interaction between tobacco and alcohol consumption and the risk of cancers of the upper aero-digestive tract in brazil. *American Journal of Epidemiology*, **150**(11), p.1129-1137.
207. **Schultz, C. P. (2000)**. Comparative FT-Raman and FT-infrared biochemical images of the same tissue sections providing new insight into tissue structure, formation and aberrations. *Proc SPIE*, **3918**, .16.
208. **Sepehr, A., Armstrong, W. B., Guo, S., Su, J., Perez, J., Chen, Z., Wong, B. J. F. (2008).** Optical coherence tomography of the larynx in the awake patient. *Otolaryngology - Head and Neck Surgery*, **138** (4), p. 425-429.
209. **Shetty, G., Kendall, C., Shepherd, N., Stone, N., & Barr, H. (2006).** Raman spectroscopy: Elucidation of biochemical changes in carcinogenesis of oesophagus. *British Journal of Cancer*, **94**(10), p.1460-1464.
210. **Shim, M. G., Song, L. M. W. K., Marcon, N., Hassaram, S., Wilson, B. C. (2000).** Assessment of *ex vivo* and *in vivo* near-infrared Raman spectroscopy for the classification of dysplasia within Barrett's oesophagus. *Proc SPIE,*. **3918**, 114-119.
211. **Shim, M. G., Wilson,B. C. (1996).** The effects of ex vivo handling procedures on the near infrared Raman spectra of normal mammalian tissues. *Photochem. Photobiol.* **63**, p.662-671.
212. **Sideroudi, T. I., Pharmakakis, N. M., Papatheodorou, G. N., Voyiatzis, G. A. (2006**). Non-invasive detection of antibiotics and physiological substances in the aqueous humor by Raman spectroscopy. *Lasers in Surgery and Medicine*, **38**(7), p.695-703.
213. **Sideroudi, T., Pharmakakis, N., Tyrovolas, A., Papatheodorou, G., Chryssikos, G. D., & Voyiatzis, G. A. (2007)**. Non-contact detection of ciprofloxacin in a model anterior chamber using Raman spectroscopy. *Proc SPIE*, **12** 3.
214. **Sieg, A., Crowther, J., Blenkiron, P., Marcott, C., & Matts, P. J. (2006).** Confocal Raman microspectroscopy - measuring the effects of topical moisturisers on stratum corneum water gradient in vivo. *Proc SPIE*, 6093.
215. **Smekal, A. (1923).** Title. *Naturwissenschaften*, **43**, p.873.
216. **Smith, E. M., Summersgill, K. F., Allen, J., Hoffman, H. T., McCulloch, T., Turek, L. P., et al. (2000).** Human papilloma virus and risk of laryngeal cancer. *Annals of Otology, Rhinology and Laryngology*, **109**(11), p.1069-1076.
217. **Smith, E., Dent, G. (2005a)**. Modern Raman Spectroscopy. In: *A Practical Approach, John Wiley & Sons, Ltd*, p.1-21.
218. **Smith, E., Dent, G. (2005b)**. Modern Raman Spectroscopy. In: *A Practical Approach, John Wiley & Sons, Ltd*, p.23-31.
219. **Smith, E., Dent, G. (2005c)**. Modern Raman Spectroscopy. In: *A Practical Approach, John Wiley & Sons, Ltd*, p.3.
220. **Smith, E., Dent, G. (2005d)**. Modern Raman Spectroscopy. In: *A Practical Approach, John Wiley & Sons, Ltd*, p.113-133.
221. **Smith, J., Kendall, C., Sammon, A. M., Christie-Brown, J., Mandalia, T., Stone, N. (2005)**. Raman spectroscopy is sensitive and specific in the detection of lymph node metastases in breast cancer. *Proc SPIE* **5862**, 1-7.

222. **Smith, J., Kendall, C., Sammon, A., Christie-Brown, J., Stone, N. (2003)**. Raman spectral mapping in the assessment of axillary lymph nodes in breast cancer. *Technology in Cancer Research and Treatment*, **2**(4), p.327-331.
223. **Solomon, D., Smith, R. R. L., Hashima, H. K. (1985).** Malignant transformation in non-irradiated recurrent respiratory papillomatosis. *Laryngoscope*, **95**(8), p.900-904.
224. **Steenland, K., Schnorr, T., Beaumont, J., Halperin, W., Bloom, T. (1988).** Incidence of laryngeal cancer and exposure to acid mists. *British Journal of Industrial Medicine*, **45**(11), p.766-776.
225. **Stell, P. M., McGill, T. (1973).** Asbestos and laryngeal carcinoma. *Lancet*, **2**(7826), p.416-417.
226. **Sterenborg, H. J. C. M., Motamedi, M., Sahebkar, F., Wicksted, J. P., Wagner Jr, R. F. (1993).** In vivo optical spectroscopy: New promising techniques for early diagnosis of skin cancer. *Skin Cancer*, **8**(1), p.57-65.
227. **Stone, N. (2001a).** Raman Spectroscopy of Biological Tissue for Application in Optical Diagnosis of Malignancy. *PhD Thesis*,
228. **Stone, N. (2001b.** Raman Spectroscopy of Biological Tissue for Application in Optical Diagnosis of Malignancy. *PhD Thesis*, p.47.
229. **Stone, N., Hart Prieto, M. C., Crow, P., Uff, J., Ritchie, A. W. (2007).** The use of Raman spectroscopy to provide an estimation of the gross biochemistry associated with urological pathologies. *Analytical and Bioanalytical Chemistry*, **387**(5), p.1657-1668.
230. **Stone, N., Kendall, C., Shepherd, N., Crow, P., Barr, H. (2002)**. Near-infrared Raman spectroscopy for the classification of epithelial pre-cancers and cancers. *Journal of Raman Spectroscopy*, **33**(7), p 564-573.
231. **Stone, N., Kendall, C., Shepherd, N., Crow, P., Barr, H. (2002).** Near-infrared Raman spectroscopy for the classification of epithelial pre-cancers and cancers. *Journal of Raman Spectroscopy*, **33**(7), p.564-573.
232. **Stone, N., Kendall, C., Smith, J., Crow, P., Barr, H. (2004)**. Raman spectroscopy for identification of epithelial cancers. *Faraday Discussions*, **126**, p.141-157.
233. **Stone, N., Stavroulaki, P., Kendall, C., Birchall, M., Barr, H. (2000**). Raman spectroscopy for early detection of laryngeal malignancy: Preliminary results. *Laryngoscope*, **110**(10 I), p.1756-1763.
234. **Suzuki, K., Miura, T., Takeuchi, H. (2001).** Inhibitory effect of copper (II) on zinc (II)-induced aggregation of amyloid β-peptide.
235. **Suzuki, M., Kato, H., Wakumoto, S. (1991).** Vibrational analysis by Raman spectroscopy of the interface between dental adhesive resin and dentin. *Journal of Dental Research*, **70(**7), p.1092-1097.
236. **Swinson, B., Jerjes, W., El-Maaytah, M., Norris, P., Hopper, C. (2005).** Optical techniques in the diagnosis of head and neck malignancy. *Oral Oncol*, **42**(3), p.221-8.
237. **Székely, G., Remenár, E., Kásler, M., Gundy, S. (2005).** Mutagen sensitivity of patients with cancer at different sites of the head and neck. *Mutagenesis*, **20**(5), p.381-385.
238. **Szládek, G., Juhász, A., Kardos, K., Szöke, K., Major, T., Sziklai, I., et al. (2005).** High co-prevalence of genogroup 1 TT virus and human papillomavirus is

associated with poor clinical outcome of laryngeal carcinoma. *Journal of Clinical Pathology,* **58**(4), p.402-405.

239. **Szyfter, K., Szmeja, Z., Szyfter, W., Hemminki, K., Banaszewski, J., Jaskuła-Sztul, R., et al. (1999).** Molecular and cellular alterations in tobacco smoke-associated larynx cancer. *Mutation Research - Genetic Toxicology and Environmental Mutagenesis,* **445**(2), p.259-274.
240. **Talamini, R., Bosetti, C., La Vecchia, C., Dal Maso, L., Levi, F., Bidoli, E., et al. (2002)**. Combined effect of tobacco and alcohol on laryngeal cancer risk: A case-control study. *Cancer Causes and Control,* **13**(10), p.957-964.
241. **Teppo, H., Soini, Y., Melkko, J., Koivunen, P., & Alho, O. (2003).** Prognostic factors in laryngeal carcinoma: The role of apoptosis, p53, proliferation (ki-67) and angiogenesis. *APMIS,* **111**(4), p.451-457.
242. **Thakur, J. S., Dai, H., Serhatkulu, G. K., Naik, R., Naik, V. M., Cao, A., et al. (2007)**. Raman spectral signatures of mouse mammary tissue and associated lymph nodes: Normal, tumour and mastitis. *Journal of Raman Spectroscopy,* **38**(2), p.127-134.
243. **The NHS Cancer Plan. (2000a).** *Funding,* **11**, p.92.
244. **The NHS Cancer Plan. (2000b).** *Research Funding,* **10**, p.86.
245. **The NHS Cancer Plan. (2000c).** *Wait Targets,* p *Executive Summary,* p.6.
246. **Thiberville, L., Moreno-Swirc, S., Vercauteren, T., Peltier, E., Cavé, C., Heckly, G. B. (2007).** In vivo imaging of the bronchial wall microstructure using fibered confocal fluorescence microscopy. *American Journal of Respiratory and Critical Care Medicine***, 175**(1), p.22-31.
247. **Thomsen, K. A., Thomsen, J. (1975).** Toluidine blue staining in laryngeal diseases. *Laryngologie Rhinologie Otologie,* **54**(2), p.114-119.
248. **Towler, M. R., Wren, A., Rushe, N., Saunders, J., Cummins, N. M., Jakeman, P. M. (2007).** Raman spectroscopy of the human nail: A potential tool for evaluating bone health? *Journal of Materials Science: Materials in Medicine,* **18**(5), p.759-763.
249. **Tsuda, H., Arends, J. (1993).** Raman spectra of human dental calculus. *Journal of Dental Research,* **72**(12), p.1609-1613.
250. **Utzinger, U., Heintzelman, D. L., Mahadevan-Jansen, A., Malpica, A., Follen, M., Richards-Kortum, R. (2001)**. Near-infrared Raman spectroscopy for in vivo detection of cervical precancers. *Applied Spectroscopy*. **55**(8), p.955-959.
251. **Utzinger, U., Richards-Kortum. R. R. (2003)**. Fibre optic probes for biomedical optical spectroscopy. *Journal of Biomedical Optics*. **8**(1), p.121-147.
252. **Vandecaveye, V., de Keyzer, F., Vander Poorten, V., Deraedt, K., Alaerts, H., Landuyt, W., et al. (2006).** Evaluation of the larynx for tumour recurrence by diffusion-weighted MRI after radiotherapy: Initial experience in four cases. *British Journal of Radiology,* **79**(944), p. 681-687.
253. **Varzim, G., Monteiro, E., Silva, R. A., Fernandes, J., Lopes, C. (2003).** CYP1A1 and XRCC1 gene polymorphisms in SCC of the larynx. *European Journal of Cancer Prevention : The Official Journal of the European Cancer Prevention Organisation (ECP),* **12**(6), p.495-499.
254. **Wang, S. Q. R., Setlow, M., Berwick, D., Polsky, A. A., Marghoob, A. W., Kopf, and R. S. Bart. (2001)**. Ultraviolet A and melanoma: A review. *Journal of the American Academy of Dermatology*. **44**(5), p. 837-846.

255. **Watanabe, A., Taniguchi, M., Tsujie, H., Fujita, M., Sasaki, S. (2007).** Early detection of recurrent hypopharyngeal cancer after radiotherapy by utilizing narrow-band imaging-report of a case. *Journal of Otolaryngology of Japan,* **110**(10), p.680-682.

256. **Weatherall, D. J., Ledingham, J. G. G., Warrell, D. A. (1987).** Aeitiological fators and pathology of neoplastic polyps, In: *The Oxford Text Book of Medicine, 2nd Ed, Published by the Oxford University Press,* **12**, p.151.

257. **Williams, A. C., Barry, B. W., Edwards, H. G. M., Farwell, D. W. (1993).** A critical comparison of some Raman spectroscopic techniques for studies of human stratum corneum. *Pharmaceutical Research,* **10**(11), p.1642-1647.

258. **Williams, A. C., Carter, E. A., Edwards, H. G. M., Barry, B. W. (1999).** Drug penetration into and permeation through human skin assessed by Raman spectroscopy. *Proc SPIE,* **3608**,.64-72.

259. **Williams, A. C., Edwards, H. G. M., Barry, B. W. (1992).** Fourier transform Raman spectroscopy. A novel application for examining human stratum corneum. *International Journal of Pharmaceutics***, 81**(2-3), R11-R14.

260. **Williams, A. C., Edwards, H. G. M., Barry, B. W. (1995).** The 'iceman': Molecular structure of 5200-year-old skin characterised by Raman spectroscopy and electron microscopy. *Biochimica Et Biophysica Acta - Protein Structure and Molecular Enzymology,* **1246**(1), p.98-105.

261. **Wilson, B. C. (2007a).** Detection and treatment of dysplasia in Barrett's oesophagus: a pivotal challenge in translating Biophotonics from bench to bedside. *J Biomed Opt.* **12**(5): 051401-4.

262. **Wilson, B. C. (2007b).** Detection and treatment of dysplasia in Barrett's oesophagus: a pivotal challenge in translating Biophotonics from bench to bedside. *J Biomed Opt.* **12**(5): 051401-13.

263. **Wilson, B. C. (2007c).** Detection and treatment of dysplasia in Barrett's oesophagus: a pivotal challenge in translating Biophotonics from bench to bedside. *J Biomed Opt.* **12**(5): 051401-10.

264. **Wolthius, R., Bakker Schut, T. C., Caspers, P. J., Buschman, H. P. J, Romer, T. J., Bruining, H. A., Puppels, G. J. (1999).** Raman Spectroscopic methods for In Vitro and In Vivo Tissue Characterization. In: *Fluorescent and Luminescent Probes, 2nd Ed, Edited by Mason, W.T.,* **32**, p.433-455.

265. **World Health Assembly. (2005).** Proceedings of the 58th World Health Assembly (WHA). *Resolution on cancer prevention and control.*

266. **World Health Organisation (2007).** http:// www.who.int/cancer/en/2007 (accessed 10th September 2007).

267. **Wu, Q., Nelon, W. H., Elliot, S., Sperry, J. F., Feld, M., Dasari, R., Manoharan, R. (2000)**. Intensities of E Coli nucleic acid Raman spectra excited selectively from whole cells with 251 nm light. *Anal Chem,* **72**, p.2981-2986.

268. **Wynder, E. L., Stellman, S. D. (1979).** Impact of long-term filter cigarette usage on lung and larynx cancer risk: A case-control study. *Journal of the National Cancer Institute,* **62**(3), p.471-477.

269. **Xu, L., Tian, J., Li, C., Ma, X. (2007).** Application of the three-dimensional reconstruction with 16-multi slice spiral CT in pharyx and larynx. *Chinese Journal of Cancer Prevention and Treatment,* **14**(1), p.60-63.

270. **Yang, Y., Liu, C. H., Savage, H. E., Schantz, S., Alfano, R. R. (1998)**. Optical fluorescence and Raman biopsy of squamous cell carcinoma from the head and neck. *Proc SPIE,* **3250**, 68-71.
271. **Yaqood, Z., Wu, J., McDowell, E. J., Heng, X., Yang, C. (2006).** Methods and application areas of endoscopic optical coherence tomography. *Journal of Biomedical Optics*, **11**(6) 063001, p1-19.
272. **Yerramshetty, J. S., Akkus, O. (2008).** The associations between mineral crystallinity and the mechanical properties of human cortical bone. *Bone***, 42**(3), p.476-482.
273. **Yu N. T, East E. J. (1975**). Laser Raman spectroscopic studies of ocular lens and its isolated protein fractions. *J Biol Chem*, **250**(6)**,** p. 2196-2202.
274. **Yu, N. T., Kuck Jr, J. F. R., Askren, C. C. (1982).** Laser Raman spectroscopy of the lens in situ, measured in an anesthetized rabbit. *Current Eye Research***, 1**(10), p.615-618.
275. **Yu, N-T., Li, X-Y., Kuck, J. F. R. (1996)**. Biomedical applications of Raman Spectroscopy: eye lens research and cardiovascular disease. In: *Biomedical applications of Raman Spectroscopy, Edited by Clark, R.J.H., Hester, R.E., Publishers John Wiley and Sons, **4**.*
276. **Zalesska-Krecicka, M., Krecicki, T., Fraczek, M., Bereś-Pawlik, E., Zatoński, T. (2005).** Autofluorescence laryngoscopy in the diagnosis of laryngeal cancer--early results. *Otolaryngologia Polska*. **59**(2), p.195-199.
277. **Zhou, Y., Li, Y. (2004).** The interaction of polyethylenimine with nucleic acids and its use in determination of nucleic acids based on light scattering. *Spectrochimica Acta - Part A: Molecular and Biomolecular Spectroscopy,* **60**(1-2), p377-384.
278. **Zonios, G., Cothren, R., Crawford, J. M., Fitzmaurice, M., Manoharan, R., Van Dam, J., et al. (1998)**. Spectral pathology. *Annals of the New York Academy of Sciences,* **838**, p.108-115.
279. **Hutchings, J., Kendall, C. A., Shepherd, N., Barr, H., Smith, B., Stone, N. (2008).** Rapid Raman microscopic imaging for potential histological screening. In: *Proc SPIE; 6853 A-33.*
280. **Barr, H., Hutchings, J., Kendall, C. A., Bazant-Hegemark, F., Stone, N. (2007)**. Endoscopic Approaches to the Treatment of Early Malignancy and their relationship to Clinical Outcome. In: *UK Key Advances in Clincal Practice Series. The Effective Management of Upper Gastrointestinal Malignancies , 2nd ed. Edited bys Allen,W., Coyle, V., and Johnston, P.G.*
281. **Baker, R., Matousek, P., Ronayne, K. L., Parker, A. W., Rogers, K., Stone. (2007)**. Depth profiling of calcifications in breast tissue using picosecond Kerr-gated Raman spectroscopy. *Analyst*, **132**, p.48-53.
282. **Mills, Gafey, Frierson (2008)**. Conventional squamous cell carcinoma, In: *Tumors of the Upper Aerodigestive Tract and Ear, 3rd Ed, Published by.....,* **26**, p45-51.

Other Spectroscopic Techniques

Raman spectroscopy is one of many optical techniques which have the potential for use in medical diagnostics. This section classifies and discusses the main alternatives and seeks to show how they inter-relate, their advantages, and disadvantages and how these techniques might be combined with Raman spectroscopy to produce more complete specimen analysis in the future.

A.1 General classification of Spectroscopic Techniques

Spectroscopy can be defined as the study of the interaction between radiation and matter. Historically, spectroscopy referred to a branch of science in which visible light was used for the qualitative and quantitative analysis of the molecular structure of matter. This definition has now broadened to encompass new techniques which utilise other forms of electromagnetic and non-electromagnetic radiation such as microwaves, radio waves, x-rays, electrons and phonons. Spectroscopy can be sub-classified according to the physical parameter measured or calculated; alternatively it can be classified according to the measurement process itself. The absorption, emission, and scattering of electromagnetic radiation by atoms or molecules are the fundamental processes in the spectroscopic techniques discussed in this section. When atoms or molecules absorb electromagnetic energy the incoming energy, if quantum matched, allows transfer of the atomic or molecular system to a higher energy level. Transfer of electromagnetic energy to the atom or molecule is called absorption. A transition from a higher energy level to a lower level were energy is transferred to the electromagnetic field is called emission. If a redirection of light occurs as a result of its interaction with matter the term scattering is used. Generally electrons are promoted to higher orbital states by excitation using ultraviolet or visible light; vibrations are excited by infrared light and rotation by microwaves. A general classification based on the measurement process used is outlined in Figure A.1.

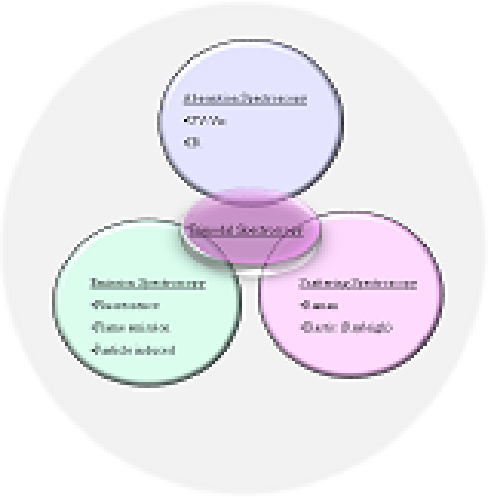

Figure A.1: A general classification of spectroscopic techniques.

Absorption Spectroscopy

Absorption spectroscopy encompasses a range of different techniques and can be sub classified in two ways. Techniques can be defined with reference to the wavelength of the incident radiation e.g. ultraviolet-visible (UV-Vis) range, infrared (IR) and near infrared (NIR) spectroscopy or may be classified according to the direction of the radiation beam after it has interacted with the target specimen as shown in Figure A.2. Radiation that passes through the specimen and is detected in the 180^{o} arc based on a plane running perpendicular to the direction of the incident radiation beam is said to be detected in transmission. Radiation that exits the specimen behind this plane is said to be detected in remission and is made up of two entities, specular reflection where radiation exits at the same angle as that of the incident radiation and diffuse reflection where it occurs at all other angles.

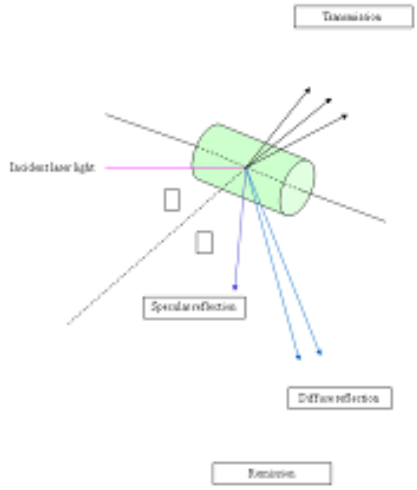

Figure A.2: Radiation detected in reflectance and transmission.

Energy levels available within the target substrate determine the wavelength of radiation absorbed and the energy of the incident photon must match that required to move electrons to a higher electronic level. This allows selective probing of samples by varying the wavelength of the incident radiation. In absorption spectroscopy the absorbed photons are not re-emitted, energy which has been transferred to the target substrate is lost in other ways e.g. thermally. Absorption spectra can be obtained from matter in gas, liquid or solid states. The absorption spectrum obtained is expressed as a plot of radiation absorbance against wavelength and is a fundamental characteristic for that compound. At a given wavelength the measured absorbance is proportional to the molar concentration of the absorbing species and the thickness of the sample. For a specific specimen λ max is the wavelength of the most intense absorption line i.e. the wavelength at which maximum transmission occurs. Each component of a solution has its own λ max hence this parameter may be used qualitatively to identify the constituents of a solution.

Ultraviolet (UV) and Visible (Vis) light spectroscopy

Ultra-violet (UV) spectroscopy has been used extensively as an analytical tool, several amino acids absorb in the ultraviolet range of the electromagnetic spectrum and the technique has been used to quantify concentrations of proteins and DNA. Recently UV resonance Raman spectroscopy has been used to detect 8-oxo-deoxyguanosine (8-oxo-dG), an oxidative lesion in DNA which is responsible for cellular mutation (Kundu, 2007). Ultraviolet-visible light spectroscopy (UV-Vis) uses incident radiation in the visible, ultraviolet or near infrared ranges of the electromagnetic spectrum. Samples tested are generally liquids although the technique can be applied to gases and solids. It is routinely used for quantitative analysis of organo-metallic solutions containing transition metal ions and some innovative uses have been made within the ceramics industry (Masui, 2004). Solutions containing these elements absorb light in the visible range of the electromagnetic spectrum and so are coloured. Absorption is influenced by the presence of other ions, and these can alter the electronic state and hence the wavelength of the absorbed light. As previously noted the Beer-Lambert law applies hence absorbance of the solution will be directly proportional to the concentration of the substance tested. By using calibration curves, which show how quickly absorbance changes with concentration, the concentration of the solution can be determined and standard spectra produced which are independent of the device used.

Infrared spectroscopy (IR)

Infrared spectroscopy is also an example of absorption spectroscopy. The transition between molecular vibrational levels is within the mid-infrared range allowing Raman spectroscopy and mid-infrared spectroscopy to be complimentary in nature when used to probe biological molecules. The two techniques have fundamental differences; in IR the absorption effect occurs as a result of a change in the permanent molecular dipole whereas in Raman spectroscopy it results from scattering of light due to an induced dipole present round the molecule. IR exploits the fact that certain molecules have unique frequencies at which they can vibrate or rotate. In molecules with little or no symmetry the IR and Raman spectra have peaks at similar positions. As a gold standard the vibrational motion of a molecule can only be fully expressed by considering both IR and Raman spectra

In infrared spectroscopy the incident radiation is polychromatic i.e. has a range of frequencies. It can only excite the molecule through vibrational transitions and absorption only occurs when the energy required by the molecule to move between vibrational levels equals that of the photons of incident light. In Raman spectroscopy the incident radiation is monochromatic and the scattered radiation measured differs by one vibrational unit of energy from the incident radiation thus no match is required between the energy of the incident radiation and the energy difference between the ground and excited electronic states (Smith & Dent 2005c; Ferrano, 2003c). Infrared absorption can be thought of as resulting from a direct resonance between the frequency of the incident radiation and the vibration frequency of that particular molecule. The increase in energy corresponds to the energy of the incident photon at the frequency of vibration resonance. This is a one-photon event in contrast to the changes that results as a result of Raman and Raleigh scattering which are considered two photon events and require much higher radiation energy (Nafie, 2001).

Electromagnetic radiation can be characterised by its' wavelength (λ). Energy is linearly related to frequency (ν) and wavenumber (ώ). The relationship between wavelength, frequency and energy (ΔE) is shown below (Eq A.1-A.4) also that of absorbance, radiation intensity and transmission (Eqn A.5-A.13).

$$\lambda = c/\nu \qquad \text{Eq. A.1}$$

$$\nu = \Delta E / h \qquad \text{Eq. A.2}$$

$$\acute{\omega} = 1/\lambda = \Delta E / hc \qquad \text{Eq. A.3}$$

$$\Delta E \; \alpha \; 1/\lambda \qquad \text{Eq. A.4}$$

Where;

c = speed of light ($3x10^{8}ms^{-1}$)
h = Planck's constant (6.626×10^{-34} Js or 4.136×10^{-15} eVs)
ώ = wavenumber (cm^{-1})

Thus the highest energy absorption is associated with radiation of the shortest wavelength and highest frequency.

The intensity of infrared absorptions can be expressed in several ways

Absorbance =A
Transmission =T
% Transmission = T (%)

$$A = \log_{10} (I_o / I) \qquad \text{Eq. A.5}$$

$$T = I / I_o \qquad \text{Eq. A.6}$$

$$T (\%) = 100 \; T \qquad \text{Eq. A.7}$$

$$\text{Hence } A = \log_{10} 1/ T \qquad \text{Eq. A.8}$$

I_o is the intensity of the incident radiation and I the intensity of the radiation after it has passed through the sample.

Absorbance is governed by the Beer-Lambert Law

$$A = \varepsilon \; b \; c \qquad \text{Eq. A.9}$$

Where;

ε = the molar absorbtivity ($Lmol^{-1}cm^{-1}$)
b = the cell length (cm).
c = the concentration of the sample in solution (mol L^{-1})

$$A = \log_{10} (I_o / I) = \varepsilon\, b\, c \qquad \text{Eq. A.10}$$

$$I = I_o\, e^{-\varepsilon b c} \qquad \text{Eq. A.11}$$

$$I_o / I = 1 / e^{-\varepsilon b c} \qquad \text{Eq. A.12}$$

In infrared spectra it is conventional to plot percentage transmission against wavenumber.

$$T\,(\%) = (I_o / I) \times 100 \qquad \text{Eq. A.13}$$

Equations A.12 and A.13 show that percentage transmission is not directly proportional to concentration so in quantitative work absorbance is used in preference (Ferraro, 2003b). IR spectroscopy is simple and reliable. it can be used for both qualitative steady state and dynamic measurements. One practical point of note is that in aqueous solutions the broad absorbance signal resulting from water must be subtracted out of spectra to allow simpler assessment.

Fourier–transform infrared spectroscopy (FT-IR) is an efficient method for processing spectral data obtained using interferometers. Nearly all IR and nuclear magnetic resonance spectroscopy are now performed using Fourier transforms as is much NIR Raman spectroscopy. Fourier-transform Raman spectroscopy has been discussed in more detail in *Section 2.2.5.*

Emission Spectroscopy

Theoretical explanation of emission spectroscopy led the way to the development of quantum mechanics. This form of spectroscopy examines the wavelength of photons emitted when an atom or molecule drops from a higher electronic state to a lower one and it is the structure of the sample that dictates the wavelength of the photons the sample can absorb and emit. The mechanism by which atoms or molecules are excited subclassifies this type of spectroscopy further. For example if electromagnetic radiation is used, fluorescence spectroscopy can result. Protons can produce particle-induced x-ray emission, and if heat is applied to a sample causing an increase in collisions between particles flame emission spectra can be detected. In fluorescence spectroscopy the absorption of a quantum of energy by the target molecule allows a transition from the ground state to a higher electronic state in which there are several vibrational levels. Collisions between the sample molecules can result in a loss of a different quantum of energy as the molecule drops from one vibrational state to a lower one within that particular electronic state. A further quantum of energy can be lost if the molecule subsequently drops to its ground state. The energy emitted during each of these events is different and hence so are the frequencies and wavelengths of the emitted light. Two types of spectra can be obtained; where the excitation radiation has a single, constant wavelength the intensity of the emission is recorded and the spectrum produced is called an emission spectrum. If different wavelengths of excitation radiation are used a series of emission spectra can be recorded and the wavelength producing the maximum intensity of emitted radiation from each spectrum can be used to form an intensity profile for that specimen as a function of the excitation wavelength, this is called an excitation spectrum.

At low concentration the intensity of fluorescence is considered to be directly proportional to the concentration of the fluorophore present. In fluorescence spectra the Raman signal is always seen at a position which has a constant wavenumber difference relative to the excitation wavenumber. It has proved difficult to obtain standard spectra in fluorescence spectroscopy as the signal can be distorted in many ways. Factors related to instrumentation include variation in the intensity and wavelength of the light source. A light source which maintains the same intensity over all wavelengths has proved elusive as has a detecting system which maintains constant efficiency over time. Factors relating to the sample include; photodecomposition, scattering of light by Raman and Rayleigh effects and variation in the intensity of the radiation throughout the sample with photons of energy emitted through fluorescence sometimes being reabsorbed.

Scattering Spectroscopy

The mechanism by which spectra are obtained by scattering techniques has been dealt with in some detail with reference to Raman spectroscopy. Diffuse elastic and elastic scattering are also examples of this form of spectroscopy and considered further in *Section A.2.2.2.* Elastic scattering spectroscopy is also known as Raleigh or light scattering spectroscopy.

Tri modal spectroscopy

The combination of three spectroscopic techniques, Raman spectroscopy, autofluorescence and elastic scattering is gaining favour and has been used for the detection of cancer of the oral cavity (Muller, 2003).

A.2 Field Classification of Spectroscopic Techniques

In Figure A.3 the general classification described above can be further refined to emphasis those techniques which are predominant in the assessment of biological tissues. At a basic level techniques for the delineation of the macroscopic, microscopic and biochemical characteristics of biological tissue can be divided into imaging techniques and those that utilise spectroscopy. The area of tissue over which these differing modalities can be practically applied further broadly classifies them into those used over a wide field (cm^2) and those used over much smaller areas, narrow or point fields (nm^2). Wilson uses this type of classification to base a review paper describing the various spectroscopic and imaging techniques currently available (Wilson, 2007a). However with rapid technological advances this classification is becoming blurred with imaging techniques such as OCT being applied over very small fields and spectroscopic techniques over much larger areas with fast mapping techniques. The remainder of this chapter uses this classification but also seeks to clarify the interrelationships between the modalities described. The relationships between field and point techniques are illustrated in Figure A.3. Increasing work the combination of a ‘scanning’ modality predominately utilising imaging field techniques with detailed examination of areas of suspicion by spectroscopic point techniques is being used; once again allowing optical medical diagnostics to achieve a further step towards clinical effectiveness.

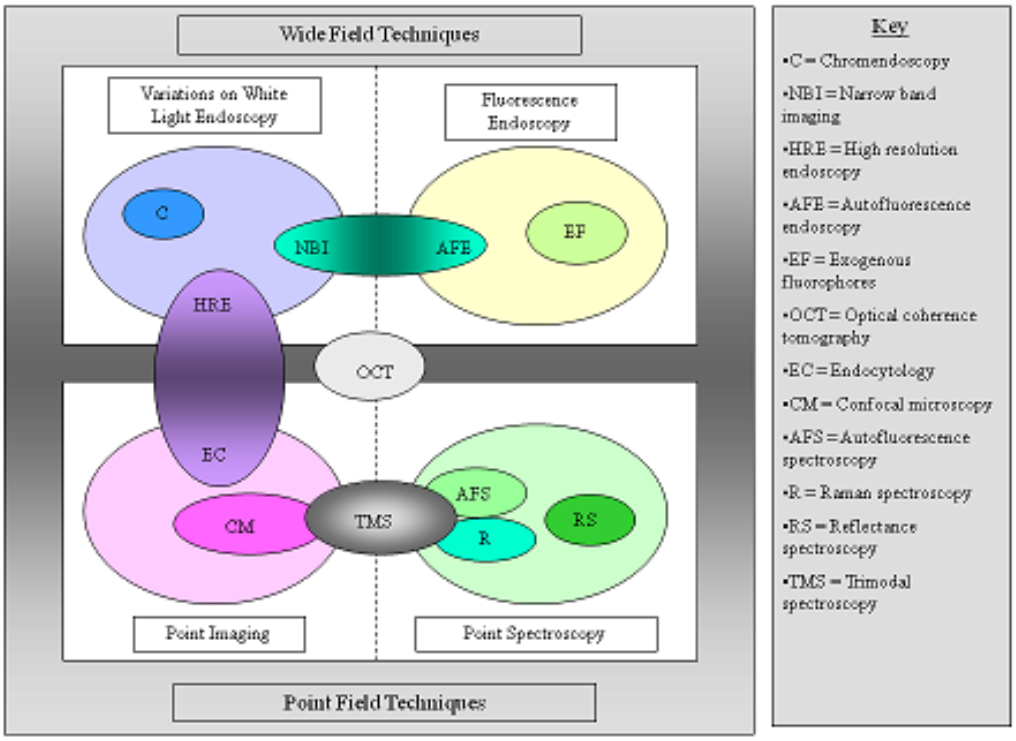

Figure A.3: Inter-relationships between spectroscopic and imaging techniques predominantly used in the assessment of biological tissues.

A.2.1 Wide Field Techniques

A.1.1.1 Variations on White Light Endoscopy

White light endoscopy (WLE) is used extensively in the routine surveillance of disease in many areas of the body. In laryngology nasendoscopy is used in all outpatient appointments where visualisation of the larynx is needed. In gastroenterology the upper and lower gastrointestinal tract have been successfully visualised by this means for many years. Areas of suspicion require biopsy and the tissue obtained undergoes histological assessment. Improvements in WLE have been driven by the need to localise these areas accurately to reduce unnecessary clinical intervention.

High resolution endoscopy

Instrument advances have made a great difference to WLE most recently with the advent of video endoscopes which are rapidly replacing fibre optic endoscopes. The use of high-density charge-coupled device (CCDs) detector arrays with 2 to 3 times the number of pixels (400 000-850 000) used in a standard WLE. High resolution (magnification) endoscopes with sophisticated optics can now focus down to close on the size of a cell, 10µm, (Nelson, 2000). At such high magnification this technique moves from a field to a point technique and at its' limit can be thought of as endocytology.

Chromoscopy

The aim of this technique is to enhance the junction between normal and dysplastic tissue by the topical application of a stain. The stain can either bind to normal or abnormal tissue and can be classified into two groups; chromogenic or modifiers. Methylene Blue is an example of a chromogenic stain; it is absorbed onto cells and highlights mucosal architecture (Eberl, 2007). Another example is crystal violet, a stain that highlights the actual nuclear component of the cell. Lugol's Iodine has been used successfully to stain islands of squamous cells in the detection of Barrett's oesophagus (Takubo, 2005). Acetic acid is an example of a 'modifier', this compound acts by breaking down the surface glycoprotein layer changing the refractive index of the tissue. It has been used very successfully in the detection of cervical neoplasia and in 'screen and treat programs' for this disease used in developing countries (Denny, 2000). Whilst there is still some debate as to the efficacy of chromendoscopy to detect oesophageal dysplasia it is now well established as a technique for the delineation of sessile adenomas in the colon (Fujii, 2001).

Narrow band imaging (NBI)

The image obtained from a standard white light microscope is produced by recombination of the red-green-blue channels. In narrow-band imaging these channels are displayed separately. This results in the highlighting of micro vascular patterns and improves the contrast between different mucosal morphologies. The improvement in contrast is due to the different attenuations of these three spectral regions. More superficial layers of tissue are biased towards blue, deeper towards red. The combination of narrow-band imaging and autofluorescence endoscopy is of interest and may improve diagnostic specificity (Wilson, 2007a). A case report has been published outlining the use of narrow-band imaging in the detection of recurrent hypopharyngeal cancer in a piriform fossa after radiotherapy (Watanabe, 2007).

A.1.1.2 Fluorescence Endoscopy (FE)

The utilisation of fluorescence endoscopy as a diagnostic tool is long standing however it gained more attention in the 1960s when the first photodynamic therapy agent was developed, haematoporphyrin derivative (HpD). In the 1970s fluorescence endoscopy was used to localise photosensitizers with the earliest work being done on the detection of bronchial tumours (Profio, 1997).

Autofluorescence endoscopy (AFE)

Biological tissues often process endogenous fluorophores capable of autofluorescence such as tryptophan, NADH, collagen, elastin and flavins. AFE has been used to improve the effectiveness of WLE for example in the detection of nasopharyngeal carcinoma (Chang, 2002). In the gastrointestinal tract it has been shown to help differentiate between benign hyperplastic polyps and adenomatous polyps which have malignant potential (McCallum, 2008). It has also been used as an adjuvant to WLE in examination of the bronchus were loss of extracellular matrix reduces the collagen signal and allows an increase in the attenuation of green fluorescence from the submucosal layer (Haubinger, 2005). Several studies in the past have assessed the ability of autofluorescence spectroscopy to be used as a diagnostic tool in the larynx (Paczona, 2003; Palasz, 2003; Arens, 2004 & 2007). All these studies showed autofluorescence could delineate pathological entities in the larynx. Normal laryngeal

mucous will fluoresce green when illuminated by a xenon lamp however the presence of malignancy appears to reduce this fluorescence and in some cases change it to a red-yellow colour (Zalesska, 2005). The use of indirect autofluorescence as a diagnostic tool for laryngeal disease has also been assessed (Arens, 2004 & 2007). In their first prospective study patients underwent autofluorescence which was compared to direct autofluorescence obtained during microlaryngoscopy. All these results were then compared to histological sections with excellent correlation. It was noted that the presence of inflammation, scarring and hyperkeratosis made assessment of the lesions more difficult. The aim of the study published in 2007 was to compare indirect autofluorescence laryngoscopy with 5-ALA-induced protoporphyrin IX (PPIX) fluorescence. Fluorescence was induced using a xenon arc lamp (375-440nm) and after initial investigation with autofluorescence laryngoscopy the 5-ALA was applied by inhalation, two hours later both investigations were performed again. The results of this study suggest that both these techniques are useful in the assessment of premalignant and malignant lesions however it is pointed out that autofluorescence has the advantage of not requiring the patient to have an exogenous substance however the changes seen in scarred laryngeal tissue using 5-ALA suggest it may be the more useful of the two techniques in this scenario. There are problems associated with AFE; where fibre optics instruments are used the signal at shorter wavelengths can be relatively poor. The advent of video endoscopes with autofluorescence capability may make this less problematic. Endogenous autofluorescence from moieties other than those of interest may also reduce specificity and sensitivity.

Exogenous Fluorophores

Exogenous fluorophores such as fluorescein applied to tissue have been shown to bind to certain biomolecular entities which can then be utilised in imaging techniques (Kiesslich, 2006).

Point Field Techniques

A.1.1.3 Point Imaging

Endocytoscopy

This technique can be seen as an extension of high resolution endoscopy. A contact endoscope with sophisticated optics allows *in vivo* images to be obtained with a cellular resolution is in the order of 2-4 µm. Endocytology can produce images of areas 100-300µm wide and to a depth of 5-15µm (Wilson, 2007b).

Confocal endoscopy

Once the preserve of microscopy confocal imaging is now used in endoscopy. Unlike high resolution (magnification) endoscopy it allows depth scanning. Point scanning is performed on tissue in a plane at a specific depth (max 100µm) and a detector rejects any scattered photons not from this plane. The combination of contact endoscopy and fluorescence contrast enhancement has been used to study bronchial wall microstructure (Thiberville, 2007) and oesophageal disease (Kiesslich, 2006). Whilst much progress has been made in this area drawbacks do exist with this technique; specimens can suffer photobleaching and the equipment is still expensive. The combination of confocal endomicroscopy with the application of exogenous fluorophores is an area on ongoing research and hold promise for the future (Wilson, 2007b).

Optical coherence tomography (OCT)

White light interferometry used as a technique for taking measurements optically has been used for many years however interest in this technique has under gone resurgence with the advent of optical coherence tomography (Huang, 1991). OCT is analogous to ultrasound but utilises electromagnetic radiation rather than sound. The basic difference between the practical application of ultra sound and OCT lies in the fact that reflected sound travels over distance and time on a scale that is easily measured (nanoseconds). Light travels at much greater speeds and to date there are no clinically applicable methods in which it can be recorded in a similar way to ultrasound. As a consequence the technology on which the two techniques are based differs a great deal. OCT systems can produce spatial resolutions in the range of 10μm however 'ultra-high' resolution systems can now give images down to1μm (Barr, 2007) whereas that from ultra sound is in the region of 100μm. OTC utilises interferometry; a technique where by two or more waves of the same frequency and phase can be superimposed. A beam of light is split into 2 or more 'coherent' parts one of which is used as a reference beam the other acts on the sample. The reflected beams are recombined with any small difference detected as 'interference'. If the superimposed waves are initially in phase the interference is constructive and increases the amplitude of the resultant wave or vice versa. Any changes in the phase of a beam will shift the interference from its maximum to minimum values making the system very sensitive to a factor that changes the phase of one of the reflected waves such as the refractive index of the specimen. An interference pattern is only generated if the two beams of light have travelled an optical distance less than the coherence length, areas of the specimen that reflect more light will create greater interference

OCT has a significant number of biomedical applications. It was first demonstrated in this context in the *in vitro* examination of a retina (Huang, 1991). It can be used easily in the clinical setting and produce images over real time. It has better resolution than magnetic resonance imaging (MRI) and USS (Yaqood, 2006). However if the reference and sample scattered radiation are not aligned signal fading can occur. OCT has been used to assess the larynx and can identify disruption of the basement membrane and disease transitional zones (Armstrong, 2006) and has also been used in the evaluation of the paediatric airway (Ridgeway, 2007) and the larynx of an awake patient. At present OCT is limited by the need to strike a balance between the power and band width of the radiation source, resolution, coherence length, expense and portability. It has good sensitivity as interferometry measures the field not the intensity of the scattered radiation and the relatively weak scattered signal can be amplified by the reference beam. At present the most serious drawback seems to be limitations in penetration depth particularly in the assessment of exophytic lesions.

A.1.1.4 Point Spectroscopy

Fluorescence spectroscopy

Autofluorescence spectroscopy (AFS) can be used to determine the optimum spectral range over which to use autofluorescence endoscopy AFE and this technique has been relatively simple to implement in the clinical setting. This is because the fibre optic probe used can be inserted via the biopsy/instrument port of the endoscopes currently used in clinical practice. This arrangement is not without practical problems; where

several biopsies are required the process can takes some time. Where an instrument is used to hold tissue, removing it to insert a probe may alter the orientation of the sample and hence the spectra obtained. To overcome these difficulties multi channelled endoscopes can be used or instruments where biopsy forceps and probe are combined. Tissue can also be fixed with the use of a probe which applies pressure to the area; however this may alter the blood flow and result in a change in the attenuation of the light. The optimum angle at which the probe is applied is less of a problem in the larynx where the areas of concern are perpendicular to the tip of the probe, unlike in the oesophagus. In the oesophagus the areas which require biopsy are in a plane parallel to the long axis of the instrument and subject to a great deal variation in position due to the intrinsic peristalsis of the oesophagus and transmitted movement resulting from the heart beating. AFS is a relatively expensive technique requiring multiple CCD cameras and the spectra obtained can show considerable point to point and patient to patient variation however the use of time resolved modes may provide additional information that helps with this problem.

The application of exogenous fluorophores can selectively highlight specific disease entities or can bind to molecules only present in normal tissue thus allowing the edges of surgical resection margins to be probed (Da Costa, 2007). In time a combination of AFE with AFS using exogenous fluorophores to probe tumour edges may allow a quantitative appraisal of the presence of tumour. The difficulties lie in the ongoing technical challenges of rapid spectroscopic scanning and the difficulties in isolating highly disease specific exogenous fluorophores.

Reflectance spectroscopy

This form of spectroscopy explores some of the micro morphological features that make up many of the criteria used in the histological diagnosis of dysplasia and cancer such as nuclear size and chromatin content. Reflectance spectroscopy is subclassified depending on its' ability to subtract the signal acquired from multiply scattered photons from the measured spectra in order to enhance the contribution made by photons which have undergone few scattering events. Reflectance spectra represent both the absorptive and scattering properties of the specimen examined (Wilson, 2007c).

Diffuse reflectance spectroscopy /Light scattering spectroscopy (LSS)

This technique has many similar features to that of fluorescence spectroscopy. It is differs from elastic scattering spectroscopy in that it is a measurement of the total spectrum of light scattered from the surface of the specimen. The light which is emitted after passing through deeper tissues and which will have undergone more interaction with the molecules of the specimen is filtered out by a polarizer. Only light which has been reflected back without undergoing any significant deeper collisions, i.e. were the polarisability is unaltered, and is collected.

Elastic scattering spectroscopy (ESS)

In ESS there is no change in energy between the incident and scattered radiation, hence no change in frequency. ESS produces spectra which are dependent on the wavelength of the excitation radiation. The scattering component in this form of spectroscopy is related to the optical index of refraction of the specimen and in biological tissue these changes occur as a result of the different densities of the cellular components; these areas are called scattering centres. ESS has been used to assess lymph nodes (Jerjes,

2005) and squamous epithelial tissue from the mouth Muller, 2003). It is fast, cheap, and reliable, giving good correlation with the key histological changes that alert to malignancy. It is successfully utilised is many areas such as the monitoring of chemotherapy drugs levels and the oxygenation of free-flaps (Swinson, 2006).

A.1.1.5 Advanced Raman Spectroscopy Techniques

A major drawback to the use of Raman spectroscopy in the study of biological tissues has always been the considerable fluorescence signal produced when visible excitation has been used. As a consequence visible Raman spectroscopy has been superseded by near infrared excitation; the techniques described in this section have been developed in part to try to overcome this problem.

Resonance Raman spectroscopy

Pre resonance Raman occurs when the energy of the excitation photon nears that required to stimulate an electron to reach a higher electronic state. In these circumstances the intensity of the Raman scattering significantly increases. If the excitation energy is sufficiently large to promote the chromophore to a higher electron energy state absorption of the photon can occur. Despite the whole molecule absorbing energy during an electronic absorption, in a mixed sample the molecules exhibiting resonance Raman will be preferentially enhanced. This is a great help in probing the individual chromophores of highly complex biological molecules however resonance Raman is only effective in certain coloured molecules and continues to have drawbacks relating to fluorescence interference and photo degradation of the sample.

Surface enhanced Raman spectroscopy (SERS) and surface enhanced resonance Raman spectroscopy (SERRS)

Since being first reported in the mid 1970s by Fleischman and later extensively developed (REF MRSp133), surface enhanced Raman spectroscopy (SERS) and subsequently surface enhanced resonance Raman spectroscopy (SERRS) have begun to play an ever increasing rôle in the development, understanding and utilisation of Raman spectroscopy. In this technique the tissue sample is held in a cell into which a metal electrode is inserted and the choice of metal can vary. Silver and gold are extensively used and the close proximity of the specimen to the roughened metal surface allows significant enhancement of the Raman signal. The voltage applied across the cell determines the size of the enhancement and relative peak intensities. SERRS combines the advantages of surface and molecular resonance enhancement. The substance being tested is usually a dye or molecule containing a dye and absorption of this dye onto the surface of the metal electrode quenches fluorescence. One of the great advantages of this technique is that although the intensity of the peaks can vary their positions are very similar to those seen in the resonance Raman spectra, or FT-Raman spectra if the substance is fluorescent. This makes the identification of the test substance and contaminants relatively straight forward. In SERRS the extra resonance enhancement seems to discriminate against contaminants which can improve the reliability of the results and is one of its advantages over SERS. SERRS can also be done using lower powered lasers and has reduced accumulation times making photodegradation less of an issue (Smith & Dent, 2005d).

Non linear Raman spectroscopy

Pulsed lasers of high power densities are now available allowing for the possibility that at a particular moment in time a molecule may be hits by two photons producing a multi-photon event. Techniques which utilise this phenomenon are called non-linear Raman spectroscopy examples of which include hyper-Raman and coherent anti-Stokes Raman spectroscopy. These techniques require more than one laser excitation source and to date have proved expensive and difficult to use.

Hyper-Raman Spectroscopy

In hyper-Raman spectroscopy (HRS) molecules can be promoted to a virtual state at double the frequency of the excitation radiation. As well as expense there are some technical difficulties that must be addressed with all forms of non-linear Raman spectroscopy. In order that multiple photons interact at the same time the beams of incident radiation must be carefully phased. In HRS the frequency of the scattered light may not be in a range capable of detection by CCDs and difficulties in detection are compounded by the inherently weak signal. The high power of the pulsed lasers also produces more heat which may cause difficulties in probing bio molecules *in vivo*.

Coherent anti-Stokes Raman spectroscopy (CARS)

This technique requires several laser excitation sources, in the past three but more recently two. In the three laser system the first photon used is of a frequency that elevates the molecule to a virtual state the same as with conventional Raman spectroscopy. The second photon has a frequency equal to that which would be apparent if the molecule underwent spontaneous Stokes Raman scattering. The third photon has a frequency used to excite the molecule into a second virtual state from which it can fall to the electronic ground state. CARS can be used in conjunction with resonance enhancement and has the great advantage that it is an anti-Stokes event and hence does suffer from fluorescence interference.

Time resolved Raman spectroscopy

This is a very exciting development in Raman spectroscopy. A pulsed laser is split into two and the second beam is delayed by a fraction of a second; a nanosecond, picosecond or even less. The first beam initiates a photochemical event and the second beam probes it producing a Raman spectra. For each laser pulse there may only be a few Raman events but over time they can produce a significant accumulative signal provided that minimal photo degradation occurs. The Raman signal can be detected much more quickly than that of fluorescence so by subjecting a specimen to fast pulses of radiation this technique can be used for fluorescence suppression. In a converse fashion if longer is taken for the emitted radiation to be collected time resolved Raman spectroscopy can be used for depth probing (Baker, 2007)

Appendix B: Staging and Classification Criteria for Laryngeal Disease.

B.1 TNM Staging

Tumours involving two anatomical sites are classified according to the site in which the greater part of the tumour is located. In invasive tumours with an associated carcinoma in situ only the invasive component is considered for classification. Superficial extension to adjacent sites is not considered invasion of adjacent structures. In tumours extending to an adjacent site, differentiation between superficial extension and deep extension is necessary. In superficial extension the involvement is considered to be limited to the mucosa; in deep extension, muscles, bones or other deep structures are invaded. Deep extension to an adjacent site can be the result of vertical invasion of adjacent structures or the result of horizontal spread *not* limited to the mucosa but also involving muscles or bones. Such extension is classified as invasion of adjacent structures.

In advanced lymphatic spread, one often finds perinodal tumour and the confluence of several lymph node metastases into one large tumour conglomerate. In the definition of the N classification, the perinodal component should be included in the size for isolated lymph node metastases; for conglomerates, the overall size of the conglomerate should be considered and not only the size of the individual lymph nodes. The pN classification is based on the size of the metastasis rather than the size of the lymph node.

The cervical lymph nodes groups;

Submental (Level IA)

Lymph nodes within the triangular boundary of the anterior belly of the digastric muscle and the hyoid bone.

Submandibular (Level IB)

Lymph nodes within the boundaries of the anterior and posterior bellies of the digastric muscle and the body of the mandible.

Upper jugular group (Level II)

Lymph nodes located around the upper third of the internal jugular vein and adjacent spinal accessory nerve, extending from the hyoid bone to the skull base. The posterior boundary is the posterior border of the sternocleidomastoid muscle, and the anterior boundary is the lateral border of the sternohyoid muscle. This group includes the jugulodigastric node, which is the most cranial jugular node.

Middle jugular group (Level III):

Lymph nodes located around the middle third of the internal jugular vein, extending from the carotid bifurcation superiorly to the omohyoid muscle or cricothyroid notch inferiorly. The posterior boundary is the posterior border of the sternocleidomastoid muscle, and the anterior boundary is the lateral border of the sternohyoid muscle.

Lower jugular group (Level IV):

Lymph nodes located around the lower third of the internal jugular vein, extending from the omohyoid muscle superiorly to the clavicle inferiorly

Dorsal cervical nodes along the spinal accessory nerve (Level V) and Supraclavicular nodes (mostly Level IV):

These two groups are combined and called the "posterior triangle group" and comprise predominantly of the lymph nodes located along the lower half of the spinal accessory nerve and the transverse cervical artery. The posterior boundary is the anterior border of the trapezius muscle, the anterior boundary is the posterior border of the sternocleidomastoid muscle, and the inferior border is the clavicle. Most are in Level IV; some may occupy the most caudal component of Level V.

Anterior compartment group (Level VI):

Lymph nodes surrounding the midline visceral structures of the neck, extending from the level of the hyoid bone superiorly to the suprasternal notch inferiorly. On each side, the lateral boundary is the medial border of the carotid sheath. Located within this compartment are the perithyroidal lymph nodes, paratracheal lymph nodes, lymph nodes along the recurrent laryngeal nerves and precricoid lymph nodes.

Prelaryngeal and paratracheal nodes

These may be further subdivided as follows:

- cranial - paratracheal (suprathyroidal), thyroidal (perithyroidal)
- caudal - paratracheal (infrathyroidal, lateral tracheal)
- prelaryngeal
- pretracheal - near the thyroid isthmus (delphian)

Retropharyngeal nodes

Parotid nodes

The parotid nodes may be subdivided into superficial i.e. in front of the tragus of the ear and on top of parotid fascia and deep parotid nodes. The latter are located underneath the parotid fascia and include intra-glandular nodes. The preauricular and infra-auricular nodes are assigned to the parotid nodes.

The buccal (facial) nodes

These nodes include the buccinator nodes located deep on buccinator muscle, the nasolabial nodes located underneath the nasolabial groove, the molar nodes located in the surface of cheek and the mandibular nodes located outside the lower jaw.

Retroauricular (mastoid, posterior auricular) and occipital nodes.

Summary—Oropharynx

T1	≤2 cm
T2	>2 to 4 cm
T3	>4 cm
T4a	Larynx, deep/extrinsic muscle of tongue, medial pterygoid, hard palate, mandible
T4b	Lateral pterygoid muscle, pterygoid plates, lateral nasopharynx, skull base, carotid artery, prevertebral fascia

- A tumour extending from the oropharynx to the nasopharynx or to the hypopharynx or to the oral cavity or larynx and limited to the mucosa (without invasion of muscles, bones or other deep structures) is classified only according to size up to T3.
- A tumour invading soft tissue of neck and paravertebral fascia/muscles is classified as T4b.
- Invasion of the larynx is defined as invasion of the outer framework (thyroid cartilage, cricoid cartilage, pre-epiglottic space) or internal structures such as arytenoid and epiglottic cartilages.

Summary—Nasopharynx

T1		Nasopharynx Soft tissue
T2	T2a	Oropharynx/nasal cavity without parapharyngeal extension
	T2b	Tumour with parapharyngeal extension
T3		Bony structures and/or paranasal sinuses
T4		Intracranial, cranial nerves, infratemporal fossa, hypopharynx, orbit, masticator space

- Tumours not involving the oropharynx and/or nasal fossa, but with parapharyngeal extension are classified T2b.
- The term “postnasal space” corresponds to nasopharynx (C11). Invasion of vertebral bodies is classified T3.

Summary—Hypopharynx

T1	≤2 cm and limited to one subsite
T2	>2 to 4 cm or more than one subsite
T3	>4 cm or with larynx fixation
T4a	Thyroid/cricoid cartilage, hyoid bone, thyroid gland, oesophagus, central compartment of soft tissue
T4b	Prevertebral fascia, carotid artery, mediastinal structures

- The term "laryngopharynx" corresponds to hypopharynx
- For classification, the hypopharyngeal surface of the aryepiglottic fold (C13.1) belongs to the hypopharynx, while the laryngeal aspect of the aryepiglottic fold (C32.1) is part of the supraglottis.
- Fixation of hemi-larynx is diagnosed endoscopically by immobility of the arytenoid or vocal cord.
- The uncommon tumours limited to one subsite but with vocal cord fixation should be classified as T3.
- Involvement of the arytenoid cartilage is classified as T3, not T4a
- A tumour extending from the hypopharynx to oesophagus and limited to the mucosa (without invasion of muscles, bones or other deeper structures) is classified only according to size up to T3.

Summary—Larynx

Summary—Supraglottis

T1	One subsite, normal mobility
T2	Mucosa of more than one adjacent subsite of supraglottis or glottis or adjacent region outside the supraglottis, without fixation
T3	Cord fixation or invades postcricoid area, pre-epiglottic tissues, paraglottic space, thyroid cartilage erosion
T4a	Through thyroid cartilage; trachea, soft tissues of neck: deep/extrinsic muscle of tongue, strap muscles, thyroid, oesophagus
T4b	Prevertebral space, mediastinal structures, carotid artery

Summary—Glottis

	Limited to vocal cord(s), normal mobility
T1	a. one cord
	b. two cords
T2	Supraglottis, subglottis, impaired cord mobility
T3	Cord fixation, paraglottic space, thyroid cartilage erosion
T4a	Through thyroid cartilage; trachea, soft tissues of neck: deep/extrinsic muscle of tongue, strap muscles, thyroid, oesophagus
T4b	Prevertebral space, mediastinal structures, carotid artery

Summary—Subglottis

T1	Limited to the subglottis
T2	Extends to vocal cord(s) with normal/impaired mobility
T3	Cord fixation
T4a	Through cricoid or thyroid cartilage; trachea, deep/extrinsic muscle of tongue, strap muscles, thyroid, oesophagus
T4b	Prevertebral space, mediastinal structures, carotid artery

- For pathological classification concerning impaired mobility or fixation of vocal cords the information from the clinical T is used for the pathologic T.

- For invasive carcinoma, the classification according to horizontal spread is based only on the invasive component.

- To indicate the presence of associated carcinoma in situ (adjacent or separate) the suffix "(is)" may be added to the respective T category of the invasive carcinoma, e.g., T2(is). The presence of an associated carcinoma in situ influences treatment of the invasive carcinoma and needs identification and separate analysis of such cases.

B.2 Histological Classification

The histological classification of laryngeal dysplasia, carcinoma-in-situ and SCC has historically been a difficult area in which to achieve consensus. Whilst the application of guidelines does leave great scope for inter-observer error there has been recent work to clarify areas of debate and it is this that is summarised below and these are the parameters used in the histological reports obtained for this work. This section contain extracts from a definitive text on this subject (Mills, 2008)

Keratosis (leucoplakia / erythroplakia)

Mucosal Keratosis found in the head and neck and not associated with dysplastic change is very common and has certain distinct features which in combination help to separate it from both dysplasia and invasive SCC. The macroscopic features of keratosis are weaker than the microscopic features in this respect.

Macroscopically

- White, thickened mucosa
- Visible increase in vascularity in underlying stroma at times
- Strips easily especially from vocal cords usually at the junction of the basal cells and stroma
- Intact basal cell layer – good differentiator from invasive SCC

Microscopically

- Normal or thickened layer of squamous mucosa
- Prominent granular cell layer
- Overlying layers of ortho-keratin often admixed with parakeratotic cells
- Orderly cell maturation
- Mitotic figures confined to the basal cell layer
- No aberrant keratinisation of individual cells

Laryngeal Dysplasia

Many grading systems have been used to classify mucosal dysplasia found within the head and neck and these have usually been based on those applied to dysplastic lesions arising in the cervix. One of the major differences is that in the head and neck dysplastic lesions often retain a considerable number of keratinised cells even in high-grade lesions.

In many systems a separate grade of carcinoma-in-situ is applied for lesions felt to have progressed beyond severe dysplasia but not to invasive SCC. In this system and for the purposes of the work these lesions are included with those classified as severely dysplastic.

Squamous dysplasia can extend a considerable distance and involve the underlying seromucinous ducts. This must be carefully assessed to distinguish dysplasia from invasive SCC and this can be very difficult particularly in frozen sections. Key features of the extension seen in dysplasia is the sharp circumscription of the nests, the lack of surrounding stromal response and the presence nearby of more easily recognised seromucinous ducts.

Mild dysplasia

- Nuclear irregularity
- Nuclear crowding, primarily in basal layer
- Essentially normal nuclear chromatin

Moderate dysplasia

- Larger, irregular nuclei
- Often peripherally condensed chromatin resulting in central clearing

- Focally prominent nucleoli
- Increase in mitotic figures in basal cell layer but not extending to superficial layers

Severe dysplasia

- Aberrant cell maturation with dyskaryotic cells
- Mitotic figures, some of which are atypical, present above the basal cell layer
- Often in the setting of partial or complete maturation with keratinisation of the overlying surface mucosa.
- At low power the presence of *individual* keratinised (dyskaryotic) cells is an important clue to the presence of significant dysplasia however surface keratinisation itself is not considered reliable in the assessment of laryngeal dysplasia

Invasive Squamous Cell Carcinoma

Well differentiated

- Obvious squamous differentiation
- Large, closely apposed cell nests
- Prominent keratinisation

Moderately differentiated

- Smaller nests of more pleomorphic cells
- Increased mitotic activity
- Clear-cut but less prominent squamous differentiation
- +/- prominent intra-lymphatic invasion

Poorly differentiated

- Highly mitotically active cells growing alone and in small nests
- Showing ragged or diffuse rather than 'pushing' infiltration
- Squamous differentiation is focal and often poorly developed
- +/- prominent intra-lymphatic invasion

There is a particular situation where in certain SCCs are present but appear to 'drop off' the basal cell layer and are overlain by essentially normal mucosa. In this situation endoscopic diagnosis is extremely difficult and biopsies must be taken with an adequate depth but they are not considered histologically as a separate entity.

Appendix C: Staging and Classification Criteria for Lymphoproliferative Disease.

C.1 Staging

At the present time it is not considered practical to propose a TNM classification for non-Hodgkin lymphoma and since no other convincing and tested staging system is available, the Ann Arbor or WHO classification is recommended with the same modifications as for Hodgkin lymphoma

Summary

Stage	Hodgkin Disease	Substage
Stage I	Single node region	
	Localized single extralymphatic organ/site	I_E
	Two or more node regions, same side of diaphragm	II_E
Stage II	Localized single extralymphatic organ/ site with its regional nodes, ± other node regions same side of diaphragm	
	Node regions both sides of diaphragm ± Localized extralymphatic organ/site	III_E
Stage III	Spleen	III_S
	Both	III_{E+S}
Stage IV	Diffuse or multifocal involvement of extralymphatic organ(s) ± regional nodes; isolated extralymphatic organ and non-regional nodes	
All stages divided	Without weight loss/fever/sweats	A
	With weight loss/fever/sweats	B

Notes

1. Right and left neck are considered separate lymph node regions.
2. Single lymph node regions are:
    - Lymph nodes of head, face and neck
    - Intrathoracic lymph nodes

- Intra-abdominal lymph nodes
- Lymph nodes of axilla or arm
- Lymph nodes of inguinal region or leg
- Pelvic lymph nodes

3. Bilateral involvement of axillae/arm lymph nodes is considered as involvement of two separate regions. The same applies to bilateral involvement of inguinal lymph nodes.
4. Direct spread of a lymphoma into adjacent tissues or organs does not influence classification.

C.2 Classification

Revised European-American Lymphoma Classification

B cell neoplasms

I. Precursor B cell neoplasms: B precursor lymphoblastic leukaemia/lymphoma
II. Peripheral B cell neoplasms
    1. B cell chronic lymphocytic leukaemia / prolymphocytic leukaemia / small lymphocytic lymphoma
    2. Lymphoplasmacytoid lymphoma / immunocytoma
    3. Mantle cell lymphoma
    4. Follicle centre lymphoma
    5. Marginal zone B cell lymphoma
    6. Splenic marginal zone lymphoma
    7. Hairy cell leukaemia
    8. Plasmacytoma / plasma cell myeloma
    9. Diffuse large B cell lymphoma
    10. Burkitt lymphoma
    11. High-grade B cell lymphoma – Burkitt-like

T cell and putative natural killer (NK) cell neoplasm

I. Precursor T cell neoplasms: T precursor lymphoblastic leukaemia/lymphoma
II. Peripheral T cell and NK cell neoplasms Peripheral B cell neoplasms
    1. B cell chronic lymphocytic leukaemia / prolymphocytic leukaemia
    2. Large granular lymphocytic leukaemia, T and NK cell types
    3. Mycosis fungoides / Szary syndrome
    4. Unspecified peripheral T cell lymphoma
    5. Angiommunoblastic T cell lymphoma
    6. Angiocentric lymphoma
    7. Intestinal T cell lymphoma
    8. Adult T cell lymphoma / leukaemia
    9. Anaplastic large cell lymphoma
    10. Anaplastic large cell lymphoma – Hodgkin's – like

Hodgkin's disease

I. Lymphocyte predominance
II. Nodular sclerosing
III. Mixed cellularity

IV. Lymphocyte depleted
V. Lymphocyte-rich classical Hodgkin's disease

WHO Classification of Neoplastic Diseases of the Haemopoietic and Lymphoid Tissues

Precursor B cell neoplasms

Precursor B cell neoplasms
B cell lymphoblastic leukaemia / lymphoma
Peripheral B cell neoplasms
B cell chronic lymphocytic leukaemia / small lymphocytic lymphoma
Variant: monoclonal gammopathy / plasmacytoid differentiation; mu heavy chain disease
Mantle cell lymphoma
Variant: blastic
Follicular lymphoma
Variant: cutaneous follicular lymphoma
Marginal zone B cell lymphoma of mucosa-associated lymphoid tissue
Variant: alpha heavy chain disease
Nodal marginal zone lymphoma +/- monocytoid B cells
Splenic marginal zone B cell lymphoma
Hairy cell leukaemia
Diffuse large B-cell lymphoma
Variants: Centroblastic
Immunoblastic
T cell or histiocyte rich
Anaplastic large B cell
Burkitt-like
Lymphomatoid granulomatosis type
Diffuse large B-cell lymphoma – subtypes
Mediastinal (thymic) large B cell lymphoma
Intravascular large B cell lymphoma
Primary effusion lymphoma in HIV patients
Burkitt Lymphoma
Variant: with plasmacytoid differentiation (AIDS-associated)
Plasmacytoma
Variants: Solitary Plasmacytoma of bone
Extramedullary plasmacytoma
Plasma cell myeloma
Variant: Indolent myeloma
Smoldering myeloma
Osteosclerotic myeloma (POEMS syndrome)
Plasma cell leukaemia
Non-secretory myeloma
Systemic light chain disease
Primary amyloidosis

T cell neoplasias

Precursor T cell leukaemia / lymphoma
- T cell lymphoblastic leukaemia / lymphoma

Peripheral BT/NK cell neoplasms – predominantly disseminated
- T cell prolymphocytic (T-PLL)
- T cell large granular lymphocyte leukaemia
- NK cell leukaemia
- Adult T cell lymphoma / leukaemia

Peripheral T cell and NK cell neoplasms – predominantly nodal
- AIL T cell lymphoma cell lymphoma
- ALC lymphoma

Peripheral T cell and NK cell neoplasms – predominantly extranodal
- Mycosis fungoides
- Sezary syndrome
- Primary cutaneous CD 30 positive T cell
- Lymphoproliferative disorders
- Primary cutaneous ALC lymphomas

Subcutaneous panniculitic – like T cell lymphoma
NK/T cell lymphoma – nasal type
Enteropathy – type intestinal T cell
Hepatosplenic T cell lymphoma

Hodgkin Lymphoma (Hodgkin disease)

Nodular lymphocyte-predominance Hodgkin lymphoma
Classical Hodgkin lymphoma
- Hodgkin lymphoma – nodular sclerosis (grades I and II)
- Hodgkin lymphoma – mixed cellularity
- Classical Hodgkin lymphoma – lymphocyte-rich
- Hodgkin lymphoma – Lymphocyte-depleted

Appendix D: Larynx study - Tables and Figures

D.1 Normalised spectra for individual pathology codes

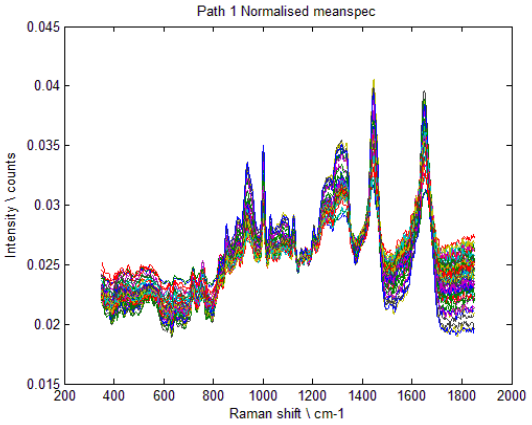

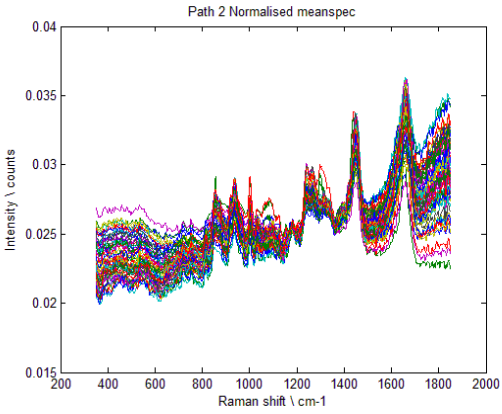

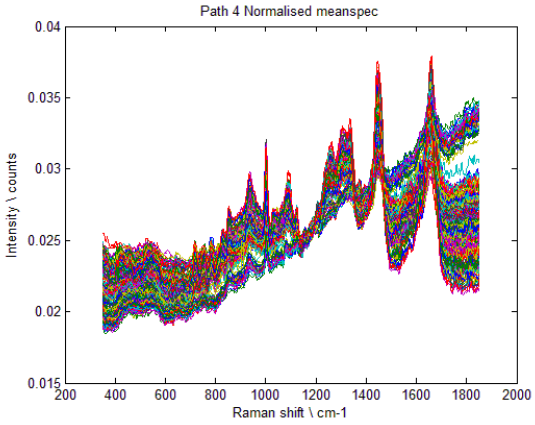

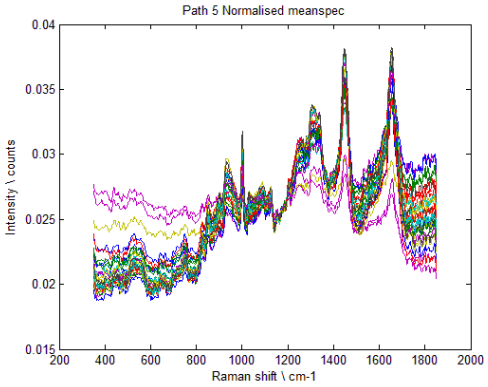

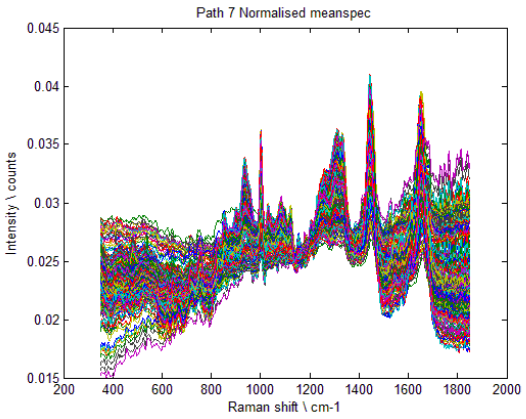

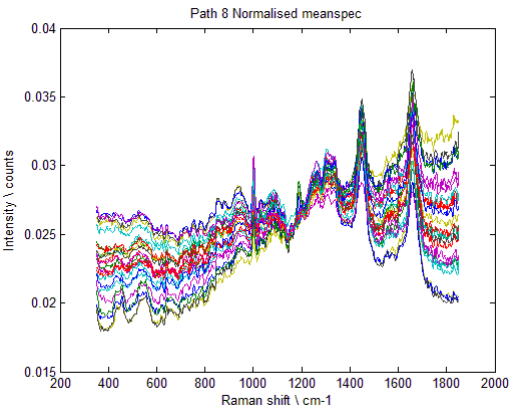

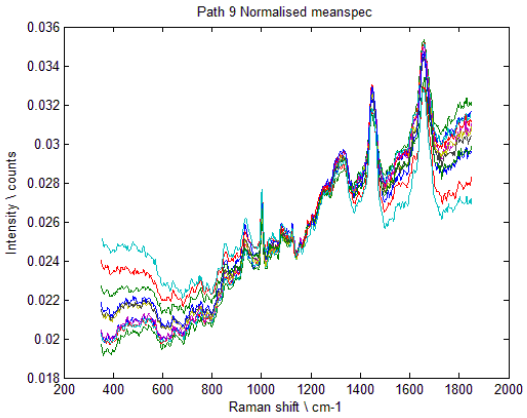
Path 9 Normalised meanspec
Intensity \ counts
Raman shift \ cm-1

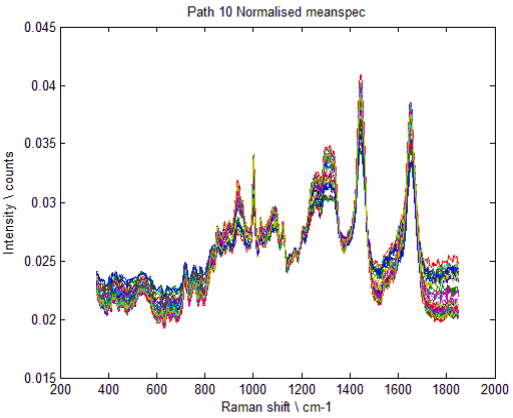
Path 10 Normalised meanspec
Intensity \ counts
Raman shift \ cm-1

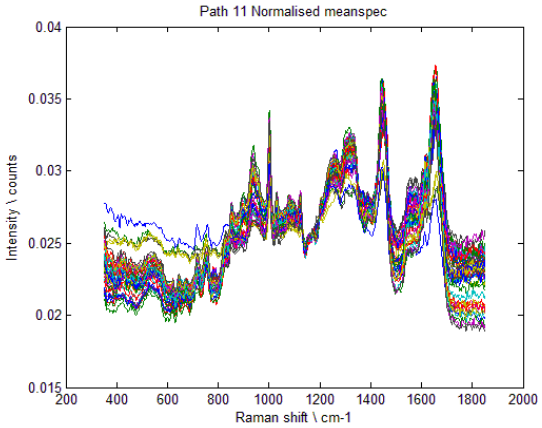
Path 11 Normalised meanspec
Intensity \ counts
Raman shift \ cm-1

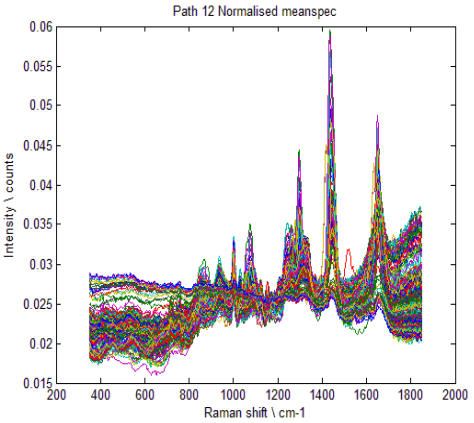
Path 12 Normalised meanspec
Intensity \ counts
Raman shift \ cm-1

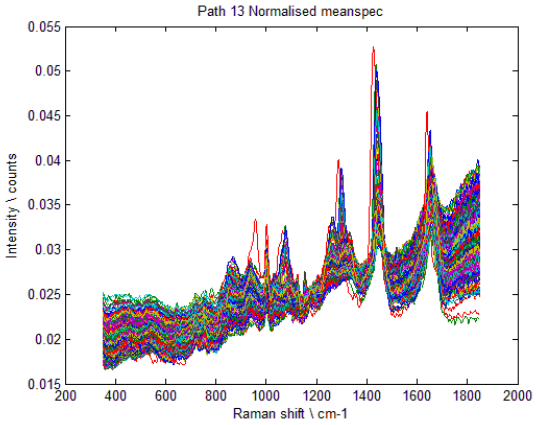
Path 13 Normalised meanspec
Intensity \ counts
Raman shift \ cm-1

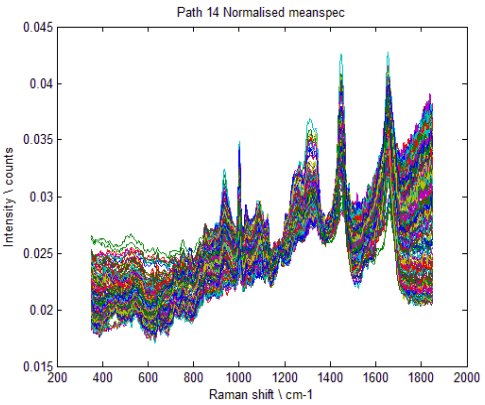
Path 14 Normalised meanspec
Intensity \ counts
Raman shift \ cm-1

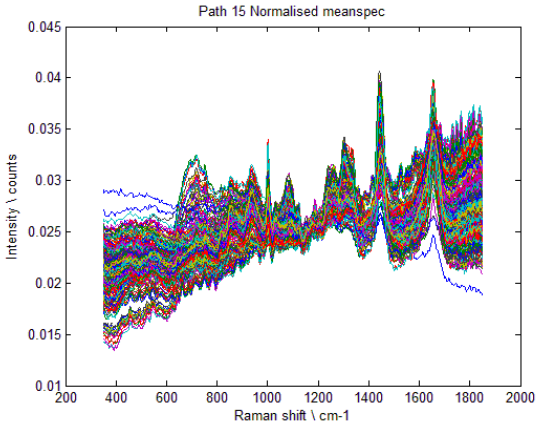
Path 15 Normalised meanspec
Intensity \ counts
Raman shift \ cm-1

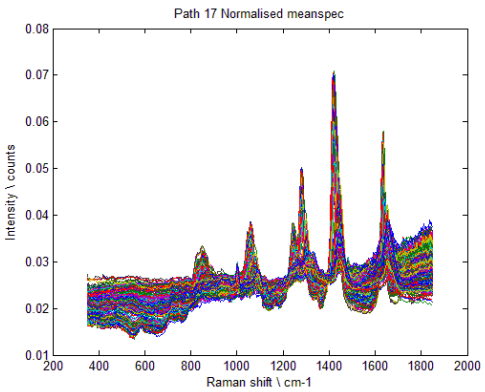
Path 17 Normalised meanspec
Intensity \ counts
Raman shift \ cm-1

D.2 Summary diagram for Larynx study mini models

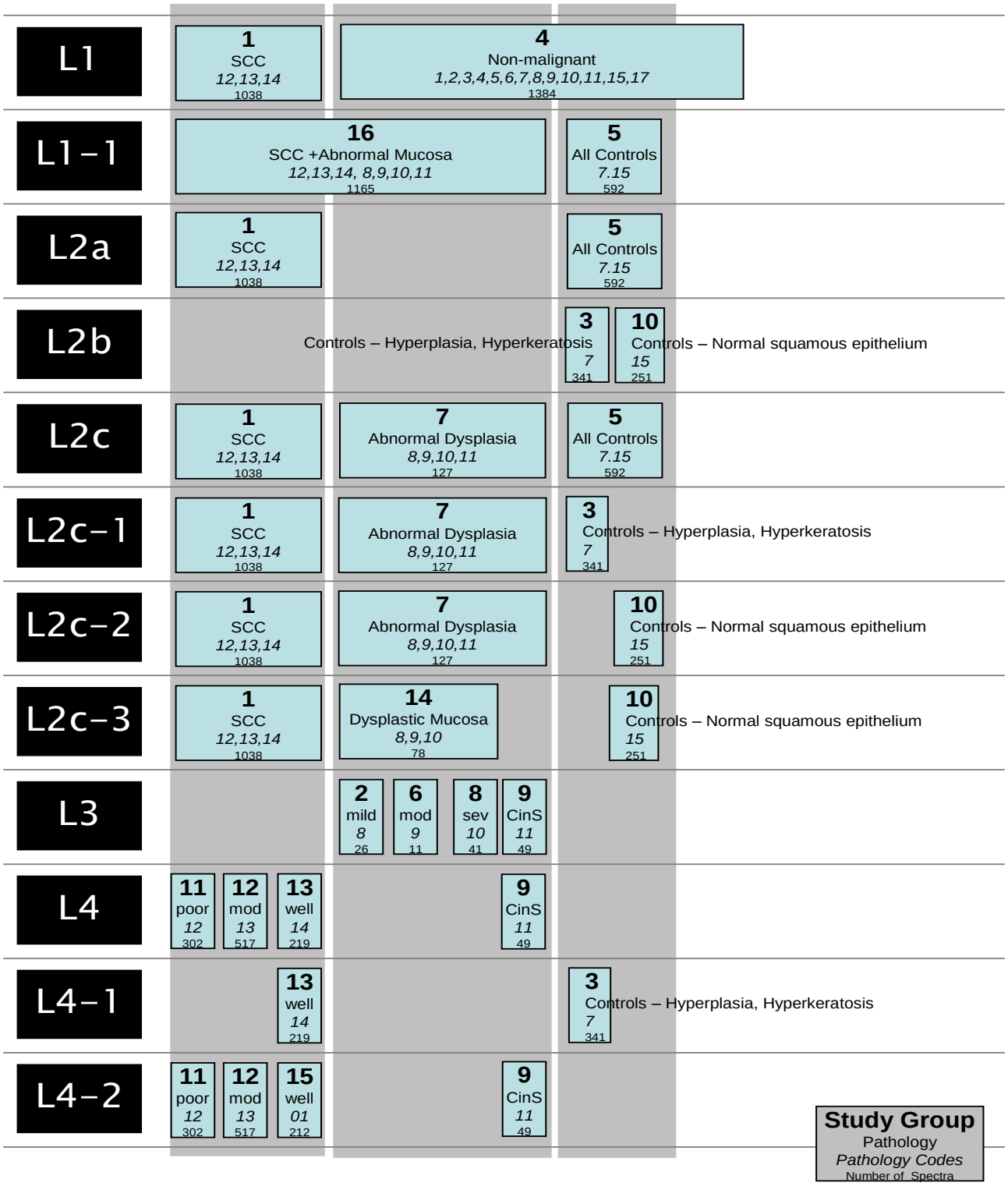

D.3 Difference spectra for larynx study mini models

D.3.1 L1

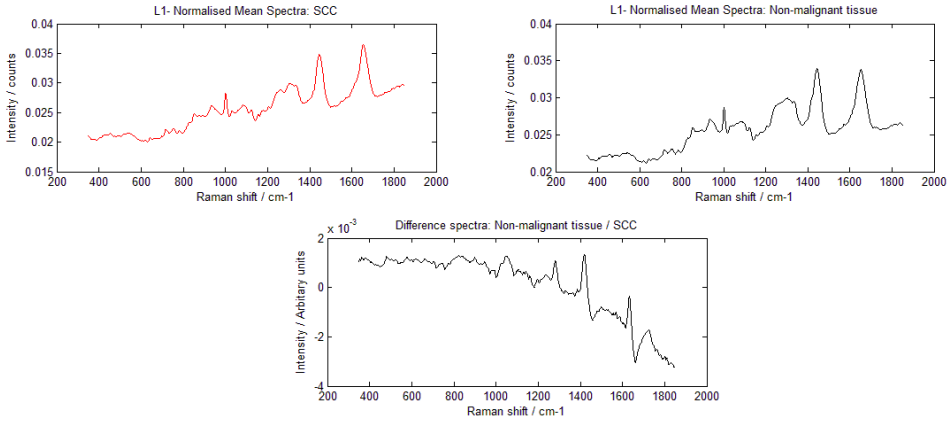

D.3.2 L1-1

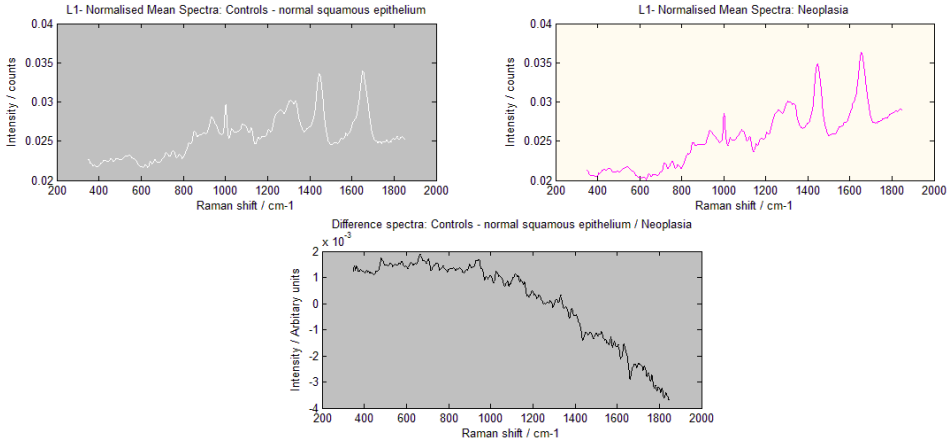

D.3.3 L2a

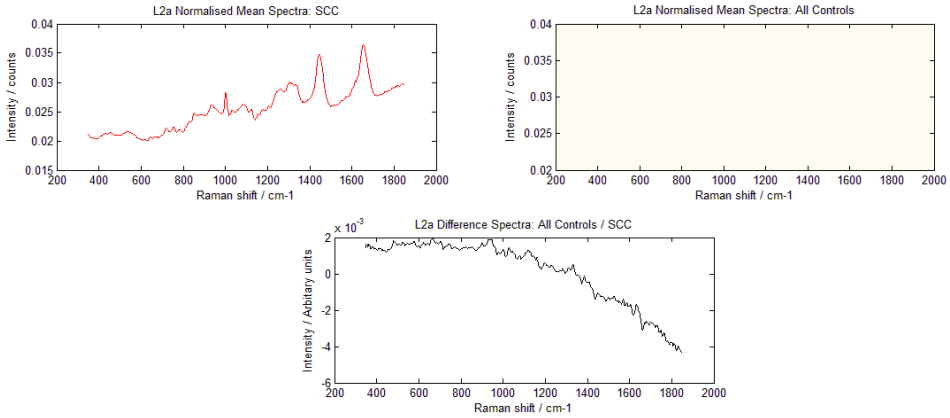

D.3.4 L2c

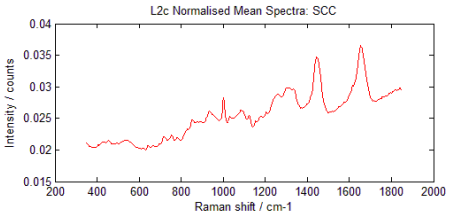

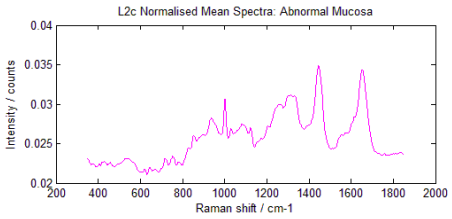

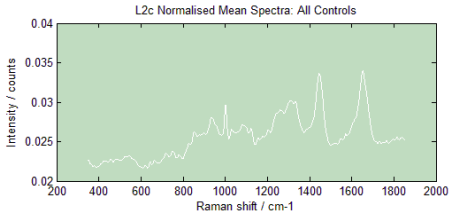

D.3.5 L2c_1

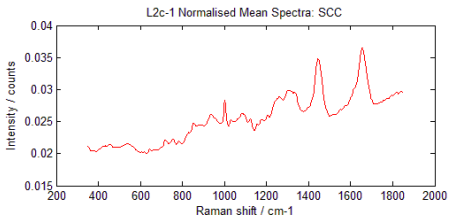

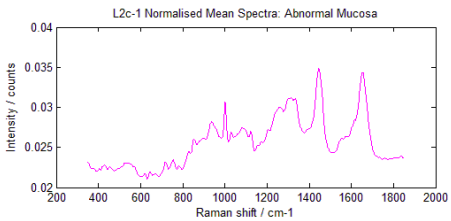

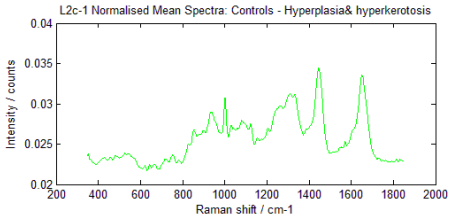

D.3.6 L2c_2

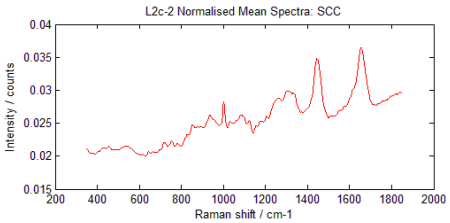

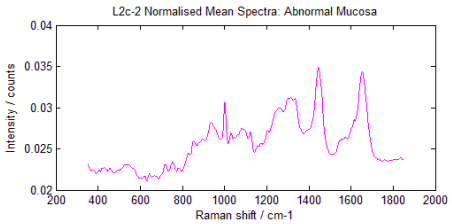

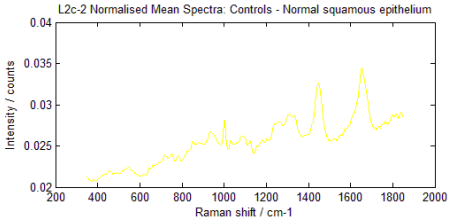

D.3.7 L2c_3

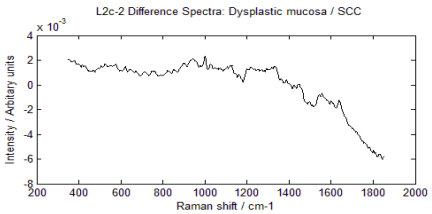

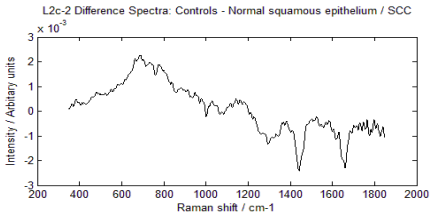

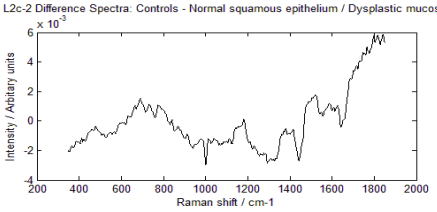

D.3.8 L3

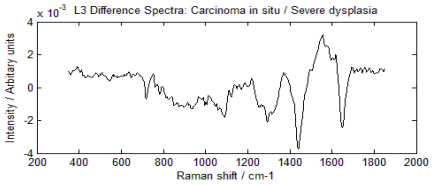

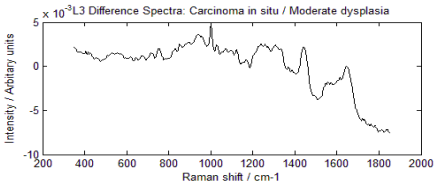

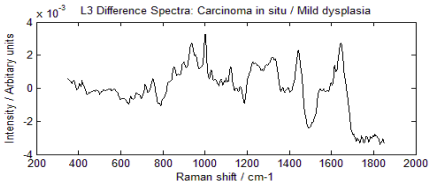

D.3.9 L4

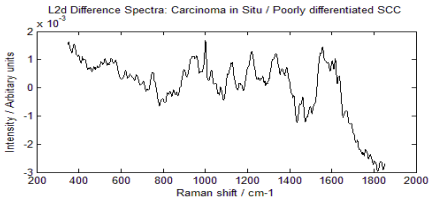

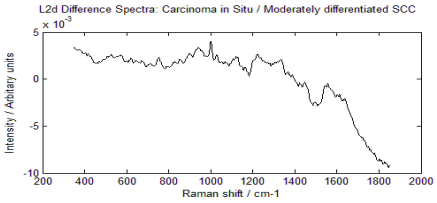

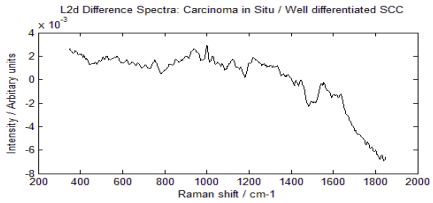

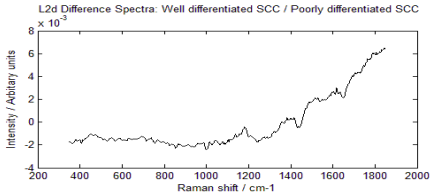
L2d Difference Spectra: Well differentiated SCC / Poorly differentiated SCC
x 10^-3
Intensity / Arbitary units
Raman shift / cm-1

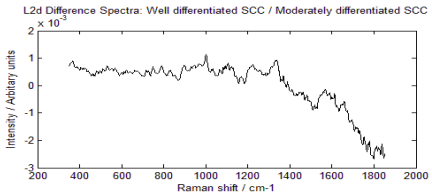
L2d Difference Spectra: Well differentiated SCC / Moderately differentiated SCC
x 10^-3
Intensity / Arbitary units
Raman shift / cm-1

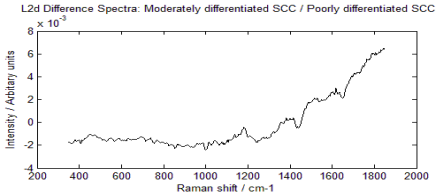
L2d Difference Spectra: Moderately differentiated SCC / Poorly differentiated SCC
x 10^-3
Intensity / Arbitary units
Raman shift / cm-1

D.4 Peak data for individual study groups (SGs)

D.4.1 SG1

SG1	Wave Number	Peak Intensity	Peak Area	Peak Mass
Group1.1	457	0.00040	0.0059	459.2781
Group1.2	543	0.00057	0.0196	541.6748
Group1.3	643	0.00050	0.0055	647.0847
Group1.4	718	0.00091	0.0142	721.7115
Group1.5	754	0.00081	0.0138	756.5217
Group1.6	782	0.00046	0.0059	785.1999
Group1.7	827	0.00039	0.0061	826.7343
Group1.8	852	0.00093	0.0132	854.1001
Group1.9	935	0.00170	0.0586	942.3764
Group1.10	1002	0.00380	0.0483	1004.7
Group1.11	1030	0.00056	0.0056	1034.1
Group1.12	1085	0.00140	0.0425	1087.6
Group1.13	1125	0.00100	0.0124	1127.6
Group1.14	1154	0.00054	0.0048	1156.4
Group1.15	1174	0.00048	0.0083	1179.5
Group1.16	1205	0.00051	0.005	1208.1
Group1.17	1244	0.00140	0.0592	1251.5
Group1.18	1303	0.00110	0.0275	1306.5
Group1.19	1339	0.00057	0.0081	1343.5
Group1.20	1446	0.00850	0.3647	1449.9
Group1.21	1654	0.00880	0.4463	1656.8

D.4.2 SG2

SG2	Wave Number	Peak Intensity	Peak Area	Peak Mass
Group2.1	431	0.00034	0.0054	433.383
Group2.2	457	0.00031	0.0035	460.3969
Group2.3	528	0.00100	0.067	541.0018
Group2.4	621	0.00045	0.0046	623.3386
Group2.5	642	0.00062	0.0052	645.2153
Group2.6	668	0.00020	0.0036	672.2422
Group2.7	698	0.00029	0.0021	700.5168
Group2.8	724	0.00037	0.0074	722.6973
Group2.9	753	0.00068	0.0119	754.1834
Group2.10	789	0.00054	0.0091	787.7874
Group2.11	828	0.00044	0.0089	826.8107
Group2.12	851	0.00064	0.0099	855.3025
Group2.13	880	0.00030	0.0039	885.698
Group2.14	947	0.00099	0.0456	946.2027
Group2.15	1001	0.00300	0.0343	1005
Group2.16	1030	0.00060	0.0076	1032.5
Group2.17	1085	0.00130	0.0456	1087
Group2.18	1129	0.00081	0.0092	1131
Group2.19	1157	0.00042	0.0048	1158.2
Group2.20	1188	0.00061	0.0159	1193.1
Group2.21	1264	0.00100	0.0428	1254
Group2.22	1302	0.00097	0.0202	1306.7
Group2.23	1339	0.00099	0.0162	1340.2
Group2.24	1360	0.00020	0.0012	1364.6
Group2.25	1388	0.00019	0.0014	1390.6
Group2.26	1401	0.00013	0.00072	1404.6
Group2.27	1449	0.00550	0.2143	1452.6
Group2.28	1513	0.00010	0.000521	1516
Group2.29	1556	0.00056	0.0095	1553.7
Group2.30	1574	0.00040	0.005	1577.5
Group2.31	1603	0.00045	0.0038	1607.2
Group2.32	1660	0.00500	0.1808	1664.3
Group2.33	1718	0.00014	0.000629	1720.2
Group2.34	1736	0.00043	0.0033	1739.2
Group2.35	1758	0.00041	0.0043	1757

D.4.3 SG3

SG3	Wave Number	Peak Intensity	Peak Area	Peak Mass
Group3.1	422	0.00046	0.0135	425.866
Group3.2	456	0.00034	0.0036	459.6935
Group3.3	481	0.00042	0.0064	486.5563
Group3.4	527	0.00024	0.0032	527.5147
Group3.5	622	0.00050	0.0051	624.9951
Group3.6	643	0.00050	0.0047	645.9511
Group3.7	666	0.00052	0.0082	669.6625
Group3.8	718	0.00075	0.0184	717.2807
Group3.9	754	0.00095	0.0183	755.2536
Group3.10	783	0.00036	0.0043	787.0599
Group3.11	826	0.00070	0.0114	826.4924
Group3.12	853	0.00140	0.0222	855.0226
Group3.13	898	0.00031	0.0036	901.9459
Group3.14	936	0.00250	0.0824	942.8756
Group3.15	1002	0.00460	0.0545	1005.1
Group3.16	1029	0.00090	0.0095	1031.4
Group3.17	1082	0.00100	0.0259	1089.6
Group3.18	1124	0.00130	0.0177	1127.5
Group3.19	1154	0.00052	0.0063	1158
Group3.20	1204	0.00069	0.0088	1205.3
Group3.21	1245	0.00130	0.0535	1250.9
Group3.22	1303	0.00094	0.0237	1306.8
Group3.23	1447	0.00910	0.3714	1448.2
Group3.24	1546	0.00025	0.0023	1547.2
Group3.25	1571	0.00060	0.0046	1573.4
Group3.26	1651	0.00960	0.5059	1654.7
Group3.27	1735	0.00020	0.002	1735.7
Group3.28	1751	0.00008	0.000567	1752.3
Group3.29	1815	0.00026	0.0021	1816.7
Group3.30	1831	0.00025	0.0017	1833.4

D.4.4 SG4

SG4	Wave Number	Peak Intensity	Peak Area	Peak Mass
Group4.1	457	0.00023	0.0026	459.7465
Group4.2	545	0.00054	0.0254	545.1677
Group4.3	643	0.00040	0.0039	645.8002
Group4.4	666	0.00023	0.0035	670.9043
Group4.5	718	0.00078	0.0154	719.4752
Group4.6	753	0.00065	0.0113	754.0636
Group4.7	782	0.00034	0.0048	786.9302
Group4.8	826	0.00056	0.0096	826.6084
Group4.9	851	0.00089	0.0113	854.9436
Group4.10	898	0.00020	0.0023	901.0539
Group4.11	936	0.00170	0.0594	942.1678
Group4.12	1002	0.00350	0.0424	1005
Group4.13	1083	0.00140	0.0938	1070.3
Group4.14	1125	0.00093	0.0121	1127.7
Group4.15	1154	0.00033	0.0036	1156.4
Group4.16	1174	0.00021	0.0024	1176.5
Group4.17	1204	0.00039	0.0041	1207.1
Group4.18	1246	0.00200	0.1475	1270.8
Group4.19	1337	0.00077	0.0191	1347.8
Group4.20	1438	0.00037	0.0651	1406.7
Group4.21	1443	0.00860	0.4286	1443.3
Group4.22	1514	0.00006	0.000752	1517.1
Group4.23	1547	0.00021	0.0033	1549.7
Group4.24	1571	0.00029	0.0025	1575.1
Group4.25	1652	0.00780	0.4242	1652.5
Group4.26	1726	0.00025	0.0045	1729.8
Group4.27	1815	0.00015	0.0022	1813

D.4.5 SG5

SG5	Wave Number	Peak Intensity	Peak Area	Peak Mass
Group5.1	422	0.00035	0.0094	425.7946
Group5.2	457	0.00034	0.004	459.1793
Group5.3	481	0.00028	0.0043	487.2255
Group5.4	546	0.00093	0.0469	550.4006
Group5.5	620	0.00017	0.0013	622.9323
Group5.6	643	0.00048	0.0044	645.5159
Group5.7	665	0.00043	0.0063	668.1827
Group5.8	719	0.00070	0.0144	719.4315
Group5.9	753	0.00082	0.0147	754.0204
Group5.10	782	0.00045	0.006	785.7827
Group5.11	826	0.00052	0.0082	825.0035
Group5.12	852	0.00110	0.0158	855.803
Group5.13	898	0.00019	0.0035	896.3932
Group5.14	936	0.00210	0.0707	942.1567
Group5.15	1002	0.00400	0.0472	1005
Group5.16	1030	0.00100	0.0144	1033
Group5.17	1084	0.00099	0.0276	1089.1
Group5.18	1124	0.00130	0.0177	1126.1
Group5.19	1155	0.00043	0.0048	1156
Group5.20	1175	0.00020	0.0026	1178.1
Group5.21	1204	0.00055	0.0068	1206.5
Group5.22	1241	0.00120	0.048	1251
Group5.23	1303	0.00083	0.0198	1306.3
Group5.24	1336	0.00110	0.0216	1341.4
Group5.25	1447	0.00830	0.3635	1448.8
Group5.26	1529	0.00013	0.0028	1521.1
Group5.27	1547	0.00031	0.0037	1549.2
Group5.28	1572	0.00045	0.0036	1573.3
Group5.29	1652	0.00860	0.4548	1654
Group5.30	1734	0.00018	0.0021	1733.3
Group5.31	1766	0.00030	0.0036	1766.3
Group5.32	1797	0.00024	0.0026	1797.3
Group5.33	1815	0.00031	0.0027	1818
Group5.34	1840	0.00032	0.0038	1840

D.4.6 SG6

SG6	Wave Number	Peak Intensity	Peak Area	Peak Mass
Group6.1	419	0.00017	0.0013	422.1675
Group6.2	434	0.00016	0.0013	436.2624
Group6.3	458	0.00017	0.002	456.6427
Group6.4	523	0.00011	0.0011	528.1066
Group6.5	570	0.00039	0.0124	563.7026
Group6.6	621	0.00016	0.0014	623.2938
Group6.7	695	0.00019	0.0017	697.3569
Group6.8	717	0.00027	0.0035	717.1443
Group6.9	755	0.00060	0.0122	754.4262
Group6.10	780	0.00032	0.005	785.2491
Group6.11	825	0.00031	0.0037	826.0311
Group6.12	851	0.00069	0.0121	855.8607
Group6.13	897	0.00025	0.0037	900.1582
Group6.14	934	0.00130	0.0374	939.7935
Group6.15	1002	0.00270	0.0293	1004.8
Group6.16	1031	0.00046	0.0106	1042.7
Group6.17	1081	0.00066	0.0111	1087.8
Group6.18	1125	0.00081	0.0119	1126.1
Group6.19	1155	0.00032	0.0038	1157.6
Group6.20	1187	0.00031	0.0036	1187.6
Group6.21	1204	0.00034	0.003	1206.3
Group6.22	1252	0.00066	0.0233	1252.5
Group6.23	1333	0.00170	0.0934	1328.9
Group6.24	1393	0.00020	0.0025	1397
Group6.25	1449	0.00460	0.1735	1452.1
Group6.26	1543	0.00045	0.0084	1550.5
Group6.27	1580	0.00014	0.002	1581.6
Group6.28	1659	0.00540	0.291	1660
Group6.29	1796	0.00032	0.0037	1800.1
Group6.30	1828	0.00027	0.0026	1829.7

D.4.7 SG7

SG7	Wave Number	Peak Intensity	Peak Area	Peak Mass
Group7.1	406	0.00022	0.0017	407.9824
Group7.2	431	0.00042	0.0074	430.3507
Group7.3	457	0.00035	0.005	461.0886
Group7.4	546	0.00130	0.0886	544.7568
Group7.5	621	0.00044	0.0039	623.4962
Group7.6	643	0.00069	0.0081	646.5979
Group7.7	671	0.00030	0.0047	674.7635
Group7.8	717	0.00110	0.0205	719.7804
Group7.9	755	0.00110	0.0213	756.7908
Group7.10	782	0.00037	0.0051	786.4228
Group7.11	825	0.00053	0.0116	825.8421
Group7.12	852	0.00120	0.0168	855.6806
Group7.13	897	0.00033	0.0077	894.6226
Group7.14	937	0.00210	0.0749	943.2572
Group7.15	1001	0.00460	0.0544	1004.9
Group7.16	1030	0.00080	0.0089	1031
Group7.17	1083	0.00120	0.0397	1087.2
Group7.18	1125	0.00140	0.0195	1127.4
Group7.19	1154	0.00022	0.0028	1155.3
Group7.20	1174	0.00021	0.0018	1177.2
Group7.21	1203	0.00061	0.0071	1204
Group7.22	1252	0.00140	0.057	1251.6
Group7.23	1335	0.00300	0.1507	1324.5
Group7.24	1446	0.00920	0.3881	1448.8
Group7.25	1545	0.00064	0.0128	1549.5
Group7.26	1573	0.00026	0.0025	1575
Group7.27	1654	0.00920	0.4727	1655.6
Group7.28	1760	0.00019	0.002	1763.7
Group7.29	1838	0.00017	0.0017	1839.3

D.4.8 SG8

SG8	Wave Number	Peak Intensity	Peak Area	Peak Mass
Group8.1	405	0.00031	0.0031	409.2234
Group8.2	417	0.00069	0.0145	428.555
Group8.3	457	0.00043	0.0071	462.1681
Group8.4	494	0.00023	0.0024	494.4893
Group8.5	548	0.00150	0.0826	549.2431
Group8.6	622	0.00051	0.0042	623.1166
Group8.7	644	0.00079	0.0089	647.5429
Group8.8	671	0.00033	0.0044	673.9281
Group8.9	717	0.00200	0.0315	720.8618
Group8.10	757	0.00110	0.0211	758.5976
Group8.11	784	0.00064	0.0074	787.0577
Group8.12	824	0.00086	0.0172	825.4015
Group8.13	852	0.00170	0.0237	855.4827
Group8.14	877	0.00025	0.002	879.1805
Group8.15	898	0.00042	0.0055	900.7851
Group8.16	937	0.00270	0.0889	943.7189
Group8.17	1001	0.00550	0.0689	1003.1
Group8.18	1030	0.00098	0.0109	1033.1
Group8.19	1060	0.00017	0.0011	1061
Group8.20	1092	0.00160	0.044	1091.1
Group8.21	1124	0.00200	0.0274	1128.1
Group8.22	1151	0.00032	0.0033	1154.2
Group8.23	1172	0.00058	0.007	1174.1
Group8.24	1203	0.00100	0.0139	1205.6
Group8.25	1253	0.00190	0.0718	1252
Group8.26	1335	0.00440	0.224	1323.1
Group8.27	1445	0.01340	0.5955	1446.3
Group8.28	1545	0.00035	0.0048	1544.6
Group8.29	1572	0.00033	0.0036	1573.1
Group8.30	1651	0.01300	0.6517	1653.1
Group8.31	1763	0.00027	0.0035	1768

D.4.9 SG9

SG9	Wave Number	Peak Intensity	Peak Area	Peak Mass
Group9.1	406	0.00024	0.0016	407.4429
Group9.2	430	0.00040	0.0073	429.0127
Group9.3	456	0.00029	0.0044	460.5541
Group9.4	550	0.00140	0.0959	545.6819
Group9.5	621	0.00053	0.0055	623.1907
Group9.6	643	0.00068	0.0078	646.8584
Group9.7	672	0.00038	0.0061	675.2568
Group9.8	716	0.00077	0.0113	718.6169
Group9.9	754	0.00160	0.0288	755.4575
Group9.10	788	0.00015	0.0018	787.1481
Group9.11	825	0.00057	0.0098	826.6526
Group9.12	852	0.00120	0.0172	855.5311
Group9.13	879	0.00007	0.0011	877.3575
Group9.14	898	0.00031	0.004	899.492
Group9.15	938	0.00240	0.0859	943.0309
Group9.16	1001	0.00530	0.0627	1003.1
Group9.17	1030	0.00110	0.0128	1032.4
Group9.18	1081	0.00080	0.0267	1087.5
Group9.19	1125	0.00160	0.0236	1127.7
Group9.20	1154	0.00025	0.0025	1156
Group9.21	1174	0.00024	0.002	1177.2
Group9.22	1203	0.00067	0.0079	1205.9
Group9.23	1239	0.00130	0.0554	1249.6
Group9.24	1302	0.00084	0.0206	1307.5
Group9.25	1337	0.00110	0.0261	1350.3
Group9.26	1390	0.00025	0.0037	1396
Group9.27	1447	0.00840	0.3058	1450.9
Group9.28	1545	0.00090	0.0247	1546
Group9.29	1574	0.00031	0.0034	1577.6
Group9.30	1614	0.00067	0.0082	1614.6
Group9.31	1656	0.00660	0.2656	1662
Group9.32	1760	0.00018	0.0017	1763.2
Group9.33	1838	0.00024	0.0029	1838.6

D.4.10 SG10

SG10	Wave Number	Peak Intensity	Peak Area	Peak Mass
Group10.1	421	0.00025	0.0052	425.4268
Group10.2	457	0.00042	0.0055	460.814
Group10.3	547	0.00086	0.0379	548.0736
Group10.4	618	0.00018	0.0018	622.9238
Group10.5	643	0.00042	0.004	645.2238
Group10.6	663	0.00024	0.002	665.4843
Group10.7	719	0.00060	0.008	721.092
Group10.8	752	0.00072	0.0111	754.6906
Group10.9	782	0.00064	0.0097	784.2356
Group10.10	827	0.00035	0.0056	825.7534
Group10.11	851	0.00076	0.0105	854.5361
Group10.12	878	0.00022	0.0046	885.0419
Group10.13	935	0.00150	0.0538	944.7339
Group10.14	1002	0.00290	0.0313	1003.1
Group10.15	1030	0.00065	0.0091	1034
Group10.16	1058	0.00009	0.000714	1063.7
Group10.17	1086	0.00098	0.0272	1090.3
Group10.18	1124	0.00098	0.013	1126.5
Group10.19	1154	0.00037	0.0034	1156.2
Group10.20	1180	0.00049	0.0079	1180.1
Group10.21	1205	0.00036	0.0042	1207.5
Group10.22	1241	0.00120	0.0484	1250.6
Group10.23	1304	0.00073	0.0171	1308.1
Group10.24	1337	0.00080	0.0119	1340.3
Group10.25	1448	0.00650	0.2582	1450.2
Group10.26	1529	0.00021	0.0029	1526.5
Group10.27	1547	0.00030	0.0034	1550.5
Group10.28	1572	0.00024	0.0022	1573.1
Group10.29	1653	0.00740	0.3805	1656.8
Group10.30	1733	0.00021	0.0022	1733.5
Group10.31	1766	0.00045	0.0048	1767.8
Group10.32	1797	0.00049	0.005	1797
Group10.33	1816	0.00050	0.0058	1818.5
Group10.34	1840	0.00069	0.0076	1841.1

D.4.11 SG11

SG11	Wave Number	Peak Intensity	Peak Area
Group11.3	459	0.00035	0.0049
Group11.6	621	0.00027	0.0026
Group11.7	644	0.00052	0.006
Group11.10	717	0.00100	0.0149
Group11.11	755	0.00097	0.0158
Group11.13	826	0.00049	0.0077
Group11.14	853	0.00110	0.0152
Group11.17	937	0.00180	0.0624
Group11.18	1002	0.00410	0.0511
Group11.19	1030	0.00075	0.0086
Group11.20	1085	0.00150	0.0513
Group11.21	1125	0.00120	0.0148
Group11.22	1154	0.00052	0.0054
Group11.24	1204	0.00064	0.0072
Group11.27	1338	0.00092	0.0157
Group11.28	1446	0.00890	0.3531
Group11.31	1545	0.00023	0.0033
Group11.34	1654	0.00950	0.4716

D.4.12 SG12

SG12	Wave Number	Peak Intensity	Peak Area
Group12.1	457	0.00045	0.0066
Group12.7	618	0.00016	0.0017
Group12.8	643	0.00049	0.0053
Group12.11	719	0.00079	0.0124
Group12.12	754	0.00067	0.0112
Group12.14	827	0.00044	0.0083
Group12.15	851	0.00088	0.012
Group12.17	935	0.00160	0.0567
Group12.18	1002	0.00340	0.0397
Group12.19	1030	0.00054	0.0057
Group12.21	1086	0.00110	0.027
Group12.22	1125	0.00089	0.0095
Group12.23	1155	0.00060	0.0051
Group12.25	1205	0.00049	0.0046
Group12.27	1336	0.00220	0.1199
Group12.28	1446	0.00810	0.3573
Group12.30	1550	0.00029	0.0034
Group12.31	1654	0.00840	0.4321

D.4.13 SG13

SG13	Wave Number	Peak Intensity	Peak Area
Group13.3	457	0.00037	0.0059
Group13.8	622	0.00024	0.0023
Group13.9	643	0.00049	0.0053
Group13.12	718	0.00092	0.0139
Group13.13	753	0.00088	0.0155
Group13.15	827	0.00049	0.008
Group13.16	852	0.00095	0.0137
Group13.18	935	0.00160	0.0585
Group13.19	1002	0.00410	0.051
Group13.20	1031	0.00075	0.0108
Group13.21	1085	0.00140	0.0444
Group13.22	1125	0.00110	0.0139
Group13.23	1154	0.00036	0.0027
Group13.25	1205	0.00055	0.0058
Group13.28	1339	0.00096	0.0137
Group13.30	1446	0.00780	0.315
Group13.32	1549	0.00032	0.0043
Group13.35	1655	0.00870	0.4502

D.4.14 SG14

SG14	Wave Number	Peak Intensity	Peak Area
Group14.3	457	0.00038	460.531
Group14.7	643	0.00072	646.51
Group14.10	755	0.00120	756.478
Group14.11	782	0.00040	786.753
Group14.12	825	0.00071	826.471
Group14.13	852	0.00120	855.925
Group14.16	938	0.00220	943.527
Group14.17	1001	0.00490	1005.1
Group14.18	1030	0.00097	1032.7
Group14.19	1083	0.00120	1087.4
Group14.20	1125	0.00150	1127.6
Group14.21	1154	0.00029	1156.6
Group14.23	1203	0.00067	1206.1
Group14.26	1301	0.00098	1305.3
Group14.27	1337	0.00110	1347
Group14.29	1446	0.00920	1449.3
Group14.33	1654	0.00950	1655.2

D.5 Mini model unique SG peaks and PIR tables for shared peaks

D.5.1 L1

Wavenumbers (cm^{-1}) unique across groups	
SG1	SG 4
1030	666
1303	898
1339	1438
	1514
	1547
	1571
	1726
	1815

Wave Number	Peak Area SG1	Peak Area SG4	Area Ratio SG4-SG1
457	1.00	1.00	0.00
543	3.32	9.77	6.45
643	0.93	1.50	0.57
718	2.41	5.92	3.52
754	2.34	4.35	2.01
782	1.00	1.85	0.85
827	1.03	3.69	2.66
852	2.24	4.35	2.11
935	9.93	22.85	12.91
1002	8.19	16.31	8.12
1085	7.20	36.08	28.87
1125	2.10	4.65	2.55
1154	0.81	1.38	0.57
1174	1.41	0.92	-0.48
1205	0.85	1.58	0.73
1244	10.03	56.73	46.70
1339	1.37	7.35	5.97
1446	61.81	164.85	103.03
1654	75.64	163.15	87.51

Wave Number	PIR SG1	PIR SG4	SG4-SG1
457	1.00	1.00	0.00
543	1.42	2.35	0.93
643	1.25	1.75	0.50
718	2.28	3.37	1.09
754	2.04	2.81	0.77
782	1.15	1.48	0.32
827	0.98	2.42	1.43
852	2.34	3.83	1.49
935	4.26	7.34	3.08
1002	9.52	15.12	5.60
1085	3.51	6.05	2.54
1125	2.51	4.00	1.50
1154	1.34	1.42	0.08
1174	1.20	0.93	-0.28
1205	1.27	1.70	0.43
1244	3.51	8.64	5.13
1339	1.43	3.34	1.90
1446	21.30	37.15	15.85
1654	22.05	33.69	11.64

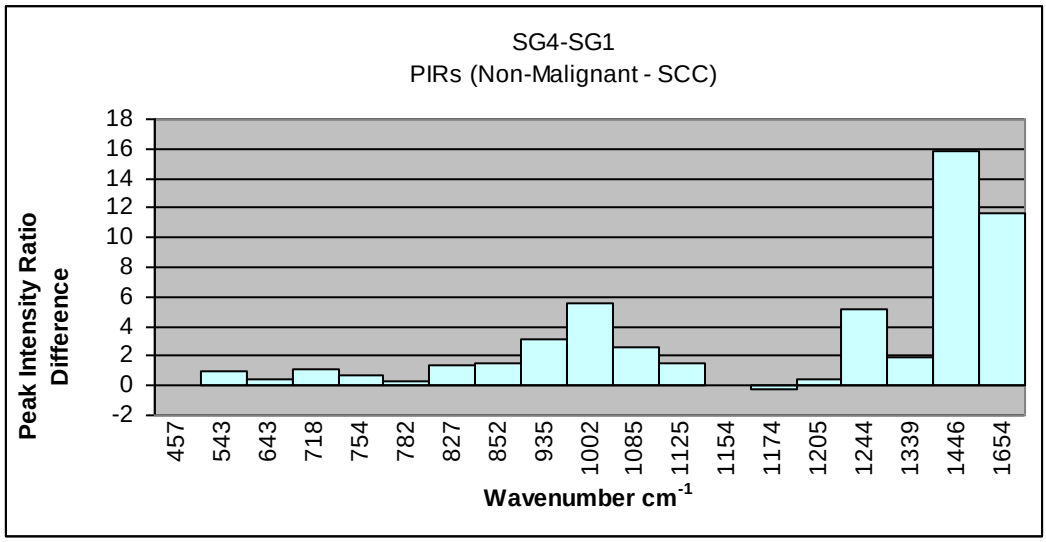
SG4-SG1
PIRs (Non-Malignant - SCC)
Peak Intensity Ratio Difference
18
16
14
12
10
8
6
4
2
0
-2
457
543
643
718
754
782
827
852
935
1002
1085
1125
1154
1174
1205
1244
1339
1446
1654
Wavenumber cm-1

D.5.2 L2a

Wavenumbers (cm^{-1}) unique across groups	
SG1	SG5
	422
	481
	620
	655
	898
	1529
	1547
	1572
	1734
	1766
	1797
	1815
	1840

Wave Number	PIR SG1	PIR SG5	SG5-SG1
457	1.00	1.00	0.00
543	1.42	2.73	1.31
643	1.25	1.41	0.16
718	2.28	2.05	-0.24
754	2.04	2.40	0.37
782	1.15	1.32	0.17
827	0.98	1.51	0.53
852	2.34	3.21	0.87
935	4.26	6.12	1.86
1002	9.52	11.67	2.14
1030	1.39	2.92	1.52
1085	3.51	2.90	-0.61
1125	2.51	3.79	1.29
1154	1.34	1.24	-0.10
1174	1.20	0.58	-0.63
1205	1.27	1.62	0.35
1244	3.51	3.50	-0.01
1303	2.76	2.42	-0.34
1339	1.43	3.21	1.78
1446	21.30	24.21	2.90
1654	22.05	25.08	3.03

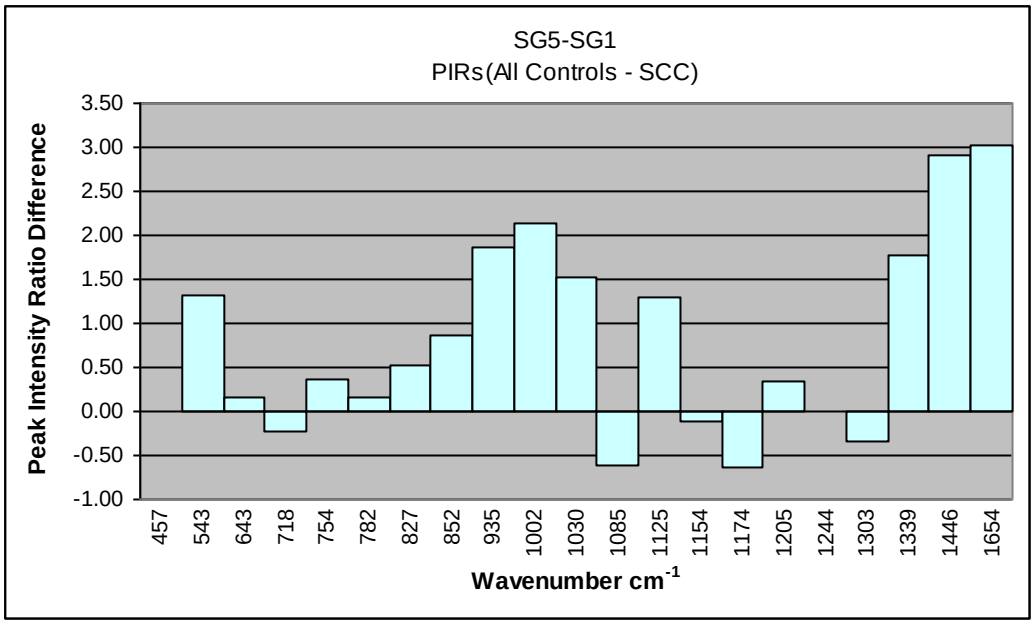

D.5.3 L2b

Wavenumbers (cm^{-1}) unique across groups	
SG3	10
481	
898	878
	1058
	1180
	1529
1751	1766
	1797
1831	1840

Wave Number	PIR SG3	PIR G10	SG3-SG10
422	1.00	1.00	0.00
456	0.73	1.71	-0.99
643	1.07	1.71	-0.64
666	1.12	0.99	0.13
718	1.61	2.41	-0.80
754	2.03	2.92	-0.89
783	0.78	2.59	-1.81
826	1.51	1.40	0.11
853	3.01	3.07	-0.06
936	5.38	6.06	-0.68
1002	9.89	11.72	-1.82
1029	1.93	2.64	-0.72
1082	2.15	3.98	-1.83
1124	2.80	3.95	-1.16
1154	1.12	1.48	-0.35
1245	2.80	4.85	-2.05
1303	2.03	2.94	-0.92
1447	19.57	26.26	-6.69
1571	1.30	0.99	0.31
1651	20.65	29.90	-9.25

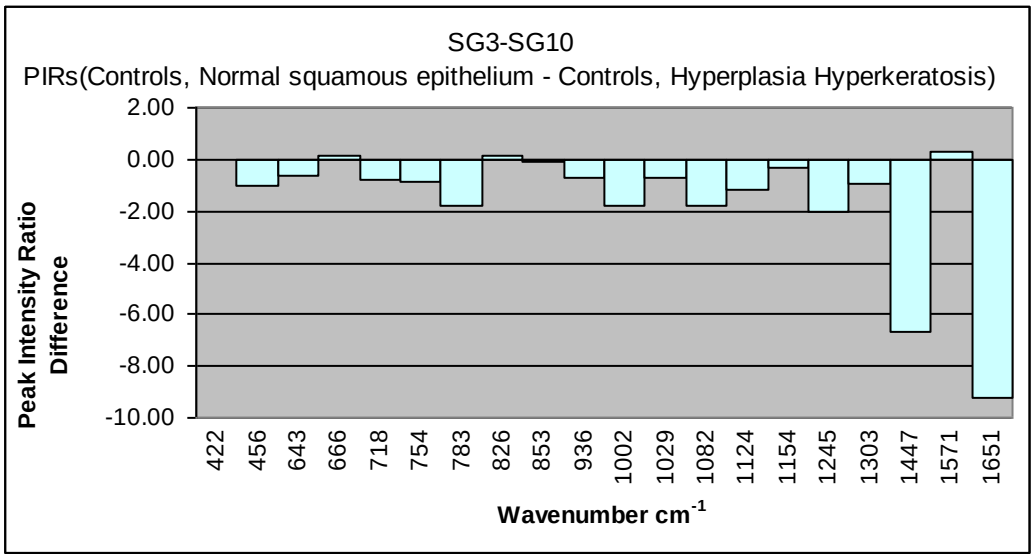

D.5.4 L2c

Wavenumbers (cm^{-1}) unique across groups		
SG1	SG5	SG7
1244	422	406
	481	431
	620	643
	665	671
	1529	1252
	1734	
	1797	
	1815	
	1241	
1303	1303	
1339		
1446		

Wave Number	PIR SG1	PIR SG5	PIR SG7	SG7-SG1	SG5-SG1	SG5-SG7
457	1.00	1.00	1.00	0.00	0.00	0.00
543	1.42	2.73	3.69	2.28	-1.31	-0.97
643	1.25	1.41	1.24	-0.01	-0.16	0.17
718	2.28	2.05	3.13	0.84	0.24	-1.08
754	2.04	2.40	3.13	1.09	-0.37	-0.72
782	1.15	1.32	1.05	-0.11	-0.17	0.28
827	0.98	1.51	1.49	0.51	-0.53	0.01
852	2.34	3.21	3.41	1.07	-0.87	-0.20
935	4.26	6.12	5.97	1.71	-1.86	0.16
1002	9.52	11.67	13.07	3.55	-2.14	-1.40
1030	1.39	2.92	2.27	0.87	-1.52	0.65
1085	3.51	2.90	3.41	-0.10	0.61	-0.51
1125	2.51	3.79	3.98	1.47	-1.29	-0.19
1154	1.34	1.24	0.61	-0.73	0.10	0.63
1174	1.20	0.58	0.60	-0.61	0.63	-0.02
1205	1.27	1.62	1.73	0.46	-0.35	-0.11
1654	22.05	25.08	26.14	4.08	-3.03	-1.06

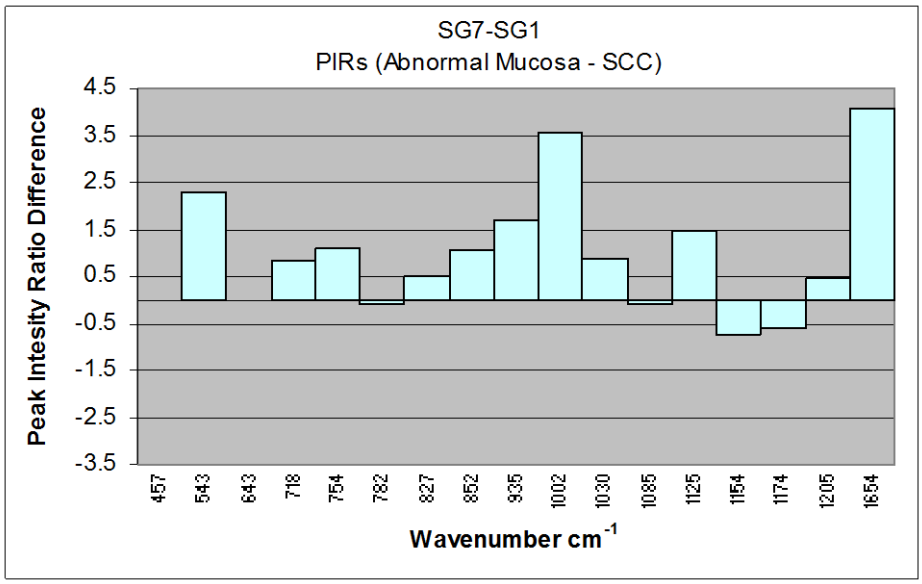
SG7-SG1
PIRs (Abnormal Mucosa - SCC)
Peak Intesity Ratio Difference
4.5
3.5
2.5
1.5
0.5
-0.5
-1.5
-2.5
-3.5
457
543
643
718
754
782
827
852
935
1002
1030
1085
1125
1154
1174
1205
1654
Wavenumber cm-1

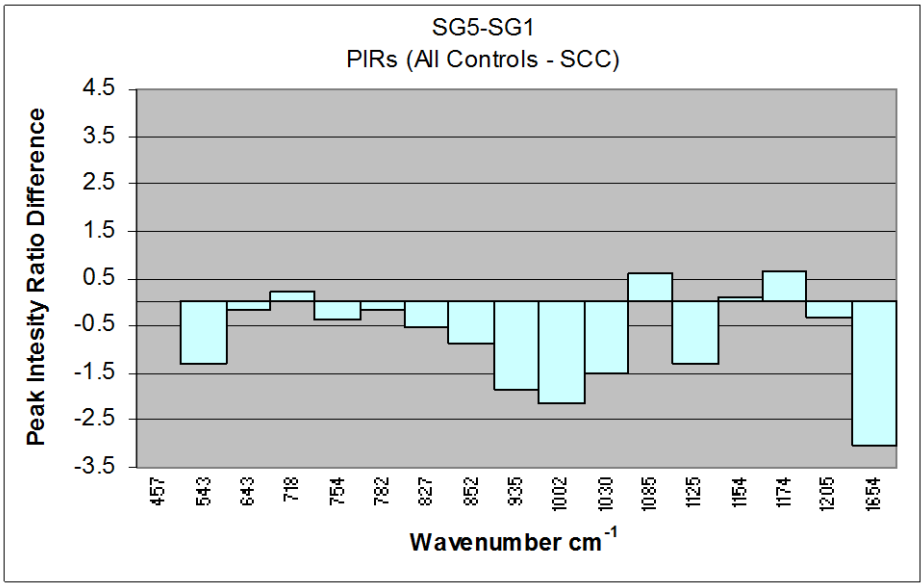
SG5-SG1
PIRs (All Controls - SCC)
Peak Intesity Ratio Difference
4.5
3.5
2.5
1.5
0.5
-0.5
-1.5
-2.5
-3.5
457
543
643
718
754
782
827
852
935
1002
1030
1085
1125
1154
1174
1205
1654
Wavenumber cm-1

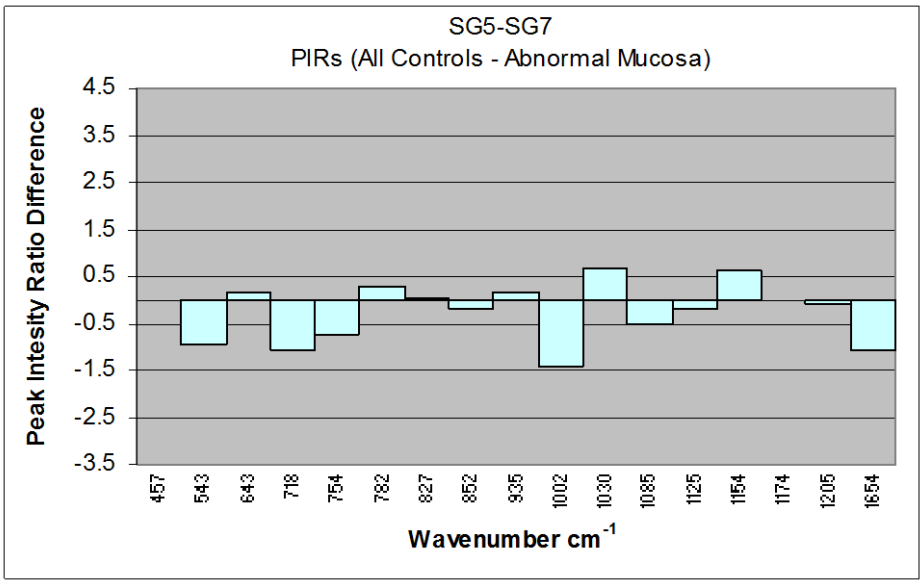
SG5-SG7
PIRs (All Controls - Abnormal Mucosa)
Peak Intesity Ratio Difference
4.5
3.5
2.5
1.5
0.5
-0.5
-1.5
-2.5
-3.5
457
543
643
718
754
782
827
852
935
1002
1030
1085
1125
1154
1174
1205
1654
Wavenumber cm-1

D.5.5 L2c_1

Wavenumbers (cm^{1}) unique across groups		
SG1	SG3	SG7
	422	406
	481	431
	527	671
	666	1760
	1735	
	1751	
	1815	

Wave Number	PIR SG1	PIR SG3	PIR SG7	SG7-SG1	SG3-SG1	SG3-SG7
457	1.00	1.00	1.00	0.00	0.00	0.00
643	1.25	1.48	1.96	0.23	0.71	-0.49
718	2.28	2.22	3.13	-0.06	0.84	-0.91
754	2.04	2.80	3.13	0.77	1.09	-0.32
782	1.15	1.07	1.05	-0.08	-0.11	0.02
827	0.98	2.08	1.49	1.10	0.51	0.58
852	2.34	4.15	3.41	1.81	1.07	0.74
935	4.26	7.41	5.97	3.15	1.71	1.44
1002	9.52	13.63	13.07	4.11	3.55	0.56
1030	1.39	2.66	2.27	1.26	0.87	0.39
1085	3.51	2.96	3.41	-0.55	-0.10	-0.45
1125	2.51	3.85	3.98	1.35	1.47	-0.13
1154	1.34	1.55	0.61	0.21	-0.73	0.93
1205	1.27	2.05	1.73	0.78	0.46	0.32
1446	21.30	26.96	26.14	5.66	4.84	0.83
1654	22.05	28.45	26.14	6.39	4.08	2.31

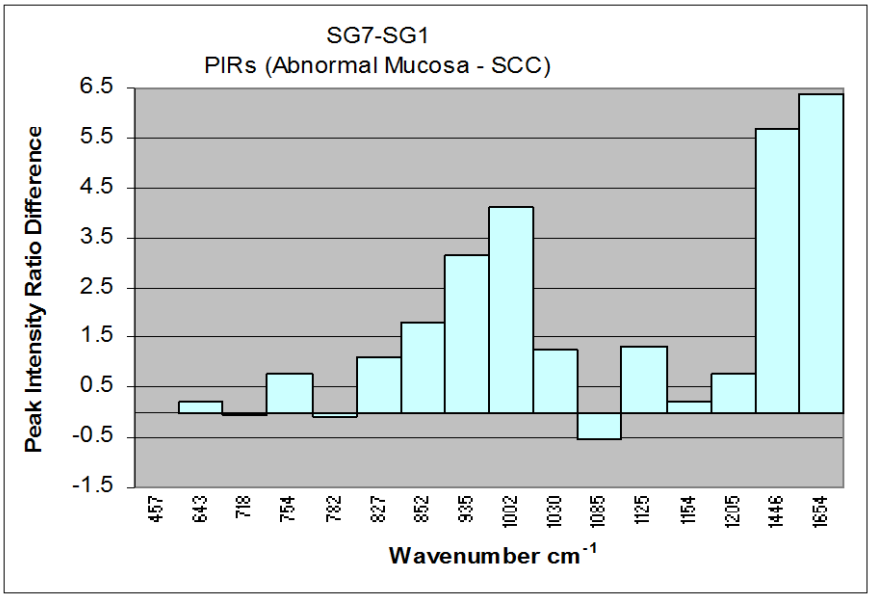
SG7-SG1
PIRs (Abnormal Mucosa - SCC)
Peak Intensity Ratio Difference
6.5
5.5
4.5
3.5
2.5
1.5
0.5
-0.5
-1.5
457
643
718
754
782
827
852
935
1002
1030
1085
1125
1154
1205
1446
1654
Wavenumber cm-1

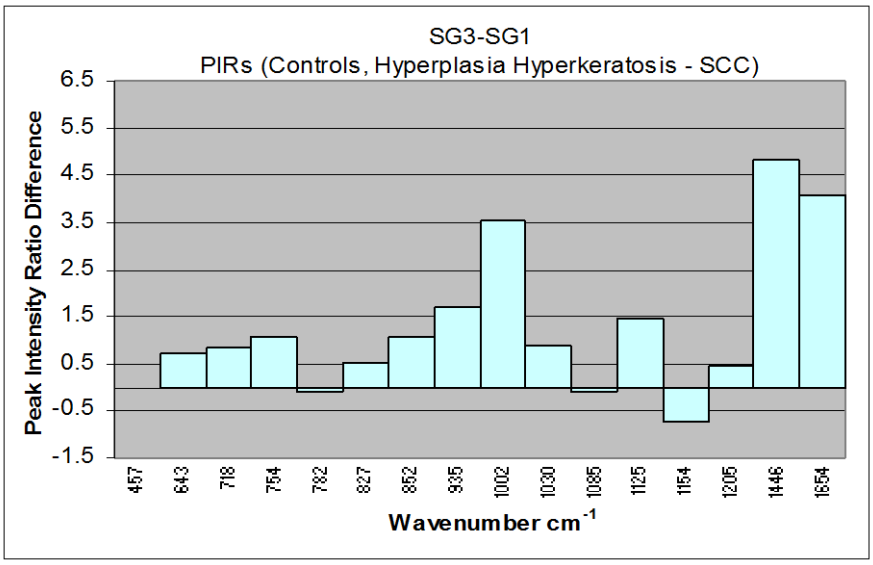
SG3-SG1
PIRs (Controls, Hyperplasia Hyperkeratosis - SCC)
Peak Intensity Ratio Difference
6.5
5.5
4.5
3.5
2.5
1.5
0.5
-0.5
-1.5
457
643
718
754
782
827
852
935
1002
1030
1085
1125
1154
1205
1446
1654
Wavenumber cm-1

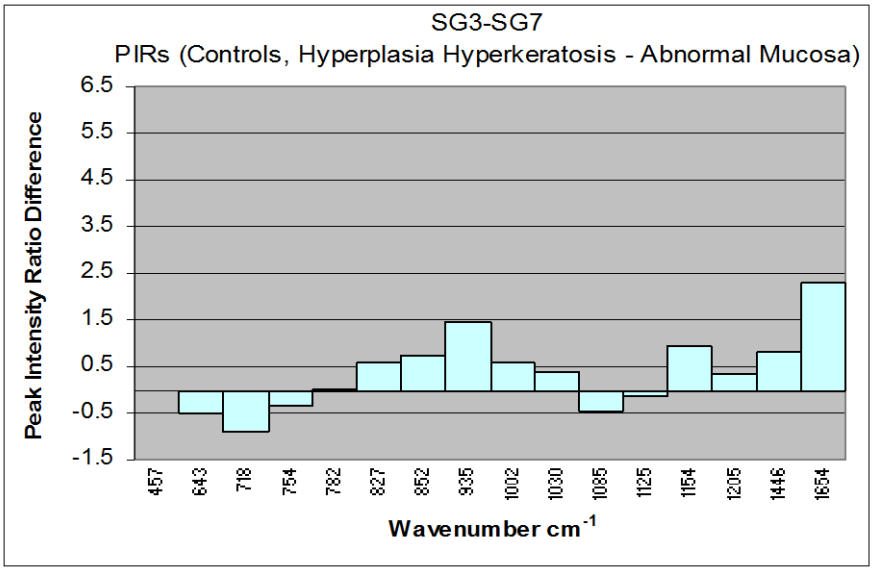
SG3-SG7
PIRs (Controls, Hyperplasia Hyperkeratosis - Abnormal Mucosa)
Peak Intensity Ratio Difference
6.5
5.5
4.5
3.5
2.5
1.5
0.5
-0.5
-1.5
457
643
718
754
782
827
852
935
1002
1030
1085
1125
1154
1205
1446
1654
Wavenumber cm-1

D.5.6 L2c_2

Wavenumbers (cm^{-1}) unique across groups		
SG1	SG10	SG7
	421	406
	663	431
	878	671
	1058	897
	1180	1252
	1529	
	1733	
	1797	
	1816	

Wave Number	SG1	SG10	SG7	SG7-SG1	SG10-SG1	SG10-SG7
457	1.00	1.00	1.00	0.00	0.00	0.00
543	1.42	3.69	2.02	2.28	1.67	0.61
643	1.25	1.96	1.00	0.71	0.96	-0.25
718	2.28	3.13	1.41	0.84	1.72	-0.88
754	2.04	3.13	1.71	1.09	1.42	-0.33
782	1.15	1.05	1.51	-0.11	-0.47	0.36
827	0.98	1.49	0.82	0.51	0.68	-0.16
852	2.34	3.41	1.79	1.07	1.61	-0.55
935	4.26	5.97	3.54	1.71	2.43	-0.72
1002	9.52	13.07	6.84	3.55	6.22	-2.68
1030	1.39	2.27	1.54	0.87	0.72	0.15
1085	3.51	3.41	2.32	-0.10	1.09	-1.19
1125	2.51	3.98	2.31	1.47	1.67	-0.20
1154	1.34	0.61	0.86	-0.73	-0.25	-0.48
1205	1.27	1.73	0.84	0.46	0.89	-0.43
1446	21.30	26.14	15.34	4.84	10.80	-5.96
1654	22.05	26.14	17.47	4.08	8.67	-4.59

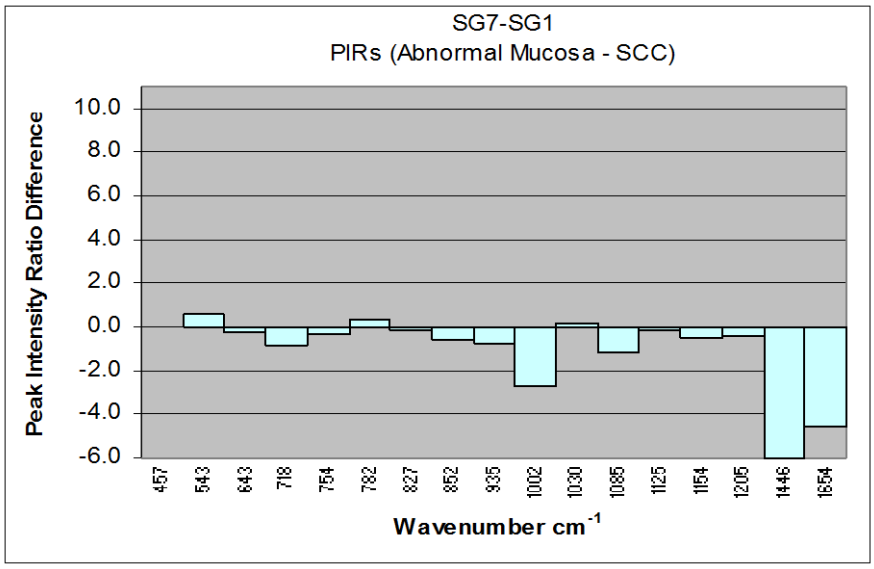
SG7-SG1
PIRs (Abnormal Mucosa - SCC)
Peak Intensity Ratio Difference
10.0
8.0
6.0
4.0
2.0
0.0
-2.0
-4.0
-6.0
457
543
643
718
754
782
827
852
935
1002
1030
1085
1125
1154
1205
1446
1654
Wavenumber cm-1

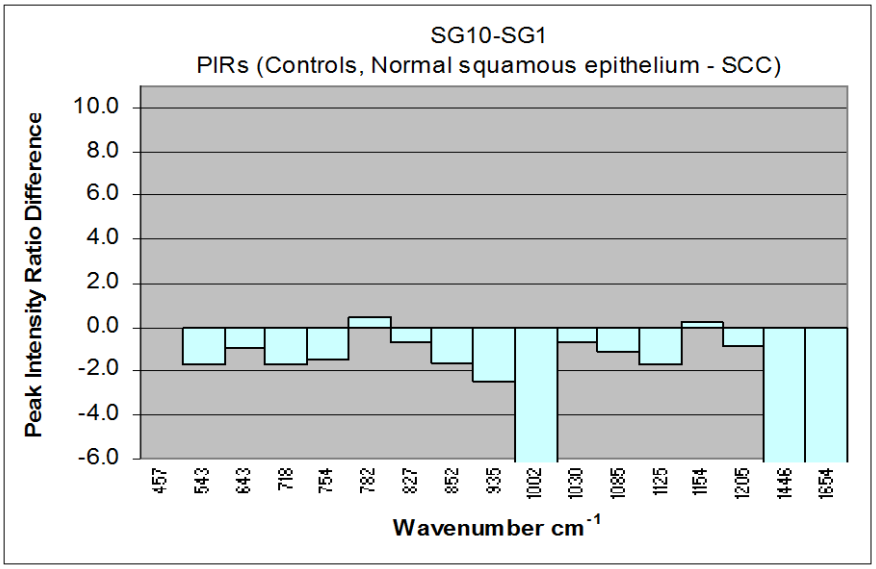
SG10-SG1
PIRs (Controls, Normal squamous epithelium - SCC)
Peak Intensity Ratio Difference
10.0
8.0
6.0
4.0
2.0
0.0
-2.0
-4.0
-6.0
457
543
643
718
754
782
827
852
935
1002
1030
1085
1125
1154
1205
1446
1654
Wavenumber cm-1

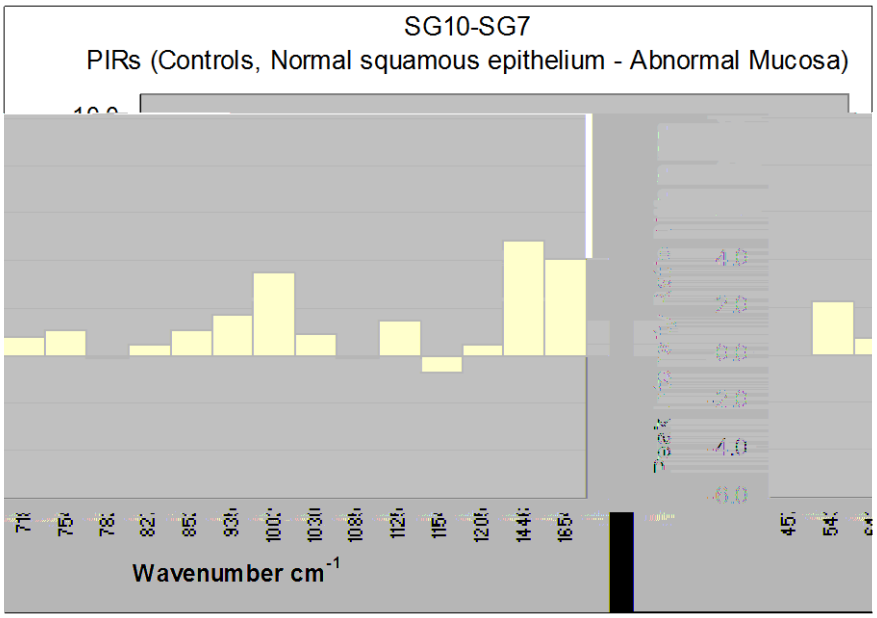
SG10-SG7
PIRs (Controls, Normal squamous epithelium - Abnormal Mucosa)
Wavenumber cm-1

D.5.7 L2c_3

Wavenumbers (cm^{-1}) unique across groups		
SG1	SG10	SG14
543	421	406
		430
		494
	547	548
	618	622
	663	671
	878	878
	1058	897
1174		1173
	1180	1252
1244	1241	1296
	1529	1389
	1547	1545
	1572	1573
	1733	1614
	1766	1760
	1797	1802
	1816	
	1840	1838

Wave Number	PIR SG1	PIR SG10	PIR SG14	SG14-SG1	SG10-SG1	SG10-SG14
457	1.00	1.00	1.00	0.00	0.00	0.00
643	1.25	1.00	1.91	-0.25	-0.91	0.66
754	2.04	1.71	3.19	-0.33	-1.48	1.15
782	1.15	1.51	1.06	0.36	0.46	-0.10
827	0.98	0.82	1.88	-0.16	-1.06	0.90
852	2.34	1.79	3.19	-0.55	-1.40	0.85
935	4.26	3.54	5.85	-0.72	-2.31	1.59
1002	9.52	6.84	13.03	-2.68	-6.18	3.50
1030	1.39	1.54	2.58	0.15	-1.03	1.19
1085	3.51	2.32	3.19	-1.19	-0.87	-0.32
1125	2.51	2.31	3.99	-0.20	-1.68	1.48
1154	1.34	0.86	0.78	-0.48	0.08	-0.56
1205	1.27	0.84	1.79	-0.43	-0.95	0.52
1303	2.76	1.72	2.60	-1.04	-0.88	-0.16
1339	1.43	1.88	2.92	0.45	-1.05	1.49
1446	21.30	15.34	24.46	-5.96	-9.12	3.15
1654	22.05	17.47	25.25	-4.59	-7.79	3.20

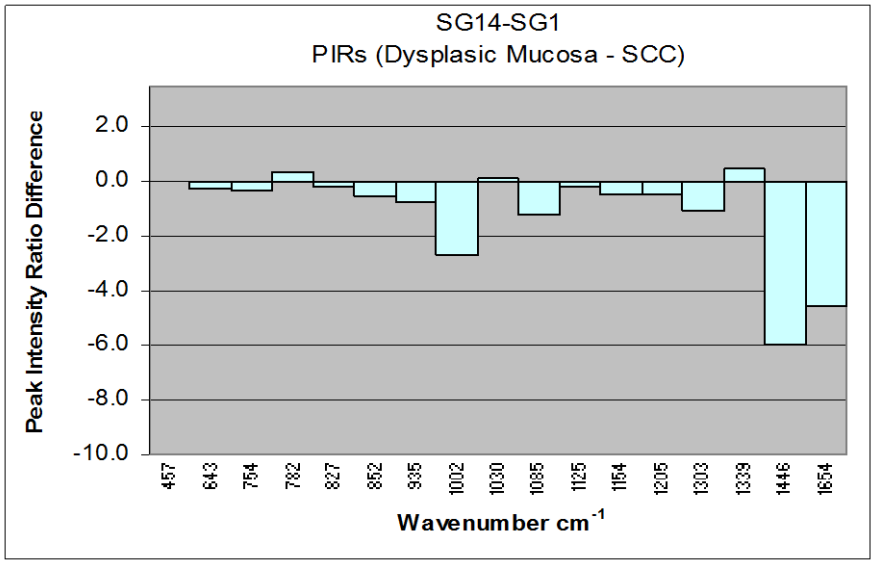
SG14-SG1
PIRs (Dysplasic Mucosa - SCC)
Peak Intensity Ratio Difference
2.0
0.0
-2.0
-4.0
-6.0
-8.0
-10.0
457
643
754
782
827
852
935
1002
1030
1085
1125
1154
1205
1303
1339
1446
1654
Wavenumber cm-1

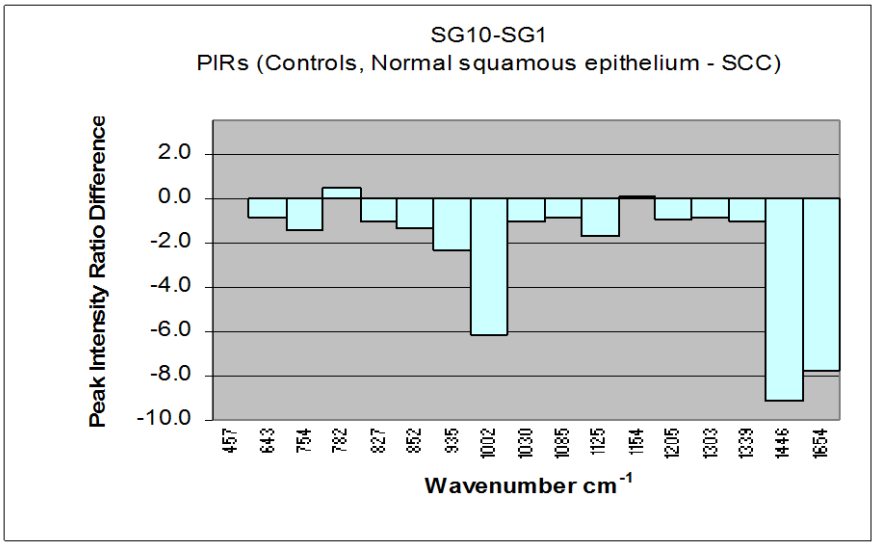
SG10-SG1
PIRs (Controls, Normal squamous epithelium - SCC)
Peak Intensity Ratio Difference
2.0
0.0
-2.0
-4.0
-6.0
-8.0
-10.0
457
643
754
782
827
852
935
1002
1030
1085
1125
1154
1205
1303
1339
1446
1654
Wavenumber cm-1

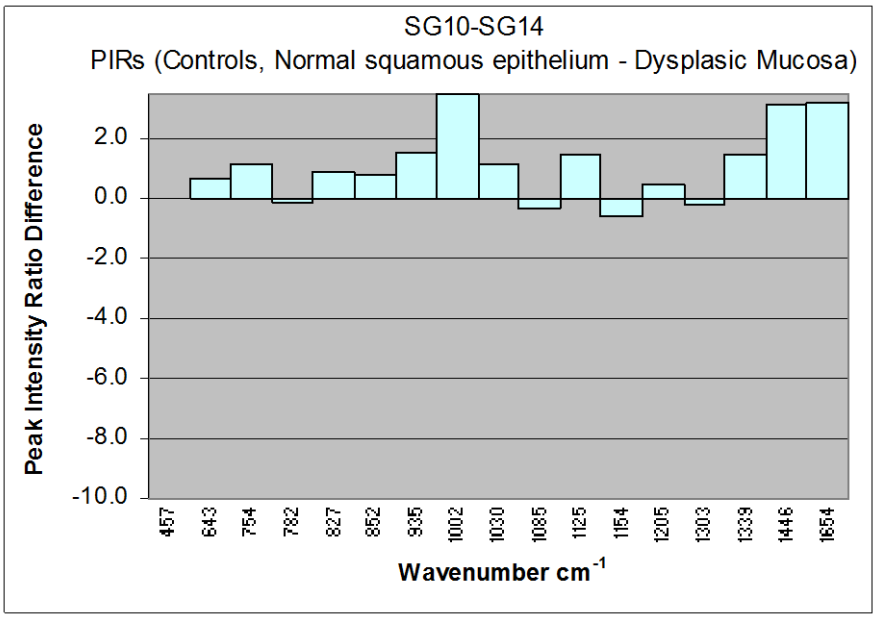
SG10-SG14
PIRs (Controls, Normal squamous epithelium - Dysplasic Mucosa)
Peak Intensity Ratio Difference
2.0
0.0
-2.0
-4.0
-6.0
-8.0
-10.0
457
643
754
782
827
852
935
1002
1030
1085
1125
1154
1205
1303
1339
1446
1654
Wavenumber cm-1

D.5.8 L3

Wavenumbers (cm^{-1}) unique across groups			
SG2	SG6	SG8	SG9
		405	406
	419	417	
431	434		430
		494	
528	523		
		548	550
642	570		
668		644	643
		671	672
698	695		
880		877	879
	897	898	898
	934	937	938
947		1060	
1085	1081		1081
		1092	
1129	1125	1124	1125
		1172	1174
1188	1187		
	1204	1203	1203
			1239
	1252	1253	
1264			
1302			1302
1360			
1388	1393		1390
1401			
1513			
1603			1614
1718			
1736			1838
1758		1763	1760
	1796		
	1828		

Wave Number	PIR SG2	PIR SG6	PIR SG8	PIR SG9	SG9-SG2	SG9-SG6	SG9-SG8	SG2-SG8	SG6-SG8	SG2-SG6
457	1.00	1.00	1.00	1.00	0.00	0.00	0.00	0.00	0.00	0.00
621	1.45	0.98	1.20	1.82	0.37	0.84	0.61	0.24	-0.23	0.47
724	1.20	1.58	4.70	2.61	1.41	1.03	-2.08	-3.49	-3.12	-0.38
753	2.20	3.58	2.58	5.45	3.25	1.87	2.87	-0.38	1.00	-1.38
789	1.74	1.87	1.49	0.51	-1.23	-1.36	-0.98	0.24	0.38	-0.14
828	1.42	1.86	2.01	1.92	0.50	0.07	-0.09	-0.59	-0.15	-0.43
851	2.07	4.07	3.99	4.09	2.01	0.02	0.09	-1.92	0.07	-1.99
1001	9.71	16.03	12.92	18.05	8.34	2.02	5.13	-3.21	3.11	-6.32
1030	1.95	2.71	2.30	3.75	1.80	1.04	1.44	-0.35	0.40	-0.76
1129	2.62	4.80	4.70	5.45	2.82	0.65	0.75	-2.07	0.11	-2.18
1157	1.36	1.90	0.75	0.86	-0.50	-1.04	0.11	0.61	1.15	-0.54
1339	3.20	10.09	10.33	3.75	0.55	-6.34	-6.59	-7.14	-0.24	-6.89
1449	17.79	27.30	31.47	28.61	10.81	1.30	-2.87	-13.68	-4.17	-9.51
1556	1.81	2.66	0.81	3.07	1.26	0.41	2.26	1.00	1.85	-0.85
1574	1.29	0.82	0.78	1.06	-0.23	0.24	0.28	0.51	0.04	0.47
1660	16.18	32.05	30.54	22.48	6.30	-9.58	-8.06	-14.36	1.52	-15.88

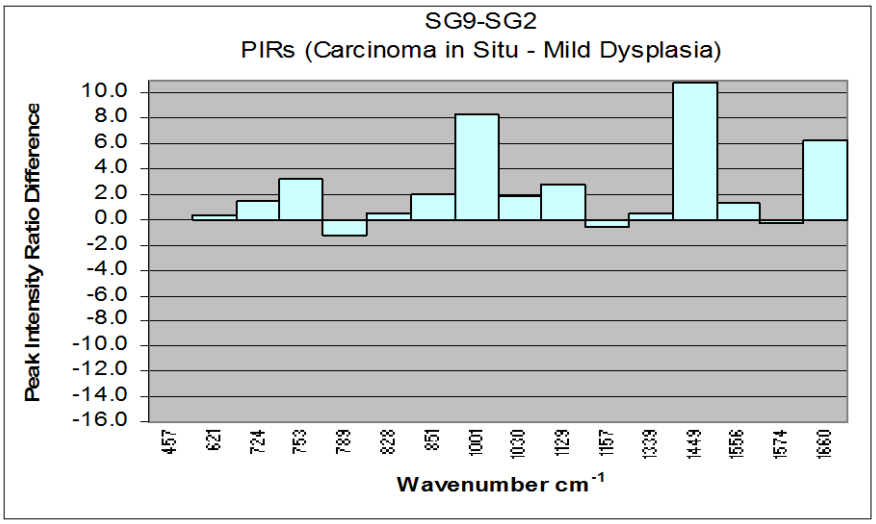
SG9-SG2
PIRs (Carcinoma in Situ - Mild Dysplasia)
Peak Intensity Ratio Difference
10.0
8.0
6.0
4.0
2.0
0.0
-2.0
-4.0
-6.0
-8.0
-10.0
-12.0
-14.0
-16.0
457
621
724
753
789
828
851
1001
1030
1129
1157
1339
1449
1556
1574
1660
Wavenumber cm-1

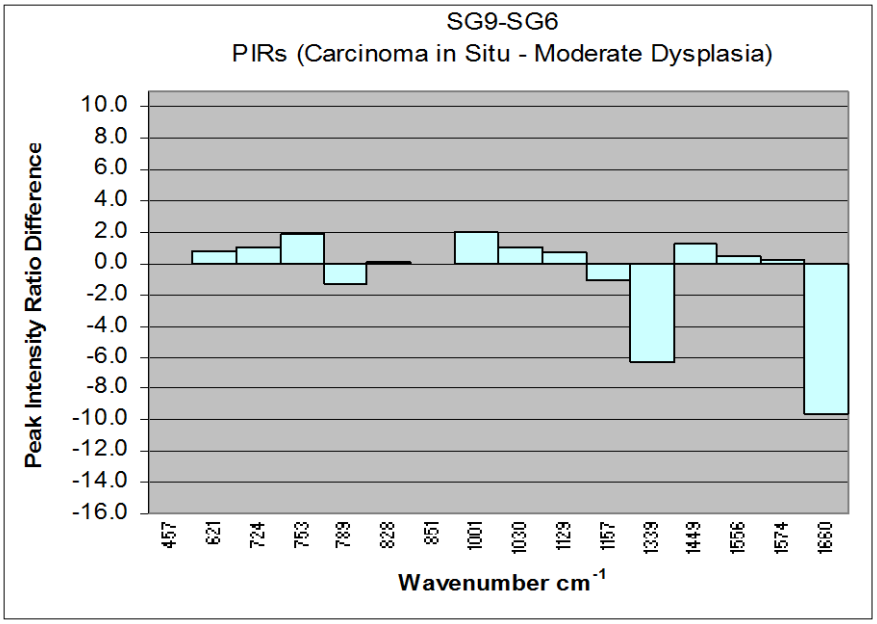
SG9-SG6
PIRs (Carcinoma in Situ - Moderate Dysplasia)
Peak Intensity Ratio Difference
10.0
8.0
6.0
4.0
2.0
0.0
-2.0
-4.0
-6.0
-8.0
-10.0
-12.0
-14.0
-16.0
457
621
724
753
789
828
851
1001
1030
1129
1157
1339
1449
1556
1574
1660
Wavenumber cm-1

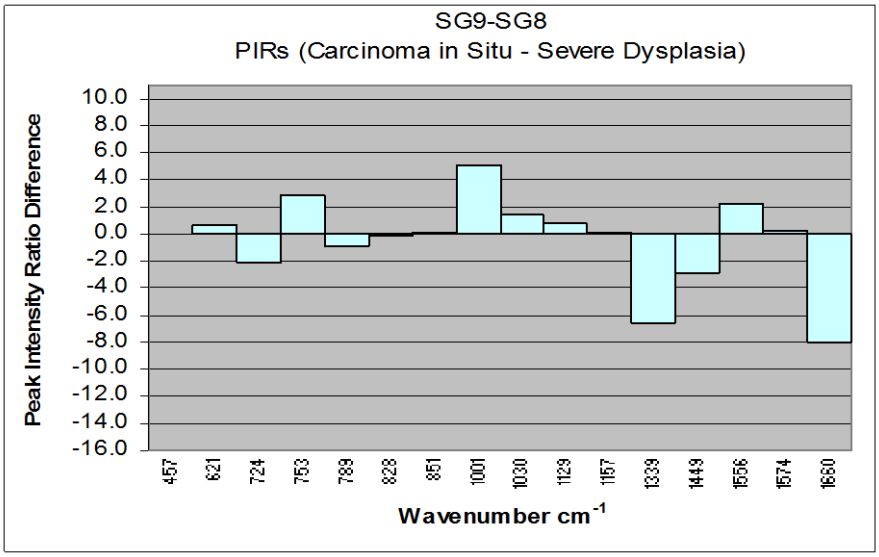
SG9-SG8
PIRs (Carcinoma in Situ - Severe Dysplasia)
Peak Intensity Ratio Difference
10.0
8.0
6.0
4.0
2.0
0.0
-2.0
-4.0
-6.0
-8.0
-10.0
-12.0
-14.0
-16.0
457
621
724
753
789
828
851
1001
1030
1129
1157
1339
1449
1556
1574
1660
Wavenumber cm-1

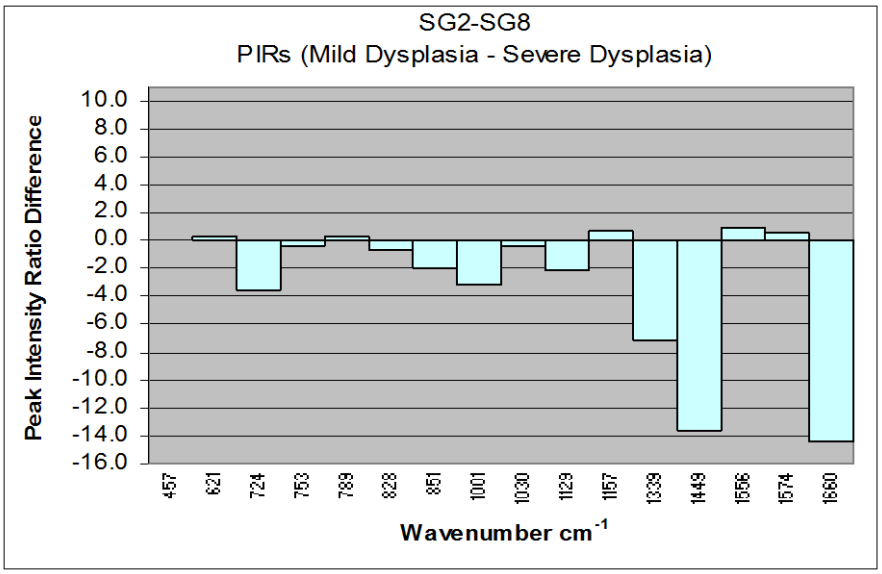
SG2-SG8
PIRs (Mild Dysplasia - Severe Dysplasia)
Peak Intensity Ratio Difference
10.0
8.0
6.0
4.0
2.0
0.0
-2.0
-4.0
-6.0
-8.0
-10.0
-12.0
-14.0
-16.0
457
621
724
753
789
828
851
1001
1030
1129
1157
1339
1449
1556
1574
1660
Wavenumber cm-1

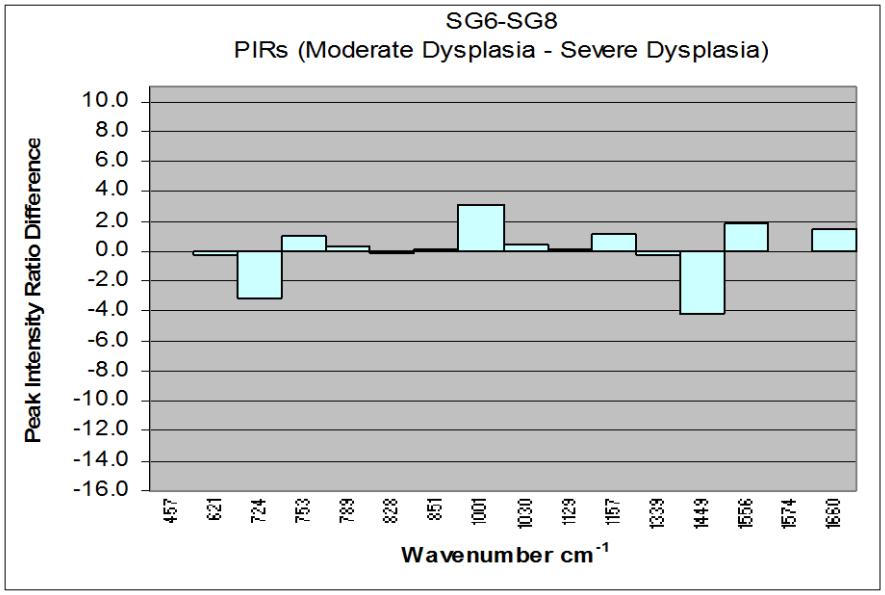
SG6-SG8
PIRs (Moderate Dysplasia - Severe Dysplasia)
Peak Intensity Ratio Difference
10.0
8.0
6.0
4.0
2.0
0.0
-2.0
-4.0
-6.0
-8.0
-10.0
-12.0
-14.0
-16.0
457
621
724
753
789
828
851
1001
1030
1129
1157
1339
1449
1556
1574
1660
Wavenumber cm-1

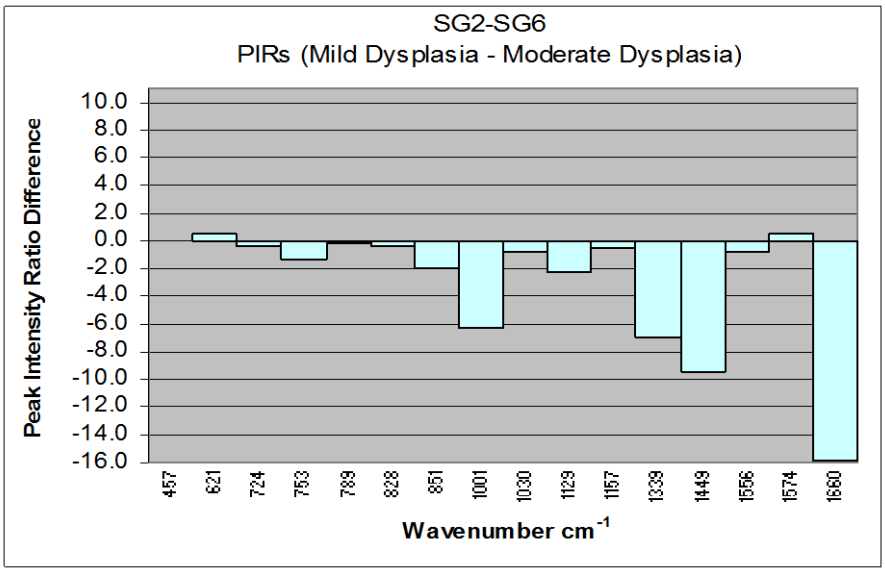
SG2-SG6
PIRs (Mild Dysplasia - Moderate Dysplasia)
Peak Intensity Ratio Difference
10.0
8.0
6.0
4.0
2.0
0.0
-2.0
-4.0
-6.0
-8.0
-10.0
-12.0
-14.0
-16.0
457
621
724
753
789
828
851
1001
1030
1129
1157
1339
1449
1556
1574
1660
Wavenumber cm-1

D.5.9 L4

Wavenumbers (cm^{-1}) unique across groups			
SG9	SG11	SG12	SG13
406	406		406
430	431		427
		476	479
	494	496	497
		519	516
	534		
550		545	546
		607	
		665	665
672	669		
	698	697	698
	782	782	783
788			
879	876	877	
	891		
898			896
		1059	
1174	1172		1174
		1181	
1239			
	1243		
		1247	
			1259
1302	1303		1302
			1371
1390			
	1507	1508	
	1521		1519
1574	1574		1573
1614	1613		1614
	1734		1733
	1755		1756
1760			
	1773		1773
	1797	1790	1791
		1807	
	1816	1817	1821
1838			1839

Wave Number	PIR SG9	PIR SG11	PIR SG12	PIR SG13	SG9-SG11	SG9-SG12	SG9-SG13	SG13-SG11	SG13-SG12	SG12-SG11
456	1.00	1.00	1.00	1.00	0.00	0.00	0.00	0.00	0.00	0.00
621	1.82	0.77	0.36	0.64	1.05	1.46	1.18	-0.13	-0.28	0.41
643	2.32	1.51	1.08	1.32	0.81	1.23	0.99	-0.18	-0.24	0.42
716	2.61	2.88	1.75	2.49	-0.27	0.87	0.13	-0.40	-0.74	1.13
754	5.45	2.79	1.48	2.38	2.66	3.97	3.07	-0.41	-0.90	1.32
825	1.92	1.42	0.98	1.31	0.50	0.95	0.62	-0.11	-0.33	0.45
852	4.09	3.17	1.94	2.56	0.92	2.15	1.52	-0.61	-0.63	1.23
938	8.17	5.19	3.53	4.31	2.99	4.65	3.87	-0.88	-0.78	1.66
1001	18.05	11.81	7.49	11.04	6.24	10.56	7.01	-0.78	-3.55	4.32
1030	3.75	2.15	1.18	2.01	1.60	2.57	1.73	-0.14	-0.84	0.97
1081	2.73	4.32	2.42	3.77	-1.60	0.30	-1.04	-0.55	-1.34	1.90
1125	5.45	3.46	1.96	2.96	1.99	3.49	2.49	-0.50	-1.01	1.50
1154	0.86	1.49	1.32	0.97	-0.64	-0.46	-0.11	-0.52	0.35	0.18
1203	2.27	1.84	1.08	1.47	0.43	1.19	0.79	-0.36	-0.40	0.76
1337	3.75	2.65	4.85	2.57	1.10	-1.10	1.17	-0.08	2.28	-2.20
1447	28.61	25.64	17.85	21.00	2.96	10.76	7.61	-4.65	-3.15	7.79
1545	3.07	0.66	0.64	0.87	2.41	2.43	2.20	0.21	-0.23	0.02
1656	22.48	27.37	18.51	23.42	-4.90	3.97	-0.94	-3.95	-4.91	8.86

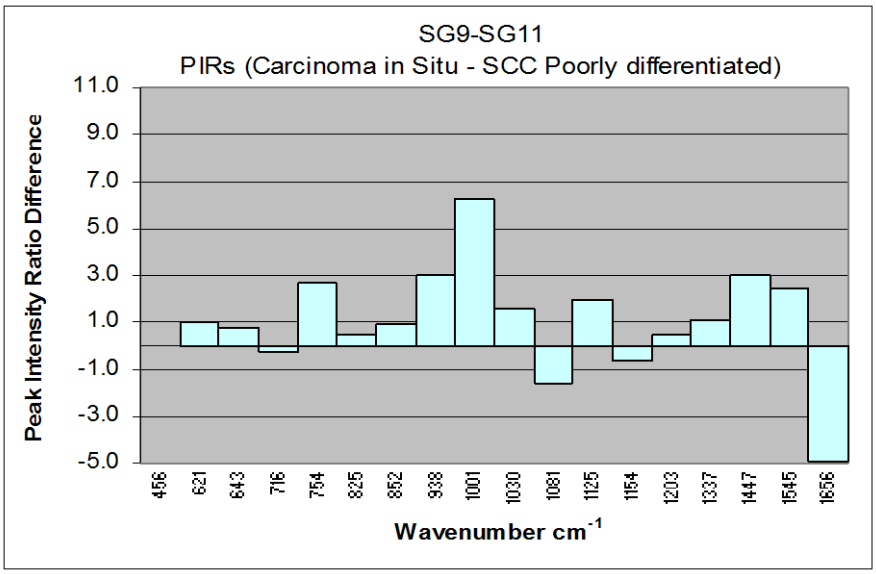
SG9-SG11
PIRs (Carcinoma in Situ - SCC Poorly differentiated)
Peak Intensity Ratio Difference
11.0
9.0
7.0
5.0
3.0
1.0
-1.0
-3.0
-5.0
456
621
643
716
754
825
852
938
1001
1030
1081
1125
1154
1203
1337
1447
1545
1656
Wavenumber cm-1

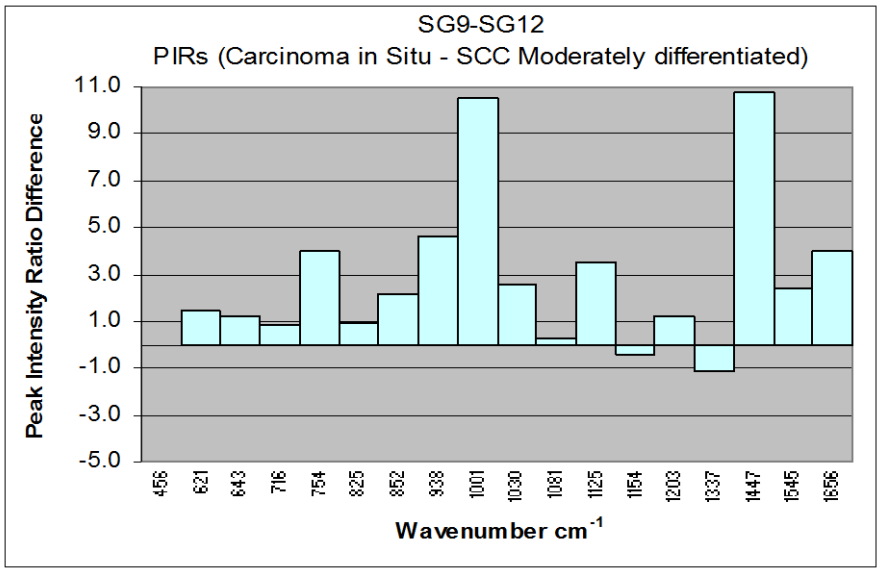
SG9-SG12
PIRs (Carcinoma in Situ - SCC Moderately differentiated)
Peak Intensity Ratio Difference
11.0
9.0
7.0
5.0
3.0
1.0
-1.0
-3.0
-5.0
456
621
643
716
754
825
852
938
1001
1030
1081
1125
1154
1203
1337
1447
1545
1656
Wavenumber cm-1

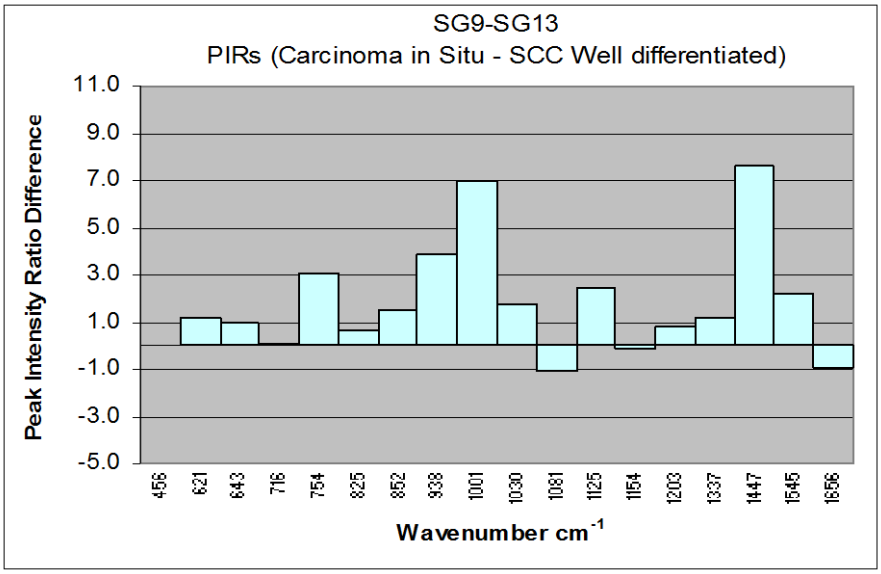
SG9-SG13
PIRs (Carcinoma in Situ - SCC Well differentiated)
Peak Intensity Ratio Difference
11.0
9.0
7.0
5.0
3.0
1.0
-1.0
-3.0
-5.0
456
621
643
716
754
825
852
938
1001
1030
1081
1125
1154
1203
1337
1447
1545
1656
Wavenumber cm-1

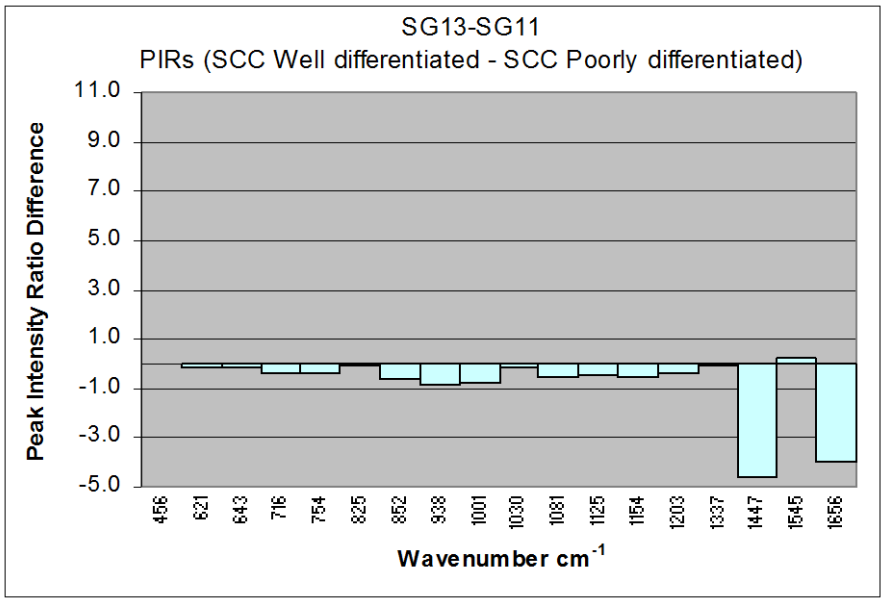
SG13-SG11
PIRs (SCC Well differentiated - SCC Poorly differentiated)
Peak Intensity Ratio Difference
11.0
9.0
7.0
5.0
3.0
1.0
-1.0
-3.0
-5.0
456
621
643
716
754
825
852
938
1001
1030
1081
1125
1154
1203
1337
1447
1545
1656
Wavenumber cm-1

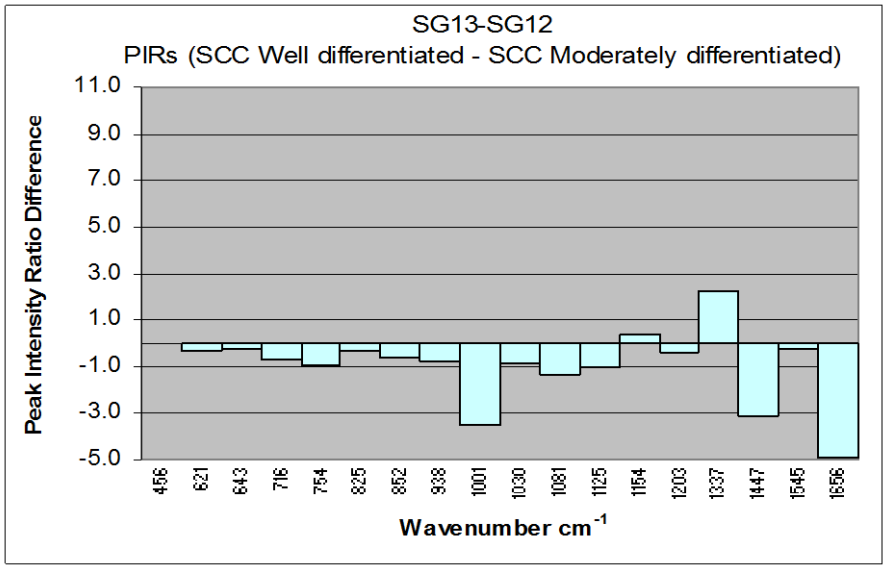
SG13-SG12
PIRs (SCC Well differentiated - SCC Moderately differentiated)
Peak Intensity Ratio Difference
11.0
9.0
7.0
5.0
3.0
1.0
-1.0
-3.0
-5.0
456
621
643
716
754
825
852
938
1001
1030
1081
1125
1154
1203
1337
1447
1545
1656
Wavenumber cm-1

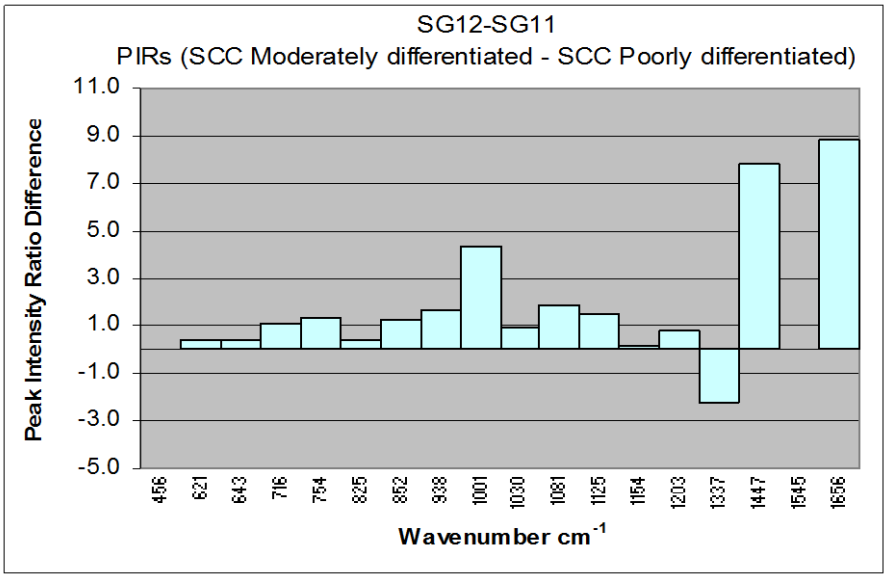
SG12-SG11
PIRs (SCC Moderately differentiated - SCC Poorly differentiated)
Peak Intensity Ratio Difference
11.0
9.0
7.0
5.0
3.0
1.0
-1.0
-3.0
-5.0
456
621
643
716
754
825
852
938
1001
1030
1081
1125
1154
1203
1337
1447
1545
1656
Wavenumber cm-1

D.5.10 L4_2

Wavenumbers (cm^{-1}) unique across groups			
SG9	SG11	SG12	SG15
406	406		406
430	431		427
		476	479
	494	496	497
		519	516
	534		
550		545	546
		607	
		665	665
672	669		
	698	697	698
	782	782	783
788			
879	876	877	
	891		
898			896
		1059	
1174	1172		1174
		1181	
1239			
	1243		
		1247	
			1259
1302	1303		1302
			1371
1390			
	1507	1508	
	1521		1519
1574	1574		1573
1614	1613		1614
	1734		1733
	1755		1756
1760			
	1773		1773
	1797	1790	1791
		1807	
	1816	1817	1821
1838			1839

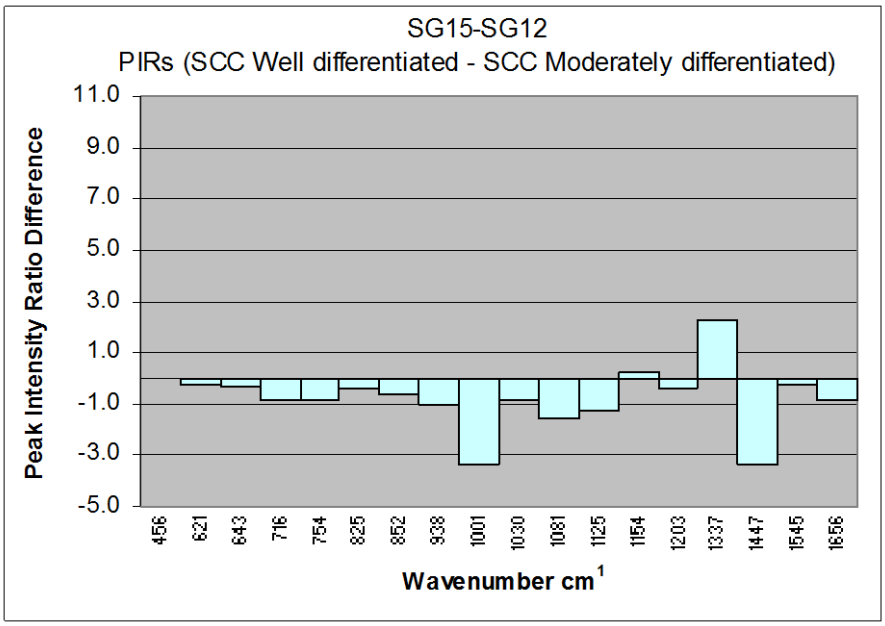
SG15-SG12
PIRs (SCC Well differentiated - SCC Moderately differentiated)
Peak Intensity Ratio Difference
11.0
9.0
7.0
5.0
3.0
1.0
-1.0
-3.0
-5.0
456
621
643
716
754
825
852
938
1001
1030
1081
1125
1154
1203
1337
1447
1545
1656
Wavenumber cm1

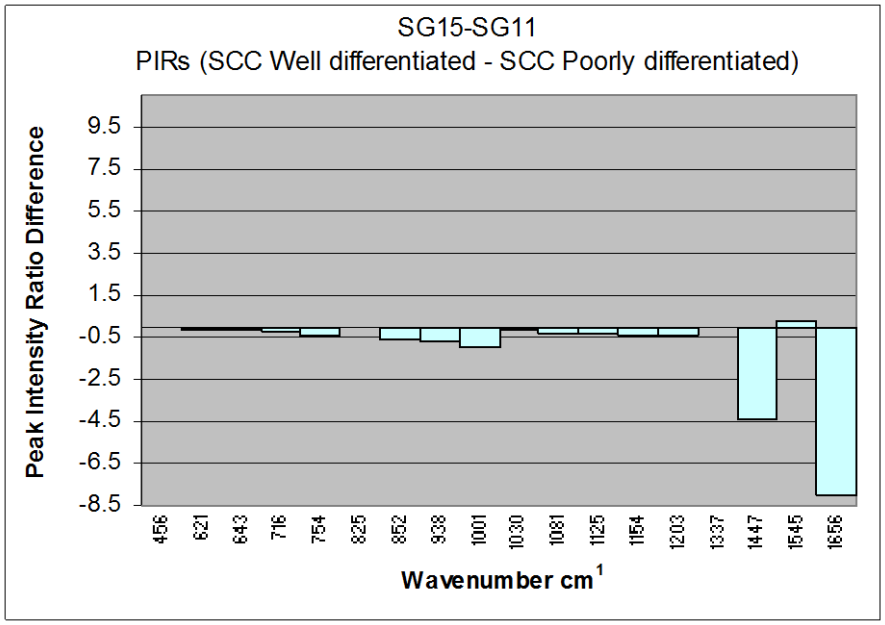
SG15-SG11
PIRs (SCC Well differentiated - SCC Poorly differentiated)
Peak Intensity Ratio Difference
9.5
7.5
5.5
3.5
1.5
-0.5
-2.5
-4.5
-6.5
-8.5
456
621
643
716
754
825
852
938
1001
1030
1081
1125
1154
1203
1337
1447
1545
1656
Wavenumber cm1

D.5.11 Summary of larynx mini models multivariate analysis results.

	L1	L1-1	L2a	L2b	L2c	L2c-1
1	300.0421	258.3151	344.7667	249.7182	213.5561	337.9797
2	2.7829	56.7493	41.6013	28.7105	29.7851	2.8279
3	150.078	25.363	19.4962	95.011	34.2954	27.5177
4	74.7436	18.7207	21.054	94.3425	32.5957	9.4957
5	13.2927	0.1891	0.3201	51.9062	0.113	93.3019
6	5.5836	219.125	268.9875	10.0596	121.6903	74.3078
7	94.0853	97.649	8.2299	2.0977	80.9551	107.7855
8	7.6865	65.9839	66.0545	4.3603	37.7285	18.9721
9	28.5302	0.0849	0.6692	4.3333	13.3636	10.5108
10	228.4783	42.9864	46.4478	0.1912	21.699	2.7146
11	135.1432	55.1824	74.5047	47.3043	54.7454	49.272
12	0.0629	14.8553	8.3755	9.2472	29.5273	5.6675
13	14.885	57.7829	33.7306	0.0019	36.3175	1.0498
14	4.458	6.9649	10.2419	5.4406	8.4914	4.8453
15	0.8887	145.989	91.7722	19.3023	74.2982	68.5529
16	1.7569	1.0229	0.0595	0.0017	26.5	27.0548
17	45.0604	61.8494	76.1229	6.7026	35.5073	11.2658
18	18.9453	2.085	0.3873	11.4611	8.7144	35.9416
19	1.5291	4.9365	10.8318	0.8854	8.8783	60.1384
20	63.6341	29.6583	1.5703	1.3593	66.5909	63.0848
21	6.7149	9.1625	1.3772	5.2367	8.0715	9.1648
22	26.6005	0.8197	27.9681	3.8515	50.1669	21.5203
23	50.0409	36.4132	22.107	3.4417	41.8755	2.7158
24	32.5562	2.4182	27.8101	0.445	2.5599	8.3516
25	71.0559	44.8853	9.9629	0.018	34.884	48.7958
Distance between Class 1 and 2 is	4.7139	8.9744	8.9188	48.8467	9.3101	16.0034
Distance between Class 1 and 3 is	4.7139				12.624	15.5775
Distance between Class 1 and 4 is					17.2031	17.9436
Distance between Class 2 and 3 is						
Distance between Class 2 and 4 is	85.6455					
Distance between Class 3 and 4 is	87.211					
Total Distance between classes is		8.9744	8.9188	48.8467	39.1372	49.5245
Training Classfication Performance						
Class 1 Percentage Correct	85.6455	95.1931	94.605	97.9472	91.8112	93.9306
Class 2 Percentage Correct	87.211	84.6284	83.4459	100	84.2905	86.5103
Class 3 Percentage Correct					77.1654	83.4646
Class 4 Percentage Correct						
Training performance	86.54	91.6335	90.5521	98.8176	88.2186	91.3679
Prediction performance	86.54	91.6335	90.5521	98.8176	0	0
F Crit	10.681	10.775	10.682	10.885	10.885	7.037

	L2c-1	L2c-2	L2c-3	L3	L4	L4_2
1	337.9797	79.9057	46.6069	53.5333	207.5909	212.2289
2	2.8279	76.6517	72.9062	16.1816	1.619	1.2787
3	27.5177	134.7785	109.3403	485.9727	25.8308	26.07
4	9.4957	35.4527	17.1352	10.5262	4.8128	5.4049
5	93.3019	9.8939	10.9579	7.2569	90.5194	90.8995
6	74.3078	51.7903	12.3766	2.5689	10.7248	10.2518
7	107.7855	9.5018	9.1142	7.7938	9.3013	9.3318
8	18.9721	4.5422	35.1909	12.3522	84.577	84.6541
9	10.5108	17.8575	5.2497	1.9706	8.5537	9.6949
10	2.7146	11.4253	37.5152	6.2579	59.4123	55.1777
11	49.272	64.6692	92.3072	0.5552	33.3613	35.3191
12	5.6675	144.8926	56.4104	0.1591	9.3678	9.3478
13	1.0498	7.3576	5.182	0.235	85.4023	88.5161
14	4.8453	0.3081	10.7124	1.9789	82.1574	81.5305
15	68.5529	14.5742	15.2854	0.1417	27.9822	26.7484
16	27.0548	87.936	47.6545	0.5976	10.6182	8.9789
17	11.2658	18.1883	35.5782	0.0509	27.72	27.8992
18	35.9416	55.0069	61.5614	0.1918	12.0315	11.5612
19	60.1384	39.9379	19.5542	0.0211	4.0865	3.8124
20	63.0848	4.2338	10.6055	0.1609	11.5576	10.68
21	9.1648	17.9414	8.3947	0.1121	43.0905	43.2298
22	21.5203	47.5714	23.1964	0.3371	16.2802	20.4906
23	2.7158	69.792	77.075	0.0537	3.1445	3.8695
24	8.3516	17.1397	7.806	0.2988	51.9213	47.7784
25	48.7958	4.1118	18.0168	0.3645	0.9454	1.2562
Distance between Class 1 and 2 is	16.0034	14.64	14.3387	56.0973	65.4779	64.12
Distance between Class 1 and 3 is	15.5775	19.5632	15.1374	96.6849	70.5998	69.18
Distance between Class 1 and 4 is	17.9436	32.8025	28.9591	78.8451	47.2946	47.35
Distance between Class 2 and 3 is				136.7591	22.7943	23.29
Distance between Class 2 and 4 is				126.4369	17.0478	17.78
Distance between Class 3 and 4 is				152.2397	13.068	13.13
Total Distance between classes is	49.5245	67.0056	58.4351	647.063	236.2823	234.86
Training Classfication Performance						
Class 1 Percentage Correct	93.9306	93.738	94.7013	96.1538	97.9592	97.96
Class 2 Percentage Correct	86.5103	90.4382	94.8207	100	90.7285	90.73
Class 3 Percentage Correct	83.4646	88.9764	82.0513	100	94.1973	94.39
Class 4 Percentage Correct				100	87.2146	87.26
Training performance	91.3679	92.726	94.0015	99.2126	91.9963	92.1296
Prediction performance	0	0	0	0	0	0
F Crit	7.037	6.967	6.895	5.573	5.457	5.529

Appendix E: Identification Table for Characteristic Raman Spectral Peaks (Kendall, 2002e).

Key:- δ - deformational vibrations ; ν - stretching vibrations; ν_s - symmetric stretching vibrations; ν_{as} - asymmetric stretching vibrations

	Assignment	Author	Tissue/Substance
207	Calcium carbonate	Wentrup-Byrne 1995	Cholesterol
275	τCCC	Cassanas 1991	Lactic acid
350	Ribose, cytosine	Hartman 1973	
370	δCCC	Cassanas 1991	Lactic acid
385	Cytosine	Hartman 1973	
400	Silica	Mahadevan-Jansen 1998a	Fibre probe on cervix
424	δCCC	Barry 1992	Human strateum corneum
425	δCCO	Cassanas 1991	Lactic acid
429	Calcium hydroxyapatite	Yu 1996	
430	Cholesterol	Yu 1996	
430	δ(OPO)	Wentrup-Byrne 1997a	Human tooth
435	Ribose	Hartman 1973	
451	O-P-O symmetric bend	Nie 1990	Chicken leg bone
481	Glycogen	Kendall C	Sigma Aldrich G0885
492	ν_s (SiOSi)	Frank 1994	silicone gel
500	Cytosine, guanine & disulphide	Hartman 1973	
500-550	Disulphide (S-S) stretch	Gnaidecka 1998	Protein
505	ν (S-S)	Fredericks 1995	Bovine serum albumin
507	Disulphide	Schrader 1995	Nails
509	Disulphide (S-S)	Ozaki 1988	
510	Disulphide (C-S-S-C gauche-gauche-gauche)	Gnaidecka 1998	Protein
518	Glucose	Goetz 1995	
525	Disulphide (C-S-S-C gauche-gauche-trans)	Gnaidecka 1998	Protein
526	ν (S-S)	Edwards 1995	Strateum corneum
526	ν (S-S)	Barry 1992	Human strateum corneum
528	ν (S-S)	Yu 1996	Protein
529	Desmosine & isodesmosine (amino acids)	Manoharan 1996	Elastin
530-1	ν (S-S)	Edwards 1995	Callus, psoriatic plaque
533	COC deformation (glycosidic ring)	Maquelin 2000	
533	Glucose	Chaiken 2000	Blood
540	Disulphide (C-S-S-C trans-gauche-trans)	Gnaidecka 1998	Protein

540	νOCO	Cassanas 1991	Lactic acid
547	Cholesterol	Yu 1996	Protein
553	Glucose	Chaiken 2000	Blood
556	ν (S-S)	Manfait 2000	
574	Tryptophan	Siebinga 1992	Eye lens
575	Cytosine, guanine & disulphide	Hartman 1973	
576	Glycogen	Kendall C	Sigma Aldrich G0885
587	Calcium hydroxyapatite	Yu 1996	Protein
591	Apatite	Nie 1990	Human tooth enamel
591	δ(OPO)	Wentrup-Byrne 1997a	Human tooth
600	ρ(CH) wagging	Barry 1992	Human strateum corneum
607	Cholesterol	Yu 1996	Protein
618	Phenylalanine(amino acid)	Frank 1994	Collagen
620	Phenylalanine(amino acid)	Frank 1994	Diseased breast tissue
620	Phenylalanine	Yu 1996	
620-2	ν (C-S)	Edwards 1995	Callus, psoriatic plaque
622	Phenylalanine	Puppels 1999	
623	ν (C-S)	Barry 1992	Human strateum corneum
623	ν (C-S)	Edwards 1995	Strateum corneum
624	Adenine	Mahadevan-Jansen 1996	DNA (Z), RNA(Z)
625	Guanine in the C3' endo/syn form	Mahadevan-Jansen 1996	DNA (Z)
626	Phenylalanine	Mahadevan-Jansen 1995	
626		Mahadevan-Jansen 1998a	Cervix tissue
626	Silica	Mahadevan-Jansen 1998a	Fibre probe on cervix
637	Ribose & disulphide	Hartman 1973	Protein
640	Guanine	Mahadevan-Jansen 1996	RNA(Z)
642	Thymine	Mahadevan-Jansen 1996	DNA (A), RNA (A)
643	ν (C-S), amide IV	Edwards 1995	Strateum corneum, Callus, psoriatic plaque
643	Tyrosine	Yu 1996	
644	Tyrosine	Puppels 1999	
644	ν (C-S), Amide IV	Barry 1992	Human strateum corneum
650	δC-COH	Cassanas 1991	Lactic acid
665	Thymine	Mahadevan-Jansen 1996	DNA (B)
668	Guanine in the C3' endo/anti form	Mahadevan-Jansen 1996	DNA (A), RNA (A)
669	ν(C-S)	Fredericks 1995	Bovine Serum albumin
669	ν(C-S)	Maquelin 2000	
669	Thymine	Puppels 1999	
670	Breathing of aromatic ring of purine bases	Mahadevan-Jansen 1996	DNA

	(guanine & adenine)		
670	Guanine	Mahadevan-Jansen 1996	DNA (C)
670	Guanine	Hartman 1973	
670	Thymine & guanine	Puppels 1991	
681	Guanine breathing ring	Puppels 1991	
682	Guanine in the C2' endo/anti form	Mahadevan-Jansen 1996	DNA (B)
692	Creatine (O-C=O) deformation	Dou 1996	
704	Calcium carbonate	Wentrup-Byrne 1995	Cholesterol
709	Glycogen	Kendall C	Sigma Aldrich G0885
700	Cholesterol	Schrader 1995	Brain
701	Cholesterol	Yu 1996	
710	Adenine	Hartman 1973	
710	ν_s (Si-C)	Frank 1994	silicone gel
720	Nucleotides	Schrader 1995	Breast cancer in mouse
720	C-N vibration	Mahadevan-Jansen 1996	Phospholipid membrane
722	Adenine	Hartman 1973	
724-7	Adenine	Mahadevan-Jansen 1996	DNA (A), DNA(B), RNA(A)
725	C-S	Siebinga 1992	Eye lens
725	CH_2 rocking	Maquelin K	
727	=C-H in plane bend	Frank 1994	Breast tissue, lipid
727	C-C stretch, proline	Frank 1995	Normal breast tissue
727	=C-H in plane bend	Frank 1994b	
728	C-C stretch, proline	Frank 1995	Oleic acid methyl ester
729	Adenine breathing ring	Puppels 1991	
729	Adenine	Mahadevan-Jansen 1996	DNA (Z), RNA(Z)
730		Pilotto 2001	DL-Lactic acid ($C_3H_6O_3$)
742-748	O-P-O	Mahadevan-Jansen 1996	DNA (Z), RNA(Z)
743	in bovine albumin	Kendall C	Sigma Aldrich A2153
746	$\rho(CH_2)$	Barry 1992	Human strateum corneum
748	Thymine	Mahadevan-Jansen 1996	DNA (B)
749	Thymine breathing ring	Puppels 1991	
750	δOCO	Cassanas 1991	Lactic acid
750	Cholesterol	Feld 1995	Carotid artery
759	Tryptophan (amino acid)	Yu 1996	
759	Tryptophan (amino acid)	Nie 1990	Human eye lens
760	Tryptophan (amino acid)	Erckens 1997	Rabbit & human cornea & Rabbit aqueous humour
760	Tryptophan & tyrosine	Erckens 1997	Rabbit lens
760	Tryptophan (amino acid)	Hartman 1973	
760	Tryptophan (amino acid)	Ozaki 1988	

760	Tryptophan (amino acid)	Miura 1995	
761	Glycogen	Kendall C	Sigma Aldrich G0885
762	Collagen	Kendall C	Sigma Aldrich C7774
770	Breathing of aromatic ring of pyrimidine bases (cytosine & thymine)	Mahadevan-Jansen 1996	DNA
777	Thymine	Mahadevan-Jansen 1996	DNA (A), RNA (A)
780	Cytosine	Mahadevan-Jansen 1996	DNA (A), RNA (A)
780	Nnucleotides	Schrader 1995	Breast cancer in mouse
780	Uracil ring	Maquelin 2000	
782	Cytosine ring breathing	Mahadevan-Jansen 1996	DNA (B)
785	O-P-O	Mahadevan-Jansen 1996	DNA (C)
787	Cytosine & uracil	Hartman 1973	
788	Thymine, cytosine, O-P-O	Puppels 1991	DNA
790	ν_s O-P-O	Puppels 1999	DNA
790	Acetone (C-C-C) stretch	Dou 1996	
800		Wang 1993	pyruvate
806-813 (809)	ν_s O-P-O	Mahadevan-Jansen 1996	DNA (A)
811	Nucleotides	Schrader 1995	Breast cancer in mouse
814	ν_s O-P-O	Manfait 2000	DNA
814	ν_s O-P-O	Mahadevan-Jansen 1996	RNA (A)
814	C-C stretch, backbone	Frank 1995	Type I collagen (human placenta)
814	C-C stretch, backbone	Frank 1994a	Collagen
814	C-C stretch, backbone in collagen	Kendall C	Sigma Aldrich C7774
815	Phosphate	Hartman 1973	
816	C-C Proline ring	Fendel 1988	Collagen type I, normal skin dermis
817	C-C stretch, backbone	Frank 1995	Infiltrating ductal carcinoma
817	C-C stretch, backbone	Frank 1994a	Diseased breast tissue
818	Haemoglobin	Mahadevan-Jansen 1995	
818		Mahadevan-Jansen 1998a	Cervix tissue
818	Silica	Mahadevan-Jansen 1998a	Fibre probe on cervix
819	**Tyrosine**	Liu CH 1992a	
820	Structural protein	Manoharan 1998	Breast
825-830	**Tyrosine (amino acid)**	Mahadevan-Jansen 1996	Histones
825-842	O-P-O	Mahadevan-Jansen 1996	DNA (B)
826	in bovine albumin	Kendall C	Sigma Aldrich A2153

827	δ(CCH) aliphatic	Barry 1992	Human strateum corneum
828	Tyrosine (amino acid)	Kendall C	Sigma Aldrich T8909
830	C-COOH stretch	Wang 1993	Lactate
830	C-COOH stretch	Pilotto 2001	DL-Lactic acid ($C_3H_6O_3$) CH_3-CHOH-COOH
830	C-COOH stretch	Wicksted 1995	Lactate
830	Tyrosine (amino acid)	Nie 1990	Human eye lens
830	**Tyrosine (amino acid)**	Mahadevan-Jansen 1996	
830	Tyrosine (amino acid)	Hartman 1973	
830	Tyrosine (amino acid)	Miura 1995	
830	νC-COOH	Cassanas 1991	Lactic acid
832	Tryptophan & tyrosine	Erckens 1997	Rabbit lens
832	Tyrosine	Puppels 1999	
832	Tyrosine	Ozaki 1988	
833	ν_{as} O-P-O	Puppels 1999	DNA
833	**Ribose phosphate**	Greve 1996	
835	ν_{as} O-P-O	Mahadevan-Jansen 1996	DNA (B)
840	Tyrosine (amino acid)	Frank 1994a	
840	Glucose	Chaiken 2000	
840-860	Polysaccharides	Shim 1996	
840-860	Polysaccharides	Gnaidecka 1997a	
840-880	Glucose	Chaiken 2000	Blood
846	Tyrosine (amino acid)	Kendall C	Sigma Aldrich T8909
847	Glucose	Mahadevan-Jansen 1998a	Sigma
849		Frank 1994a	Breast
850	Proline	Liu CH 1992a	
850	**Tyrosine (amino acid)**	Mahadevan-Jansen 1996	
850	Tyrosine (amino acid)	Miura 1995	
850		Kendall C	Bovine albumin Sigma Aldrich A2153
850	δ(CCH) aromatic	Barry 1992	Human strateum corneum
850-3	δ(CCH) aromatic	Edwards 1995	Strateum corneum, Callus, psoriatic plaque
853	Tyrosine (amino acid)	Nie 1990	Human eye lens
853	Tyrosine (amino acid)	Puppels 1999	DNA
853	Glycogen	Kendall C	Sigma Aldrich G0885
854-6	**Tyrosine (amino acid)**	Mahadevan-Jansen 1996	Histones
855	Tyrosine	Ozaki 1988	
855	C-C stretch Proline ring	Frank 1994a	Collagen
855	C-C stretch, proline	Frank 1995	Type I collagen (human placenta)
856	Proline	Nie 1990	Chicken leg bone

856		Mizuno 1994	Polysaccharides in glioma grade III (human brain tissue)
856	CC strectch, COC stretch, 1,4 glycosidic link	Maquelin 2000	
856	C-C stretch collagen backbone & Proline ring	Frank 1994a	Diseased breast tissue
856	C-C stretch, proline	Frank 1995	Infiltrating ductal carcinoma (breast)
856	ν(CC) skeletal vibrations, keratotic	Carter 1998	Healthy human skin dermis
856	C-C stretch collagen backbone & Proline ring	Lucassen 1998	
856	Tryptophan & tyrosine	Erckens 1997	Rabbit lens
856	C-C stretch Proline ring in collagen	Kendall C	Sigma Aldrich C7774
857	Tyrosine	Yu 1996	
858	C-C stretch in elastin	Kendall C	Sigma Aldrich E1625
859	C-C Proline ring	Fendel 1988	Collagen type I, normal skin dermis
860	Collagen	Redd 1993	Fibrocystic human breast tissue
860	Lactate	Erckens 1997	Human aqueous humour
865	Ribose, Tryptophan (amino acid)	Hartman 1973	Protein
866	Lactic acid	Pilotto 2001	DL-Lactic acid ($C_3H_6O_3$) CH_3-CHOH-COOH
868	C-C stretch, hydroxyproline	Frank 1995	Oleic acid methyl ester
870	C-C stretch, hydroxyproline	Frank 1995	Normal breast tissue
870	Proline (amino acid)	Feld 1995	Malignant breast tissue
870		Frank 1994b	Breast
872	C-C stretch of 4-hydroxyproline in collagen	Kendall C	Sigma Aldrich C7774
873	hydroxyproline	Nie 1990	Chicken leg bone
874	C-C stretch, hydroxyproline	Frank 1995	Type I collagen (human placenta)
874	C-C stretch of 4-hydroxyproline	Frank 1994a	Collagen
876	C-C stretch, hydroxyproline	Frank 1995	Infiltrating ductal carcinoma (breast)
876	C-C stretch of 4-hydroxyproline	Frank 1994a	Diseased breast tissue
879	Tryptophan (amino acid)	Nie 1990	Human eye lens
880	Tryptophan (amino acid)	Ozaki 1988	
880	Tryptophan (amino	Miura 1995	

	acid)		
880	Tryptophan (amino acid)	Frank 1994a	
880	Tryptophan (amino acid)	Erckens 1997	Rabbit & human cornea
880	Tryptophan & tyrosine	Erckens 1997	Rabbit lens
880	Tryptophan (amino acid)	Erckens 1997	Rabbit aqueous humour
883	CH_2 rocking,	Edwards 1995	Strateum corneum,
883	$\rho(CH_2)$	Barry 1992	Human strateum corneum
885	Ribose, Tryptophan (amino acid)	Hartman 1973	Protein
890	Structural protein	Manoharan 1998	Breast
890		Frank 1994b	Breast
890-1	CH_2 rocking,	Edwards 1995	Callus, psoriatic plaque
892	CH_2 rocking, collagen hydroxyproline	Lucassen 1998	Skin
893		Kendall C	Bovine albumin Sigma Aldrich A2153
895	DNA backbone	Puppels 1999	DNA
896	Proline	Kendall C	Sigma Aldrich T8449
915	Ribose	Hartman 1973	Protein
917	Deoxyribose (CH_2 deformation)	Mahadevan-Jansen 1996	DNA (B)
920	**Glucose**	Mahadevan-Jansen 1998a	Sigma
920	C-C stretch in elastin	Kendall C	Sigma Aldrich E1625
920	Lactic acid	Pilotto 2001	DL-Lactic acid ($C_3H_6O_3$)
920	C-C stretch Proline ring	Frank 1994a	Diseased breast tissue, collagen
920	C-C Proline ring	Frank 1995	Type I collagen (human placenta) & infiltrating ductal carcinoma (breast)
920	C-C stretch Proline ring in collagen	Kendall C	Sigma Aldrich C7774
921	C-C Proline ring	Fendel 1988	Collagen type I, normal skin dermis
921	C-C stretch Proline ring	Mahadevan-Jansen 1996	Collagen
925	DNA backbone	Puppels 1999	DNA
928	DNA backbone, α helix	Puppels 1991	Protein
928-940	C-C Proline, valine	Mahadevan-Jansen 1998a	
930	Tryptophan (amino acid)	Hartman 1973	Protein
930	rCH_3	Cassanas 1991	Lactic acid
931	CH_3 rocking, collagen proline	Lucassen 1998	Skin
931	$\rho(CH_3)$, ρ(C-C) α-helix	Barry 1992	Human strateum corneum
932	Skeletal C-C, α helix	Puppels 1999	DNA
932-5	CH_3 rocking, C-C	Edwards 1995	Strateum corneum, Callus,

	stretch α helix keratin		psoriatic plaque
934	C-C stretch, backbone	Frank 1994a	Collagen
934	C-C Proline ring	Frank 1995	Type I collagen (human placenta)
935-945	(C-C) skeletal vibrations, α helix	Mahadevan-Jansen 1998	α-helix protein secondary structure
935	Collagen	Redd 1993	Fibrocystic human breast tissue
936	C-C stretch backbone, hydroxyproline & collagen	Caspers 1998	Skin
936	C-C stretch, backbone in collagen	Kendall C	Sigma Aldrich C7774
937	Glycogen	Kendall C	Sigma Aldrich G0885
937	C-C stretch, backbone	Frank 1994a	Diseased breast tissue
937	C-C Proline ring	Frank 1995	Infiltrating ductal carcinoma (breast)
937	α-helix	Schrader 1995	nails
938	ν(C-C) skeletal vibrations, keratotic	Carter 1998	Healthy human skin dermis
938	Peptide backbone stretch	Yu 1996	
938	C-C backbone	Mahadevan-Jansen 1996	Collagen
939	C-C-N stretching	Fredericks 1995	Bovine Serum albumin
940	C-C-N stretching in bovine albumin	Kendall C	Sigma Aldrich A2153
940	ν(C-C) of proline and valine	Gniakeda 1997	Normal human skin
940	Triple helix vibrations	Fendel 1988	Collagen type I, normal skin dermis
941	C-C stretch	Ozaki 1988	Protein
944	ν(C-C)	Baraga 1992a	Asian skin
950	4-hydroxyproline	Feld 1995	Malignant breast tissue
955	Hydroxyapatite	Manoharan 1992	
956	Carotenoids	Mizuno 1994	Human brain tissue, acoustic neuroma
956	$\rho(CH_3)$, δ(CCH) olefinic	Barry 1992	Human strateum corneum
960	Calcification - hydroxyapatite	Mizuno 1994	Human brain tissue, central neurocytoma
960	Calcification - hydroxyapatite	Clarke 1987	Aortic valve leaflets & coronary artery segments
960	P-O symmetric stretch	Nie 1990	Chicken leg bone
960	P-O symmetric stretch	Baraga 1992a	Atherosclerotic plaque calcified salts
960	Hydroxyapatite, P-O symmetric stretch	Yu 1996	Calcified plaque
960	Cholesterol	Keller 1994	
961	Apatite	Nie 1990	Human tooth enamel
961	$Y_s(PO)$ of PO_4^{3-} in apatite	Wentrup-Byrne 1997a	Human tooth
961	Phosphate groups	Rava 1991	Calcified atherosclerotic plaque
966	Hydroxyapatite	Clarke 1987	Calcified plaque

966	Desmosine & isodesmosine (amino acids)	Manoharan 1996	Elastin
966	Triple helix vibrations	Fendel 1988	Collagen type I, normal skin dermis
968	C-OH	Manfait 2000	
972	=C-H out of plane deformation	Frank 1994a	Breast tissue
972	C-C Proline ring	Frank 1995	Normal breast tissue, Oleic acid methyl ester
972	=C-H out of plane deformation	Frank 1994b	Breast
975	Ribose	Hartman 1973	Protein
975	Deoxyribose (CH_2 deformation)	Mahadevan Jansen 1996	DNA (B)
978	Symmetric phosphate ion stretching	Mahadevan Jansen A	Phospholipids, glucose-1-phosphate
978	Symmetric phosphate ion stretching	Mahadevan Jansen A	Human cervix
978	Phosphorylated proteins and nucleic acids	Mahadevan Jansen 1995	Human cervical biopsies
982	CH_2 rocking	Edwards 1995	Strateum corneum
1000-1100	Glucose	Chaiken 2000	Blood
1000-1150	C-C skeletal vibrations	Mahadevan Jansen 1996	Phospholipid membrane, hydrophobic chains
1000-1250	Phosphate groups	Sajid J 1997	DMPC (dimyristoylphosphatidycholine), a typical lipid, brain
1000-1200	C-C stretch – lipids	Carter 1998	Healthy human skin
1000	Phenylalanine in bovine Albumin	Kendall C	Sigma Aldrich A2153
1001	Phenylalanine(amino acid)	Kendall C	Sigma Aldrich T8324
1001	Phenylalanine(amino acid)	Feld 1995	Malignant breast tissue
1001		Lieber 2000	Ovary
1001-1004	Phenyl ring breathing mode	Shim 1996	
1002	υ(C-C) aromatic ring	Edwards 1995	Strateum corneum, Callus, psoriatic plaque
1002	(C-C) skeletal vibrations, β sheet	Mahadevan-Jansen 1996	β-sheet protein secondary structure
1002	Phenylalanine(amino acid)	Yu 1996	
1002	Phenylalanine(amino acid)	Frank 1994a	
1002	Phenylalanine(amino acid)	Frank 1994a	Collagen
1002	Hydroxyproline, tyrosine	Frank 1995	Type I collagen (human placenta)

1002	ν(CC) aromatic ring	Barry 1992	Human strateum corneum
1003	ν(CC) aromatic ring stretch of phenylalanine residue in keratin	Carter 1998	Healthy human skin
1003	Phenylalanine(amino acid) breathing mode	Mizuno 1994	Human brain tissue, protein
1003	C-N stretch	Erckens 1997	Urea
1003	C-N stretch of urea	Wicksted 1995	Urea
1003	C-N stretch of urea	Lucassen 1998	
1004	Phenylalanine(amino acid)	Erckens 1997	Rabbit lens, aqueous humour, cornea & human cornea
1004	Aromatic ring (breathing mode)	Gniakeda 1997	Normal human skin
1004	Phenylalanine(amino acid)	Maquelin 2000	
1004	Phenylalanine(amino acid)	Puppels 1999	
1004	Phenylalanine(amino acid)	Puppels 1991	
1004	Phenylalanine(amino acid)	Frank 1994a	Diseased breast tissue
1004	Phenylalanine(amino acid)	Frank 1995	Infiltrating ductal carcinoma (breast)
1004	Phenylalanine(amino acid) + Trp aromatic ring	Fredericks 1995	Bovine Serum albumin
1004	Carotenoid	Redd 1993a	Beta carotene, Human breast carcinoma
1004		Kendall C	Sigma Aldrich C7774

1004	P-O symmetric stretch	Nie 1990	Chicken leg bone
1005		Redd 1993a	Normal human breast tissue
1005	Beta carotene	Frank 1995	Breast
1005		Redd 1993b	Human breast tissue Renal cell carcinoma (1003)
1005	Phenylalanine(amino acid)	Hartman 1973	Protein
1006	C-N stretch of urea	Wicksted 1995	Urea, rabbit aqueous humour
1006	Phenylalanine, amino acid	Mahadevan-Jansen 1998	Collagen, histones
1006	Phenylalanine, amino acid	Ozaki 1988	Protein
1006	Carotenoids	Mizuno 1994	Human brain tissue, acoustic neuroma
1008	C-N stretch	Wang 1993	Urea NH_2-CO-NH_2
1008	Carotenoids	Redd 1993b	Carotenoids in normal colon
1010	C-N stretch	Erckens 1997	Human aqueous humour
1013	Urea N-C-N stretch	Dou 1996	
1014	Tryptophan (amino acid)	Mahadevan-Jansen 1998	
1015	Tryptophan (amino acid)	Hartman 1973	Protein
1016	Tryptophan – amino acid	Manoharan 1995	DNA in water
1017	DNA backbone C-O stretch	Puppels 1999	
1030	Collagen	Kendall C	Sigma Aldrich C7774
1031	Proline	Yu 1996	
1031	ν(CC) skeletal cis	Barry 1992	Human strateum corneum

	conformation		
1031-32	υ(C-C) keratin	Edwards 1995	Strateum corneum, Callus, psoriatic plaque
1032	Phenylalanine(amino acid)	Erckens 1997	Rabbit & human cornea Rabbit lens Rabbit aqueous humour
1032	Phenylalanine(amino acid)	Puppels 1999	
1032	proline	Frank 1995	Type I collagen (human placenta)
1034		Lieber 2000	Ovary
1035	Ribose, Phenylalanine(amino acid)	Hartman 1973	Protein
1035	C-C skeletal cis	Lucassen 1998	
1043	Proline	Frank 1995	Infiltrating ductal carcinoma (breast)
1043	Formalin artefact	Frank 1994a	breast tissue
1046	Lactic acid	Pilotto 2001	DL-Lactic acid ($C_3H_6O_3$) CH_3-CHOH-COOH
1048	Glycogen	Kendall C	Sigma Aldrich G0885
1050	νC-CH_3	Cassanas 1991	Lactic acid
1050	CO stretch, CCC trans skeletal stretch	Carter 1998	Healthy human skin dermis
1057	DNA backbone C-O stretch	Puppels 1999	
1060	δOD	Cassanas 1991	Methyl lactate
1061	Lipid	Caspers 1998	Strateum corneum
1062	υ(C-C) skeletal trans conformation lipid	Edwards 1995	Strateum corneum
1062	ν(CC) skeletal trans conformation	Barry 1992	Human strateum corneum
1064	C-C stretch	Sajid 1997	
1065	C-O stretch & C-O-C sym. stretch - phospholipids	Mizuno 1994	Human brain tissue
1066	C-C stretch	Frank 1994b	Breast
1066	C-C stretch	Frank 1994a	breast tissue
1066	Proline	Frank 1995	Normal breast tissue
1066	C-O, C-O-C stretch	Ozaki 1988	Phospholipids
1066	Lipid	Gnaidecka 1998	
1066		Lieber 2000	Ovary
1067	Proline	Frank 1995	Oleic acid methyl ester
1069	Hydroxyapatite shifted due to environment	Mahadevan Jansen A	Human cervix
1070	Symmetric phosphate ion stretching	Mahadevan Jansen A	Glucose -1-phosphate, collagen
1070	Symmetric phosphate ion stretching	Mahadevan Jansen A	Human cervix
1070	Collagen/elastin	Mahadevan Jansen 1995	

1070		Utzinger 2001	Cervix
1070	Phosphate / carbonate	Baraga 1992a	Atherosclerotic plaque
1070	Phosphate / carbonate	Yu 1996	
1071	apatite	Nie 1990	Human tooth enamel
1071	$Y_{as}(PO)$	Wentrup-Byrne 1997a	Human tooth
1072	P-O asymmetric stretch	Nie 1990	Chicken leg bone
1074		Manoharan 1994	Adipose tissue
1074	Triglycerides	Baraga 1992a	Adipose tissue from human aorta
1078	C-N stretch	Alfano 1991	Benign breast tissue
1078-1090	C-C, C-O stretch in lipids. C-C, PO_2 stretch in nucleic acids	Shim 1996	
1079	C-C stretch	Frank 1994a	Breast tissue
1079		Frank 1995	Normal breast tissue
1079	C-C stretch	Frank 1994b	Breast
1080	C-C stretch & PO2- sym. stretch - phospholipids	Mizuno 1994	Human brain tissue
1082	υ(C-C) skeletal random conformation lipid	Edwards 1995	Strateum corneum
1082		Frank 1995	Oleic acid methyl ester
1082	PO2- vibration in phospholipids and nucleic acids	Gniakeda 1997	Normal human skin
1082		Redd 1993a	Normal human breast tissue, Lipid (TPE)
1082	Lipid	Redd 1993	Human breast tissue
1082	Lipid	Lucassen 1998	
1082		Gnaidecka 1998	Protein
1082	ν(CC) skeletal random conformation	Barry 1992	Human strateum corneum
1083	Glycogen	Kendall C	Sigma Aldrich G0885
1084	Lactic acid	Pilotto 2001	DL-Lactic acid ($C_3H_6O_3$) CH_3-CHOH-COOH
1085	Calcium carbonate	Wentrup-Byrne 1995	Cholesterol
1085	C-C stretch	Yu 1996	Lipid
1085	Phenylalanine(amino acid)	Hartman 1973	Protein
1085	Phosopholipids	Feld 1995	Malignant breast tissue
1086	C-C stretch, PO_2 stretch	Ozaki 1992	Phospholipids
1087	Symmetric stretching of phosphate groups of the polynucleotide chain	Sajid 1997	DNA
1090	νCO	Cassanas 1991	Lactic acid
1090	PO^-_2	Mahadevan-Jansen 1998	DNA (C)

1091	PO^-_2	Mahadevan-Jansen 1998	DNA (B)
1094	DNA O-P-O	Puppels 1999	
1094	DNA O-P-O	Puppels 1991	
1095	ν_s of two ionised phosphate oxygens in the diphosphate ester	Mahadevan-Jansen 1998	DNA (B)
1095	PO^-_2	Mahadevan-Jansen 1998	DNA (Z), RNA(Z)
1095	CC stretch, COC deformation 1-4 glycosidic link	Maquelin 2000	
1099	PO^-_2	Mahadevan-Jansen 1998	DNA (A), RNA(A)
1100	Formalin	Keller 1994	Formalin
1100	PO_2 stretch	Hartman 1973	Protein
1100	ν_s of two ionised phosphate oxygens in the diphosphate ester	Mahadevan-Jansen 1998	DNA (A)
1100	Lipid disorganised	Gnaidecka 1998	
1100-1110	(C-C) skeletal vibrations	Mahadevan-Jansen 1998	Unordered protein secondary structure
1104	C-C stretch lipid	Yu 1996	
1108	Desmosine & isodesmosine (amino acids)	Manoharan 1996	Elastin
1118		Frank 1995	Normal breast tissue
1119		Frank 1995	Oleic acid methyl ester
1119	C-C stretch	Frank 1994a	Breast tissue
1119	C-C stretch	Frank 1994b	Breast
1122	C-C stretch lipid	Yu 1996	
1123	Glycogen	Kendall C	Sigma Aldrich G0885
1123	**Glucose**	Mahadevan-Jansen 1998a	Sigma
1125		Hartman 1973	
1125		Frank 1995	Infiltrating ductal carcinoma (breast)
1126	C-N stretch	Puppels 1999	Protein
1126	C-C stretch - phospholipids	Mizuno 1994	Human brain tissue
1126	ν(CC) skeletal trans conformation	Barry 1992	Human strateum corneum
1127	υ(C-C) skeletal trans conformation lipid & keratin	Edwards 1995	Strateum corneum, Callus, psoriatic plaque
1127	Lipids	Caspers 1998	Strateum corneum
1127		Frank 1995	Type I collagen (human placenta)
1128	C-C stretch	Sajid 1997	
1128	Heme vibrational mode	Shim 2000	

1129	C-C stretch, lipid	Carter 1998	Healthy human skin strateum corneum & epidermal membrane
1130	Trans C-C stretch – phospholipids	Mizuno 1994	Human brain tissue, glioma grade III
1130	Lipid	Carter 1998	Healthy human skin strateum corneum & epidermal membrane
1130	C-C stretch, lipid	Gnaidecka 1998	
1130	C-O stretch glucose	Dou 1996	
1130	Low density lipoproteins	Yu 1996	
1131	Lactic acid	Pilotto 2001	DL-Lactic acid ($C_3H_6O_3$)
1135	νCO, rCH_3	Cassanas 1991	Lactic acid
1150	Carotenoid	Brennan 1997a	Human artery
1150	C=C Carotenoid	Keller 1994	Food
1150	Cholesterol	Feld 1995	Carotid artery
1155	C-C stretch, $\delta(COH)$	Lucassen 1998	
1155	$\nu(CC)$, $\delta(COH)$	Barry 1992	Human strateum corneum
1156	CN stretch	Fredericks 1995	Bovine Serum albumin
1156	Carotenoid	Frank 1994a	
1156	Carotenoid	Redd 1993a	Human breast carcinoma, Beta carotene
1157		Redd 1993a	Normal human breast tissue
1157	Carotenoid	Redd 1993b	Human breast tissue Renal cell carcinoma (1155)
1157	Carotenoid	Mizuno 1994	Human brain tissue, acoustic neurinoma, beta carotene
1158	Carotenoid	Feld 1995	Carotid artery
1158	**Carotenoid**	Redd 1993b	Carotenoids in normal colon
1158	**NH_2 rocking vibration**	Wicksted 1995	Urea
1159	C-N	Siebinga 1992	Protein in eye lens
1160	Carotenoid	Larrson 1974	Blood plasma
1162	Ribose	Hartman 1973	
1166		Frank 1995	Type I collagen (human placenta)
1167		Frank 1995	Infiltrating ductal carcinoma (breast)
1172	$\nu(CC)$	Barry 1992	Human strateum corneum

1175	C-O stretching	Mahadevan 1995	Human cervical biopsies
1176	Tyrosine, Phenylalanine	Puppels 1999	Protein
1180		Utzinger 2001	Cervix
1180	Tyrosine	Manoharan 1998	Breast
1180	Tyrosine	Miura 1995	
1180	Cytosine, guanine, adenine	Hartman 1973	
1197	Carotenoid	Frank 1994a	
1200-1700	Collagen	Wentrup-Byrne 1997a	Dentine
1205	Tyrosine + Phenylalanine	Kendall C	Bovine albumin, Sigma Aldrich A2153
1206	4-hydroxyproline (amino acid), tyrosine	Frank 1994a	Diseased breast tissue
1206	4-hydroxyproline (amino acid)	Frank 1994a	Collagen
1206	Hydroxyproline, tyrosine	Frank 1995	Type I collagen (human placenta) & infiltrating ductal carcinoma (breast)
1207	Tyrosine	Nie 1990	Human eye lens
1207	Tyrosine + Phenylalanine (amino acid)	Fredericks 1995	Bovine Serum albumin
1207		Lieber 2000	Ovary
1208	Thymine	Mahadevan-Jansen 1998	DNA (B)
1210	hydroxyproline	Nie 1990	Chicken leg bone
1210		Utzinger 2001	Cervix
1210	Tryptophan, phenylalanine	Hartman 1973	
1211	Tyrosine, Phenylalanine, Thymine	Puppels 1999	Protein
1226-1243	Amide III - ν(C-N)	Miura 1995	β pleated sheet protein secondary structure in β-Poly-L-alanine
1227	Heme vibrational mode	Shim 2000	
1227-1247	Amide III (C-N stretch, N-H in plane bending) β-sheet	Mahadevan-Jansen 1998	β-sheet protein secondary structure
1230	Uracil in RNA	Yazdi 1999	Cultured breast cells
1230-1240	Amide III β-sheet	Carey 1982	
1230-1245	Amide III - ν(C-N)	Miura 1995	β pleated sheet protein secondary structure in β-Poly-L-glutamate
1234	Antisymmetric stretching of phosphate groups of the polynucleotide chain	Sajid 1997	DNA
1235-1270	Amide III (C-N stretch, N-H in plane bending) unordered	Mahadevan-Jansen 1998	
1237	Amide III	Nie 1990	Human eye lens
1238	Amide III, random coil	Erckens 1997	Rabbit & human cornea

1238	Amide III in elastin	Kendall C	Sigma Aldrich E1625
1238	Cytosine, uracil, Amide III	Hartman 1973	
1239	Thymine	Mahadevan-Jansen 1998	DNA (A), RNA (A)
1240	Amide III - ν(C-N)	Miura 1995	β pleated sheet protein secondary structure in β-Poly-L-lysine
1240	Vibration of pyrimidine bases (cytosine & thymine)	Mahadevan-Jansen 1996	DNA
1240	Amide III ν(C-N)	Alfano 1991	Benign breast tumour
1240	Amide III	Frank 1994a	
1240	Amide III in collagen	Kendall C	Sigma Aldrich C7774
1240	Amide III - ν(C-N)	Liu CH 1992a	Uterus cancer
1240	Amide III	Keller 1994	Caractous lens
1240	Thymine	Puppels 1999	Protein
1240-1260	Amide III unordered	Carey 1982	
1243	Amide III	Keller 1994	Liver - collagen
1243	Amide III	Nie 1990	Chicken leg bone
1243	Amide III	Erckens 1997	Rabbit lens
1243-48	Amide III - ν(C-N)	Miura 1995	irregular protein secondary structure in β-Poly-L-lysine pH4
1244	$\delta(CH_2)$ wagging, ν(CN) amide III disordered	Barry 1992	Human strateum corneum
1245	νCO, δOH	Cassanas 1991	Lactic acid
1245	Amide III, random coil	Mizuno 1994	Human brain tissue, glioma grade III
1245	Keratotic	Carter 1998	Healthy human skin dermis
1245		Utzinger 2001	Cervix
1245	Amide III: keratin, disordered collagen	Lucassen 1998	
1245-1305	Amide III (C-N stretch, N-H in plane bending)	Mahadevan-Jansen 1998	Histones
1246	Amide III	Fredericks 1995	Bovine Serum albumin
1246	Amide III ν(C-N)	Mahadevan 1995	Collagen & DNA
1246	Amide III ν(C-N)	Mahadevan 1995	Human cervix precancer
1246	Amide III (C-N stretching vibrations)	Mahadevan 1995	Human cervical biopsies
1246	Amide III (C-N stretching vibrations)	Liu CH 1992a	
1246	Amide III (C-N stretching vibrations)	Gnaidecka 1998	Protein
1247	Amide III	Frank 1995	Type I collagen (human placenta) & infiltrating ductal carcinoma (breast)
1247	Amide III	Frank 1994a	Diseased breast tissue
1247		Keller 1994	Neutrogena sarcoma (brain) - collagen
1247	Amide III	Frank 1994a	Collagen

1247	Amide III - ν(C-N)	Liu CH 1992a	Endometrium cancer
1247	Collagen	Redd 1993	Fibrocystic human breast tissue
1248	Amide III	Manoharan 1998	Breast
1248	PO2- vibration in phospholipids and nucleic acids	Gniakeda 1997	Normal human skin
1248	Amide III (C-N stretch, N-H in plane bending)	Mahadevan-Jansen 1998	Collagen
1249	Amide III - ν(C-N)	Miura 1995	irregular protein secondary structure in β-Poly-L-glutamate pH 11
1250	Cytosine, uracil, Amide III	Hartman 1973	
1250	Amide III	Brennan 1997a	Human artery
1250	Amide III	Ozaki 1992	
1250	Cytosine	Mahadevan-Jansen 1998	DNA (B)
1250	Amide III	Fendel 1988	Collagen type I, normal skin dermis
1252	Amide III	Baraga 1992b	Aorta
1253	Amide III random coil protein	Schrader 1995	Breast cancer in mouse
1254	Adenine	Puppels 1991	Protein
1254	Amide III (C-N stretch, N-H in plane bending)	Mahadevan-Jansen 1998	Elastin
1255	Cytosine	Puppels 1999	Protein
1256	Glycogen	Kendall C	Sigma Aldrich G0885
1258-1304	Amide III (C-N stretch, N-H in plane bending)	Mahadevan-Jansen 1998	α-helix protein secondary structure
1260-1310	Amide III (C-N stretch, N-H in plane bending)	Miura 1995	α-helix protein secondary structure
1259	Amide III	Frank 1994a	Silicone gel
1260	Tyrosine	Miura 1995	Unordered protein secondary structure
1260	Structural protein	Manoharan 1998	Breast
1260	Symmetric CH_3 deformation	Frank 1994a	Silicone gel
1260	Amide III	Nie 1990	Chicken leg bone
1260	Amide III	Feld 1995	Malignant breast tissue
1260-1280	Amide III	Fredericks 1995	Bovine Serum albumin
1261	Lipid	Manoharan 1994	
1262	Amide III - ν(C-N)	Liu CH 1992a	Benign or normal cervix
1262	Amide III - ν(C-N)	Liu CH 1992a	Benign or normal uterus
1262	Amide III - ν(C-N)	Liu CH 1992a	Benign or normal endometrium
1262	Amide III - ν(C-N)	Liu CH 1992a	Benign or normal ovary
1264	Amide III in collagen	Kendall C	Sigma Aldrich C7774
1265-1300	Amide III (C-N stretch, N-H in plane bending)	Carey 1982	α-helix protein secondary structure

1265-1348	Amide III - ν(C-N)	Miura 1995	α-helix protein secondary structure in α-Poly-L-alanine
1265	=C-H in plane deformation	Frank 1994b	Breast
1265	=C-H in plane deformation	Frank 1994a	breast tissue
1265	Amide III	Frank 1995	Normal breast tissue
1267	=C-H in plane deformation	Keller 1994	
1267	Amide III	Frank 1995	Infiltrating ductal carcinoma (breast)
1267	δ (=C-H)	Mahadevan-Jansen 1998	Phospholipid membrane
1267	δ (=C-H)	Keller 1994	Coronary Artery, unsaturated fatty acids
1267	Amide III	Frank 1994a	Lymph node
1267	Amide III	Frank 1994a	Diseased breast tissue
1267	Amide III	Frank 1994a	Collagen
1268	Amide III	Frank 1995	Oleic acid methyl ester
1268	Amide III - ν(C-N) and δ(NH) in bovine albumin	Kendall C	Sigma Aldrich A2153
1269	Amide III	Frank 1995	Type I collagen (human placenta)
1269	Amide III α-helix	Mizuno 1994	Human brain tissue
1270		Utzinger 2001	Cervix
1270	Amide III - ν(C-N)	Liu CH 1992a	Endometrium cancer
1271	Amide III - ν(C-N) and δ(NH)	Gniakeda 1997	Normal human skin
1271	Amide III (C-N stretch, N-H in plane bending)	Mahadevan-Jansen 1998	Collagen
1273	Amide III	Fendel 1988	Collagen type I, normal skin dermis
1274	δ(NH) wagging, ν(CN) amide III α-helix	Barry 1992	Human strateum corneum
1280	Amide III	Clarke 1993	Phospholipid membrane
1290	Amide III - ν(C-N)	Miura 1995	α-helix protein secondary structure in α-Poly-L-glutamate
1295	Amide III - ν(C-N)	Miura 1995	α-helix protein secondary structure in α-Poly-L-lysine
1296	$\delta(CH_2)$	Barry 1992	Human strateum corneum
1296	Keratotic	Carter 1998	Healthy human skin dermis
1296	$\delta(CH_2)$	Edwards 1995	Strateum corneum
1297	Lipid	Carter 1998	Healthy human skin strateum corneum & epidermal membrane
1300	ν(C-C) ν(C-N)	Alfano 1991	Benign breast tissue
1300	Amide III	Sajid 1997	Bovine insulin
1300	C-H bending	Liu CH 1992a	Lipid
1300	Phospholipids - CH_2	Mizuno 1994	Human brain tissue

	twist and wagging		
1300	Lipids – fatty acids	Manoharan 1998	Breast
1300	δCH	Cassanas 1991	Lactic acid
1300	Adenine , cytosine	Hartman 1973	
1302	Lipid	Redd 1993a	Lipid (TPE)
1302	Lipid	Redd 1993b	Human breast tissue
1302		Redd 1993a	Normal human breast tissue
1302	Lipid	Redd 1993	Human breast tissue
1303	CH_2 twisting	Frank 1994b	Breast
1303	Triglycerides	Baraga 1992a	Adipose tissue from human aorta
1303	Adenine	Puppels G	
1303	δ CH_2	Mahadevan-Jansen 1998	Phospholipid membrane
1303	CH_2 twisting	Frank 1994a	Normal breast tissue
1303	CH_3CH_2 twisting	Frank 1994a	Diseased breast tissue
1303	CH_3CH_2 twisting	Frank 1995	Normal breast tissue & infiltrating ductal carcinoma
1304	CH_3CH_2 twisting	Frank 1995	Oleic acid methyl ester
1306	Lipid	Redd 1993b	Human colon
1309	CH_2 twisting & wagging in lipids	Gniakeda 1997	Normal human skin
1310-16	Δ(CH_2)	Edwards 1995	Callus, psoriatic plaque
1316	Histidine	Kendall C	Sigma Aldrich T8776
1316	Guanine	Mahadevan-Jansen 1998	DNA (Z), RNA(Z)
1317	CH_2 twisting	Redd 1993a	Skin
1318	Guanine	Mahadevan-Jansen 1998	DNA (A), RNA (A)
1319	CH_3CH_2 twisting	Frank 1995	Type I collagen (human placenta)
1319	CH_3CH_2 twisting	Frank 1994a	Collagen
1320	Guanine	Hartman 1973	
1321	in bovine albumin	Kendall C	Sigma Aldrich A2153
1322	C-H	Siebinga 1992	
1325	Tryptophan (amino acid) ring vibrations	Liu 1992a	
1325	Nucleic acid ring vibrations	Feld 1995	
1330	Tryptophan (amino acid) ν(C-C)	Liu 1992a	Cervix cancer
1330	Tryptophan (amino acid) ν(C-C)	Liu 1992a	Uterus cancer
1330	Tryptophan (amino acid) ν(C-C)	Liu 1992a	Ovary cancer
1330	C-H	Mahadevan Jansen 1998a	Nucleic acid bases & DNA, phospholipids
1330	C-H	Mahadevan Jansen	Human cervix precancer

		1998a	
1330		Utzinger 2001	Cervix
1330	DNA	Yazdi 1999	Cultured breast cells
1330	δCH	Cassanas 1991	Lactic acid
1333	Glycogen	Kendall C	Sigma Aldrich G0885
1333	Guanine	Mahadevan Jansen 1998	DNA (B)
1334	CH deformation	Maquelin 2000	
1335	Nucleic acids	Manoharan 1995	Colon
1335	Adenine	Mahadevan Jansen 1998	DNA (A), RNA (A)
1337	Nucleic acid, purine bases (adenine, guanine)	Boustany 1999	Colon
1337	Nucleic acid, purine bases (adenine, guanine)	Fodor 1985	
1337	Purine bases (adenine, guanine)	Manoharan 1995	DNA in water
1337	**Adenylates**	Boustany 1999	Colon mucosa
1338	**Tryptophan, amino acid**	Mahadevan Jansen 1998	
1339	Adenine	Mahadevan Jansen 1998	DNA (B)
1339-41		Edwards 1995	Strateum corneum, Callus, psoriatic plaque
1340	Tryptophan (amino acid)	Erckens 1997	Rabbit & human cornea
1340	Tryptophan (amino acid)	Erckens 1997	Rabbit aqueous humour
1340	Nucleic acid	Feld 1995	Colon adenocarcinoma
1343	CH_3CH_2 wagging	Frank 1994a	Diseased breast tissue
1343	CH_3CH_2 wagging	Frank 1994a	Collagen
1343	CH_3CH_2 wag	Frank 1995	Type I collagen (human placenta) & infiltrating ductal carcinoma (breast)
1343		Wicksted 1995	Rabbit aqueous humour
1343	**Adenine**	Hartman 1973	
1350	**Glucose**	Mahadevan-Jansen 1998a	Sigma
1358		Redd 1993	Normal renal parenchyma & renal cell carcinoma
1359		Redd 1993	Hepatocellular carcinoma
1360		Redd 1993	Normal hepatic parenchyma
1360		Redd 1993a	Myoglobin
1360		Erckens 1997	Human aqueous humour
1361	**Tryptophan**	Mahadevan-Jansen 1998	
1365	Guanine, tryptophan	Hartman 1973	
1372	Lipid	Redd 1993	Human colon
1375		Redd 1993a	Myoglobin

1376	Thymine, guanine, adenine	Puppels 1991	
1377	Glycogen	Kendall C	Sigma Aldrich G0885
1380	δCH_3 δOH	Cassanas 1991	Lactic acid
1385	$\delta(CH_3)$ symm	Barry 1992	Human strateum corneum
1400	Uracil, adenine	Hartman 1973	
1400		Utzinger 2001	Cervix
1401	Symmetric CH_3 bending in proteins	Mahadevan 1995	
1410	δOH	Cassanas 1991	Methyl lactate
1412	Antisymmetric CH_3 deformation	Frank 1994a	Silicone gel
1420	δOH, νCO	Cassanas 1991	Lactic acid
1421	$\delta(CH_3)$	Barry 1992	Human strateum corneum
1421	Guanine, adenine	Puppels 1991	
1438	$\delta(CH_2)$ scissoring	Barry 1992	Human strateum corneum
1438	CH_2 deformation	Shim 1996	
1439	CH_2 scissoring deformation	Frank 1994a	breast tissue
1439	CH_3, CH_2 deformation	Frank 1995	Normal breast tissue
1439	CH_2 deformation	McCreery 1995	Human breast biopsy
1439	CH_2 deformation due to lipids and proteins	Mizuno 1994	Human brain tissue
1439	CH_2 scissoring deformation	Frank 1994b	Breast
1440	Lipid	Manohran 1994	
1441	CH_2 bending	Feld 1995	Fibrous atherosclerotic plaque
1441	Lipid	Keller 1994	Liver
1442	CH_3, CH_2 deformation	Frank 1995	Oleic acid methyl ester
1442	Lipid	Redd 1993b	Human breast tissue Colon tissue
1442		Redd 1993a	Normal human breast tissue
1442	Lipids – fatty acids	Manoharan 1998	Normal breast tissue
1443	elastin	Kendall C	Sigma Aldrich E1625
1444	Lipid	Redd 1993a	Lipid (TPE)
1444	Triglycerides	Baraga 1992a	Adipose tissue from human aorta
1445	$\delta(CH_2)$ or $\delta(CH_3)$	Liu CH 1992a	Cervix cancer
1445	$\delta(CH_2)$ or $\delta(CH_3)$	Liu CH 1992a	Uterus cancer
1445	$\delta(CH_2)$ or $\delta(CH_3)$	Liu CH 1992a	Benign or normal cervix
1445	$\delta(CH_2)$ or $\delta(CH_3)$	Liu CH 1992a	Benign or normal endometrium

1445	$\delta(CH_2)$ or $\delta(CH_3)$	Liu CH 1992a	Benign or normal ovary
1445	$\delta(CH_2)$ or $\delta(CH_3)$	Alfano 1991	Human breast tissue. Benign and Malignant tumours
1445	CH_2 deformation	Frank 1994a	breast tissue
1445	CH_2 bending mode	Manoharan 1998	Normal breast tissue
1445	CH_3CH_2 deformation in collagen	Kendall C	Sigma Aldrich C7774
1447	CH_3CH_2 bending modes in bovine albumin	Kendall C	Sigma Aldrich A2153
1448	CH_2 deformation	Nie 1990	Chicken leg bone
1448	Deoxyribose	Mahadevan-Jansen 1998	DNA (B)
1448-9	$\Delta(CH_2)$ scissoring	Edwards 1995	Strateum corneum, Callus, psoriatic plaque
1449	CH_2 deformation	Frank 1994a	Lymph node
1450	Glucose	Chaiken 2000	Blood
1450	CH bending	Erckens 1997	Rabbit & human cornea
1450	CH bending	Erckens 1997	Rabbit aqueous humour
1449	CH_3CH_2 bending modes	Fredericks 1995	Bovine Serum albumin
1450	CH_3CH_2 deformation	Frank 1994a	Diseased breast tissue
1450	CH_2 bending	Brennan 1995	Human artery
1450	CH_2 bending mode	Manoharan 1998	Diseased breast tissue
1450	$\delta(CH_2)$ or $\delta(CH_3)$	Liu CH 1992a	Endometrium cancer
1450		Liu CH 1992a	Elastin & collagen
1450	CH_3, CH_2 deformation	Frank 1995	Infiltrating ductal carcinoma
1451	C-H bend	Baraga 1992a	Normal human aorta
1451	CH_3, CH_2 deformation	Frank 1995	Type I collagen (human placenta)
1451	CH_3CH_2 deformation	Frank 1994a	Collagen
1451	CH_2 bending	Ozaki 1988	
1451-1454	CH_2 bending	Mahadevan Jansen 1998a	Histones
1452	Structural protein	Manoharan 1998	Breast
1452	$\delta(CH_2)$ scissoring in lipids & $\delta(CH_2)$ $\delta(CH_3)$ in proteins	Gniakeda 1997	Normal human skin
1452	CH_2 bending	Feld 1995	Malignant breast tissue
1452	CH_2 in plane bending	Rava 1991	Normal aorta
1453	$\delta(CH_2)$ or $\delta(CH_3)$	Liu CH 1992a	Ovary cancer
1453	$\delta(CH_2)$ or $\delta(CH_3)$	Liu CH 1992a	Benign or normal uterus
1453	C-H bending modes	Baraga 1992b	Aorta
1454	CH_3 bending CH_2 scissors	Mahadevan Jansen 1998a	Elastin & collagen & phospholipids

1454	CH_3 bending CH_2 scissors	Mahadevan Jansen 1998a	Human cervix
1454	CH_3 asymmetric bending of proteins	Mahadevan 1995	
1454		Utzinger 2001	Cervix
1455	δCH_3	Cassanas 1991	Lactic acid
1455	Glycogen	Kendall C	Sigma Aldrich G0885
1455	CH_2 deformation	Frank 1994b	Breast
1456	CH_3 bending in elastin	Kendall C	Sigma Aldrich E1625
1456		Lieber 2000	Ovary
1457		Pilotto 2001	DL-Lactic acid ($C_3H_6O_3$) CH_3-CHOH-COOH
1458	Nucleic acid	Feld 1995	Colon adenocarcinoma
1460	Pentose sugar vibration due to δ CH_2	Mahadevan-Jansen 1998	DNA
1462	Deoxyribose	Mahadevan-Jansen 1998	DNA (B)
1475	δCH_3	Cassanas 1991	Lactic acid
1480	Vibration of purine bases (adenine & guanine)	Mahadevan-Jansen 1996	DNA
1480	DNA	Yazdi 1999	Cultured breast cells
1485	Nucleic acids	Manoharan 1995	Colon
1485	Purine bases	Manoharan 1995	DNA in water
1485	Nucleic acid, purine bases (adenine, guanine)	Boustany 1999	Colon
1485	Nucleic acid, purine bases (adenine, guanine)	Fodor 1985	
1487	Nucleic acid	Manoharan 1995	Colon
1491	Formalin	Frank 1994a	
1500-1650	Heme	Ozaki 1988	
1509	Phenylalanine	Fredericks 1995	Bovine Serum albumin
1510	Adenine, guanine	Puppels 1991	
1512		Lieber 2000	Ovary
1517	Carotenoid	Frank 1994b	
1520-1670	Tryptophan & tyrosine	Yazdi 1999	Cultured breast cells
1520	C=C Carotenoid	Keller 1994	Food
1520	Carotenoid	Larrson 1974	Blood plasma
1522	Carotenoid	Feld 1995	Carotid artery
1523	Carotenoid	Redd 1993	Human breast tissue Renal cell carcinoma
1523		Redd 1993a	Normal human breast tissue

1524	Carotenoid	Mizuno 1994	Human brain tissue, acoustic neuroma
1525	Carotenoid	Redd 1993a	Beta carotene
1525	Carotenoid	Redd 1993a TS	Human breast carcinoma
1525	Carotenoid	Redd 1993a	Human breast carcinoma
1528	**Carotenoid**	Manoharan 1994	Carotenoids in normal colon
1529	**Carotenoid**	Redd 1993b	Carotenoids in normal colon
1540	Amide II	Sajid 1997	Bovine insulin
1541	Tyrosine	Siebinga 1992	
1547	Tryptophan	Nie 1990	Human eye lens
1550	Tryptophan	Hartman 1973	
1552	δ(NH), ν(CN) Amide II	Barry 1992	Human strateum corneum
1553	**Tryptophan**	Mahadevan-Jansen 1998	
1554		Frank 1994b	Type I collagen (human placenta) & infiltrating ductal carcinoma (breast)
1555	Tryptophan	Manoharan 1995	DNA in water
1556	Tryptophan	Fredericks 1995	Bovine Serum albumin
1570	Vibration of purine bases (adenine & guanine)	Mahadevan-Jansen 1996	DNA
1570	nucleotides	Schrader 1995	Breast cancer in mouse
1575	Guanine, adenine tryptophan	Hartman 1973	
1576	Nucleic acid	Feld 1995	Colon adenocarcinoma
1577	Guanine, adenine	Puppels 1991	
1580	nucleotides	Schrader 1995	Breast cancer in mouse
1580	DNA	Yazdi 1999	Cultured breast cells
1580		Utzinger 2001	Cervix
1585	Nucleic acid, purine bases (adenine, guanine)	Boustany 1999	Colon
1585	Nucleic acid, purine bases (adenine, guanine)	Fodor 1985	
1585	υ(C-O) olefinic	Edwards 1995	Strateum corneum, Callus, psoriatic plaque
1585	ν(C=C) olefinic	Barry 1992	Human strateum corneum
1593	Purine bases	Manoharan 1995	DNA in water
1600		Hartman 1973	

1602	Phenylalanine	Siebinga 1992	
1602	Tyrosine	Manoharan 1995	Tyrosine, colon adenocarcinoma
1606	Phenylalanine	Fredericks 1995	Bovine Serum albumin
1607	Phenylalanine in bovine albumin	Kendall C	Sigma Aldrich A2153
1610	Tyrosine	Boustany 1999	Colon mucosa
1610	Tyrosine	Spiro 1987	Protein bands
1612	C=C stretching	Manoharan 1995	Benzene
1616	Tyrosine	Fredericks 1995	Bovine Serum albumin
1617	Tyrosine, phenylalanine	Puppels 1991	
1620	Tryptophan, tyrosine, phenylalanine, uracil	Hartman 1973	
1620	Tryptophan	Boustany 1999	Colon mucosa
1620	Tryptophan	Spiro 1987	Protein bands
1622	Tryptophan	Manoharan 1995	DNA in water
1637	Amide I ν(C=O)	Frank 1994a	Diseased breast tissue
1637	Amide I ν(C=O)	Frank 1994a	Collagen
1640	OH bending	Erckens 1997	Water
1642	Amide I ν(C=O)	Mahadevan-Jansen 1998	Collagen
1648-1661	Amide I ν(C=O)	Mahadevan-Jansen 1998	Histones
1645	Bending mode		Water
1645	Amide I (C=O stretch)	Miura 1995	α-helix protein secondary structure in α-Poly-L-lysine
1645-1660	Amide I (C=O stretch)	Carey 1982	α-helix protein secondary structure
1665-1680	Amide I (C=O stretch)	Carey 1982	β-sheet protein secondary structure
1660-1670	Amide I (C=O stretch)	Carey 1982	Unordered protein secondary structure
1645-1655	Amide I (C=O stretch)	Miura 1995	α-helix protein secondary structure
1665-1680	Amide I (C=O stretch)	Miura 1995	β-sheet protein secondary structure
1655-1665	Amide I (C=O stretch)	Miura 1995	Unordered protein secondary structure
1654-1662	Amide I (C=O stretch) α-helix	Mahadevan-Jansen 1998	α-helix protein secondary structure
1665-1680	Amide I (C=O stretch)	Mahadevan-Jansen 1998	β-sheet protein secondary structure
1654-1685	Amide I (C=O stretch)	Mahadevan-Jansen 1998	Unordered protein secondary structure
1650	Amide I	Baraga 1992a	Normal human aorta
1650	lipid	Boustany 1999	Colon mucosa
1650	Pyrimidine bases	Manoharan 1995	DNA in water

	(cytidine, thymidine) ?		
1650	C=C lipid bands	Boustany 1999	Colon
1650	Amide I ν(C=O)	Sajid 1997	Bovine insulin
1650		Wang 1993	Ascorbate
1650		Erckens 1997	Rabbit aqueous humour
1650	Amide I (C=O stretch) ν(C=O)	Brennan 1994	Human artery
1650-1666	C=C vibration cis-isomer in fatty acid chain	Mahadevan-Jansen 1998	Phospholipid membrane
1651	Amide I, ν(C=O)	Alfano 1991	Benign breast tissue and malignant tumours
1651-1664	Amide I, ν(C=O)	Carter 1998	Healthy human skin
1651	Amide I, ν(C=O) in collagen	Kendall C	Sigma Aldrich C7774
1651	Amide I, (C=O stretch)	Liu CH 1992a	Ovarian cancer
1651-4	υ(C-O) Amide I, α helix	Edwards 1995	Strateum corneum, Callus, psoriatic plaque
1652	Lipid	Redd 1993a Zhe Chuan Feng, Kwok to Yue, Gansler TS	Lipid (TPE)
1652	Lipid	Redd 1993	Human breast tissue
1652	Amide I	Miura 1995	α-helix protein secondary structure in α-Poly-L-glutamate
1652	ν(C=O) Amide I α-helix	Barry 1992	Human strateum corneum
1653	Lipid	Redd 1993	Human breast tissue Human colon
1653		Redd 1993a	Normal human breast tissue
1653	Amide I protein	Mizuno 1994	
1653	Amide I (C=O stretch) in bovine albumin	Kendall C	Sigma Aldrich A2153
1654	α-helix	Schrader 1995	nails
1654	C=C stretch Olefinic	McCreery 1994	Breast biopsy tissue
1654	C=C stretch	Frank 1994a	Breast tissue
1654	Amide I	Frank 1995	Normal breast tissue
1654	C=C stretch	Frank 1994b	Breast
1655	C=C stretch of unsaturated fatty acid chains	Baraga 1992b	Aorta
1655	Amide I	Frank 1995	Oleic acid methyl ester
1655	Amide I protein (C=O stretch)	Keller 1994	Coronary Artery

1655	Amide I (C=O stretch)	Frank 1994a	Lymph node
1655	Amide I (C=O stretch)	Liu 1992a	Endometrial cancer
1655	Amide I (C=O stretch)	Miura 1995	α-helix protein secondary structure in α-Poly-L-alanine
1656	Amide I (C=O stretch)	Mahadevan Jansen 1998a	Collagen
1656	Amide I (C=O stretch)	Mahadevan Jansen 1996	Human cervix
1656	Amide I (C=O stretch)	Mahadevan Jansen 1995	
1656		Utzinger 2001	Cervix
1656	Amide I (C=O stretch)	Liu 1992a	Benign or normal endometrium
1656	Amide I (C=O stretch)	Miura 1995	irregular protein secondary structure in β-Poly-L-glutamate pH 11
1657	Amide I (C=O stretch)	Liu 1992a	Cervical cancer
1657	Lipids – fatty acids	Manoharan 1998	Breast
1657	Lipids	Manoharan 1995	Colon
1657	Amide I (C=O stretch)	Feld 1995	Malignant breast tissue
1657	Amide I	Frank 1995	Infiltrating ductal carcinoma (breast)
1657	Amide I (C=O stretch)	Frank 1994a	Diseased breast tissue
1658	Amide I (C=O stretch)	Ozaki 1992	
1658	Amide I	Baraga 1992b	Aorta
1659	Amide I, ν(C=O)	Alfano 1991	Benign breast tumours
1659	Amide I (C=O stretch)	Liu CH 1992a	Benign or normal ovary
1659	Amide I (C=O stretch)	Liu CH 1992a	Benign or normal cervix
1659	Amide I (C=O stretch)	Liu CH 1992a	Benign or normal uterus
1659	Amide I (C=O stretch)	Liu CH 1992a	Uterus cancer
1659	Amide I (C=O stretch) ά helical	Mizuno 1994	Human brain tissue
1659	Amide I (C=O stretch)	Fredericks 1995	Bovine Serum albumin
1659	Amide I (C=O stretch)	Greve 1996	
1661	Amide I ν(C=O) in elastin	Kendall C	Sigma Aldrich E1625
1661	Amide I ν(C=O)	Gniakeda 1997	Normal human skin
1662	Nucleic acid	Feld 1995	Colon adenocarcinoma
1662	Triglycerides	Baraga 1992a	Adipose tissue from human aorta
1662	Nucleic acids	Manoharan 1996	Colon
1664	Amide I (C=O stretch)	Carter 1998	Healthy human skin
1664		Lieber 2000	Ovary
1665	Amide I (C=O stretch)	Miura 1995	irregular protein secondary structure in β-Poly-L-lysine pH 4
1665	Amide I (C=O stretch)	Frank 1994a	Collagen
1665	Amide I	Frank 1995	Type I collagen (human placenta)
1665	Amide I (C=O stretch)	Keller 1994	Liver - collagen
1665	Carbonyl vibration mode	Feld 1995	Fibrous atherosclerotic plaque

1666	C=O stretching modes of pyrimidine bases	Sajid 1997	DNA
1667	Structural protein	Manoharan 1998	Malignant breast
1668	Amide I (C=O stretch)	Mahadevan-Jansen 1998	Elastin
1669	Amide I (C=O stretch)	Nie 1990	Human eye lens
1669	Protein	Schrader 1995	Breast cancer in mouse
1669	Amide I (C=O stretch)	Miura 1995	β pleated sheet protein secondary structure in β-Poly-L-alanine
1669	Amide I (C=O stretch)	Rava 1991	Normal aorta
1670-1680	C=C vibration trans-isomer in fatty acid chain	Mahadevan-Jansen 1998	Phospholipid membrane
1670	Amide I	Nie 1990	Chicken leg bone
1670	Amide I (C=O stretch)	Mahadevan-Jansen 1998	Pure protein - β pleated sheet
1670	Amide I (C=O stretch)	Mahadevan-Jansen 1998	Collagen
1670	Amide I (C=O stretch)	Frank 1994a	
1670	Amide I (C=O stretch)	Erckens 1997	Rabbit lens
1670	Amide I (C=O stretch)	Miura 1995	β pleated sheet protein secondary structure in β-Poly-lysine
1672	Amide I (C=O stretch)	Miura 1995	β pleated sheet protein secondary structure in β-Poly-L-glutamate
1683	Amide I (C=O stretch)	Mahadevan-Jansen 1998	Bound protein - regular uncharacterised secondary structure
1717	**C=O stretching modes of purine bases**	Sajid 1997	DNA
1725		Wang 1993	Lactate
1725	νC=0	Cassanas 1991	Lactic acid
1726	Lactate	Goetz 1995	
1736	**ester stretching mode C=O**	Sajid 1997	DMPC (dimyristoylphosphatidylcholine), a typical lipid
1740	ν(C=O) -lipid	Keller 1994	Food, coronary artery
1743		Frank 1995	Oleic acid methyl ester, normal human breast tissue
1743	C=O stretch	Frank 1994a	Breast tissue
1743	C=O stretch	Frank 1994b	Breast
1743	ν(C=O) lipid	Barry 1992	Human strateum corneum
1747	C=0 stretch	Baraga 1992b	Aorta
1750	C=O	Fendel 1988	Normal skin dermis
1752	Triglycerides	Baraga 1992a	Adipose tissue from human aorta
1768	ν(COO)	Barry 1992	Human strateum corneum
2579	S-H stretch	Erckens 1997	Rabbit lens
2700-2880	Collagen C-H stretch	Wentrup-Byrne 1997a	Dentine
2717-23	υ(CH) aliphatic	Edwards 1995	Strateum corneum, Callus, psoriatic plaque
2723	ν(CH) aliphatic	Barry 1992	Human strateum corneum

2730		Frank 1994b	Breast
2800-3000	CH stretch – lipids	Carter 1998	Healthy human skin
2850-2960	CH_3, CH_2 stretching in alkyl/ acyl chains	Sajid 1997	DMPC (dimyristoylphosphatidycholine), a typical lipid
2850	ν_s(C-H) in (Ethylene CH_2=CH_2)	Mahadevan-Jansen 1998	Phospholipid membrane (constant with temperature)
2850	C-H stretching vibration	Fendel 1988	Normal skin dermis
2852	$\upsilon(CH_2)$ symmetric	Edwards 1995	Strateum corneum
2852	$\nu_s(CH_2)$ in lipids & proteins	Gniakeda 1997	Normal human skin
2852	$\nu_s(CH_3)$ - lipid	Carter 1998	Healthy human skin
2852	$\nu(CH_2)$ symm	Barry 1992	Human strateum corneum
2857	C-H stretch (-CH_3 sym.)	Frank 1994a	Breast tissue
2857	C-H stretch (-CH_2 sym.)	Frank 1994b	Breast
2872	$\upsilon(CH_2)$ asymmetric	Edwards 1995	Callus, psoriatic plaque
2875	C-H stretch (-CH_3 asym.)	Frank 1994a	Breast tissue
2875	C-H stretch (-CH_2 asym.)	Frank 1994b	Breast
2880	ν_{as}(C-H)	Mahadevan-Jansen 1998	Phospholipid membrane
2880	C-H stretch	Nie 1990	Human tooth enamel
2882	C-H stretch	Nie 1990	Chicken leg bone
2883	$\upsilon(CH_2)$ asymmetric	Edwards 1995	Strateum corneum
2883	$\nu(CH_2)$ sym.- lipid	Carter 1998	Healthy human skin
2883	$\nu(CH_2)$ symm, $\nu(CH_2)$ asymm	Barry 1992	Human strateum corneum
2885	CH_3 stretch	Erckens 1997	Lactate
2886	C-H stretching vibration	Fendel 1988	Normal skin dermis
2898	C-H stretch (-CH_3 sym.)	Frank 1994b	Breast
2890	ν_{as}(C-H) in (Ethylene CH_2=CH_2)	Mahadevan-Jansen 1998	Phospholipid membrane
2890	CH_2 symmetric stretch	Wicksted 1995	Glucose
2890	CH_2 stretch	Erckens 1997	Rabbit & human cornea
2890	CH_2 stretch	Erckens 1997	Glucose
2890	CH stretch	Erckens 1997	Rabbit & human aqueous humour
2893	**Glucose & lactate**	Wicksted 1995	Rabbit aqueous humour
2894-5	Lactate & glucose	Goetz 1995	
2898	C-H stretch (-CH_3 sym.)	Frank 1994a	Breast tissue
2918	C-H stretch	Nie 1990	Chicken leg bone
2929	C-H stretch (-CH_3 sym.)	Frank 1994a	Breast tissue
2929	C-H stretch (-CH_3 sym.)	Frank 1994b	Breast
2930	$\nu(CH_2)$ – lipid	Keller 1994	Coronary Artery
2931	$\upsilon(CH_3)$ symmetric	Edwards 1995	Strateum corneum, Callus, psoriatic plaque
2931	$\nu(CH_3)$ symm, $\nu(CH_2)$ asymm	Barry 1992	Human strateum corneum
2932	C-H stretch	Nie 1990	Human tooth enamel
2935	$\nu(CH_2)$ sym.- lipid	Carter 1998	Healthy human skin
2935	C-H stretch	Erckens 1997	Rabbit lens

2939	**Glucose & lactate**	Wicksted 1995	Rabbit aqueous humour
2942	C-H	Hartman 1973	
2942	$\nu_{as}(CH_3)$ – lipids and proteins	Gniakeda 1997	Normal human skin
2943	Glucose	Goetz 1995	
2945	CH stretch	Erckens 1997	Rabbit & human cornea
2945	CH_3 stretch	Erckens 1997	Lactate
2945	CH stretch	Erckens 1997	Rabbit & human aqueous humour
2945	Lactate	Goetz 1995	
2950	CH_2 anti-symmetric stretch	Wicksted 1995	Glucose
2950	CH_2 stretch	Erckens 1997	Glucose
2958	$\nu(CH_3)$ asymm	Barry 1992	Human strateum corneum
2960	C-H stretch (-CH_3 asym.)	Frank 1994a	Breast tissue
2960	C-H stretch (-CH_3 asym.)	Frank 1994b	Breast
2975	C-H stretch	Hartman 1973	
2982	**Glucose & lactate**	Wicksted 1995	Rabbit aqueous humour
2983	$\upsilon(CH_3)$ symmetric	Edwards 1995	Strateum corneum, Callus, psoriatic plaque
2990	CH_3 stretch	Erckens 1997	Lactate
2995	Lactate	Goetz 1995	
3006	=C-H stretch	Frank 1994a	Breast tissue
3006	C-H stretch	Frank 1994b	Breast
3059-60	υ(CH) olefinic	Edwards 1995	Strateum corneum, Callus, psoriatic plaque
3060	ν(CH) olefinic	Barry 1992	Human strateum corneum
3063	C-H stretch	Erckens 1997	Rabbit lens
3245	νOH	Cassanas 1991	Methyl lactate
3390	OH mode	Erckens 1997	Rabbit lens

Appendix F: Glossary of Terms.

Adenocarcinoma – Malignant tumour derived from glandular epithelial tissue.
Adenomatous polyps – Benign tumour derived from glandular epithelial tissue.
Aetiological factors – Factors causing or contributing to the cause of a disease or condition.
Afferent - Conducting inward and in a medical context usually towards an organ, the opposite of efferent.
Age standardisation– This makes allowances for the difference in the age structure of a population over time and between sexes.
Allogenic - Involving, derived from, or being individuals of the same species that are sufficiently unlike genetically to interact antigenically.
Angiogenesis - The formation and differentiation of blood vessels.
Antigens - Any substance foreign to the body that evokes an immune response either alone or after forming a complex with a larger molecule such as a protein and that is capable of binding with a product of the immune response such as an antibody or T cell.
Antioncogene – A type of tumour suppressor gene
Anti-Stokes scattering - Radiation scattered with a frequency higher than the incident radiation beam and accompanied by a loss of vibrational energy by the molecule.
Apoptosis - A form of programmed cell death in which a sequence of events leads to the elimination of cells without the release of harmful substances into the surrounding area.
Attenuation – A decrease in the pathogenicity or vitality of a microorganism or in the severity of a disease.
Autoimmune disorder – A disease caused by antibodies or T cells that attack molecules, cells, or tissues of the organism producing them.
Autologous - Derived from the same individual.
Barrett's oesophagus – A disease diagnosed from biopsy and found in the distal oesophagus where intestinal metaplasia has occurred and the normal stratified squamous mucosa is replaced by columnar epithelial cells containing goblet cells. It is associated with an increased risk of developing adenocarcinoma.
Benign - Of a mild type or character that does not threaten health or life, opposite of malignant.
Carcinogens - A substance or agent causing cancer.
Carcinoma - Malignant tumour derived from epithelial tissue
Case-controlled study – A study which identifies and compares patients who have the outcome of interest (cases) and control patients who do not have the same outcome. In order that an assessment can be achieved as to whether the cases had an exposure of interest such as an environmental, behavioural factor or exposure to a drug or some other therapeutic intervention.
Caudal - Situated in or directed toward the hind part of the body.
Cell-mediated immune response - The immune response that is mediated primarily by T cells and especially cytotoxic T cells rather than by antibodies secreted by B cells.
Centrosymmetric – Molecules where a reflection of any point through the centre of the molecule produces an identical configuration e.g. ethene (C_2 H_4).
Cerebral oedema - An abnormal or excessive accumulation of serous fluid in the connective tissue of the brain.

Chemotherapy - The use of chemical agents in the treatment or control of disease.
Clinical stage – The degree to which a disease has progressed as determined by clinical examination and non-surgical investigations.
Cohort - A group of individuals having a statistical factor such as age or risk in common.
Confocal – With the same foci
Contrast enhancement - A technique by which the degree of differentiation between different structures as seen in certain diagnostic imaging techniques can be improved by the administration of a contrast agent.
Cranial - Of or relating to the skull or cranium.
Cryogenetics - The study of specific chromosomal translocations.
Cytology - A branch of biology dealing with the structure, function, multiplication, pathology, and life history of cells.
Cytotoxic - Toxic to cells.
Dark current - The current produced by emission from components of the system itself.
Differentiation - The sum of the developmental processes whereby apparently unspecialized cells, tissues, and structures attain their adult form and function.
Dipole moment – This is the measure of the polarity of a covalent bond.
Distal - Situated away from the point of attachment or origin or a central point.
Ploidy - The degree of repetition of the basic number of chromosomes.
Dysplasia – An abnormal growth or development as of organs or cells leading to an unequivocal neoplastic change which has the potential to further progress towards malignancy.
Efferent - Conducting outward and in a medical context usually from an organ, the opposite of afferent.
Electromagnetic field – This is defined as a physical field produced by electrically charged objects.
Endogenous - Caused by factors within the body or arising from internal structural or functional causes, opposite of exogenous.
Exogenous - Caused by factors outside the body, opposite of endogenous.
Exophytic - Tending to grow outward beyond the surface epithelium from which it originates.
Extralymphatic deposits - Lymphoma arising outside the main lympho-reticular system.
Fcrit - The value over which a PC score represents true variance within a dataset.
Fibroelastic - Consisting of both fibrous and elastic elements.
Fibromuscular - Consisting of both fibrous and muscular elements.
Field - The area of tissue over which these differing modalities can be practically applied and divided into wide field and point or narrow field.
Fluorescence – This is an optical phenomenon in which molecular absorption of a photon of energy triggers the emission of a further photon which pocesses a longer wavelength.
Fluorophores - Molecular species that fluoresce.
Formalin fixed - Tissue sections preserved for histological assessment by the application of formalin.
Frozen sections – Tissue section acquired by the use of a freezing microtome, avoiding the use of chemical agents in their preparation.

GASER scale – A scale used to define the depth of field of a laser.
Genotype - All or part of the genetic constitution of an individual or group.
Glioblastoma - A malignancy of the central nervous system derived from astrocyte cells.
Glioma – A benign tumour arising from glial cells.
Gold standard - The standard with which other tests or procedures are compared.
Grade - The degree of severity of a disease or abnormal condition.
Haematoxylin and Eosin (H&E) – Stains used in the histological processing of frozen and formalin fixed tissue for pathological analysis.
Heterogeneous - Derived from another species or from another individual.
Heterozygous - Having two genes at corresponding loci on homologous chromosomes different for one or more loci.
Histopathology - A branch of pathology that deals with the minute structure of diseased tissue as discernible with the microscope.
Humoral immune response - Part of the immune response that involves antibodies secreted by B cells and circulating in bodily fluids.
Hyperkeratosis – A thickening of the strateum corneum.
Hyperplasia - An abnormal or unusual increase in the elements composing a part of a tissue e.g. cells.
Immunoassay - A technique or test used to detect the presence or quantity of a substance, such as a protein, which is based on its capacity to act as an antigen or antibody.
Immunocompromised - Having an impaired or weakened immune system.
Immunoglobulin – An antibody.
Immunophenotype - The immunochemical and immunohistological characteristics of a cell or group of cells**.**
Immunosuppression - Suppression of the natural immune responses for example by disease or drugs.
Incidence – The rate of occurrence of new cases of a particular disease in a population being studied over a period of time.
Inclusion bodies - Cytoplasmic or nuclear aggregates of stainable substances usually proteins.
Inelastic scattering - When monochromatic radiation passes through a substance it can be scattered or absorbed. Most of the scattered light is elastically scattered with the same frequency as that of the incident light, but a small proportion of the incident light is inelastically scattered with the difference in energy changing the vibrational state of the molecule probed. Inelastic scattering is the process measured in Raman spectroscopy.
Inter-observer error - The differences in interpretation by two or more individuals making observations of the same phenomenon.
Ischaemia – A lack of supply of blood to a body part due to obstruction of the inflow of arterial blood.
Laparotomy – A surgical technique for opening the abdominal cavity.
Low-grade / high-grade – Terminology used to classify NHLs on the natural history of the diseases.
Lycopenes – A red pigment that occurs in many fruits e.g. tomatoes.

Macrophages - A cell of the immune system which may be fixed or freely motile, is derived from a monocyte, functions in the destruction of foreign antigens, and serves as an antigen-presenting cell. Macrophages can also be called phagocytes.
Meningeoma - A slow-growing, benign, encapsulated tumour arising from the meninges.
Metaplasia - Abnormal replacement of cells of one type by cells of another.
Metastatic – Spread of a cancer beyond the confines of the organ or tissue from which it is primarily derived.
Modifier – A compound that acts by breaking down the surface glycoprotein layer of a tissue resulting in a change in the refractive index of the tissue.
Molar concentration - This is the measure of concentration of a solute in a solution of a given volume and is also called molarity.
Morbidity - The incidence of a disease in a specific population.
Morphological - Relating to or concerned with form or structure.
Mortality - The number of deaths in a given time or place.
Mutagenic - A substance capable of inducing genetic mutation.
Nasendoscopy - An endoscopic technique for examination of the pharynx and larynx.
Neoplasia - The process of abnormal and uncontrolled growth of cell, the product of which is a neoplasm (a tumour).
Normalisation - The process of removing statistical error in repeated measured data.
Numerical aperture - This is a way of describing the collection angle of a lens and is related to the refractive index of the material surrounding the lens and the maximum angle of collection from the optical axis of the lens.
Objective - This is the lens that receives and focuses the first light rays from the object being observed.
Otolaryngology - A medical specialty concerned especially with the ear, nose, and throat.
Peltier cooling – A form of thermoelectric cooling using the Peltier effect where by a heat pump transfers heat from one side of a device to the other side against the temperature gradient.
Peyer's patches - Isolated lymphoid follicle found in the ileum.
Phagocytosis - The process of engulfing and usually destruction of particulate matter by phagocyte cells. This process is a vital bodily defence mechanism against infection by microorganisms and against occlusion of mucous surfaces or tissues by foreign particles and tissue debris.
Phonons – These are quantised modes of vibration occurring in crystal lattices.
Photobleaching - The photochemical destruction of a fluorophore.
Polarisability - This is the relative tendency of a charge distribution to be distorted from its normal shape by the presence of an external electric field, e.g. a nearby ion or dipole.
Polymorphism - The existence of a gene in several allelic forms.
Prevalence - The number of cases of a disease or condition affecting a specific population at a given time.
Pro-carcinogen - The precursor to a carcinogen.
Prognosis - The prospect of survival and recovery from a disease as anticipated from the usual course of that disease or indicated by certain special features.
Prophylactic – To guard or prevent the spread or occurrence of disease or infection.

Pseudostratified - Relating to or being an epithelial surface consisting of closely packed cells which appear to be arranged in layers but all of which are in fact attached to the basement membrane.
Raman spectroscopy - An inelastic scattering technique, which exploits the frequency shift that occurs in incident light due to the excitation of vibrational and rotational states in illuminated molecules.
Resonance - The tendency of a system to oscillate at maximum amplitude at a certain frequency.
Salvage surgery – Surgery undertaken after failed treatment by a different treatment modality.
Schwannoma – A tumour arising from the myelin sheaths surrounding nerve cells.
Sensitivity - The proportion of individuals with the disease that are correctly classified as having the disease.
Sessile – Attached directly by a broad base.
Signal-to-noise ratio – This is the ratio of a signal power to the noise power corrupting the signal.
Sjögren's disease – An autoimmune disorder affecting the parotid salivary gland.
Specificity - The proportion of individuals without the disease that are correctly classified as not having disease.
Spectral resolution – A measure of the power to resolve individual feature within a spectrum.
Specular reflection - The perfect reflection of light from a surface.
Squamous - A stratified epithelium that consists at least in its outer layers of small cells arranged in layers.
Staging - A process by which cancers are divided into groups which behave in a similar ways.
Standard deviation – The standard deviation of a population of values is a measure of the spread of its values and is defined as the square root of the variance.
Stokes scattering - Radiation scattered with a frequency lower than the incident beam and accompanied by a gain of vibrational energy by the molecule.
Stratified - Arranged in layers, especially relating to an epithelium surface.
Surgical sieve – A form of disease classification relating to pathological processes e.g. infective, inflammatory, neoplastic.
Synergistic - Having the capacity to act together in a way that is greater than the sum of the individual processes involved.
Transcutaneous - Passing, entering, or made by penetration through the skin.
Tri modal spectroscopy - The combination of three spectroscopic techniques; Raman spectroscopy, autofluorescence and elastic scattering.
Tumour - An abnormal benign or malignant new growth of tissue that possesses no physiological function and arises from uncontrolled usually rapid cellular proliferation.
Variance – The variance of a random variable or probability distribution is a measure of its statistical dispersion and comprises of the averaging of the squared distance of its possible values from the expected value. The square root of variance is the standard deviation.

Appendix G: Nomenclature

α	polarisability
A	Absorbance
AC	adenocarcinoma
AFE	Autofluorescence endoscopy
AFE	autofluorescence endoscopy
AFS	autofluorescence spectroscopy
AIDS	Acquired Immunodeficiency Syndrome
AJCC	American Joint Committee on Cancer
ANOVA	
APCs	antigen-presenting cells
ATLL	adult T cell leukaemia and lymphoma
b	cell length (cm)
BAO-H&N	British Association of Otorhinolaryngologists-Head & Neck Surgeons
BSA	bleomycin sensitivity assay
C	Celsius
c	speed of light ($3x10^{8}ms^{-1}$)
C.B.E	
CaF_2	calcium fluoride
CARS	coherent anti-Stokes Raman spectroscopy
CCD	charge coupled device
CCND1	cyclin D1 gene
CEA	carcino-embryonic antigen
CO_2	carbon dioxide
CS	clinical stage
CSF	cerebro-spinal fluid
CT	computed tomography scanning
CTVE	computer tomography virtual endoscopy
Cu (II)	copper
CW	continuous wave
DNA	deoxyribose nucleic acid
ΔE	Change in vibrational or rotational energy of a molecule
EBV	Epstein-Barr virus
ENT	ear, nose and throat
E_{out} / E_{in}	energy of the emitted and incident radiation
ε	molar absorbtivity ($Lmol^{-1}cm^{-1}$)
ESR	erythrocyte sedimentation rate
C_2H_4	ethene
Ev	energy of molecule in a particular vibrational state
E_{vib}	energy absorbed or emitted in order to alter the vibrational state
F	force (N)
FBC	full blood count
FE	fluorescence endoscopy
FNAC	fine needle aspiration cytology
FT-IR	Fourier transform infrared spectroscopy
FTRS	Fourier transform Raman spectroscopy

GMC	General Medical Council
GNHST	Gloucestershire NHS Trust
GORD	gastro-oesophageal reflux disease
GP	General Practitioner
h	Planck's constant (6.626×10^{-34} Js or 4.136×10^{-15} eVs)
H&E	haematoxylin and eosin
He-Ne	Helium-Neon
HIV	human immunodeficiency virus
HL	Hodgkin's lymphoma
HNSCC	head and neck squamous cell carcinoma
H_2O	water
HpD	haematoporphyrin derivative
HPV	human papilloma virus
HRS	hyper-Raman spectroscopy
HTLV-1	human T cell leukaemia virus 1
IACS	Indian Association for the Cultivation of Science
InGaAs	indium-gallium-arsenide
IR	infrared
K	Boltzmann constant
K	spring constant (Nm^{-1})
λ	wavelength
LD	lymphocyte depleted
LDA	linear discriminant analysis
LDH	lactate dehydrogenase
LIF	laser-induced fluorescence spectroscopy
LOH	loss of heterozygosity
LOO	leave one out (cross-validation technique)
LP	lymphocyte-predominant
LR	lymphocyte rich
LSS	light scattering spectroscopy
MPE	maximum permissible exposure
MC	mixed cellularity
MRI	magnetic resonance imaging
N	Newton
NADH	
NBI	narrow band imaging
Nd:YAG	neodymium-yttrium-aluminium-garnet laser
NHL	non-Hodgkin's lymphoma
NHS	National Health Service
NIR	near-infrared
NO	nitric oxide
Non-VC	Non vocal cord tissue
N_o	numbers of molecules in the ground state
NS	nodular-sclerosing
N_v	numbers of molecules in an excited vibrational state
O_2	oxygen
OCT	optical coherence tomography
8-oxo-dG	8-oxo-deoxyguanosine

PS	pathological stage
PC	principle component
PCA	principle component analysis
PET	positron emission tomography
pH	The measure of acidity or alkalinity of a solution.
PM	photomultiplier tubes
PPIX	5-ALA-induced protoporphyrin IX
REAL	Revised European American Lymphoma classification
RNA	ribose nucleic acid
RS	Raman spectroscopy
SAC	Speciality Accreditation Committee
SCC	squamous cell carcinoma
SERRS	surface enhanced resonance Raman spectroscopy
SERS	surface enhanced Raman spectroscopy
SNR	signal-to-noise ratio
SPECT	super-imposed dual isotope scanning
T	absolute temperature
T (%)	% Transmission
T	Transmission
TNM	tumour, node, metastasis
TTV	transfusion transmitted virus
UICC	Union Internationale Contre le Cancer
UK	United Kingdom
ULWD	ultra-long-working-distance
USA	United States of America
USS	ultrasound scan
UV	ultra-violet
UV-Vis	ultraviolet-visible
ν	frequency
ν_{out} / ν_{in}	frequency of emitted and incident radiation
ν_{vib}	frequency of energy absorbed or emitted in order to alter the vibrational state
V	volt
VC	vocal cord
Vis	visible
ώ	wavenumber (cm^{-1})
WHA	World Health Assembly
WHO	World Health Organization
WLE	white light endoscopy
Zn (II)	zinc

Appendix H: Ethical Approval

H.1 Larynx studies

Avon, Gloucestershire and Wiltshire NHS
Health Authority

Gloucestershire LREC
Gloucestershire Royal Hospital
Great Western Road
Gloucester
GL1 3NN
Tel: 01452 395726
Fax: 01452 395720
Email: Hazel.Gage@glouc-tr.swest.nhs.uk

Our Ref: 02_58G(17_10).doc

17 October 2002

Miss Linda Orr
SpR in Ear Nose & Throat Surgery
c/o ENT Department
Gloucestershire Royal Hospital
Great Western Road
Gloucester
GL1 3NN

Dear Miss Orr

Study No 02/58G : An investigation into the ability of raman spectroscopy to differentiate between normal tissue and tissue affected by cancer in the larynx and pharynx

Thank you for submitting the amendments for the above study. I have now reviewed the amendments and will be advising the committee that in my view there is now no objection on ethical grounds to the proposed study. Therefore, I am happy to give you approval on the understanding that you will follow the conditions of the approval set out below. The following documents were reviewed by the committee:-

- LREC application form
- Protocol
- Consent Form
- Consent Checklist for Investigators
- General Information
- Information for Patients about the study
- Curriculum Vitae

a) It is the responsibility of the investigator to notify the LREC immediately of any information received by him/her, or of which he/she becomes aware which would cast doubt upon, or alter, any information contained in the original application, a later amendment application or verbal resume submitted to the LREC. The committee should be informed immediately if this information would raise questions about the safety and/or continued conduct of the research.

b) The need to comply with the Data Protection Act 1998.

c) The need to comply with the Research Governance Framework for Health and Social Care (Department of Health 2001). Further information regarding this document can be obtained from Gloucestershire Research & Development Support Unit on 01452 395726.

d) The need to refer proposed amendments to the protocol to the LREC for further review and to obtain LREC approval thereto prior to implementation (except only in cases of emergency where the welfare of the subject is paramount).

e) The requirement to furnish the LREC with details of the progress of the research project periodically (usually annually) and **failure to do this could result in approval to continue with the study being withdrawn.** Please also inform us of the conclusion and outcome of the research project and inform the LREC should the research be discontinued or any subject withdrawn altogether.

f) It is the responsibility of the person conducting any Trial to ensure that all professional staff and management of NHS Trusts involved are notified that it is taking place.

Gloucestershire LREC is fully compliant with the International Conference on Harmonisation/ Good Clinical Practice (ICH GCP) Guidelines for the Conduct of Trials Involving the Participation of Human Subjects.

Please indicate your agreement to comply with the requirements outlined in this letter by signing both copies of this letter and returning one to Hazel Gage. Full approval does not commence until the signed copy is returned.

Yours sincerely

Hazel Gage

Dr M J Richards
Chairman, Gloucestershire LREC

cc Dr Sally Pearson, Gloucestershire Hospital NHS Trust

I agree to comply with the requirements outlined in this letter.

18/OCT 2002
Signed

18/OCT/2002
Date

H.2 Lymph node studies

Avon, Gloucestershire and Wiltshire NHS
Health Authority

Gloucestershire LREC
Gloucestershire Royal Hospital
Great Western Road
Gloucester
GL1 3NN
Tel: 01452 395726
Fax: 01452 395720
Email: Hazel.Gage@glouc-tr.swest.nhs.uk

Our Ref: 02_57G(16_10).doc

16 October 2002

Miss Linda Orr
SpR in Ear Nose & Throat Surgery
c/o ENT Department
Gloucestershire Royal Hospital
Great Western Road
Gloucester
GL1 3NN

Dear Miss Orr

Study No 02/57G : Investigation into the ability of raman spectroscopy to differentiate between normal and diseased lymphoid tissue found in the neck

Thank you for submitting the amendments for the above study. I have now reviewed the amendments and will be advising the committee that in my view there is now no objection on ethical grounds to the proposed study. Therefore, I am happy to give you approval on the understanding that you will follow the conditions of the approval set out below. The following documents were reviewed by the committee:-

- LREC application form
- Protocol
- Consent Form
- Consent Checklist for Investigators
- General Information
- Information for Patients about the study
- Curriculum Vitae

a) It is the responsibility of the investigator to notify the LREC immediately of any information received by him/her, or of which he/she becomes aware which would cast doubt upon, or alter, any information contained in the original application, a later amendment application or verbal resume submitted to the LREC. The committee should be informed immediately if this information would raise questions about the safety and/or continued conduct of the research.

b) The need to comply with the Data Protection Act 1998.

c) The need to comply with the Research Governance Framework for Health and Social Care (Department of Health 2001). Further information regarding this document can be obtained from Gloucestershire Research & Development Support Unit on 01452 395726.

d) The need to refer proposed amendments to the protocol to the LREC for further review and to obtain LREC approval thereto prior to implementation (except only in cases of emergency where the welfare of the subject is paramount).

e) The requirement to furnish the LREC with details of the progress of the research project periodically (usually annually) and **failure to do this could result in approval to continue with the study being withdrawn.** Please also inform us of the conclusion and outcome of the research project and inform the LREC should the research be discontinued or any subject withdrawn altogether.

f) It is the responsibility of the person conducting any Trial to ensure that all professional staff and management of NHS Trusts involved are notified that it is taking place.

Gloucestershire LREC is fully compliant with the International Conference on Harmonisation/ Good Clinical Practice (ICH GCP) Guidelines for the Conduct of Trials Involving the Participation of Human Subjects.

Please indicate your agreement to comply with the requirements outlined in this letter by signing both copies of this letter and returning one to Hazel Gage. Full approval does not commence until the signed copy is returned.

Yours sincerely

Hazel Gage
pp **Dr M J Richards**
Chairman, Gloucestershire LREC

cc Dr Sally Pearson, Gloucestershire Hospital NHS Trust

I agree to comply with the requirements outlined in this letter.

Signed **Date** 19 Oct 2002

Appendix I: Publications and Awards

I.1 Publications

2003 C. Kendall, P Crow, J. Smith, L. Orr, N. Chandratreya, H. Barr, N. Stone. 'Raman spectroscopy for cancer diagnostics'. Lasers in Medical Science. 18 (suppl 1): O145, 48-49.

2009 Kendall, C, Isabelle, M, Hutchings, J, Babrah, J, Orr, L, Baker, R, Bazant-Hegemark, F, Stone, N, 'Vibrational spectroscopy: a clinical tool for cancer diagnostics.' Analyst, 134, 1029-1045.

2010 Raman spectroscopy of lymph nodes in the head and neck. L. Orr, C. A. Kendall, J. C. Hutchings, M. Isabelle, J. Horsnell, N.Stone. P Soc Photo-Opt Ins (SPIE), Photonic Therapeutics and Diagnostics VI. 2010; 7548C-70

I.2 Awards and Prizes

National Cancer Research Trial

South West Society of Otolaryngology – Prize for excellence in research 2005.